Influence of Structuredness on the Pressure Drop through a Packed Pebble Bed

by

Franco Cecil Barnard

Dissertation submitted in partial fulfilment of the degree

Master of Engineering

in the

School of Mechanical and Nuclear Engineering,

Faculty of Engineering

at the

North-West University

Potchefstroom

Promoters: **Prof. P.G. Rousseau**
Prof. C.G.dK. Du Toit

November 2011

Acknowledgments

I would like to thank both my study leaders, Professor Rousseau and Professor Du Toit, who led me through this journey. They taught me a great deal and I am very thankful for the opportunity given to me. I would also like thank my wife, Jana, for her support, love and patience. And last, but not least, I want to thank my Heavenly Father, without whom I would not have been able to successfully complete this dissertation.

ABSTRACT

Title:	Influence of structuredness on the pressure drop through a packed pebble bed
Author:	Franco Cecil Barnard
Promoters:	Prof. P.G. Rousseau
	Prof. C.G.dK. du Toit
School:	School of Mechanical and Nuclear Engineering
Degree:	Master of Engineering, M.Eng.

During this study an experimental test facility was designed and constructed with the purpose of conducting experiments to measure the pressure drop through packed beds of spheres with varying levels of structuredness. The test facility had to be designed so that the uncertainty in the measured friction factors would be below ±10% and commissioned to ensure that results with an acceptable degree of accuracy could be obtained.

Experiments were done on a randomly packed bed and a structured packed bed in order to demonstrate the proper operation of the test facility. The resulting experimental data was compared with applicable correlations found from relevant literature. The nuclear safety standards commission (KTA (1981)) correlation, as well as the relation of Ergun (1952) was chosen for comparison with the experimental data obtained from the experiment on the randomly packed bed. The correlation of Wentz and Thodos (1963) was selected for comparison with the experimental data obtained from the structured packed bed experiment.

The friction factors obtained from the experimental data was found to be higher than the friction factors calculated with the different correlations for the respective packing configurations. This could be attributed to the manufacturing process of the packing configurations that resulted in the surface finish of the particles to be extremely coarse. In order to obtain the desired porosity within the structured packed bed, cylindrical rods were utilised to separate the particles to prevent contact between them. Wentz and Thodos (1963) also made use of cylindrical rods, called distention rods, to make varying porosity possible within the structured packed beds. The

cylindrical rods that were utilised during these experiments are larger (in diameter) than those described in the literature, which could have contributed to the higher pressure drop through the structured packed bed. Furthermore, it was found that the friction factors derived from the experimental data increased as the modified Reynolds number was increased. This is a phenomenon that is not fully understood at this time and further study is proposed.

The operation of the experimental test facility was successfully demonstrated. The measurements were shown to be repeatable and the uncertainty of the friction factors derived from the measured data obtained from the test facility was less than 10%, which is satisfactory. Therefore, the ability to measure the pressure drop through packed beds of spheres with varying degrees of structuredness has now been established as a result of this research.

TABLE OF CONTENTS

LIST OF FIGURES

LIST OF TABLES

NOMENCLATURE

B	Bias limit
c	Constant (viscous forces)
℃	Degrees celsius
D	Diameter of packed bed
d	Diameter
f	Friction factor
g	Universal gravity constant
kg	Kilogram
kPa	Kilopascal
L	Length
M	Sample size
m	Constant (inertial forces)
m	Meter
mm	Millimetre
mA	Milliamps
MPa	Megapascal
ΔP	Differential pressure
P	Precision limit
R	Radius
Re	Reynolds number
s	Seconds
S	Standard deviation
t	Coverage factor
U	Uncertainty
u	Velocity
V	Volume
W	Watt
WS	Wetted surface
x	Value along X-axis / radial direction
X	Sample measurement
$\bar{X}$	Mean value of a sample

z	Value along Z-axis / vertical direction

ABBREVIATIONS

AC	Alternating current
ADAM	Advantech data acquisition module
AIAA	American institute for aeronautics and astronautics
BCC	Body-centred cubic
BPL	By-pass loop
CFD	Computational fluid dynamics
DAQ	Data acquisition
DB	Distribution board
DC	Direct current
DRE	Data reduction equation
EES	Engineering equation solver
FCC	Face-centred cubic
HPTU	High pressure test unit
HTTF	Heat transfer test facility
HTTU	High temperature test unit
KTA	Kerntechnischer ausschuss (German) Nuclear safety standards commission (English)
PBMR	Pebble bed modular reactor
PC	Personal computer
PFD	Process flow diagram
PL	Pump loop
P&ID	Process and instrumentation diagram
RMS	Root mean square
RSS	Root sum square
SC	Simple cubic
SAPB	Small annular packed bed
SCPB	Small cylindrical packed bed
TSL	Test section loop
URS	User requirement specification

SUBSCRIPTS

b	Packed bed
c	Central
d	Distance
h	Hydraulic
i	Counter
inf	Infinite
k	Counter
m	Modified
o	Superficial
p	Particle
r	Result
s	Sphere
t	Transition
v	Void
w	Wall

GREEK SYMBOLS

Δ	Differential
ε	Porosity
θ	Sensitivity coefficient
π	Pi
ρ	Density
φ	Friction factor
Ω	Ohm

CHAPTER 1 : INTRODUCTION

Packed beds of spheres are widely used in industry for chemical engineering applications. These chemical engineering processes include gas absorption, catalytic conversion, extraction and distillation. One of the many advantages of using a packed bed of spheres is in the high surface area it creates relative to the total bed volume. Packed beds of spheres are also studied for application in high temperature gas-cooled nuclear reactors.

Packed beds do not exclusively consist only of spherical particles. In the industry many shapes and sizes of particles can be used in packed beds. Packing types used in industry and experiments include, amongst others, pulverised coke, packed columns of cylinders, weaved carbon fibre packing, packing of rings and stacked plates.

Packed beds of spheres are mostly used with the spheres being randomly distributed. The random structure of the packing results when the spherical particles are randomly deposited into a container without carefully arranging it. Geometrically ordered packed beds of spheres are much less prevalent. This is due to the fact that obtaining a perfect packing structure with spheres takes substantial effort, which would make the packing much more expensive and not a viable option for practical application on a large scale.

The structured packing does however have potential advantages. It is believed by several experts that the pressure drop through a structured (geometrically ordered) packing is less than through a randomly packed bed. These experts include, amongst others, Wentz and Thodos (1963) and Du Toit (2008). It has also been proven from their work that the heat transferred from the energy source in the packing to the cooling fluid within a structured packing is more enhanced than in the case of a randomly packed bed. This can be attributed to the structured packed bed being quasi-homogeneous in its structure throughout the packing. The homogeneous structure leads to quasi-homogeneous porosity, causing the flow fields through the packing also to be homogeneous.

Even though the packed bed of spheres has been studied in great detail over many years, the majority of correlations to calculate the hydrodynamic properties only account for the magnitude of the porosity, and not for the nature of the packing that results in that porosity. Therefore, this phenomenon needs to be studied further in order to understand the influence of the porous

structure better. However, many experts have conducted experiments on structured packings to better understand the phenomenon.

One of the institutes that investigated the phenomena related to the pressure drop through a packed bed of spheres is the North-West University. The North-West University developed the Heat Transfer Test Facility (HTTF) to support of the development of the Pebble Bed Modular Reactor (PBMR). The PBMR was envisaged as a Generation IV high temperature gas-cooled nuclear reactor. The HTTF consists of two separate test units, namely the High Temperature Test Unit (HTTU) and the High Pressure Test Unit (HPTU). During this research study only the functioning of the HPTU was considered.

Tests were conducted on the HTTF for following two reasons:

- To validate the correlations that are currently used to model the relevant heat transfer and fluid flow phenomena required for the integrated simulation of the pebble bed core through a comprehensive set of separate effect tests. Du Toit (2008); and
- To generate results that could be employed to validate the different simulation methodologies applied in the integrated models that represent the entire pebble bed core through a comprehensive set of integrated effects tests. Du Toit (2008).

Tests conducted on the HPTU contributed to both of the above-mentioned objectives. Amongst others, the following tests were performed on the HPTU whilst employing nitrogen gas as the working fluid:

- Pressure drop tests for structured packed beds with homogeneous porosity. Three different porosities (0.36; 0.39; 0.45) were each tested at four instances in order to prove the repeatability of the experiment, Du Toit (2008).
- Pressure drop tests were also conducted on a small annular packed bed (SAPB) and a small cylindrical packed bed (SCPB) to investigate the differences in effect between these two configurations. The SAPB and the SCPB were both randomly packed beds. Tests done on the SAPB and the SCPB were each also repeated for four instances, Du Toit (2008).

In order to vary the Reynolds number for the different tests, the pressure level was varied between 1 bar and 50 bar. In this way the density was increased fifty-fold and consequently the Reynolds number as well. However, the high pressure levels at which the tests had to be

conducted had a significant effect on increasing the initial cost of the test facility. The high pressure levels, combined with the potential hazards associated with using Nitrogen gas as the working fluid also complicated and increased the cost of conducting the experiments.

The results obtained from the HPTU tests were compared with values predicted by the KTA (1981) correlation, as well as the correlation by Wentz & Thodos (1963). The KTA (1981) correlation represents an empirical correlation and is recommended to analyse cylindrical pebble bed reactors. The correlation of Wentz and Thodos (1963) was used to compare the results obtained from the experiment done on the structure packed beds of which the particles were separated from each other by cylindrical rods. Wentz and Thodos (1963) refer to these rods as “distensions”.

1.1 AIM OF THE PROJECT

The high cost of operating the HPTU facility implies that exhaustive studies cannot be done at the North-West University without substantial financial support from alternative funding sources. The aim of this project was therefore to design a new, much less complicated test facility to quantify the pressure drop through packed beds of spheres with different levels of structuredness, but within an acceptable degree of accuracy. Besides being substantially less expensive, this project also aimed at developing a test facility that would be very simple and safe to operate to allow under-graduate engineering students to conduct their future experiments.

Such a test facility could be employed to conduct numerous and exhaustive tests in a much more economical way and, assist in getting an enhanced understanding of the specific effect that the structuredness of a packed bed has on the pressure drop through it.

1.2 OVERVIEW OF THE DISSERTATION

A literature survey presented in this dissertation covers the findings identified in the literature concerning the effect that structuredness has on the hydrodynamic properties of a packed bed of spheres. A brief discussion is also provided in the literature survey of the end effects, the wall effects and the effects of porosity on the hydrodynamic properties of a packed bed of spheres.

The level of accuracy at which experimental data is obtained during an experimental study is of utmost importance. Therefore, a description of the various aspects that contribute to the uncertainty of measurements is discussed in general. The process by which errors propagate into the final result is also described.

The phenomena that influence the pressure drop through a packed bed of spheres need to be taken into consideration in order to design a suitable test facility. It is also very important to use the correct measuring instruments and to use these instruments in the correct manner. The following steps were taken to ensure that the test system is properly designed:

- A user requirement specification (URS) is set up in order to define the constraints of the test facility. The URS can be found in section 4.1 of this dissertation;
- A process flow diagram (PFD) is developed to illustrate the working of the system. The PFD can be found in section 4.2.1 in this dissertation;
- Instrument design is done to ensure the proper operation of the instrumentation;
- The PFD is integrated with the instrumentation design to form the process and instrumentation diagram (P&ID). The P&ID can be found within section 4.2.2;
- From the PFD and P&ID all the system components are designed in detail;
- The system is manufacturable;
- After the system is manufactured, the test facility is commissioned; and
- Finally the experimental tests are conducted as intended.

In order to operate the test facility effectively, a detailed description is provided on how the test facility should be operated. The entire system is described with the aid of figures and notations. This description also serves as a user manual to conduct experiments with the test facility.

CHAPTER 2 : LITERATURE SURVEY

2.1 INTRODUCTION

The hydrodynamic properties of a packed bed of spheres have been extensively studied over many years. Hydrodynamic properties refer to the way in which a structure reacts to fluid flowing through it. Numerous attempts have been made over time to fully characterise a packed bed of spheres. In the literature there are many correlations derived from experiments done on many variations of packed beds of spheres. Blake (1922) suggested plotting dimensionless parameters to analyse the pressure drop through a packed bed of spheres. He suggested plotting the bed friction factor against the modified Reynolds number. Ergun (1952) was the first to propose that the pressure drop through porous media can be expressed as the sum of the viscous and inertial forces acting on the fluid as it passes through the porous media. The findings of Ergun (1952) became the foundation on which most researchers after him would base their analysis on of a packed bed of spheres.

Many parameters affect the hydrodynamic properties of flow through a packed bed of spheres or porous media. The parameters affecting the hydrodynamic properties of a packed bed that are most commonly found in the literature are the porosity of the packing, the effect of confining walls on the packing, the end effects acting on the flow through a packing, the channelling effect, the structure/orientation of the packing and the shape of the particles comprising the packing. The parameters mentioned above do not act individually and are interconnected.

The effect that the structure of a packing has on the hydrodynamic properties of a packing is one of the phenomena that is still not fully understood. A single correlation that can accurately account for different types of structured packings does not currently exist. It has also not been possible to define what the level of structuredness of a packing is. However, in the literature accounts can be found of studies done on the hydrodynamic properties of structured packings. It will be attempted in the survey that follows to present the findings from the literature concerning the effect that structuredness has on the hydrodynamic properties of a packing.

2.2 THE EFFECT OF PACKING STRUCTURE ON ITS HYDRODYNAMIC PROPERTIES

The structured packings that will be considered during this literature survey will consist primarily of packed beds with spheres. However, packings of rings and plates will also be considered. The packings of rings and plates will be discussed in section 2.2.2.

2.2.1 PACKED BEDS OF SPHERES

One of the first attempts made to understand the effect that the structure of a packed bed of spheres has on the flow phenomena through the packing was made by Wentz and Thodos (1963). Their main objective was to conduct tests of the highest accuracy possible at that time. They made use of a wind tunnel to pass air though the different packing geometries under study. The geometries and porosities they selected for the experiment are given in Table 1. An illustration of each of these structures can be seen in Figure 1.

Table 1: Experimental test sections used by Wentz and Thodos (1963).

Orientations	Porosities [ε]
• Simple Cubic	0.480, 0.729, 0.882
• Body-centred Cubic (BCC)	0.354, 0.615, 0.728
• Face-centred Cubic (FCC)	0.743

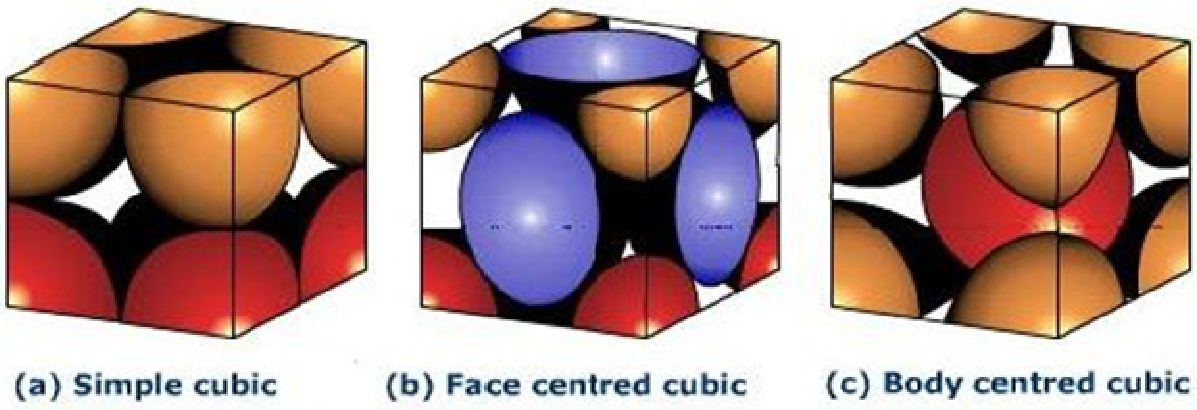

Figure 1: Graphical description of the Simple Cubic (SC), Body-centered Cubic (BCC) and the Face-centered Cubic (FCC) unit cells.

The large porosities were made possible by using distended beds. Distending the bed was done by using thin rigid wires. The shape of the wind tunnel that was used for the experiment was cylindrical. The packings were fitted into the cylindrical wind tunnel by cutting the packing into a cylindrical shape and sliding it into the wind tunnel. According to Wentz and Thodos (1963) the reason for cutting the packing into a cylindrical shape was to eliminate the effect that confining walls had on the packings. The effect from confining walls will be discussed in more detail later in section 2.4.

Confining walls of a packed bed react to the particles of a paced bed in such a manner that is influences the structure and porosity of the packing near the wall. The confining walls would then cause the area of the packing near the wall to react differently to the flow through it than the area of the packing that is not affected by the confining wall.

Wentz and Thodos (1963) used the experimental results that they obtained from the experiments done on the geometrically ordered packed and distended beds to calculate the friction factors for each using Eq (1). The experiment was carried out in two different manners. Firstly the pressure drop was measured with the inlet and outlet effects included. Then the pressure drop was measured without the inlet and outlet effects. They found in both cases that the results converged onto a single line. It was also noted that the absence of the end effects resulted in a lower friction factor.

The end effects of a packed bed refer to the effect that the inlet to and the outlet from the packing has on the flow through it. The end effects will be discussed in more details in section 2.3. The inlet effect occurs due to the fact that the porosity of the packing starts at unity in the pipe section leading to the packing and rapidly increases to as one progress through the first few rows of spheres into the packing. The outlet effect is much the same as the wall effect. The supporting structure holding the packed bed in place at the end of the packing causes the porosity in that region to vary and this has an effect on the flow through the end section of the packing.

The equation provided below (Eq 2) was derived by Wentz and Thodos (1963) from their experimental results to calculate the friction factor through a structured packing. According to Wentz and Thodos (1963), this equation is applicable to any geometrically ordered packing. This is due to the fact that all the data from simple cubic, body-centred cubic and face-centred cubic packings converged onto a single line when the friction factors were calculated. All the

other effects that could affect the friction factor of a packed bed were normalised so that only the structure of the packing could have an influence.

The above-mentioned results did not correlate well with the relation of Ergun (1952) given in Eq (3). The Ergun relation was derived from experiments done on randomly packed beds which excluded the effects of confining walls (1952). It was found that the friction factor for a geometrically ordered packing (packed and distended) was lower than that of a random packing. The results as presented by Wentz and Thodos (1963) can be seen in Figure 2.

$$f = \frac{\Delta P}{\rho u^2 / 2g} \frac{d_p}{L} \frac{\varepsilon^3}{1-\varepsilon} \tag{1}$$

$$f = \frac{0.396}{Re_m^{0.05} - 1.2} \tag{2}$$

$$f = 1.75 + \frac{150}{Re_m} \tag{3}$$

With the description of each variable as shown below:

- f - Friction factor of the packing;
- ΔP - Pressure drop through the packing;
- d_p - Particle diameter;
- ε - Porosity of the packing;
- ρ - Density of the fluid;
- u - Superficial velocity of the fluid;
- g - Gravitational constant;
- L - Length of the packing; and
- Re_m - Modified Reynolds number.

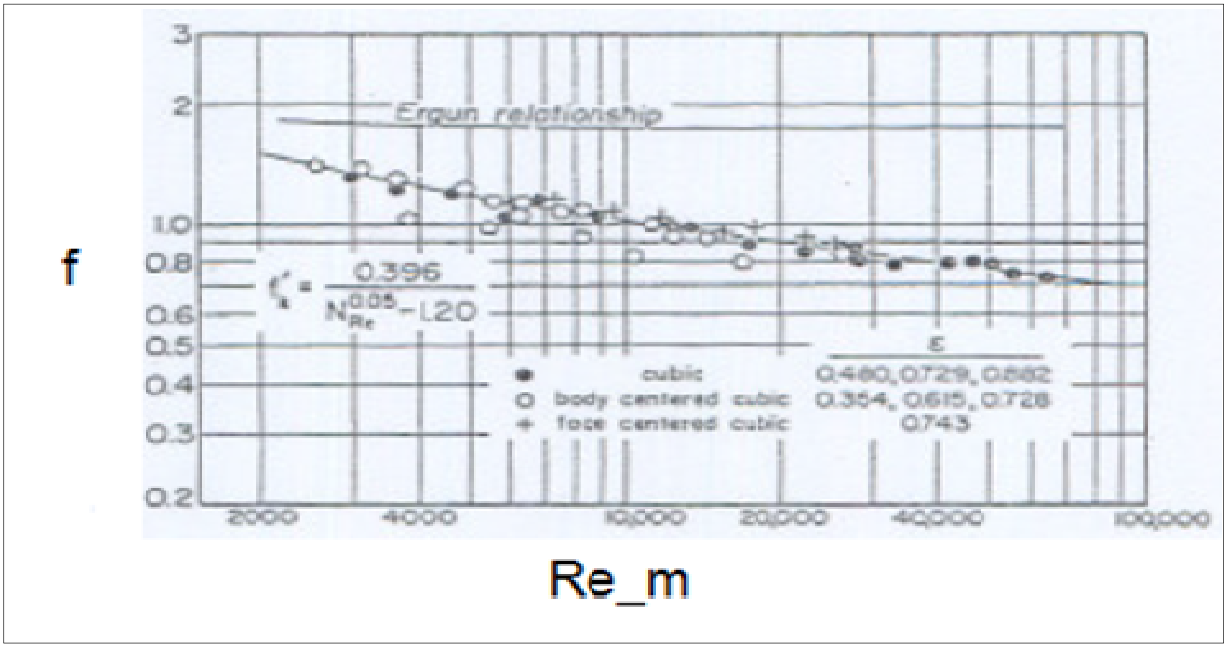

Figure 2: Friction factor vs. Modified Reynolds number for the overall pressure drop in the packed and distended bed of spheres Wentz and Thodos (1963).

As mentioned in the Introduction chapter, pressure drop tests were done on structured packings at the North-West University. These tests were done by utilising the HPTU. The homogeneous porosity packed beds, also mentioned in the Introduction chapter, are distended structured packings. The SAPB and the SCPB are randomly packed beds where the spheres were deposited into the annular and round cylinders. The average test results obtained from the HPTU are shown in Figure 3 below.

The blue line (top) in Figure 3 represents the friction factor predicted by the KTA correlation for randomly packed beds. The black and brown dots plotted on the blue line are the friction factor values obtained from the measurements of the tests done on the HPTU for the SCPB and the SAPB. The purple line (bottom) is the friction factor predicted by the KTA correlation for homogeneous porosity packed beds. The diamond, round and triangular dots plotted over the purple line are the friction factor values obtained from the measurements from the tests for the homogeneous porosity packed beds done on the HPTU.

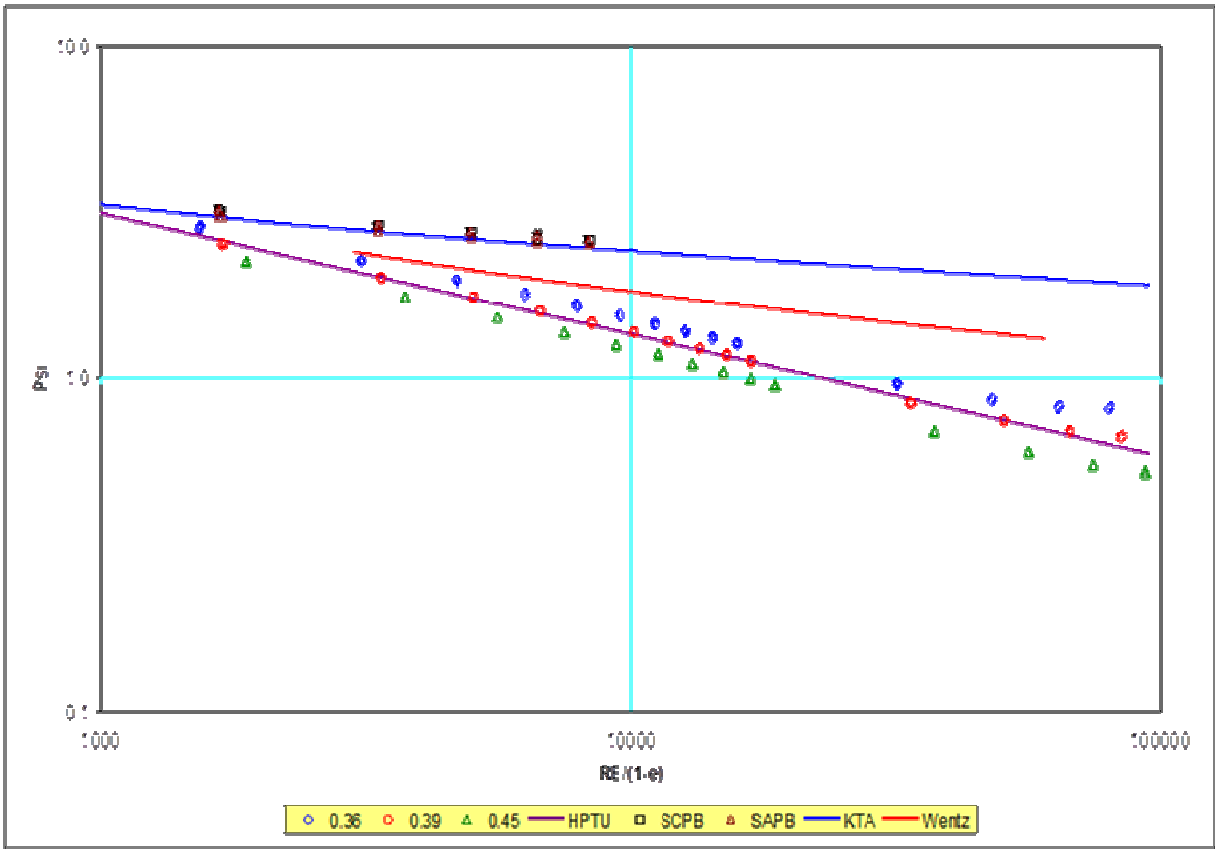

Figure 3: Combined friction factors for PDTS 0.36, PDTS 0.39, PDTS 0.45, SCPB, SAPB and the KTA and Wentz correlations Du Toit (2008).

According to the KTA correlation a difference in porosity is not supposed to affect the friction factor at a certain level of structuredness when it is plotted as a function of the modified Reynolds number. For a random packing (the blue line) it seems that the friction factor is not sensitive to a change in porosity. This conclusion is made because of the fact that for a certain modified Reynolds number the friction factor does not change much between the SCPB and the SAPB, which has different porosities. However, for the structured packings it can be clearly seen from Figure 3 that the friction factor is sensitive to a change in porosity when it is plotted as a function of the modified Reynolds number. For a selected modified Reynolds number the friction factor seem to decrease as the porosity of the packing increases.

Another observation that can be made from Figure 3 is the friction factor's sensitivity to a change in the structuredness of a packing when it is plotted as a function of the modified

Reynolds number. For a certain modified Reynolds number the friction factors for the structured packings are much lower that for the case with two randomly packed beds (SAPB and SCPB). The graphs in Figure 3 suggest that the friction factor is much lower for a structured packing for a selected type of flow.

Susskind and Becker (1967) also investigated the effect of the structure of a packing on the hydrodynamic properties of a packing. They used a rhombohedra array which was modified eleven times to give as many different types of packing. The modification was made by separating the spheres from each other while keeping each sphere in contact with the sphere above and below it. The rhombohedra array and the modifications to it can be seen in Figure 4. A description of how each of the rhombohedra array was modified eleven times can be seen in Table 2.

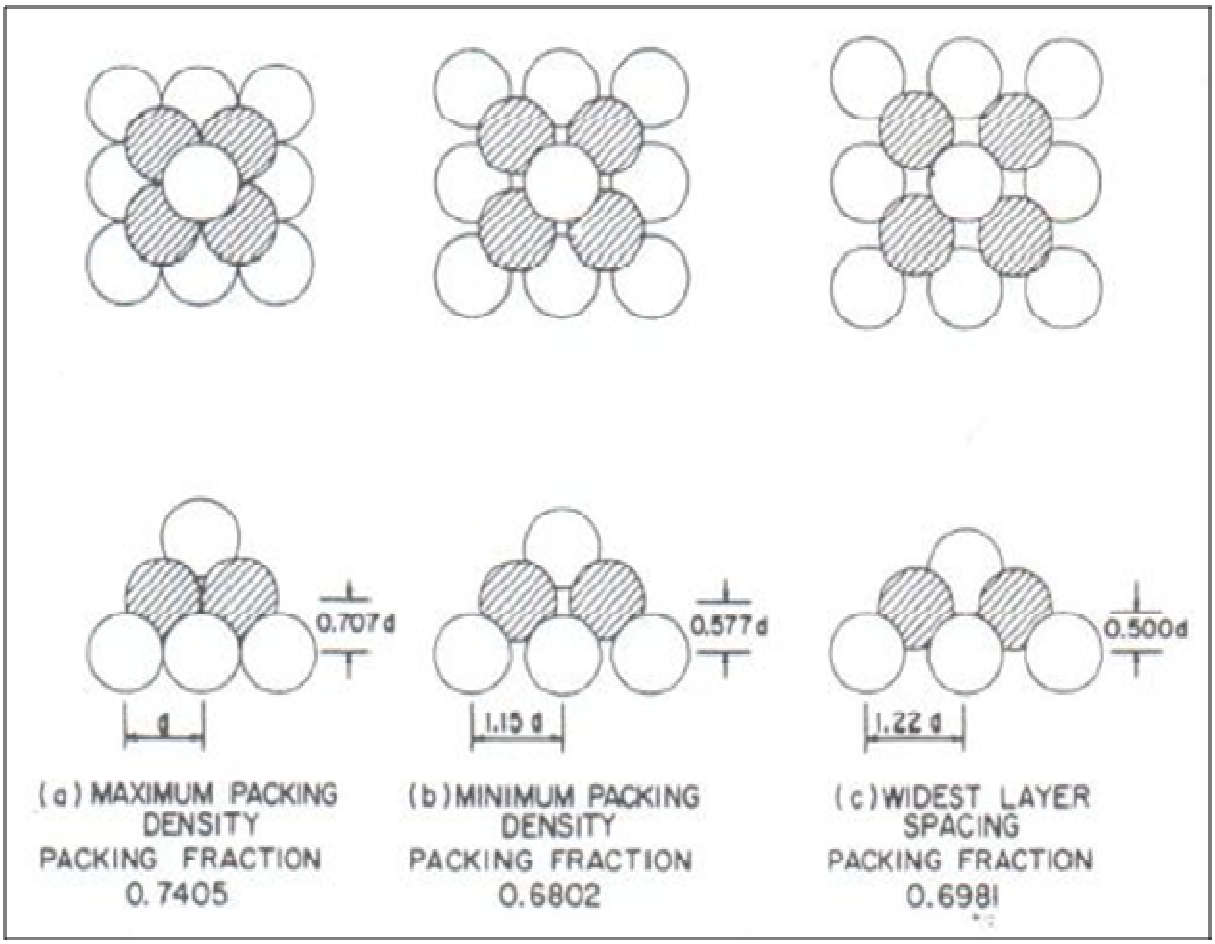

Figure 4: Rhombohedra array and the modifications to it. Susskind and Becker (1967).

The columns in Table 2 describe all the physical properties of each of the 11 packings that were tested by Susskind and Becker (1967). Column 1 provides alphabetical notations for each of the 11 packings. The second column shows how far the spheres were laterally separated from each other to obtain each of the specific structures. The d_d indicates how far the sphere centers were apart and the D_p is the diameter of the sphere. The three columns named Bed, Wall and Overall give the bulk porosity, wall region porosity and overall porosity of each of the 11 packings respectively. The last column shows what the diameters of the spheres were for each of the packings.

Table 2: Characteristics of test beds. Susskind and Becker (1967).

Test Bed	d_d/D_p	Bed	Wall	Overall	D_p, in.	D_p, cm
A	1.0000	0.2595	0.4775	0.2693	0.2500	0,6350
B	1.0340	0.2821	0.4765	0.2915	0.2500	0.6350
C	1.0460	0.2890	0.4772	0.3061	0.5000	1,2700
D	1.0720	0.3013	0.4711	0.3083	0.2500	0.6350
E	1.1110	0.3143	0.4623	0.3212	0.2500	0.6350
F	1.1240	0.3171	0.4581	0.3201	0.1250	0.3175
G	1.1270	0.3177	0.4583	0.3297	0.5000	1,2700
H	1.1540	0.3198	0.4450	0.3246	0.2500	0.6350
I	1.1910	0.3155	0.4238	0.3167	0.1250	0.3175
J	1.2000	0.3128	0.4174	0.3175	0.2500	0.6350
K	1.2210	0.3038	0.4007	0.3120	0.5000	1,2700

It was found that a change in the lateral distance between the spheres resulted in different porosities. According to Susskind and Becker (1967) the centres of the spheres could be moved apart laterally to a maximum distance of 1.225 diameters. Beyond this distance the rhombohedra array could no longer be maintained. The porosity would increase as the lateral distance increased, but only up to a point. The turning point was found to be at approximately 1.154 sphere diameters. Beyond this point the porosity started to decrease again. As the distance between the spheres was increased, straight channels of low friction started to form, as seen in Figure 4 above. The further the spheres were moved apart, the larger these low friction channels would open up.

The experiment conducted by Susskind and Becker (1967) was done with water. The rhombohedra packing was packed into a square container with a width and depth of 275.67mm (10.85in.) and a height of 762mm (30in.). The confining walls did not change the structure of the packings. The spheres were placed in such a manner that the packings fitted perfectly into the container. The pressure measurements were done at 311.15mm (12.25in.) above and 1276.35mm (50.25in.) below the packing by means of three different apparatuses. This meant that the pressure drop of the system without a packing would have to be determined so that it could be subtracted from the experimental data to deliver only the pressure drop of the packing under consideration.

From the experimental results, shown in Figure 5, that were presented by Susskind and Becker (1967) it was shown that as the distance between the spheres and the porosity increased, for packings A to H, the friction factor for the packing decreased. However, for packings I to K, as the distance between the spheres increased the porosity started to decrease. It is expected that the friction factors would start to increase as the porosity of the packings started to decrease. However, this was not the case. The friction factors of the packings continued to decrease, but at a slower rate. It is important to note that the friction factor was corrected for the effect that the wall has on the porosity of the packing.

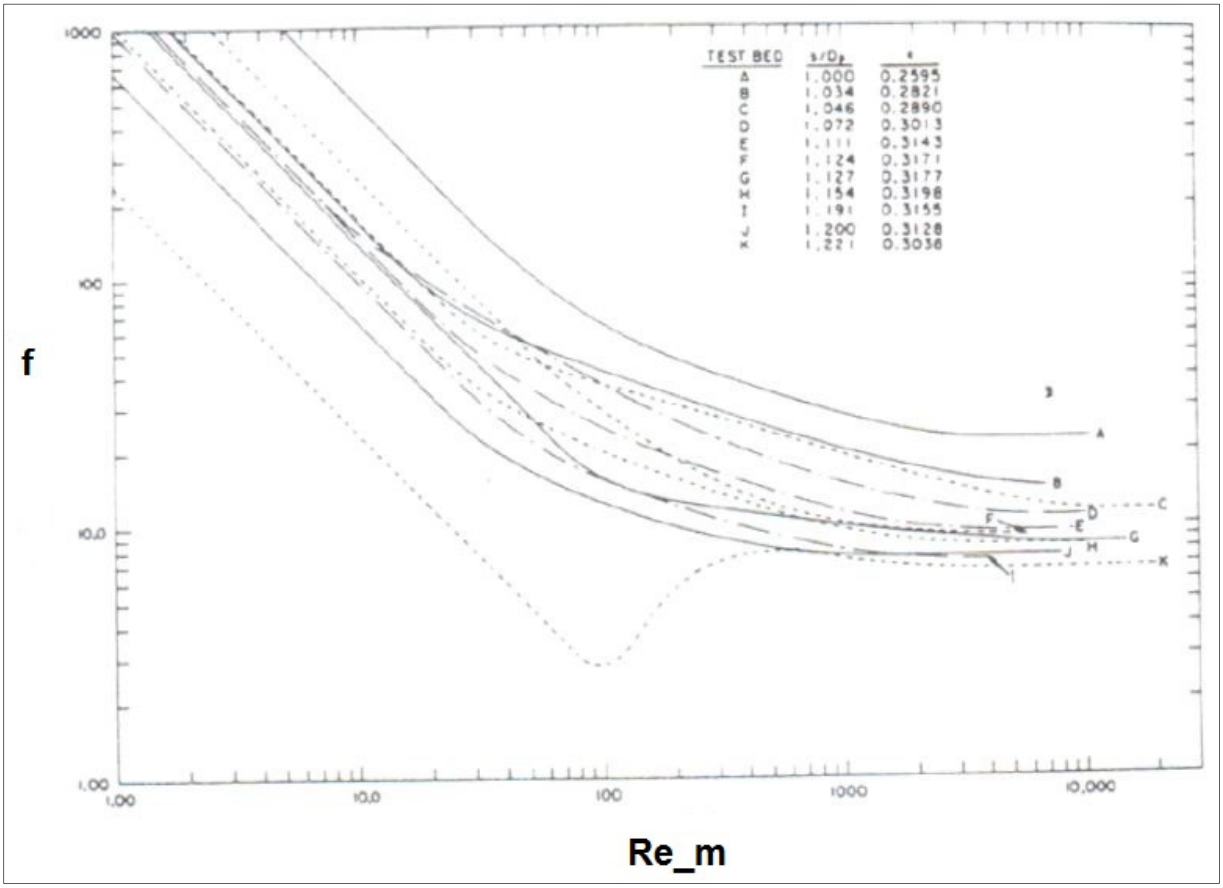

Figure 5: Results obtained by Suskind and Becker (1967).

The reason for this continuous decrease in friction factor was due to the straight low-friction channels that started to form as the distance between the spheres increased. For packing K, where the spheres were at a maximum distance from each other, the relation of the friction factor to modified Reynolds number started to resemble that of an empty low friction pipe. Therefore, laterally separating a rhombohedra array's particles beyond a certain point would cause the array not to represent a packed bed of spheres anymore.

Due to the closeness in parameters of packing F and G, Susskind and Becker compared the relations obtained from the experiments done on these two packings. They found that the relations were close to one another but that the slight difference in porosity between the packings lead to a difference in the friction factor of the packings. They corrected the porosity of the one packing to that of the other. This correction made to the porosity of the packings, was

to normalise the porosity of two packings for which the porosity differs. The porosity correction was done by using $(1-\varepsilon)/\varepsilon^3$. The friction factor would be divided by $(1-\varepsilon)/\varepsilon^3$ for the current porosity and multiplied by $(1-\varepsilon)/\varepsilon^3$ for the desired porosity. It was found that, after the porosity correction was applied, there was less than 3% difference between the average friction factors of the two relations.

Porosity corrections were also applied to compare the friction factors of packing B and C, C and D as well as E and G. It was found for the first two comparisons (B with C and C with D) the difference in average friction factors of the two relations was approximately 3%. By applying the porosity correction to E and G the difference in average friction factors of the two packings was approximately 10%

The differences in spacing between the spheres of the combinations mentioned above are at a ratio of 1.0116 for B to C, 1.0248 for C to D, 1.0026 for F to G and 1.0144 for E to G. This shows that the closer the rhombohedra array comes to the turning point, Point I in Table 2, the smaller the spacing must be between the spheres for the porosity correction to work. It also gives the impression that as the rhombohedra array approaches the turning point, it starts acting less like a packed bed. It can be seen in Figure 6 below, that the relation between the packing fraction, which is the inverse of the porosity of a packing, has a linear relation with the particle spacing up to packing D. Beyond point D the linear nature of the relation is lost and the thermal fluid properties resembling that of a packed bed of spheres start to change.

From the study done by Susskind and Becker (1967) it is clear that the bypass effect, caused by the increase in the spacing of the spheres, has a significant effect on the friction factor of a packed bed. The effect of these bypass channels starts to overshadow the effect of the porosity of the packing as the channel size increases. Susskind and Becker (1967) therefore concluded that the structure of a packing has a larger influence on the friction factor, than the porosity of the packing. However, it was also found that Susskind and Becker (1967) could not derive a suitable correlation that would satisfy all the experimental data that they obtained during their study.

The entrance and exit effects of the packings were tested by Susskind and Becker (1967). It was found that for a packing with a length of more than seven ball diameters the entrance and exit effects were negligible. No mention was made by the authors on the effects that the difference in particle size could have on the outcome of the experiment.

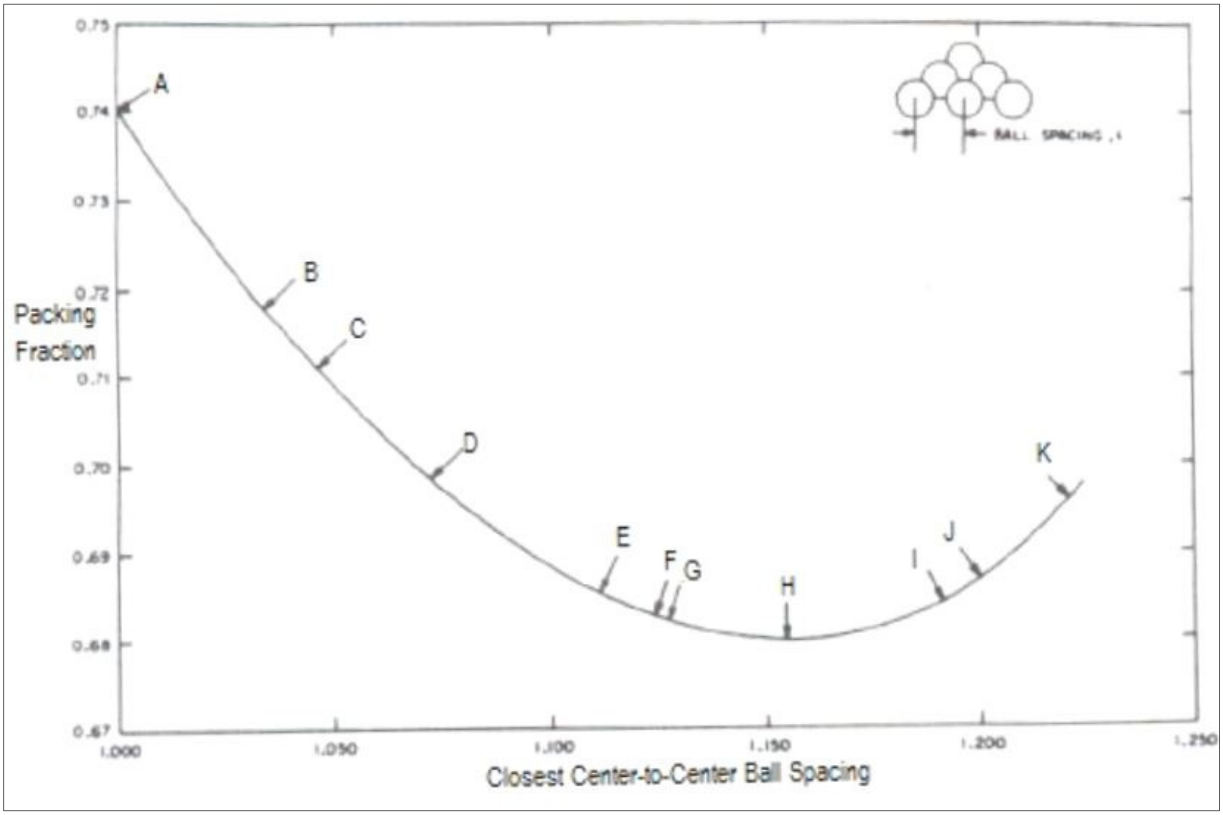

Figure 6: Packing fraction of the rhombohedra array vs. the particle spacing. Susskind and Becker (1967).

In the studies of Handley and Heggs (1968) pressure drop was tested through a range of different porous media. The first tests they performed were with beds of randomly packed steel, lead, bronze, lead glass and soda glass spheres. They also conducted tests on steel cylinder packings, as well as steel and porcelain ring packings. Lastly, geometrically ordered aluminium plate packings were tested for pressure drop.

Compressed air was chosen as the working fluid to determine the pressure drop across the different packings. The flow of air was controlled by a gate valve and measured with an orifice meter. The pressure drop was measured by means of water and mercury manometers. The temperature of the air passing through the packings was measured at the outlet of the packing. The insulation used on the inside of the test section was a flexible expanded rubber sleeve. As the particles were poured into the test section, the rubber sleeve would conform to the outside

shape of the packing, effectively eliminating the effects that the wall would have on the flow phenomena.

The packed beds were tested for bed-to-particle (D/d_p) diameter ratios of between 8 to 22 and bed length-to-particle diameter ratios (L/d_p) of between 11 to 32. The results of the experiments were compared with the linear form of the Ergun equation as shown in Eq (4), with c and m being equal to 1.75 and 150 respectively. The constants c and m represent the viscous and inertial forces respectively. The variables f and Re_m correspond to the Friction factor and the modified Reynolds number respectively.

$$fRe_m\left(\frac{\varepsilon^3}{1-\varepsilon}\right) = mRe_m + c \qquad (4)$$

It was observed from the data obtained by Handley and Heggs (1968) that the diameter ratios, (D/d_p) and length ration (L/d_p) did not have a noticeable effect on the pressure drop through the packings. Due to the linear relation of the experimental data obtained by Handley and Heggs (1968) between the modified friction factor and the modified Reynolds number, as represented by Eq (4), the Ergun (1952) approach of treating the pressure drop through a packed bed of spheres as the sum of the viscous and inertial forces was proven to be correct. The experimental data obtained by Handley and Heggs (1968) is represented in Figure 7. The modified friction factor mentioned in Figure 7 is the left-hand term in Eq (4), and the modified Reynolds number is Re_m.

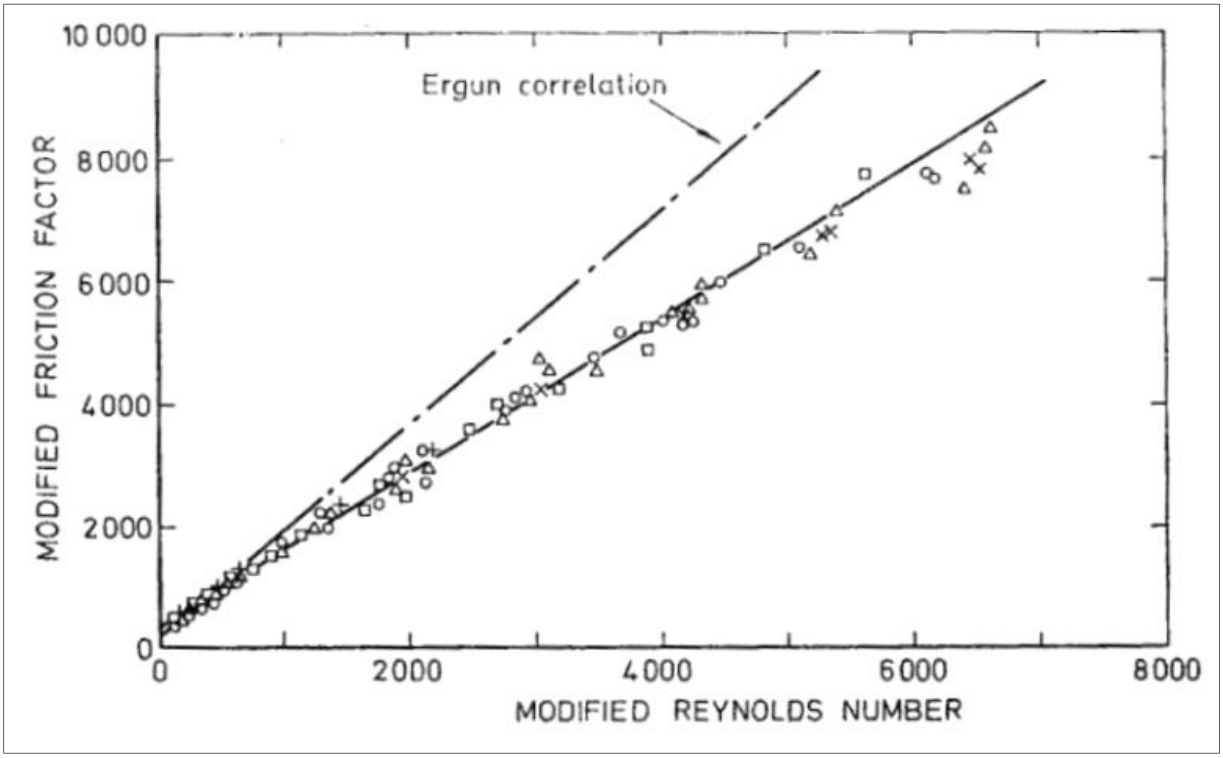

Figure 7: Experimental data of Handley and Heggs compared to the relation of Ergun. Handley and Heggs (1968).

According to Handley and Heggs (1968) the tortuosity of flow caused by the packing seems to have a significant influence on the pressure drop of the flow through the packing. Tortuosity of flow refers to the manner in which a fluid flows. For a straight pipe with no blockage in it the tortuosity of a fluid flowing through in would be minimal. In the case of a packed bed of spheres, the sphere would cause a blockage in the way of the flow. This would cause the fluid to have to wriggle its way through the packing thus increasing its tortuosity of the flow through the packing. The inertial tortuosity of flow through a packed bed can be related to the number of times the flow has to change direction. The more times the flow has to change direction, the higher the inertial component of the friction factor of the packing will be.

The viscous forces of the flow through a packed bed can be related to more than one parameter. The amount of surface area of a packing and the velocity of the flow over that surface are two of the parameters that influence the viscous forces that act on the fluid passing

through a packing. The effect of a varying diameter of the flow passage also contributes to the viscous forces that act on the fluid flowing through a packing.

The viscous forces and inertial tortuosities of a packing can contribute to the friction factor of a packing in various combinations. When there are stagnant pockets inside a packed bed of spheres, it will increase the inertial tortuosity of the packing while decreasing the viscous forces caused by the packing. In a packing where there are many bends and turns with large flow passages the inertial tortuosity of the packing will be large and the viscous forces caused by the packing will be small. On the other hand, if the flow passages are narrow the viscous forces cause by the packing will also be large. In the event of straight narrow passages of flow the inertial tortuosity of the flow will be small with a large viscous forces acting on the flow through the packing. To be able to define what the level of structuredness of a packing is one might consider using the tortuosity of a packing as one of the deciding factors according to Handley and Heggs (1968).

In the works of Atmakidis and Kenig (2009) the effects of confining walls on the pressure drop through geometrically structured and random packings were investigated. They made use of computational fluid dynamics (CFD) software to construct the different packings and simulate the flow of water through them. Bed-to-particle diameter ratios from 1 to 7 were investigated due to the fact that the effect of confining walls is very significant in this range.

Four geometrically ordered packings were investigated in the study of Akmakidis and Kenig (2009). Two BCC packings with bed-to-particle diameter ratios of 1.00 and 2.68 and two FCC packings with bed-to-particle diameter ratios of 3.00 and 5.50 were used in the simulations. The four random packings were constructed using a ballistic deposition method. This ballistic deposition method would drop a certain number of test particles into the cylindrical pipe and only secure the position of the particle with the lowest possible position and discard the rest of the particles. It would continue to repeat this procedure until the entire packing was assembled. The bed-to-particle diameter ratios used for the random packing were 2.00, 3.00, 5.00 and 7.00.

A random packing has a very complex geometry to simulate with CFD software, therefore an unstructured tetrahedral grid was chosen as an approximate discretization of the computational domain. To ensure high quality mesh elements at all possible contact points in the packing, the particles were all shrunk by 2%.

The friction factors obtained by Atmakidis and Kenig (2009) from their CFD simulations are shown in Figure 8 and Figure 9. They compared their results with the friction factors predicted by a number of correlations available in the literature. It was found in the case of the random packing that the results correlated very well with the values predicted by the correlation of Reichelt (1972). The values predicted by the correlation by Carman (1937) deviated the most from the CFD results due to the fact that the correlation of Carman (1937) does not take the inertial effects into account.

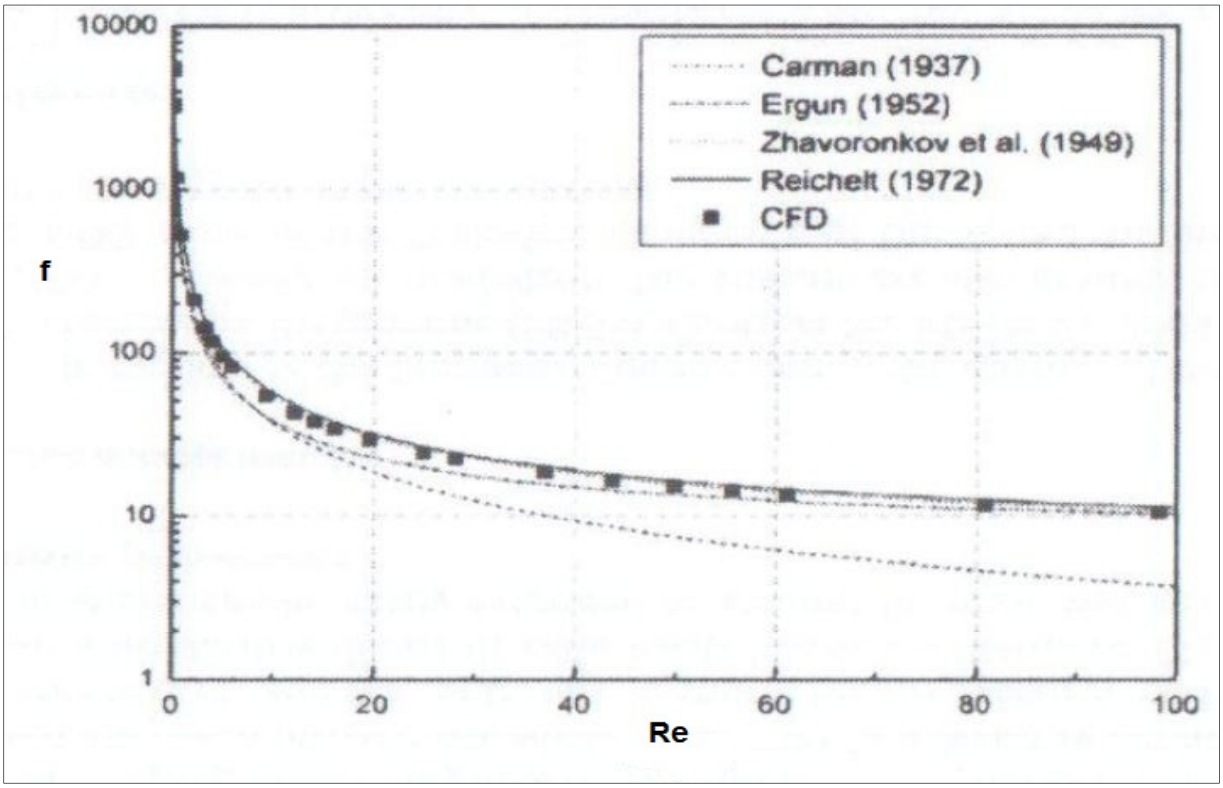

Figure 8: Results obtained by Atmakidis and Kenig for the pressure drop through random packings. Atmakidis and Kenig (2009).

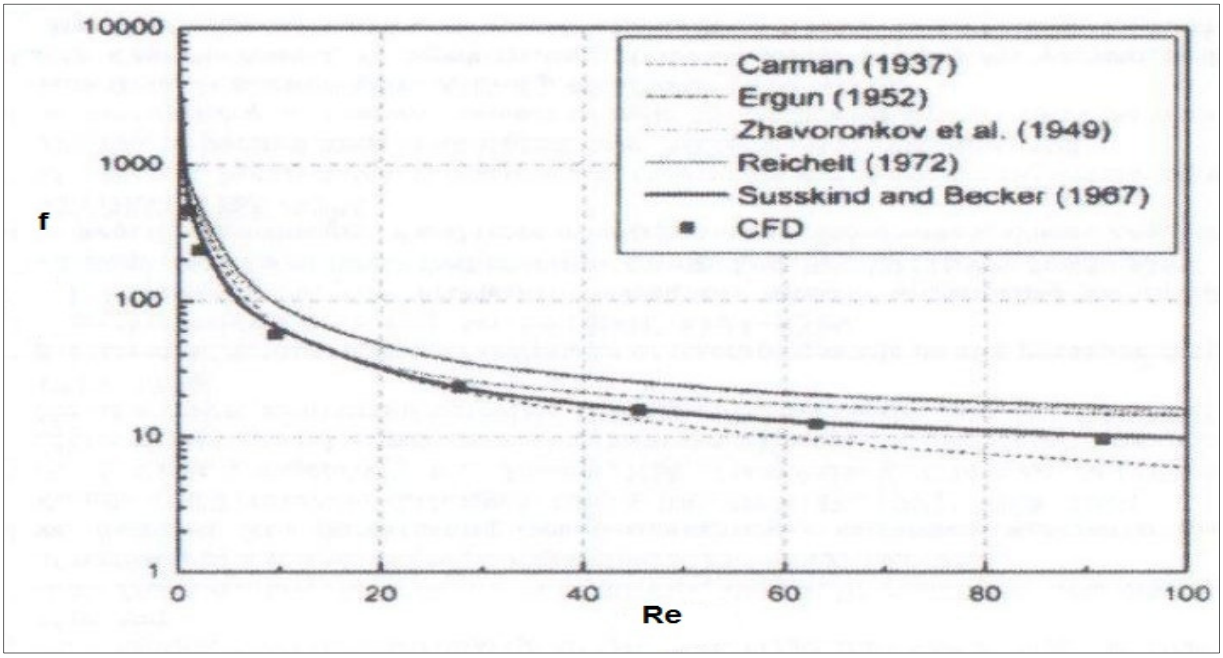

Figure 9: Results obtained by Atmakidis and Kenig for the pressure drop through structured packings. Atmakidis and Kenig (2009).

The friction factors of the structured packings correlate well with the values predicted by the correlation derived by Susskind and Becker (1967) for structured packings. As expected, the friction factor for a structured packing is less than that of a random packing. According to the authors Atmakidis and Kenig (2009) the reason for the pressure drop through structured packings being lower than that of the random packings is due to the structuredness creating a by-pass effect for the flow throughout the entire packing. The structured nature of the packing causes flow channels of lower friction than that in a random packing. It was also observed that the channelling effect near the wall was very high for the structured packing.

In the studies conducted by Yang and Wang (2010) the effects of different types of structured packings were investigated with regards to their hydrodynamic and heat transfer properties. They made use of six different structures during their simulations. A graphic representation of their test unit can be seen in Figure 13 below. The dimensions of the parameters illustrated in Figure 13 and a list of the structures chosen for the study are shown in Table 3 below.

The square channel that the structures were tested in had a length of more than 10 times the particle diameter. This can be seen in Figure 13 b, with the inlet block, the packed channel and the outlet bock shown. The packing length was eight cell units for every packing. The three dimensional Navier-Stokes equations were solved during the computation.

The first test that they conducted was to compare the hydrodynamic properties of the SC, BCC and FCC packings against each other. The pressure drops through the packings were compared and it was found that the pressure drop through the SC packing was the lowest as the Reynolds number increased. The pressure drop through the FCC packing was the highest, leaving the BCC packing in the middle. Following this, the three packings were compared with regards to their friction factors. It was found that the friction factor of the SC packing was the highest and that of the FCC packing was the lowest. It is expected that the pressure drop and the friction factor would be directly equivalent to each other, causing the SC packing to have the lowest friction factor. The reason that the friction factor and the pressure drop is not necessarily directly equivalent to each other is because of the fact that the friction factor normalises all the parameters that play a role in restricting the flow through the porous media. This implies that if the SC and the FCC packing had the same porosities, the pressure drop through the SC packing would be the highest. The results of this first experiment of Yang and Wang (2010) are presented in Figure 10.

Yang and Wang (2010) examined the flow field of the water through the packings and they concluded that the reason for the SC packing having a higher friction factor is because of vortices developing between the spheres. These vortices increase the turbulent mixing of the packing. Vortices also appear in the BCC packing, but they are smaller in size and the turbulent mixing of the packing is consequently reduced. The flow through the FCC packing show streamline flow with no vortices developing in the packing. This results in the FCC packing having a much lower friction factor.

The next comparison that Yang and Wang (2010) made was between the FCC, FCC Flat Ellipsoid and the FCC Long Ellipsoid packings. The friction factor for the FCC packing was the highest with the FCC Flat Ellipsoid's friction being just below it. The friction factor for the FCC Long Ellipsoid was much lower than that of the other FCC packings. It is expected that the more streamlined, or aerodynamic, shape of the FCC Long Ellipsoid packing caused its friction factor to be much lower. The results for this experiment of Yang and Wang (2010) are presented in Figure 11.

The last comparison by Yang and Wang (2010) was between the uniform and non-uniform BCC packings. The uniform BCC structure was such that all the spheres in the structure had the same size. For the non-uniform BCC structure the body centred sphere had a smaller diameter than that of the rest while all the spheres still had contact with each other. It was found that the friction factor of the uniform BCC packing was the lower of the two. This can most likely be attributed to the flow through the uniform BCC packing being less tortuous. A graphical illustration of what each of the above mentioned packings look like can be seen in Figure 14. The results for this experiment by Yang and Wang (2010) are provided in Figure 12.

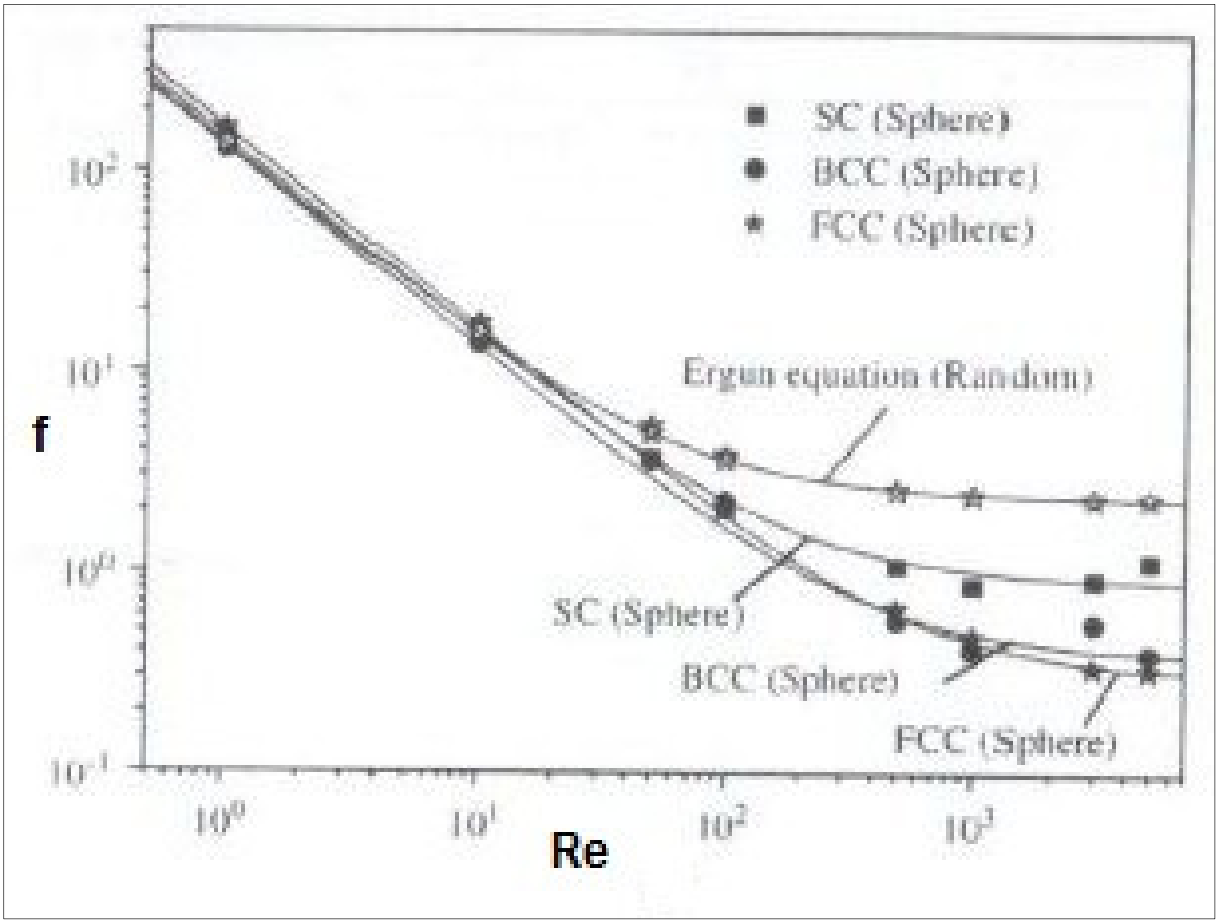

Figure 10: Results of Yang and Wang (2010) when comparing SC BCC and FCC.

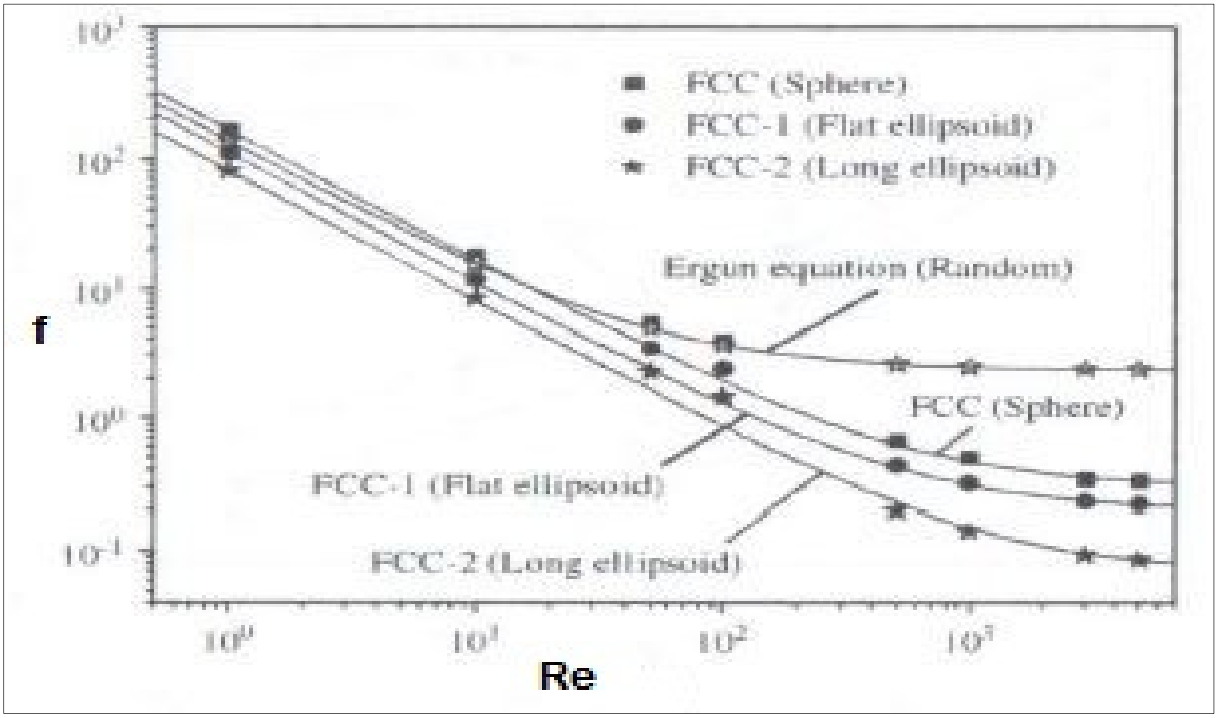

Figure 11: Results of Yang and Wang (2010) when comparing FCC, FCC 1 and FCC 2.

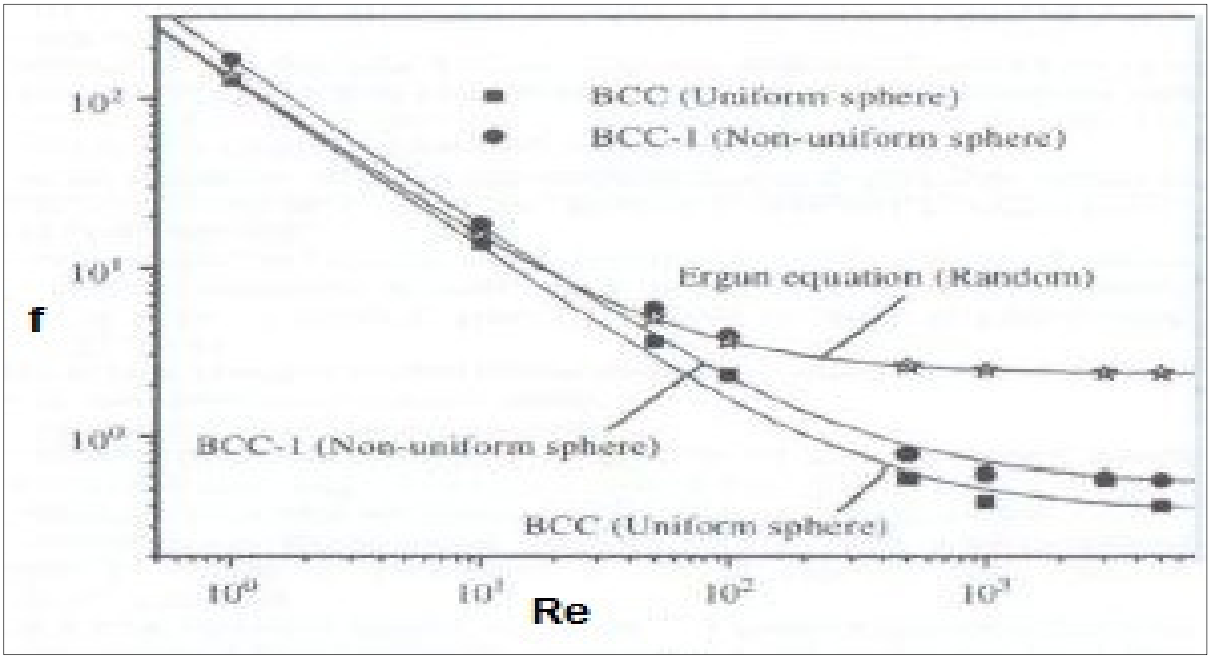

Figure 12: Results of Yang and Wang (2010) when comparing BCC and BCC 1.

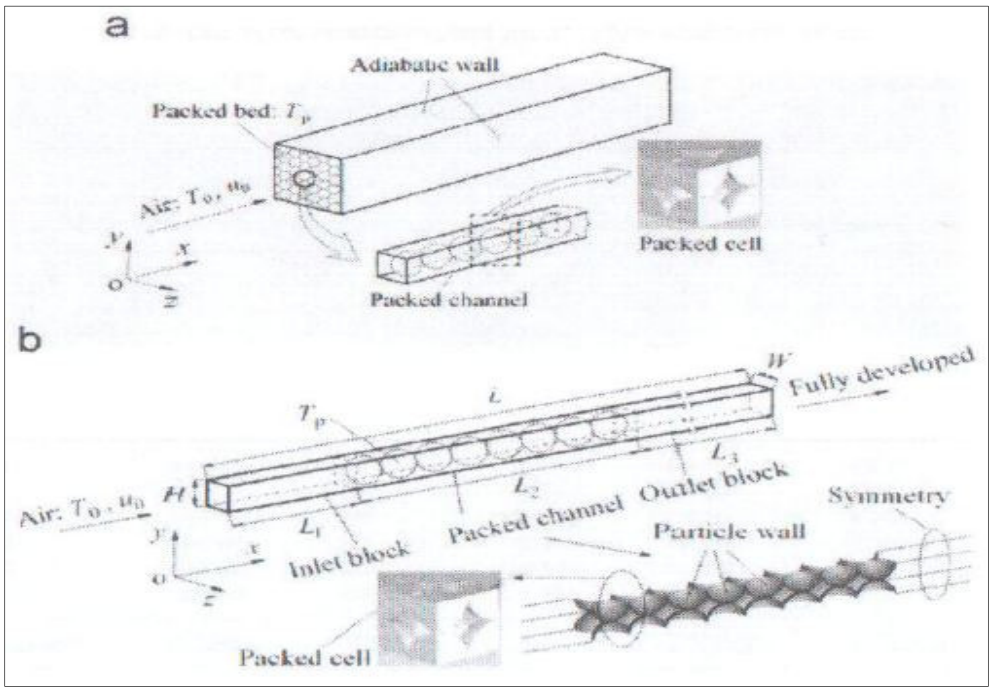

Figure 13: Physical model – (a) structured packed bed and (b) representative computational domain, Yang and Wang (2010).

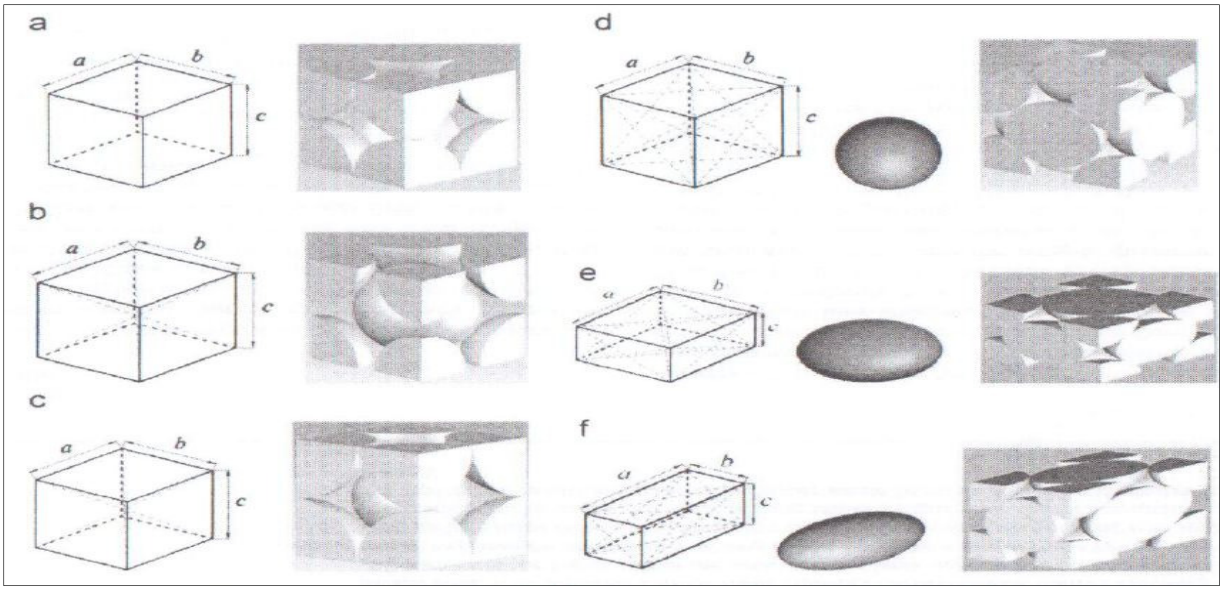

Figure 14: Different packing cells a - SC, b - Uniform BCC, c - Non-uniform BCC, d - FCC, e - FCC Flat Ellipsoid, f - FCC Long Ellipsoid. Yang and Wang (2010).

Table 3: The packings chosen by Yang and Wang for their CFD analysis. Yang and Wang (2010).

Packing Model	a (mm)	b (W) (mm)	c (H) (mm)	L1 (mm)	L2 (mm)	L3 (mm)	Porosity	D_p (mm)	D_h (mm)
SC (Sphere)	12.12	12.12	12.12	30	96.96	80	0.492	12.00	7.75
BCC Uniform Sphere)	14.00	14.00	14.00	30	123.95	80	0.340	12.00	4.12
BCC-1 (Non-uniform Sphere)	12.12	12.12	12.12	30	108.96	80	0.293	10.64	3.00
FCC (Sphere)	17.14	17.14	17.14	30	149.12	80	0.282	12.00	3.14
FCC-1Flat Ellipsoid)	21.58	21.58	10.79	30	187.73	80	0.281	12.00	2.86
FCC-2 (Long Ellipsoid)	27.21	13.61	13.61	30	236.72	80	0.282	12.00	2.92

Throughout this part of the literature survey, it was found that the pressure drop through a structured packing is always less than that for a random packing. Different structured packings also have different friction factors. This makes it difficult to define exactly what a structured packing is. Only Wentz and Thodos (1963) found that the various structured packings they experimented with resulted in the same friction factor. They made use of distended packings with very high porosities.

It was also found that the shape of a particle inside a structured packing has a significant effect on the friction factor of the packing. It would seem that when the shape of the particles is streamlined or aerodynamic in the direction of the flow, the friction factor of the packing would be lower.

It would further seem from the above-mentioned literature that there is no direct correlation that can completely characterise all kinds of spherical packings. It is however clear that there is a distinct difference between the hydrodynamic properties for structured and random packings, regardless of the structure chosen for the structured packing.

2.2.2 PACKED BEDS OF PLATES AND RINGS

In order to test the pressure drop through a geometrically ordered array, Handley and Heggs (1968) made use of packings of 3.175 mm thick aluminium plates. Six plate lengths were used at three different packings each. The plate lengths were 203.2mm, 101.6mm, 50.8mm, 25.4mm, 12.7mm and 6.35mm and the plate spacings were 1.3208mm, 2.6416mm and 5.9436mm. This gives a total of 18 stacking orientations that were tested.

According to Handley and Heggs (1968), adjacent sets of plates were oriented at 90° angles relative to each other. This would mean that the flow would take place between parallel plates within a set of plates. The flow would have to change its direction by 90° when the flow would cross over from one plate set to another. Therefore, the longer the plates, the fewer intersections there would be for a specific packing length. The shear force that the surface of the plates exert on the fluid would contribute to the viscous force term of the Ergun type equation and each 90° bends would consequently contribute to the inertial force term of the Ergun type equation.

The experimental results obtained by Handley and Heggs (1968) can be seen in Figure 15. The fact that each plate packing resulted in a linear relation clearly shows that the Ergun type correlation of the additive nature of the viscous and inertial forces in porous media is also applicable to packings of plates. These results were compared with the results obtained from the packings of spheres that they also tested. For all 18 combinations of plate spacings and lengths, the slope of the linear relation is larger for the spherical packings than in the case of the plate packings. As mentioned earlier, the y-axis intersection c and the x-axis intersection m represent the viscous and inertial forces respectively. This implies that the inertial resistance of the spherical packings is always larger than found for plate packings.

For the 12.7 mm and 6.35 mm plate lengths, the modified friction factor axis intersection, shown in Figure 15, of the linear relations is always less than that of the spherical packings. This implies that the viscous force that the plate packings exert on the flow through it is less than that of the spherical packings. The instances where the friction factor axis intersections are negative should be ignored according to Handley and Heggs (1968). They explained that this negative intersection occurs due to the fact that extremely small pressures were measured.

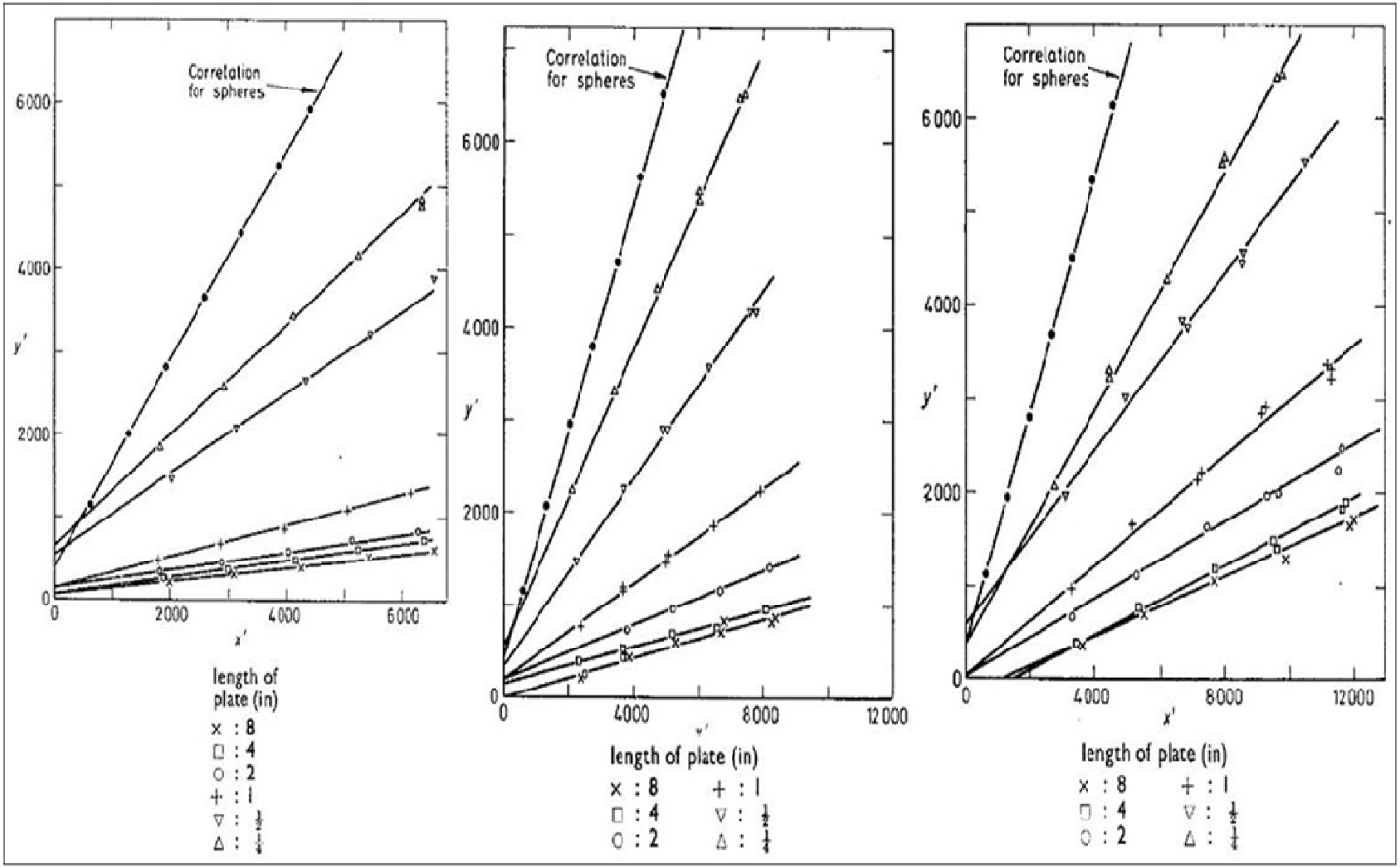

Figure 15: Results obtained from the 18 different geometrically ordered aluminum plate packings tested by Handley and Heggs (1968) with the modified friction factor (y-axis) vs. the modified Reynolds number (x-axis).

2.3 THE END EFFECTS

The end effects of a spherical packing include the effect that the inlet to the packing and the outlet from the packing have on the hydrodynamic properties of the fluid. The entrance and exit effects of the packings were tested by Susskind and Becker (1967) and they found that the entrance and exit effects were negligible for a packing with a length longer than seven ball diameters. It could be seen from the data obtained by Handley and Heggs (1968) that the bed length-to-particle diameter (L/d_p) ratio did not have a noticeable effect on the pressure drop through the packings. This was due to the fact that the bed (L/d_p) diameter ratios were between 11 to 32 which is larger than the bed (L/d_p) diameter ratio of 7 proposed by Susskind and Becker (1967).

Furthermore, Wentz and Thodos (1963) investigated the end effect during their study of the pressure drop through structured packings. The length of the packings tested by Wentz and Thodos (1963) were only five ball diameters long. It was found by Wentz and Thodos (1963) that the friction factor for a packing without end effects is 1.13 times lower than that with the end effects included. In Figure 2 and Figure 16 the experimental results of Wentz and Thodos (1963) is given with end effects included and excluded respectively.

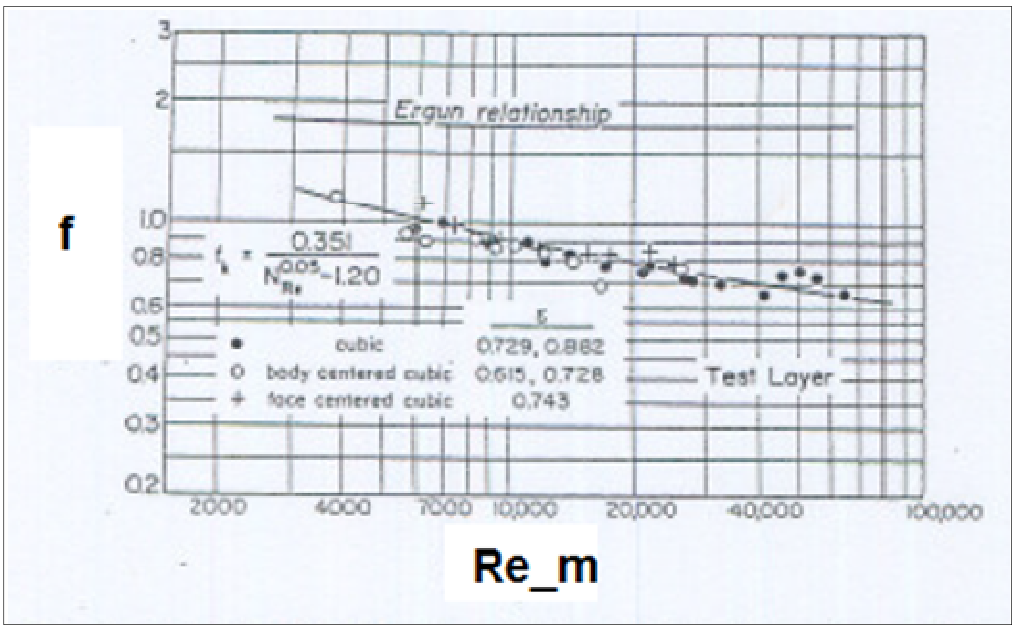

Figure 16: Friction factor vs. Modified Reynolds number for the pressure drop in the packed and distended bed of spheres Wentz and Thodos **(1963)** with no end effects.

According to the work of Achenbach (1995) the inlet effect on the flow through the packing is only evident for the first 0.75 particle diameters. Achenbach (1995) also found that the outlet effect of a packing on the flow through it is evident for the last 2.5 particle diameters of the packing. Graphs plotted by Achenbach (1995) for the porosity distribution in the axial direction as a function of particle diameter can be seen in Figure 17 and Figure 18.

In Figure 17 the porosity distribution of the packing is given for the inlet to the packing in the direction of the flow. In Figure 18 the porosity distribution of the packing is given from the end of the packing in the opposite direction of the flow. The z shown in Figure 17 and Figure 18 indicates the vertical direction, or the direction in which the working fluid is flowing through the packing.

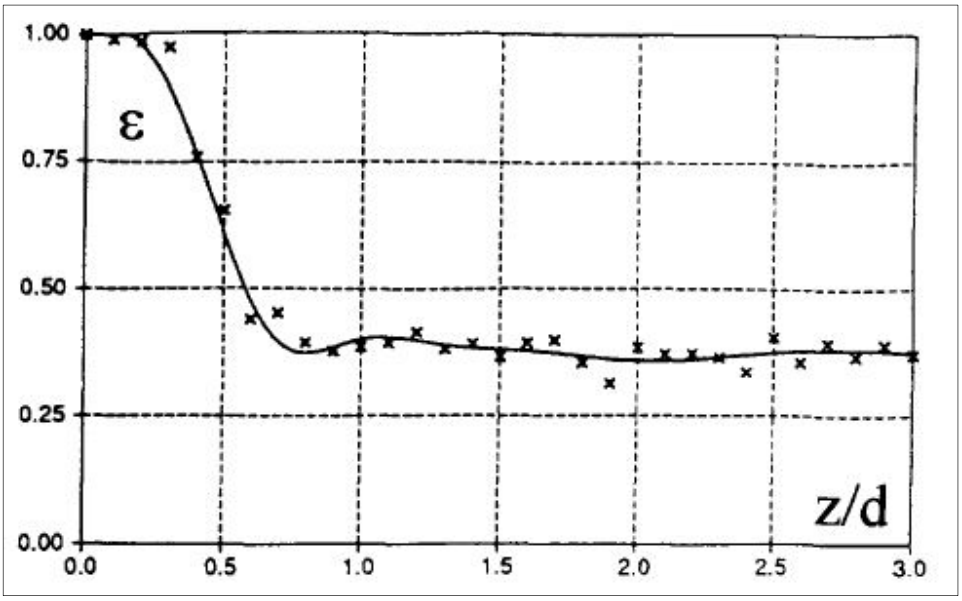

Figure 17: Porosity distribution from the inlet of a packing. Achenbach (1995).

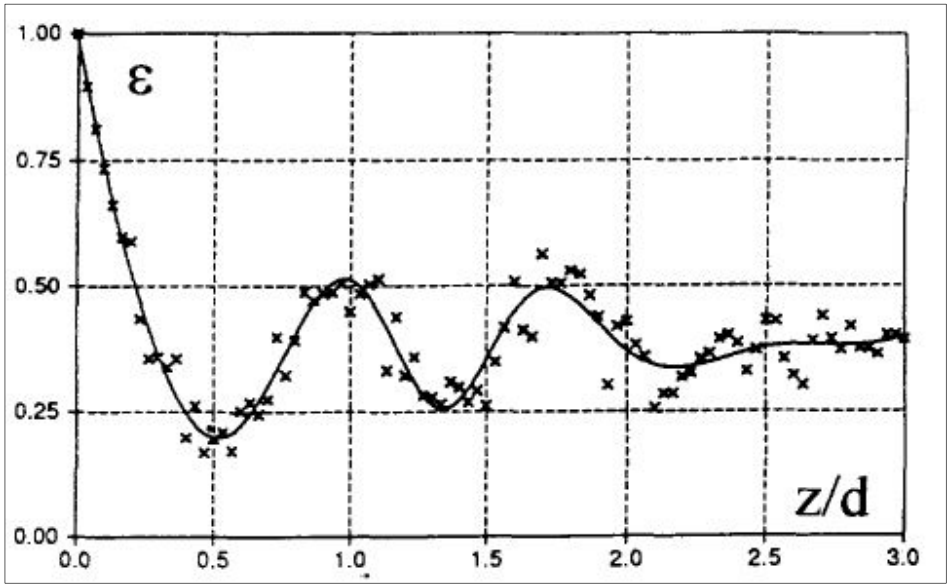

Figure 18: Porosity distribution from the bottom of a packing. Achenbach (1995).

2.4 THE WALL EFFECTS

The effect of confining walls on the structure in the wall region is significant for any packing type. The confining wall causes higher porosity of the packing in close proximity to the wall. An increased porosity near the wall has a bypass effect on the flow passing through the packing. When an average porosity for a packing is assumed and the bypass effect is significant in the wall region, it could lead to a large error in determining the hydrodynamic properties of a packing.

The effect of the confining wall is directly related to the bed-to-particle diameter ratio (D/d_p). The region in which D/d_p has an influence has been widely studied. According to Cohen and Metzner (1981) the effect of the confining wall is negligible for D/d_p larger than 30:1 and 50:1 for Newtonian and non-Newtonian fluids respectively.

According to Metha and Hawley (1969), when D/d_p is less than 50:1, its effect on the hydraulic diameter of the packing should not be neglected. Metha and Hawley (1969) proposed a modification to the hydraulic radius of the packing to compensate for the effect of wall on the hydrodynamic properties of the packing. The hydraulic diameter for a packed bed of spheres, according to Metha and Hawley (1969), can be seen in Eq (5). Metha and Hawley (1969),

however failed to explain what exactly the effects of the confining walls are on a packing. The V_v, V_b, WS_s and WS_w in Eq (5) are the void volume, packed bed volume, wetted surface of the spheres and the wetted surface of the walls respectively.

$$R_h = \frac{\frac{V_v}{V_b}}{\frac{WS_S}{V_b Volume\ of\ Bed} + \frac{WS_W}{V_b}} \tag{5}$$

It was found by Handley and Heggs (1968) that a D/d_p between 8:1 and 22:1, its effect on the pressure drop was not significant. Atmakidis and Kenig (2009) are of the opinion that for D/d_p up to 7:1, its influence on the pressure drop through a packed bed of spheres is significant.

The confining walls also have an effect on the radial porosity distribution of a packed bed of spheres. The confining walls cause the porosity to vary in a cosinusoidal fashion with a damped oscillatory pattern for random packings.

Achenbach (1995) agreed that the confining wall causes a cosinusoidal porosity variation in the near wall region and that the effect of the wall vanishes at about 6 particle diameters from the wall. He also proposed that the packed bed be divided into two regions, the near wall region and the bulk region. Equations for the calculations of the porosities in the bulk, near wall and central regions are provided in Eq (6) to (8).

$$\varepsilon = 0.78\left({}^{d_p}/_{D}\right)^2 + 0.375 \tag{6}$$

$$\varepsilon_w = 63.6\left(\frac{D}{d_p} + 15\right)^{-2} + 0.43 \tag{7}$$

$$\varepsilon_c = \varepsilon_w - \frac{\varepsilon_w - \varepsilon}{\left(1 - {}^{d_p}/_{D}\right)^2} \tag{8}$$

Cohen and Metzner (1981) also confirmed the cosinusoidal variation of the porosity in the radial direction through a packed bed due to the effect of confining walls. Cohen and Metzner (1981) proposed a tri-regional approach in solving for the porosity distribution. The tri-regional model consists of the near wall region, the transition region and the bulk region. The near wall region is located within the first 0.25 particle diameters from the wall. The transition region is from 0.25

particle diameters up to 8 particle diameters from the wall, whereas the bulk region is in excess of 8 particle diameters. The equations for calculating the porosity in the near wall and transition regions can be seen in Eq (9) and (10). The radial porosity distribution as determined by Cohen and Metzner (1981) can be seen in Figure 19.

$$\frac{1-\varepsilon_w}{1-\varepsilon} = 4.5\left(x - \frac{7}{9}x^2\right) \quad (9)$$

$$\frac{\varepsilon_t-\varepsilon}{1-\varepsilon} = 0.3463e^{-0.4273x}\cos(2.4509x - 2.2011)\pi \quad (10)$$

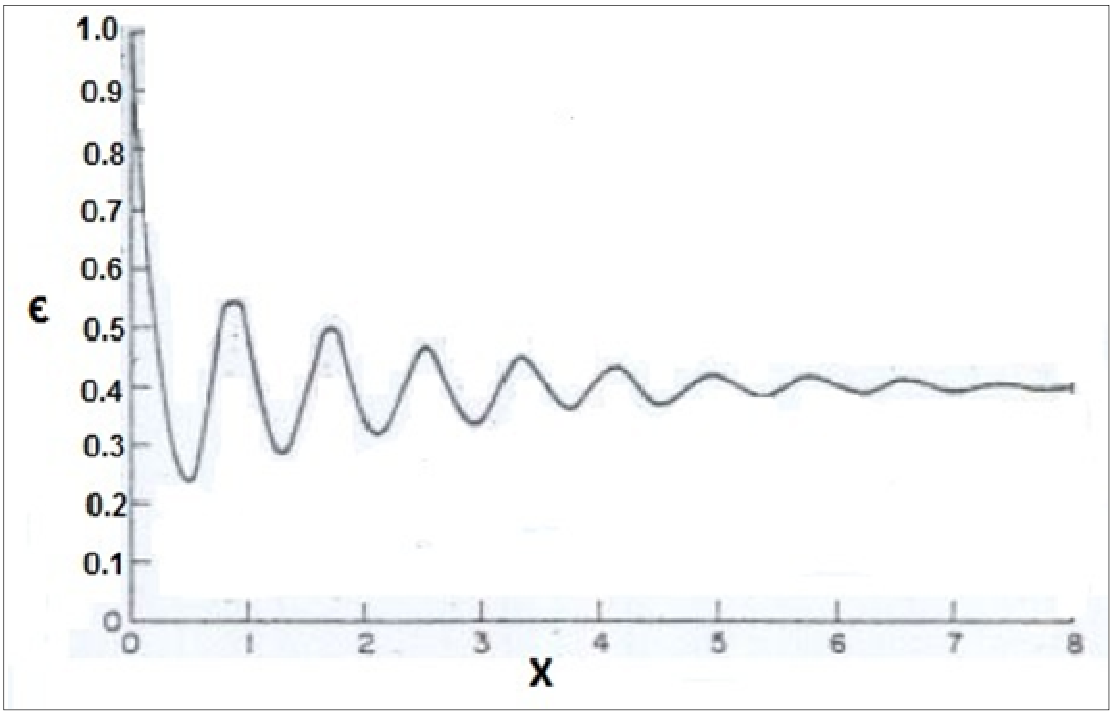

Figure 19: Radial distribution of the porosity in a packed bed of spheres. Cohan and Metzner (1981).

The contribution of each of the tri-regional areas to the total flow area of the packing as D/d_p increases can be seen in Figure 20. It is illustrated in Figure 20 how the different regions interact with varying D/d_p. The smaller D/d_p becomes, the larger the influence of the confining

walls will be on the hydrodynamic properties of the packing. Up to D/d_p equal to approximately 15, the transient and wall region comprises the entire area of the packed bed. It is only beyond this point that the bulk region starts to contribute to the total area of the packing. As D/d_p approaches infinity, the effects of the wall approaches zero.

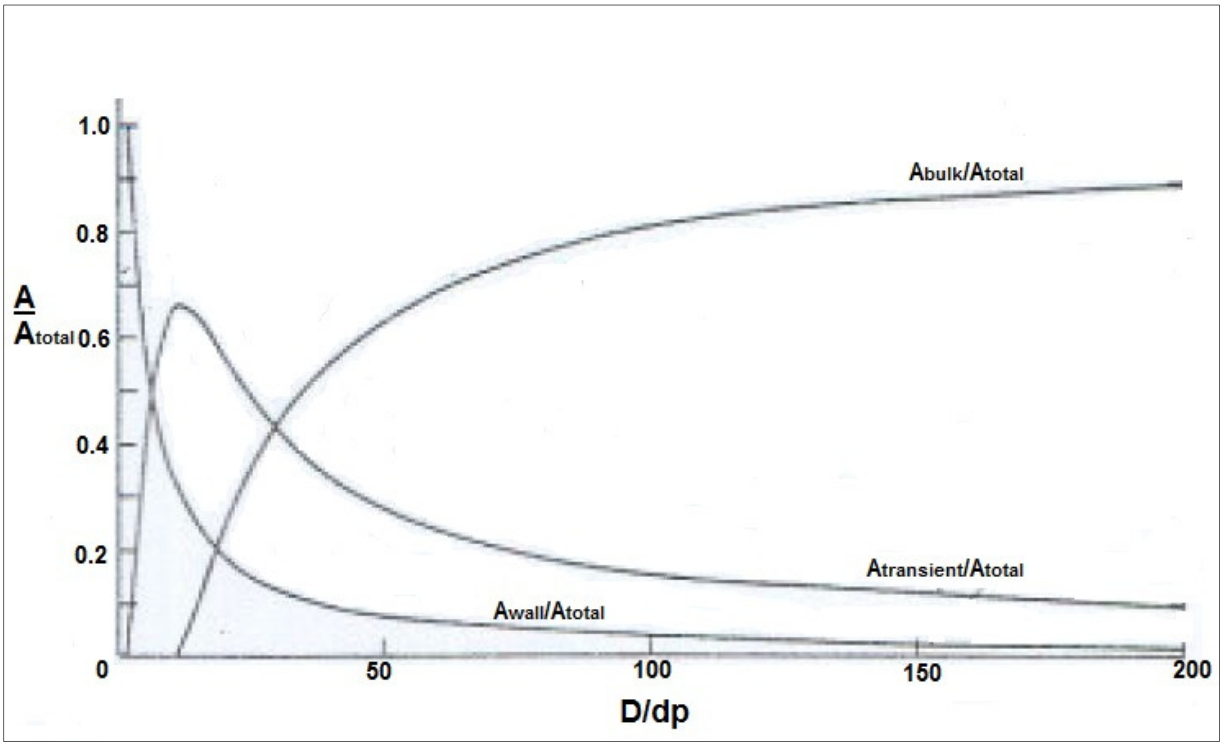

Figure 20: Contribution of each of the three regions to the fraction of area as the packing diameter increases. Cohan and Metzner (1981).

As mentioned earlier, Atmakidis and Kenig (2009) used CFD codes to construct random and structured packings. They compared their radial porosity distribution with the values predicted by the correlation of De Klerk (2003) in order to validate the method for constructing these models. The correlation for the distribution of the porosity in the radial direction of a random packing of spheres by De Klerk (2003) is shown in Eq (11) and (12), where ε is the porosity and x is the radial distance from the outside of the packing. It was determined that the radial porosity distribution of the random packing correlated well with the correlation derived by De Klerk (2003). The results of the comparison can be seen in Figure 21.

The radial porosity distribution of the structured (regular) packing did not correlate well with the values predicted by the findings of De Klerk (2003). The structured packing seems to approach a porosity of unity near the wall. The porosity then decreases drastically within the first particle diameter from the wall and beyond 1 particle diameters from the wall the porosity seems to stabilise. It does not follow the same cosinusoidal variation as that of the random (irregular) packing. In a structured packing there is no transition phase from a near wall area to the bulk of the packing. The packing is immediately structured all the way through the packing.

$$\varepsilon(x) = 2.14x^2 - 2.53x + 1; [x \leq 0.637] \quad (11)$$

$$\varepsilon(x) = \varepsilon_{inf} + 0.29e^{(-0.6x)}\left[\cos\left(2.3\pi(x - 0.16)\right)\right] + 0.15e^{(-0.9x)}; [x > 0.637] \quad (12)$$

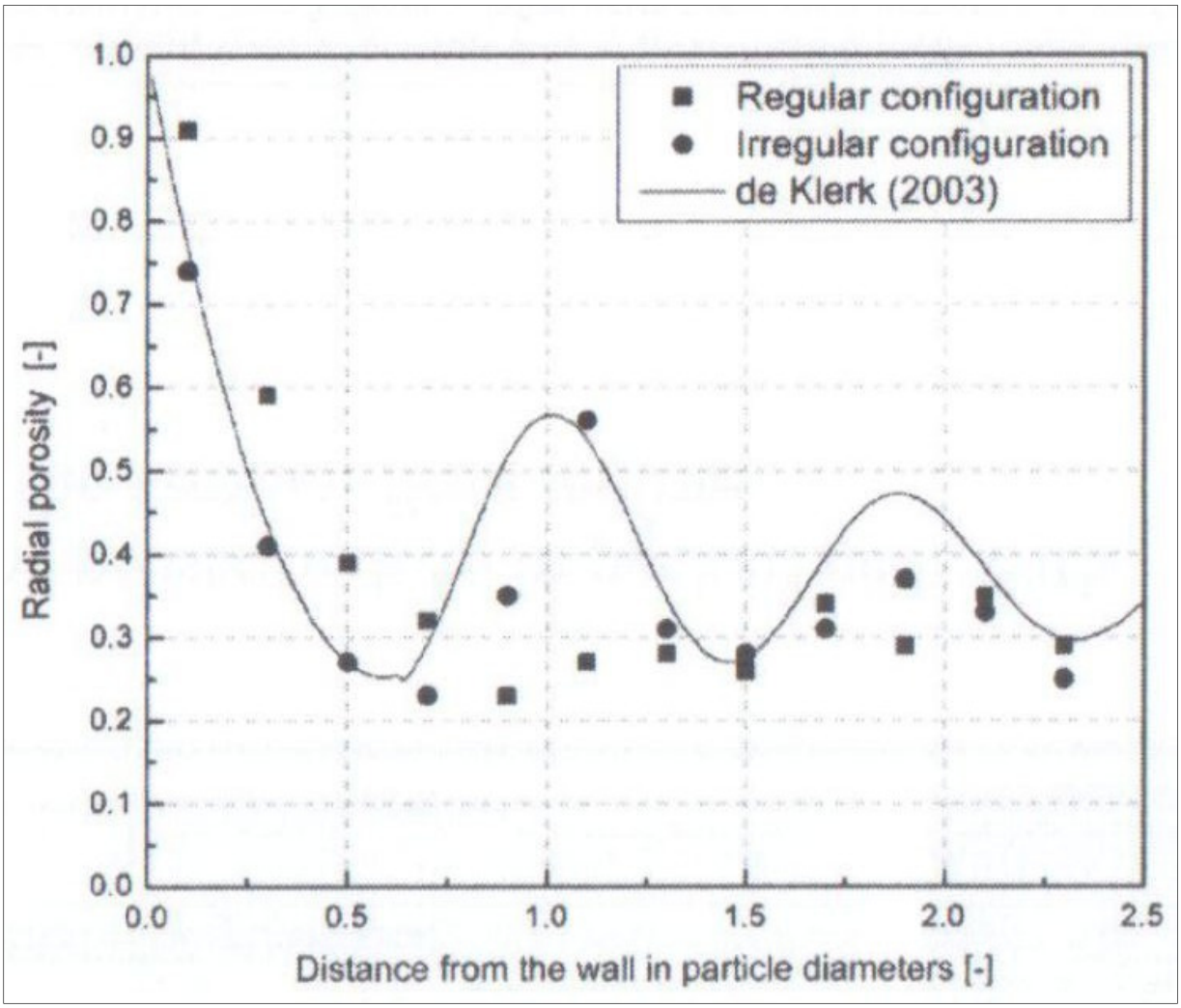

Figure 21: Radial porosity distribution as determined by Atmakidis and Kenig (2009).

2.5 THE POROSITY OF A PACKING

Porosity (ε) is defined as the ratio of the volume of the voids relative to the total volume of a packing. The total volume of a packing is the sum of the void volume and the solid particle volume of the packing. The porosity of a packing is one of the parameters that has a substantial

effect on the pressure drop through the packing. As the porosity of the packing increases, the pressure drop through the packing will decrease. This is due to the fact that an increase in the overall void volume inside a packing causes the fluid in the voids to flow more freely.

From the experimental data that Wentz and Thodos (1963) obtained, amongst others, the overall pressure drop against the superficial kinetic energy of the air flowing through the packings of spheres. They found that the relation was linear with a slope of 0.9 for each packing. They also found that the linear lines are separated from each other due to their different porosities. A closer packing would give a higher pressure drop than that of a more dispersed packing.

From the study by Yang and Wang (2010) mentioned earlier, the pressure drop was plotted against the Reynolds number for each of the pressure drop experiments performed. They also found that within packings with higher porosities, the pressure drop was lower than the pressure drop for the packings with lower porosities. Ergun (1952) presented a plot of the pressure drop through a packing against the mass flow rate through the packing. It was also found by Ergun (1952) that, as the porosity of the packing increased, the pressure drop through the packing would decrease.

The effect that a change in porosity has on the pressure drop through a packed bed of spheres was investigated by Achenbach (1995) and Barthels (1972). It can be seen in Figure 22 that, at low porosities, the pressure drop is not very sensitive to a change in the porosity of the packing. At higher porosities the pressure drop becomes increasingly sensitive to a change in porosity. According to Achenbach (1995), at a porosity of 0.4, a 1% change in the porosity would lead to a corresponding 4% change in the pressure drop. This sensitivity of the pressure to a change in the porosity of a packing illustrates the importance of accurately determining the porosity of a packing when conducting pressure drop experiments. In Figure 22 the dimensionless parameter, n, indicates in what range the Reynolds number is. A n=1 represents a laminar flow range whilst n=0.1 represents a turbulent flow range.

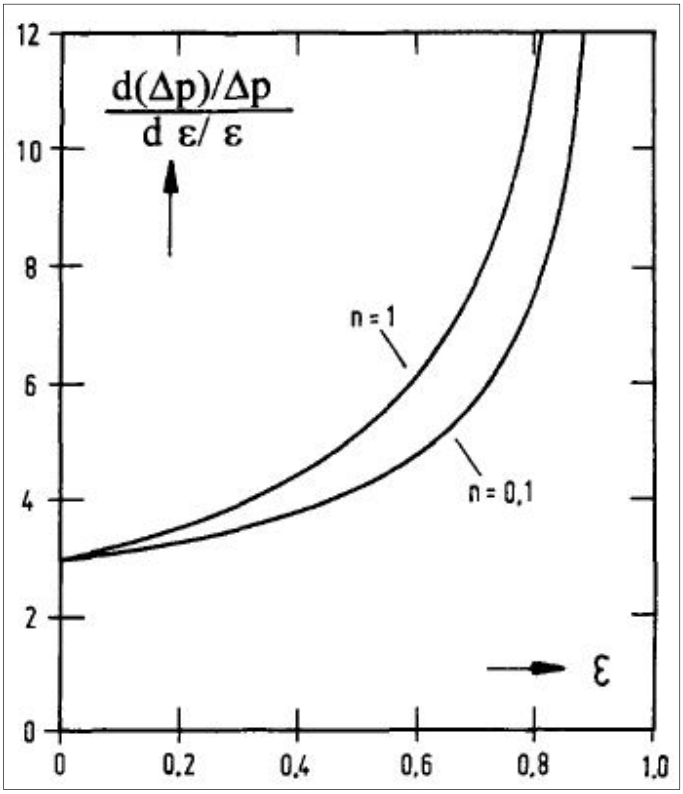

Figure 22: Sensitivity of the pressure drop through a packed bed of spheres to a change in the porosity. Achenbach (1995).

Determining what the porosity of a packing is might not always be possible. An opportunity consequently presented itself to formulate a correlation that could be used to accurately predict the porosity of a packed bed of spheres. It was found that the best parameter to relate the average porosity to is the bed-to-particle diameter ratio (D/d_p).

In the literature relations can be found for calculating the average porosity of a random packing when the bed-to-particle diameter ratio is the only known parameter of the packing. Achenbach (1995), Sato and Hirose (1973), Jeschar (1965) and De Klerk (2003) derived equations for calculating the porosity of a packing. The relation of Achenbach (1995) is shown in Eq (6). The equations of Sato and Hirose (1973), Jeschar (1965) and De Klerk (2003) can be seen in Eq (13) to (15) respectively. The relation of Jeschar (1965) was developed for low porosity random

packings, whereas the relation of De Klerk (2003) was developed for higher porosity random packings.

$$\varepsilon = 0.3517 + 0.4657\frac{d_p}{D}; \frac{d_p}{D} < 0.4 \quad (13)$$

$$\varepsilon = 0.375 + \frac{0.34}{\left(\frac{D}{d_p}\right)} \quad (14)$$

$$\varepsilon = 0.41 + 0.35e^{\left(-0.39\left(\frac{d}{d_p}\right)\right)} \quad (15)$$

Atmakidis and Kenig (2009) compared the average porosities of the four random and four structured packings which they developed through CFD code and ballistic deposition models, with the relations of Jeschar (1965) and De Klerk (2003). It was found that the average porosities of the random packings were higher than the values calculated by the relations of Jeschar (1965) and De Klerk (2003). The average porosities of the four random packings were closest to the relation of De Klerk (2003). According to Atmakidis and Kenig (2009), this difference in average porosity can be attributed to the 2% they shrunk the particles to ensure a high quality mesh for their CFD simulation. The average porosity of the structured packing was also in good correlation to the relation proposed by De Klerk (2003).

2.6 CONCLUSION

The preceding literature survey investigated how the structure of a packed bed of spheres influences its hydrodynamic properties. A number of different studies clearly demonstrated that when the structure of two packings is the only parameter that represents the difference between them, the pressure drop through the two packings will differ. It was also found that the pressure drop is lower in structured packing when compared to a randomly packed bed. Packings of plates and rings were also investigated in brief.

Other physical effects that could influence the hydrodynamic properties of a packed bed were also investigated. These effects include the end effects, the wall effects and the effect of porosity on the pressure drop through a packed bed of spheres.

The end effects influence the way in which the working fluid reacts to the first and last few particles of the packed bed of spheres. It was found that the inlet effect is much small that the outlet effect.

During the literature survey it was shown what effect confining walls have on a packing structure. Three distinct regions were evident due to the effect of the confining walls namely the wall region, transition region and the bulk region. The smaller the bed-to-particle diameter ration is, the larger the bulk regions contribution becomes relative to the total flow region of the packed bed.

The porosity of a packing was also identified to have an influence on the pressure drop through a packed bed of spheres. As the porosity of the packing increases, the pressure drop though the packing will decrease. The sensitivity of the pressure drop through a packed bed in the laminar and turbulent flow range to a change in the porosity of a packing was also investigated.

The next chapter will provide an overview of how the uncertainty assessment will be conducted and present the equations that will be utilised to calculate the estimated error of an experiment.

CHAPTER 3 : UNCERTAINTY ASSESSMENT

3.1 INTRODUCTION

In science, not knowing the absolute exact result of an experiment is known as uncertainty. This means that there is always a level of uncertainty associated with an experimental result. This uncertainty is the range around the exact result within which the measured or observed result of the experiment may lie, providing you have the true value.

Obtaining the exact results of any experiment in science is impossible. If the errors that occur during an experiment cannot be sufficiently reduced or accounted for, the outcome of the experiment may be rendered useless. Therefore, it is important to minimize and quantify the errors that are being made. Because experimental errors are inherently part of the experiment (Stern and Muste (1999)), it is important to estimate, as accurately as possible, the potential error that is being made. An assessment of the uncertainty of the experimental data is done to accurately estimate the errors made during the course of an experiment.

Over the past 60 years many methodologies have been developed to report on the assessment of experimental uncertainty. In this document the methodology of Stern & Muste (1999) will be followed which is based on the methodology developed by the American institute for aeronautics and astronautics, AIAA (1995), and by Coleman & Steele (1999).

When an experiment is conducted, there are two kinds of errors that can compromise the integrity of the data obtained from an experiment. All the errors are then combined to form the total uncertainty, U, of a measurement. The two errors are the following:

- Precision Error; and
- Bias Error.

3.2 EXPERIMENTAL ERROS

3.2.1 PRECISION LIMIT

A precision error is defined by Stern & Muste (1999) as any error that has to do with the scatter of the data obtained from an experiment. In other words it is a measure of the variation of the data around the mean value. This contributes to the repeatability of the measurement

according to Wikipedia (2011). The repeatability of an experiment is also affected by, amongst others, the possible drift in the instrumentation and other factors which could be associated with the bias error. When the precision error is small, the experimental data deliver consistent results if the measurement is repeated a number of times.

The standard deviation (S) and the coverage factor (k) of the data set is needed to quantify the precision error (P). The sample standard deviation is defined as the typical quantity by which the sample observation deviates from the mean according to Devore & Nicholas (2005). To calculate the standard deviation of a set of data points (sample) measured under a fixed test condition, the following formula is used:

$$S = \sqrt{\frac{1}{M-1}\sum_{i=1}^{M}(X_i - \bar{X})^2} \tag{16}$$

M is the number of measured points in the sample, X_i is one of the measured points and $\bar{X}$ is the mean value of the sample. A coverage factor $t = 2$ or $t = 3$ is used, for a normal distribution, if a respective confidence level of 95% and 99% is desired. This would mean that the precision limit for a single test is given as:

$$P_i = tS \tag{17}$$

The precision limit for a result, P_r, is then given as the Root Sum Square (RSS) of the product of the precision limits and the sensitivity coefficients of the respective variables in the Data reduction equation (DRE) as shown in Eq (19). The sensitivity coefficient is defined as the partial derivative of the DRE to the specific variable in Eq (18).

$$\theta_i = \frac{\partial r}{\partial X_i} \tag{18}$$

$$P_r^2 = \sum_{i=1}^{j} \theta_i^2 P_i^2 \tag{19}$$

3.2.2 BIAS LIMIT

The bias limit gives an indication of how accurately the measurement system of an experiment can measure, according to Wikipedia (2011). The following factors contribute significantly to the bias limit (Longo & Stern, 2005):

- The calibration errors that occur;
- The accuracy of the data acquisition system;
- The error in data reduction; and
- The conceptual errors.

The bias limits presented in Eq (22) can consist of multiple errors as a result of the factors mentioned above. These errors are then combined using the RSS method. This is illustrated in Eq (20). To convert a bias error to a bias limit with a 95% confidence level it must be multiplied by a coverage factor of 2. An uncertainty can only be obtained when an error distribution has been assumed. To assume an error distribution, the error must be multiplied by a coverage factor. The value of the coverage factor is dependent on the type of error distribution that was assumed for the uncertainty.

Note that in many instances it is first required to convert the bias error for a given instrument to a standard deviation. This is done by dividing it by $\sqrt{3}$ if limits of $\pm\alpha$ are specified without a confidence level and there is reason to expect that extreme values are likely (It is normally appropriate to assume a rectangular distribution, with a standard deviation of $\alpha/\sqrt{3}$ according to Du Toit (2011)). The bias error can also be divided by $\sqrt{6}$ if limits of $\pm\alpha$ are given without a confidence level, but there is reason to expect that extreme values are unlikely. (It is normally appropriate to assume a triangular distribution, with a standard deviation of $\alpha/\sqrt{6}$ according to Du Toit (2011)). This is illustrated in Eq (21) where t is the coverage factor and b_i is the bias error.

$$B_i^2 = \sum_{k=1}^{j} (B_i)_k^2 \tag{20}$$

$$B_i = t b_i \tag{21}$$

According to Stern & Muste (1999) the bias limit can be estimated using the following equation.

$$B_r^2 = \sum_{i=1}^{j} \theta_i^2 B_i^2 + 2 \sum_{i=1}^{j-1} \sum_{k=i+1}^{j} \theta_i \theta_k B_{ik} \tag{22}$$

Where θ_i and θ_k are the sensitivity coefficients (to be discussed later) and B_i is the total bias limit for a single measurement and B_{ik} is the bias limit in two measurement points related to each other. The first term in Eq (22) contains the sensitivity coefficient and the bias limit of a

single measurement point. The second term in Eq (22) is a cross correlation between two measured points. It contains the sensitivity coefficients and bias limit for measurement points related to each other.

3.2.3 TOTAL UNCERTAINTY

The total uncertainty of a measured point is given as the RSS of the errors discussed above. In Eq (23) U_r represents the total uncertainty, P_r is the precision limit and B_r is the bias limit of a single measured point (Stern & Muste, 1999).

$$U_r^2 = P_r^2 + B_r^2 \tag{23}$$

3.3 ERROR PROPAGATION

In Figure 23 the propagation of an error into the experimental results in demonstrated Stern & Muste (1999). The above-mentioned errors are made for each variable being measured. These errors find their way from the point of origin right into the experimental result. It passes through the individual measurement systems and the data acquisition system into the DRE where it is directly linked to the experimental result.

The impact of an error in a measured variable on the experimental result is a function of the sensitivity of the experimental result to a change in the variable.

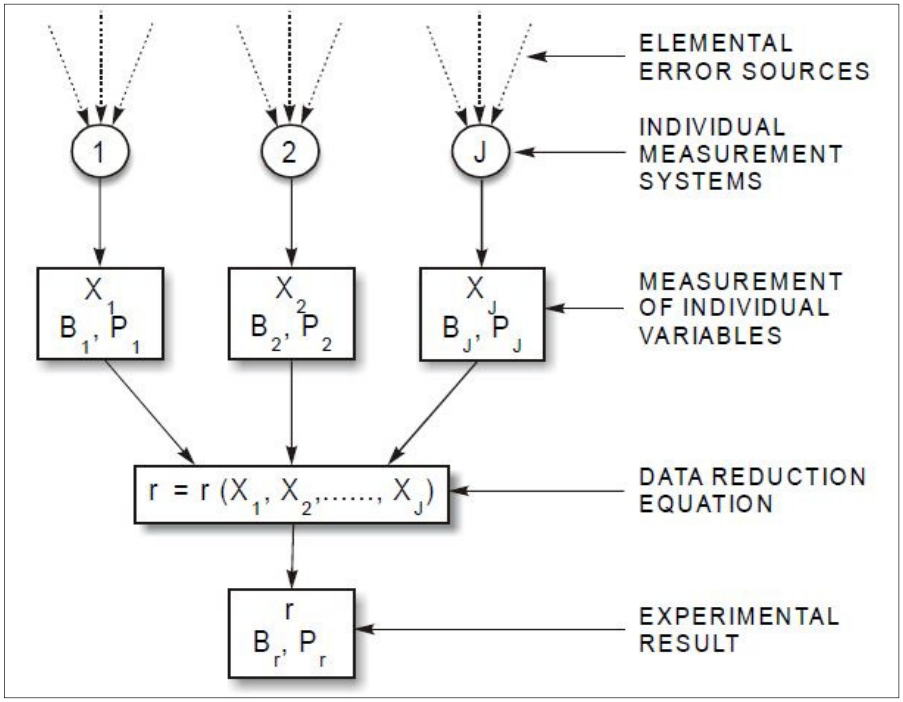

Figure 23: Propagation of errors into experimental results. Stern and Muste (1999).

The sensitivity coefficient θ_i is defined as the partial derivative (The gradient of the DRE with respect to a certain variable.) of the DRE with respect to one of the variables in the DRE. A sensitivity coefficient is derived for each of the variables that make out the DRE. An illustration of the sensitivity coefficient is shown in Figure 24 as represented by Stern & Muste (1999). The effect of the sensitivity equation on the uncertainty of the result is dependent on the rate of change of gradient of the DRE to a specific variable.

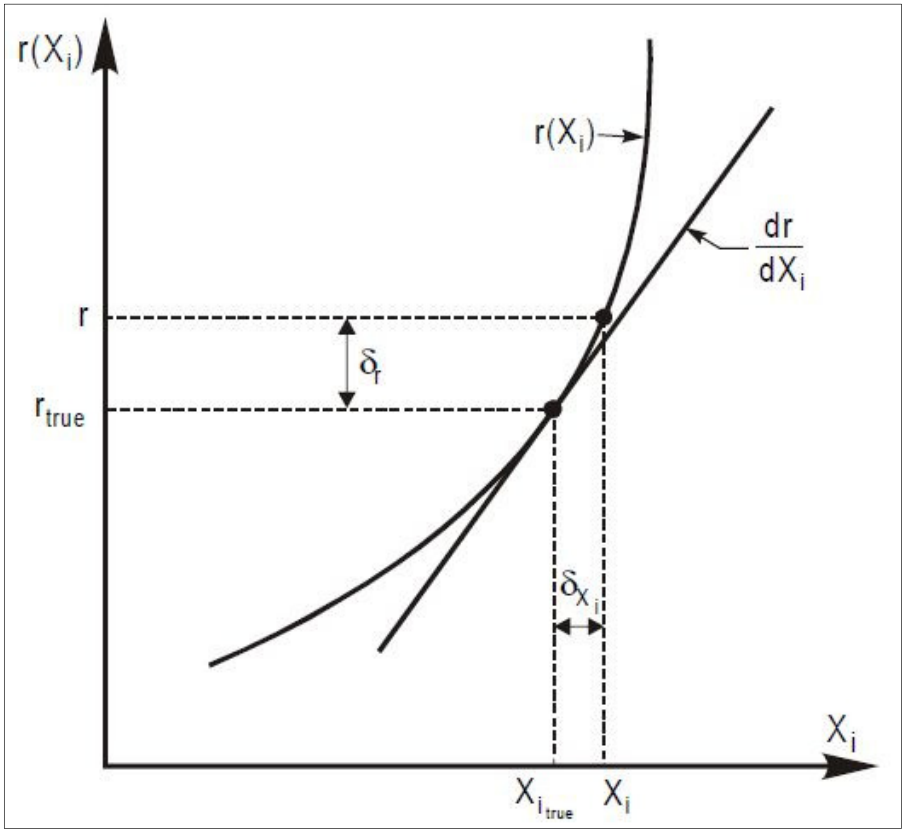

Figure 24: Schematic of error propagation from a measured variable into the result. Stern and Muste (1999).

3.4 ASSUMPTION

The following assumptions were made for the uncertainty assessment of the experiment in this study.

- The estimation of uncertainties would be made at a 95% confidence level;
- The cross correlation terms in the precision and bias limits were negligible; and
- Except for the Precision and Bias errors, no other errors would be taken into account when estimating the uncertainty.

3.5 CONCLUSION

This chapter discussed the aspects and generic methodology of conducting an uncertainty assessment. Different kinds of errors were discussed and how they propagate into the final results. The following chapter will describe the design of the test facility utilised to conduct the pressure drop measurements. The user requirement specification will firstly be provided and then the conceptual and detail designs of the test facility will follow. Each of the separate sections that make out the test facility will be discussed on their own.

CHAPTER 4 : SYSTEM DESIGN

When designing a test facility it is extremely important that each of the components of the facility performs its operation within a pre-defined specification. It is also important that all the components that form a test facility be integrated to perform the primary and secondary tasks set out by the pre-defined specification for what the test facility needs to do.

During the design of the test facility under consideration there were systems from multiple engineering disciplines that needed to be designed and integrated. The physical size, the mechanical system contributed to the largest portion of the test facility. The mechanical system also took the most time to manufacture. The rest of the test facility consisted of electrical and electronic systems.

4.1 USER REQUIREMENT SPECIFICATION (URS)

The pre-defined specification mentioned earlier must first be set up before the rest of the design of the system can commence. The pre-defined specification comes in the form of a URS. The URS provides the constraints within which the design must be done. The URS was constructed during consultations with the promoters. In Table 4 all the specifications of the URS are set out.

Table 4: User Requirement Specification.

No.	Specification	Description
URS-1	$Re_m \geq 50{,}000$	Highly turbulent flow conditions must be possible.
URS-2	Eliminate Wall Effects on the Packed Bed	Packing must be formed to the shape of its container without changing the structure or porosity of the packing.
URS-3	$\frac{D}{d_p} \geq 4.5$	Bed-to-particle diameter ratio must be larger than 4.5 to get a good representation of the core of a packing.
URS-4	$\frac{L}{d_p} \geq 20$	Bed length-to-particle diameter ratio must be larger than 20 to eliminate end effects.
URS-5	Packed bed must be visible to the operator	Make use of a transparent container to house the packed bed. This should be done for educational and experimental purposes

URS-6	Total experimental uncertainty of less than 10% must be achieved	High accuracy experimental data is critical when conducting an experiment. Make use of measurement instrumentation of the highest accuracy. Apply the instrumentation in the correct way.
URS-7	Operation of system must be easy and safe	• Don't use toxic working fluid; • Don't pressurise the system above 600kPa; • Don't leave any moving parts exposed to the environment; • Make all the system controls easily accessible; and • Earth the electrical component to avoid electrical shock.
URS-8	Make use of readily available components	Make use of commercial off the shelf components as far as possible.
URS-9	Design system to be compact	Testing facility must be able to easily fit into any laboratory and the system must also be semi-portable.
URS-10	System must be bled for air	Add bleed valves to the highest points to be able to bleed the system for air. Also add bleed valves wherever else necessary.
URS-11	System must be able to drain easily	Add drain valves to the system at the lowest points. Also add drain valves to any other position where the working fluid might be trapped.
URS-12	Design cost	Keep design cost to a minimum without compromising the quality of the design.
URS-13	Use Labview as the operational software	Graphs of each measurement instrument must be shown. A general layout of the testing facility must also be shown.
URS-14	System water pressure	The maximum pressure of the water in the piping system should not exceed 600kPa.
URS-15	Flow through test section	Fine control of the flow through the test section should be made possible.

4.2 CONCEPTUAL DESIGN

From the boundaries set out by the URS the conceptual design of the test facility could be done. The next step was to develop the PFD and the P&ID for the test facility. The names and descriptions of all the components shown in the PFD and the P&ID are given in Table 5 below.

Table 5: Description of the notations on the PFD and the P&ID.

No.	Name	Description
1	Test section	This is where the packed bed of spheres is located.
2	Control valves	The control valves on the test section loop.
3	Control valve	The control valve on the bypass loop.
4	Pump	The pump for delivering the flow and pressure to the system.
5	Inlet	Inlet where the working fluid is added.
6	Bleed valve	These bleed valves are used to bleed air from the system and drain the system. (URS-10) (URS-11).
7	Flow meter	This is for measuring the mass flow that passes through the packed bed.
8	Temperature meter	To measure the temperature of the water entering the packed bed.
9	Isolation valves	These valves are used to isolate the test section from the rest of the system.
10	Differential pressure transmitter	This meter measures the pressure drop through the packed bed.
11	Data acquisition (DAQ) system	The DAQ receives all the signals provided by the instrumentation and convert it to an analogue signal for the Personal Computer (PC).
12	Electricity supply and distribution system	The electricity supply system supplies the necessary electricity to all the components that need it.

4.2.1 PROCESS FLOW DIAGRAM (PFD)

The PFD is a line diagram illustrating the basic layout of the test facility and how it works. The PFD of the test facility is shown in Figure 25 below. From the PFD it can be seen that the

working fluid is added to the system at the inlet to the system (5). The inlet to the system must always be open to the atmosphere to ensure that the system is never excessively pressurised. The bleed valves (6) allows for the air in the system to be replaced by the working fluid. A pump (4) is used to circulate the working fluid through the system.

The system consists of two primary loops, namely the test section loop and the bypass loop. The flow through each of the loops is controlled by a control valve, (2) and (3). These valves enable the operator of the system to either fully constrict the flow through the test section or to allow all the flow through the test section. The operator can also vary the flow through the test section to achieve any flow desired.

The bypass-loop was added to the design of the system to make the operation of the system more stable. By making use of the bypass loop, the pump can potentially be operated in its most optimal range whilst the flow through the test section loop is varied to achieve different flow rates and pressured drops through the packed beds.

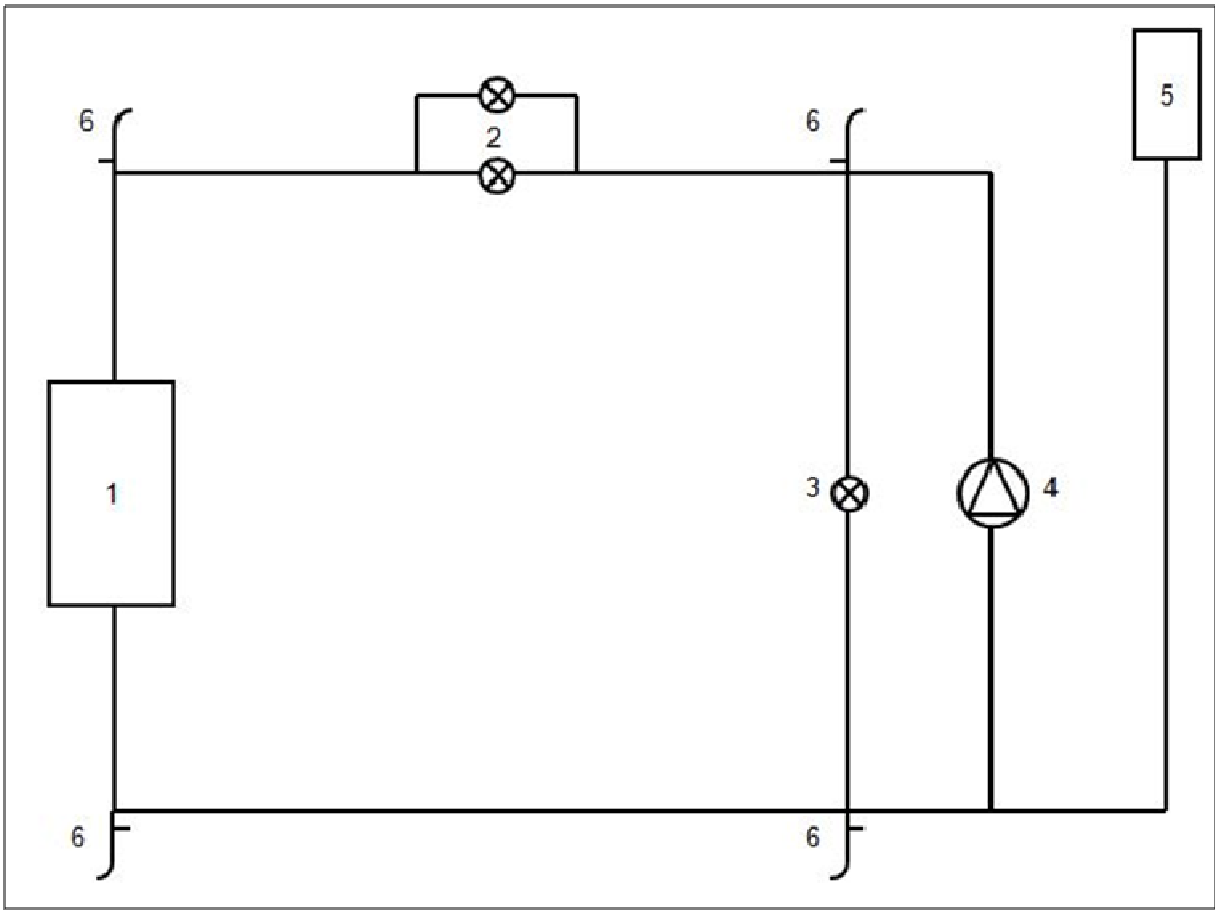

Figure 25: Process Flow Diagram (PFD) of the testing facility.

4.2.2 PROCESS AND INSTRUMENTATION DIAGRAM (P&ID)

The P&ID for the test facility is divided into three systems. The largest of the systems, the main system, is described in the PFD. This includes the primary structure, piping, the test section, as well as the associated measurement instrumentation.

The remaining two systems consist of the data acquisition system (11) and lastly the electrical supply and distribution system (12).

As mentioned above, the Main System of the test facility includes the primary structure. The primary structure has to be sufficiently durable to support the entire piping system, the various measurement instrumentation, the test section, the DAQ system, as well as the electricity

supply and distribution system. In order to support this combined weight, the primary structure had to be constructed from steel square tubing. Wheels, with lockable brakes, were added to the bottom section of the primary structure for portability.

The measurement instrumentation required for the experiment included a flow meter, a temperature meter and differential pressure transmitters. The components mentioned above were used in addition to the components that were described in the PFD.

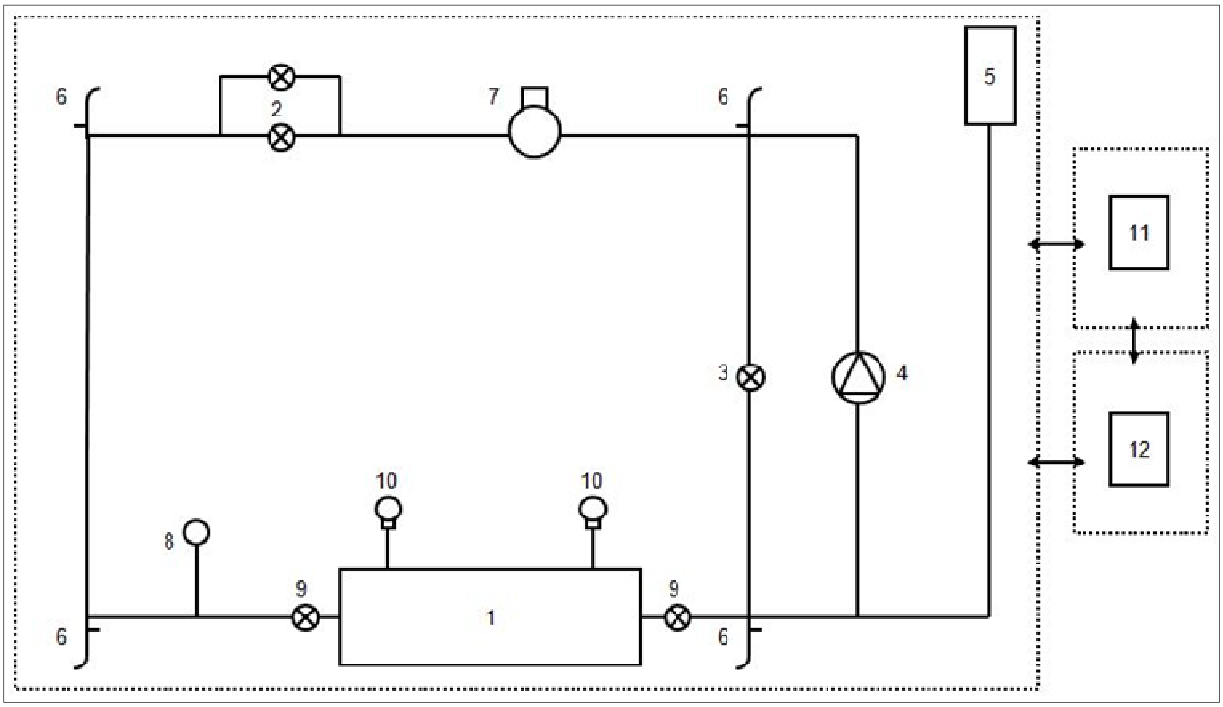

Figure 26: P&ID of the test facility.

The DAQ system receives the signals from the measurement instrumentation and converts the signals to analogue signals. It then supplies these signals to a central computer where the data is logged and converted into graphs for interpretation. The DAQ System consists of DAQ modules which are used to receive the signals from the various measurement instrumentation. The DAQ modules are also responsible for the conversion of the signals from an analogue to a digital format. The central computer makes use of the Labview software platform to interpret

and log the data received from the measurement instrumentation. Labview also supplies the operator with real-time graphs of the operation of the system.

The electricity supply and distribution system distribute electricity to all the components within the test facility and its various sub-components. The electricity is supplied to the test facility via a 3-phase, five wire electricity outlet. The test facility has its own distribution board (DB) with a main breaker switch and an earth leakage switch. Furthermore, the DB has circuit breakers switches between the electricity supply and the main components of the test facility for protection purposes. The test facility operates on AC (Alternating Current) (Single and three phase), as well as DC (Direct Current) (12V) electricity.

Each piece of measurement instrumentation was supplied with its own switch to isolate the component from the remainder of the electrical system. Indicator lights have also been installed at each switch to give the operator an indication whether the individual components are receiving electrical power. The test facility was furthermore able to be completely isolated from the external electricity supply. The DB and all other enclosures that contained electrical components could be locked to restrict operation only to the operator of the testing facility.

4.3 DETAIL DESIGN

The detail design of the test facility is divided into three separate systems. These systems include the main system, the DAQ system and the electricity supply and distribution system. The detail design and integration of all the systems and their respective components are described in the sections that follow..

4.3.1 DETAIL DESIGN OF THE MAIN SYSTEM

4.3.1.1 WORKING FLUID

The first step in designing the main system was selecting the appropriate working fluid. According to the URS, the working fluid should not be a toxic substance and must be readily available (URS-7). Two fluids that best suited the requirements were air and water. Water was consequently selected as the working fluid due to its density being much higher than that of air. This increased density of water would allow for higher Reynolds numbers (URS-1) to be achieved during the experiments under same flow velocity and geometry of the packed bed.

4.3.1.2 TEST SECTION DESIGN

The test section included the packed bed, the packed bed container and the fittings for connection to the piping system. The URS specified that the container which house the packed bed should to be transparent (URS-5). A cylindrical perspex pipe was chosen as the packed bed container. Perspex pipes can be found in a large range of sizes and it can sufficiently cope with the maximum pressure of 600 kPa as specified in the URS (URS-14).

The calculations were done by utilising Engineering Equation Solver (EES) software. The test section design was done by making use of the KTA (1981) correlation for pressure drop through a packed bed of spheres. The requirements for the design of the test section are specified in the URS. They include the range of modified Reynolds numbers ($Re_m \geq 50{,}000$) (URS-1), Bed-to-particle diameter ratio ($D/d_p \geq 4.5$; URS-3) and bed length-to-particle diameter ratio ($L/d_p \geq 20$; URS-4). The combination of all these requirements led to the specific set of physical parameters of the test section as presented in Table 6. The test section fits into the piping system by means of flanges. The flanges enable the test section to be removed from the piping system with ease.

The thermal fluid design of the testing facility was done by dividing the testing facility into sub-sections and then solving the conservation equations for each of these sub-sections. The conservation equations include the conservation of mass, momentum and energy equations. By solving these equations in EES, all the required parameters were obtained for the selection of suitable measurement instrumentation. The upper and lower boundaries for the measurement instrumentation are provided in Figure 27 and Figure 28 respectively.

The pressure drop through the rest of the piping system was estimated during the design of the test section, It was estimated that approximately 12m of 80mm (3 in.) galvanised steel pipe would be used. Also included were 3x90degree elbows joints, 8xT-pieces, 4xgate valves and 6x reducer fittings from 80mm (3in.) to 65mm (2.5in.). The estimated pressure drop through the piping system was approximately 67kPa. The pressure drop through the piping system would contribute approximately 26.27% to the total pressure drop including the packed bed.

Table 6: Physical parameter of test section.

Physical Parameter	**Dimension**
Length of perspex pipe	1000 mm
Inside diameter of perspex pipe	140 mm
Particle diameter (d_p)	30 mm
Bed-to-particle diameter ratio (D/d_p)	4.67
Bed length-to-particle diameter ratio (L/d_p)	20
Maximum modified Reynolds number (Re_m)	Up to 101 102 @ $T_{water} = 60\ °C$
Maximum mass flow through test section	15.49 kg/s
Maximum pressure drop through test section	255 kPa
Maximum pressure drop through test section loop	255 kPa + 67 kPa = 322 kPa

4.3.1.3 Development and Manufacturing of Packed Beds

Two packed beds with different structures were designed with the Solid Works™ software. These includde one randomly packed bed and one structured packed bed. Both the packings were manufactured through rapid prototyping as complete units. The material used in the rapid prototyping process is known as PA 2200. The data sheet with the material properties of PA 2200 is given in Figure 61 in APPENDIX A.

The randomly packed bed was developed using coordinates from the particles in the annular packed bed of the HTTU, Du Toit (2008). The models of the annular bed in the HTTU were generated numerically. Care was taken to ensure that the section chosen to represent the randomly packed bed was taken from the bulk region of the annular packing. The particles used in the annular packed bed had a diameter of 60 mm. Once the packing was developed, it was scaled for the particle size to be 30 mm. The average porosity of the random packing was

determined as 0.434. The porosity of the random packing was verified through testing. The test was conducted by submerging the random packed bed in water and measuring the overall displacement of the water. The reason that the porosity of the random packing is slightly higher than the 0.39 expected from the numerical HTTU beds is due to the fact that some of the particles of the random packing were dislodged during transportation. This could not be corrected in a viable manner, except for possible re-manufacture, which was not possible due to funding and time constraints.

The structured packed bed was developed by arranging spherical particles in a FCC structure. To obtain an average porosity of 0.36, the particles were distended from each other by ridged 2 mm rods between the spheres. The length of the distension rods are 1.49 mm in length. The effect of the distensions was included when the porosity of the structured packing was determined.

Once both the packings were designed, they were cut into cylindrical form to fit into the perspex pipe. By not simply putting whole particles into the perspex cylinder the walls of the perspex cylinder could not influencing the structure of the packing. Thus, the wall effects were eliminated from the packings (URS-2). The particles of the packings were designed to be hollow for cost savings (URS-12). The hollow particles on the circumference of the packings were filled with silicone prior to insertion into the perspex pipe in order to form the test section. This was done to avoid bypass flow between the packing and the container and also to avoid stagnant flow pockets.

4.3.1.4 Measurement Instrumentation Design

During the design of the test section, information was obtained for the selection of measurement instrumentation. The specifications of the differential pressure transmitters, the flow meter and the temperature meter are provided in this section.

The differential pressure transmitters need to withstand a system pressure of 600 kPa (URS-14). They must also be able to measure maximum differential pressure of 255 kPa. The differential pressure transmitters had to withstand temperatures of 60 ℃ or more. The differential pressure transmitters need to convert their pressure readings into a 4 - 20 mA signal for use in the data acquisition system.

To accurately measure (URS-6) the entire range of differential pressures, as illustrated in Figure 27 and Figure 28, more than one differential pressure transmitter was required. The ranges specified for the differential pressure transmitters were calculated during the detail design phase of the testing facility. Three differential pressure transmitters were selected from the range offered by Endress & Hauser pressure measurement instrumentation. Two Deltabar S PMD 235 and one Deltabar S PMD 70 differential pressure transmitters were utilised to measure the differential pressure over the packed beds. The necessary specifications for each of the differential pressure transmitters are provided in Table 7 below. The calibration certificates for each of the differential pressure transmitters can also be obtained in Figure 62 to Figure 64 of APPENDIX A.

Table 7: Specifications of the differential pressure transmitters.

Name	**Endress & Hauser Deltabar S PMD 235**	**Endress & Hauser Deltabar S PMD 235**	**Endress & Hauser Deltabar S PMD 70**
Range	0 to10 kPa	0 to 50 kPa	-300 to 300 kPa
Accuracy	±0.1% of set span	±0.1% of set span	±0.075% of set span
Overload	42 MPa	42 MPa	10 MPa
Temperature Range	Up to 120 ℃	Up to 120 ℃	-20 to 85 ℃
Output	4 to 20 mA	4 to 20 mA	4 to 20 mA
Electricity Supply	12 VDC	12 VDC	12 VDC

The flow meter should be able to accurately measure flow rates of up to 15.49 kg/s. It should also be able to withstand a system pressure and temperature of 600 kPa (URS-14) and 60 ℃ respectively. These specifications were obtained from the detail design of the testing facility. The Proline Promag 50W50 flow meter from Endress & Hauser was consequently selected.

It works on the principle of Faraday's law of induction. The flow meter creates a magnetic field though which the water flows. The water, being a conductor, induces a voltage as it passes through the magnetic field. The voltage is proportional to the velocity at which the water passed through the magnetic field. The volume flow of the water is then calculated from the knowledge of the pipe size.

The flow cross section of the Proline Promag 50W50 is 50 mm in diameter. In order for the flow meter to measure at maximum accuracy there were certain requirements than the installation of the flow meter needs to adhere to. These requirements include the following:

- The inlet run to the flow meter must be ≥ 5 times the flow meter diameter, thus 250 mm;
- The outlet run from the flow meter must be ≥ 2 times the flow meter diameter, thus 100 mm;
- The vibration of the flow meter needs to kept to a minimum; and
- The total distance between the two mounting points of the pipes that supports the flow meter must be < 10 m.

The calibration certificate for the flow meter can be seen in Figure 65 in APPENDIX A. The necessary specifications of the flow meter are given in Table 8 below.

Table 8: Specifications of the flow meter and temperature meter.

Name	**Endress & Hauser Proline Promag 50W50**	**Wika PR 5333A PT 100**
Range	0,6 to18 kg/s	-20 to 85 ℃
Accuracy	0.5% of set span	0.1% of set span
Overload	4 MPa	-
Temperature Range	Up to 80 ℃	-200 to 850 ℃
Output	4 to 20 mA	4 to 20 mA
Electricity Supply	220 VAC	12 VDC

The Wika PR5333A PT - 100 was selected to accurately measure the temperature of the water during the experiment. A 2-wire configuration was used to provide sufficient accuracy for the purpose of the experiment. It can withstand and measure any condition that might be encountered in the testing facility. The necessary specifications of the PT 100 are provided in Table 8.

4.3.1.5 Piping System Design and Pump Selection

The complete system could be designed once the test section had been designed and all the measurement instrumentation had been selected. The next step was to develop the piping system by which the water would be transported to all the measurement instrumentation and the test section. A pump was also selected that could deliver the required flow and head to overcome the pressure losses through the entire testing facility. The detail design of the parameters of the testing facility was calculated with EES. The code of the EES program is provided in APPENDIX C. The minimum and maximum flow parameters through the test section can be seen in Figure 27 and Figure 28 respectively.

When designing a pipe system it is important to note that the maximum water velocity inside steel pipes with threaded connections must be smaller than 5 m/s according to Rousseau (2008). At water velocities less than 5 m/s the forces of the water on bends and elbows of steel pipes are acceptably low. The piping system consists of galvanised steel pipes which come in a wide range of sizes which was readily available (URS-8).

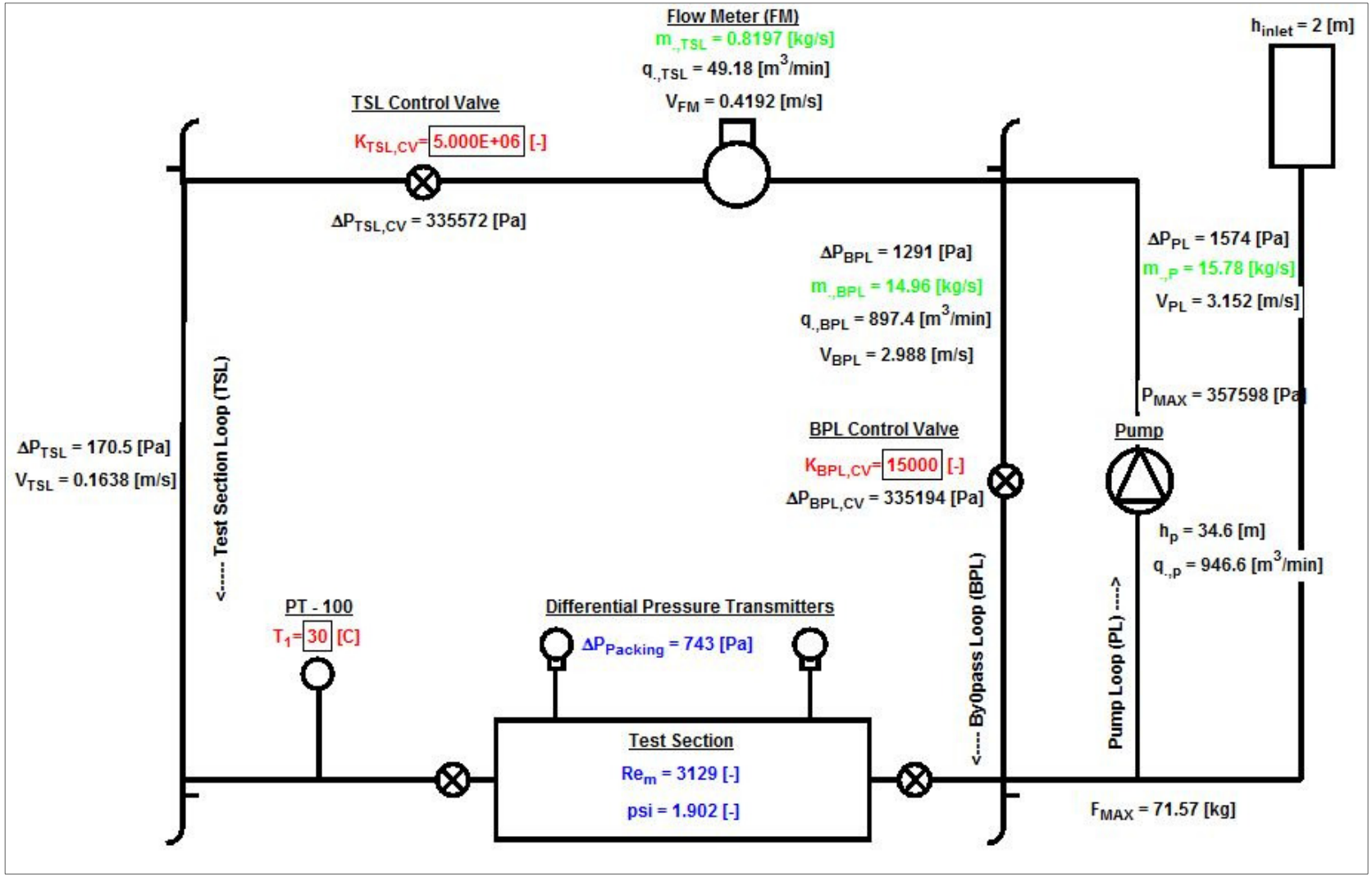

Figure 27: Detail design of testing facility parameters with EES (Minimum flow through test section).

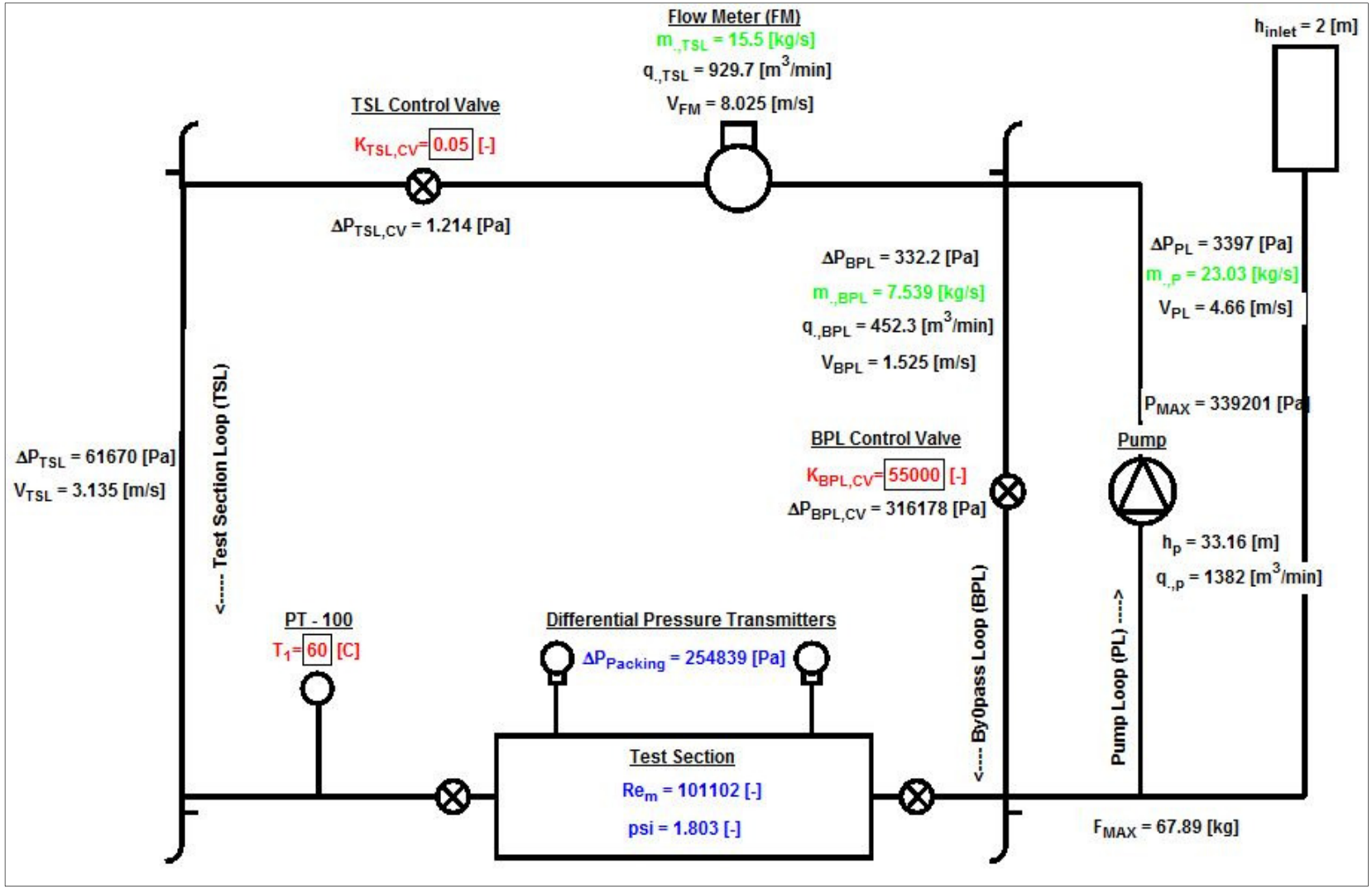

Figure 28: Detail design of testing facility parameters with EES (Maximum flow through test section).

The maximum mass flow of 23.03 kg/s was expected in the piping system at the outlet of the pump. This meant that the 80 mm (3") galvanised steel pipe had a maximum flow velocity of 4.66 m/s in the section of pipe that is directly connected to the pump. In the test section loop (TSL) the maximum fluid velocity would consequently be 8.025 m/s. This high velocity is due to the fact that the flow meter needs to be connected to a 50mm (2") galvanised steel pipe to measure accurately, as explained earlier. Due to the fact that the 50 mm pipe section leads straight into and from an 80 mm pipe without any bends, the effect of the fluid momentum is negligible on the piping system.

The piping system would have an inlet pipe that will always be open to the atmosphere. The inlet pipe's highest point would be higher than the highest point in the remainder of the testing facility. This inlet pipe would be connected to the piping system just before the inlet to the pump. This meant that the static pressure at the inlet of the pump would be equivalent to the height of the column of water in the inlet pipe. The maximum pressure in the piping system would be at the outlet of the pump and it would be the sum of the static head from the inlet pipe and the static head that the pump can deliver with relation to the friction of the piping system. The maximum pressure would be 358 kPa which is well below the 600 kPa specified in the URS (URS-14).

Controlling the flow through the test section would be achieved by adding a bypass pipe system in parallel with piping system passing through the test section. Each of the piping loops would be fitted with their own gate valve to regulate the flow through each. In the piping loop passing through the test section, known as the TSL, two gate valves would be used in parallel. One of the two gate valves would be a 19 mm (0.75") gate valve and the other would be an 80 mm (3") gate valve. At low flow rates through the TSL the 19 mm (0.75") gate valve would enable the operator of the system to control the flow more finely (URS-15). At higher flow rates the 80 mm (3") gate valve would be sufficient to control the flow through the TSL. In the by-pass loop (BPL) an 80 mm (3") gate valve would be used to control the flow through the section.

The entire piping system and all the components and fittings connected directly to it can be seen in Figure 29. A detail drawing showing all the "as-built" dimensions needed for the manufacturing of the piping system can be seen in Figure 66 in APPENDIX A.

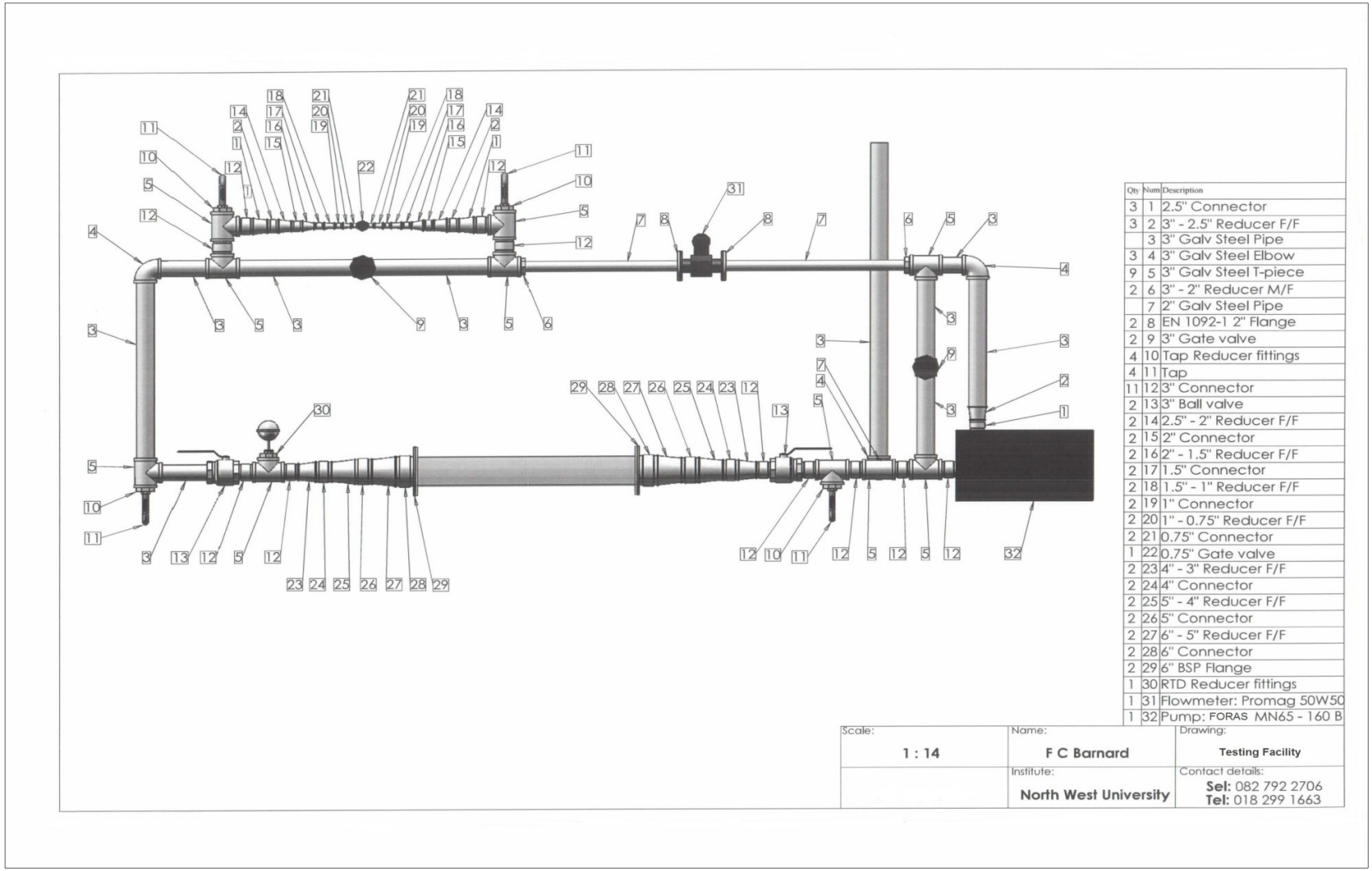

Figure 29: Main system and all of its components.

From the calculation of the piping system, it was found that the pump must deliver 23.03 kg/s (1382 m^3/min) at a head of 320 kPa (33.16 m). The 11kW Foras MN 65-160/B centrifugal pump was chosen. The specifications of the Foras MN 65-160/B centrifugal pump can be seen in APPENDIX A in Figure 67 and Figure 68. As the control valves change the system curve of the testing facility, the operating point moves along the pumping curve. This can be seen in Figure 30. Because there is no static head that needs to be overcome in this test facility the operational curve of the test facility passes through the origin of the graph. This specific range of operational points on the pumping curve was selected since these represent the pump's highest efficiency levels.

The centrifugal pump can handle water temperatures between 0 ℃ and 90 ℃. It can handle a maximum system pressure of up to 1 MPa. Therefore, the pump would be able to withstand the conditions to which the testing facility would be subjected.

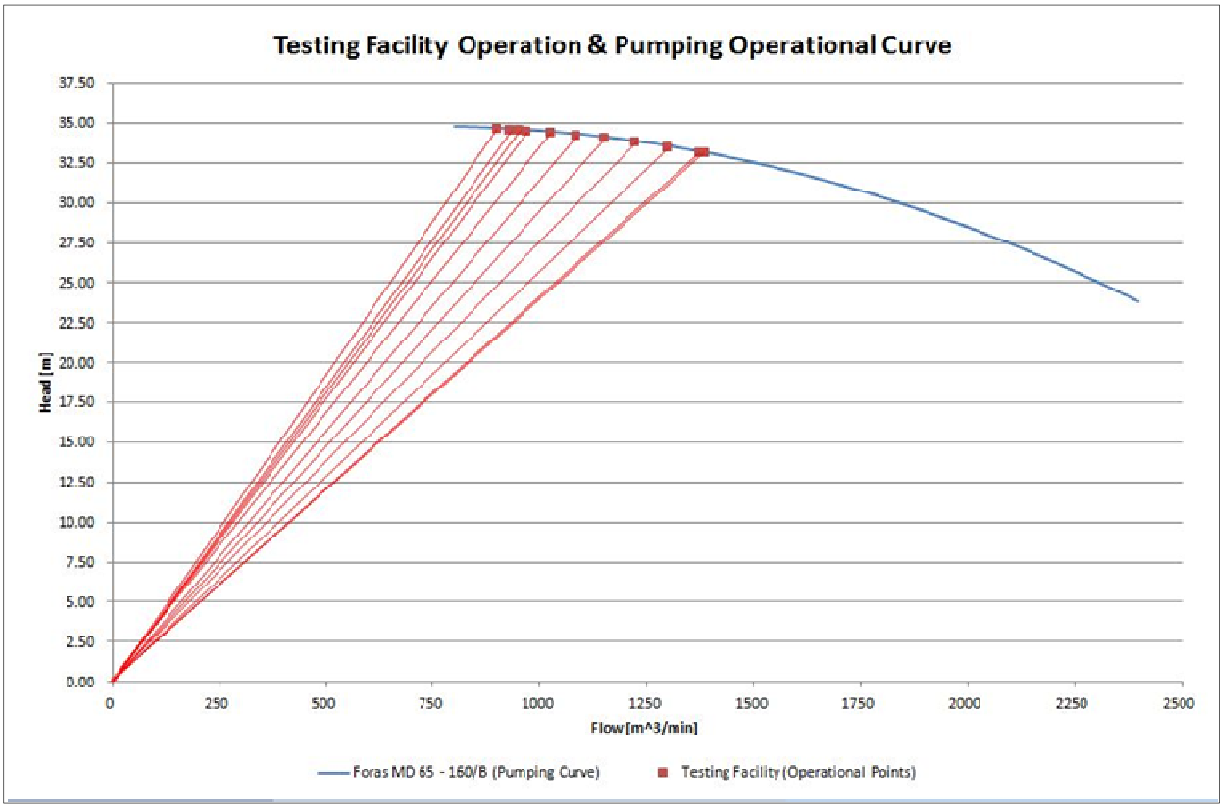

Figure 30: Testing facility system curves plotted over the pumping curve.

4.3.1.6 Design of the Frame

The entire test facility, the DAQ system and the electricity supply and distribution system had to be mounted on a frame with sufficient strength to support the weight, compact enough to fit into the allocated space in the laboratory. It also had to be fitted with wheels to make it semi-portable.

The frame was constructed from 76 mm x 2 mm square tubing and was fitted with six wheels for portability. The differential pressure transmitters were fastened to 50 mm diameter pipes placed vertically behind the test section on the frame. The layout of the frame can be seen in Figure 31. A detailed sketch of the frame indicating all the necessary dimensions of the frame for construction can be seen in Figure 69 in APPENDIX A. In APPENDIX A, a diagram showing the combination of the test facility and the frame can be seen in Figure 70.

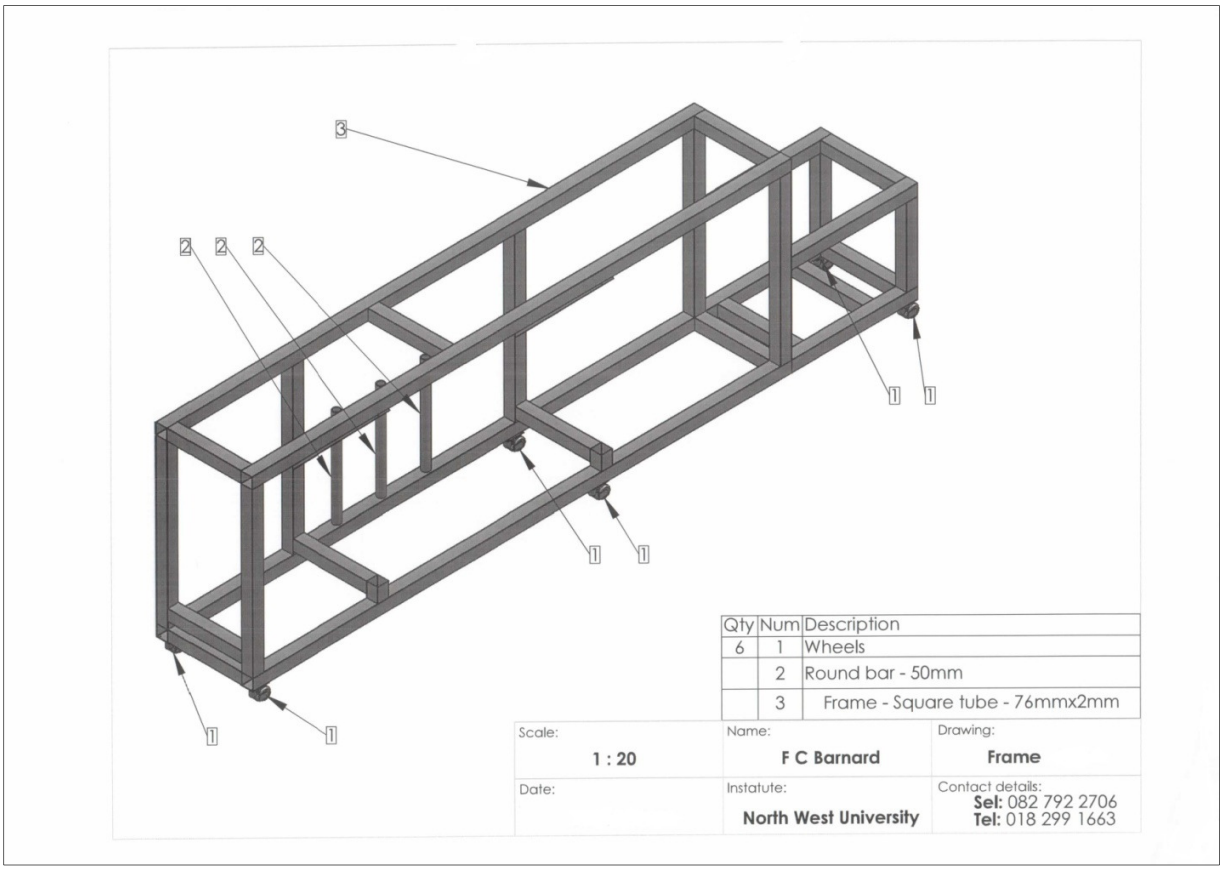

Figure 31: Frame to support the testing facility, the DAQ system and the electricity supply and distribution system.

4.3.1.7 Design of the Pressure Measurement Piping System

The differential pressure transmitters were connected to the test section in such a way that all the meters would simultaneously be able to measure the pressure drop over the same section of the packed bed. The differential pressure metering system was also constructed in such a way that the user can switch between the different sections of the packed bed for the various measurements to be taken without disconnecting any of the meters. The description of how the differential pressure measurement system works is provided in this section.

The pressure drop had to be measured over more than one section of the packed bed under consideration. The reason for the measurements being done on multiple sections of the packed bed is to give a more detailed description of the pressure drop variation over the packed bed. The sections and their respective lengths can be seen in Figure 32.

The inlet and outlet sections, in Figure 32, of the packed bed had to be two particle diameters long. The inlet and outlet sections were included so that the end effects would not be part of the pressure drop measurements made on the test section, and two particle diameters would be enough to absorb those effects (Achenbach, 1995). Sections 1 and 3 in Figure 32 are both 3 particle diameters long. The differential pressure measurements over these two sections were used to verify that the end effects did not form part of the sections measured for the experiment. The core of the packed bed under consideration consisted of sections 2 and 4. These two sections each had a length of 5 particle diameters.

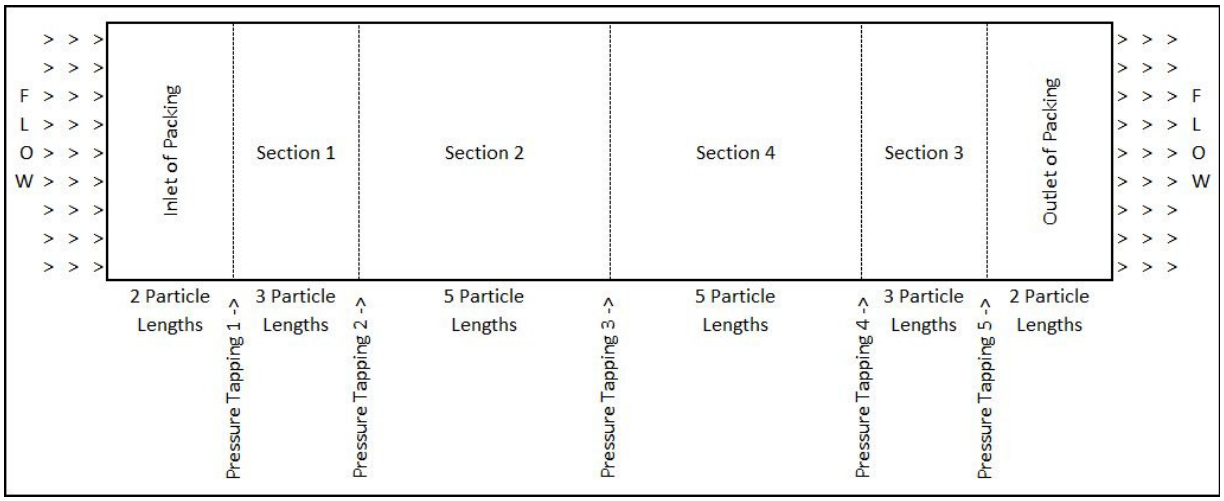

Figure 32: Sections of the packed bed and their corresponding pressure measurement points.

The pressure measurements were taken at the boundaries of the sections as shown in Figure 32. At each of the pressure tapping points the pressure was measured for four locations around the packing. The four pressure measurement points were placed as such that none of the particles that form the packed bed would influence the pressure measurement. Holes were drilled through the perspex container and then threaded. The connector fittings were then screwed into the holes. High pressure flexible pipes were used to connect the pressure tappings with the differential pressure transmitters.

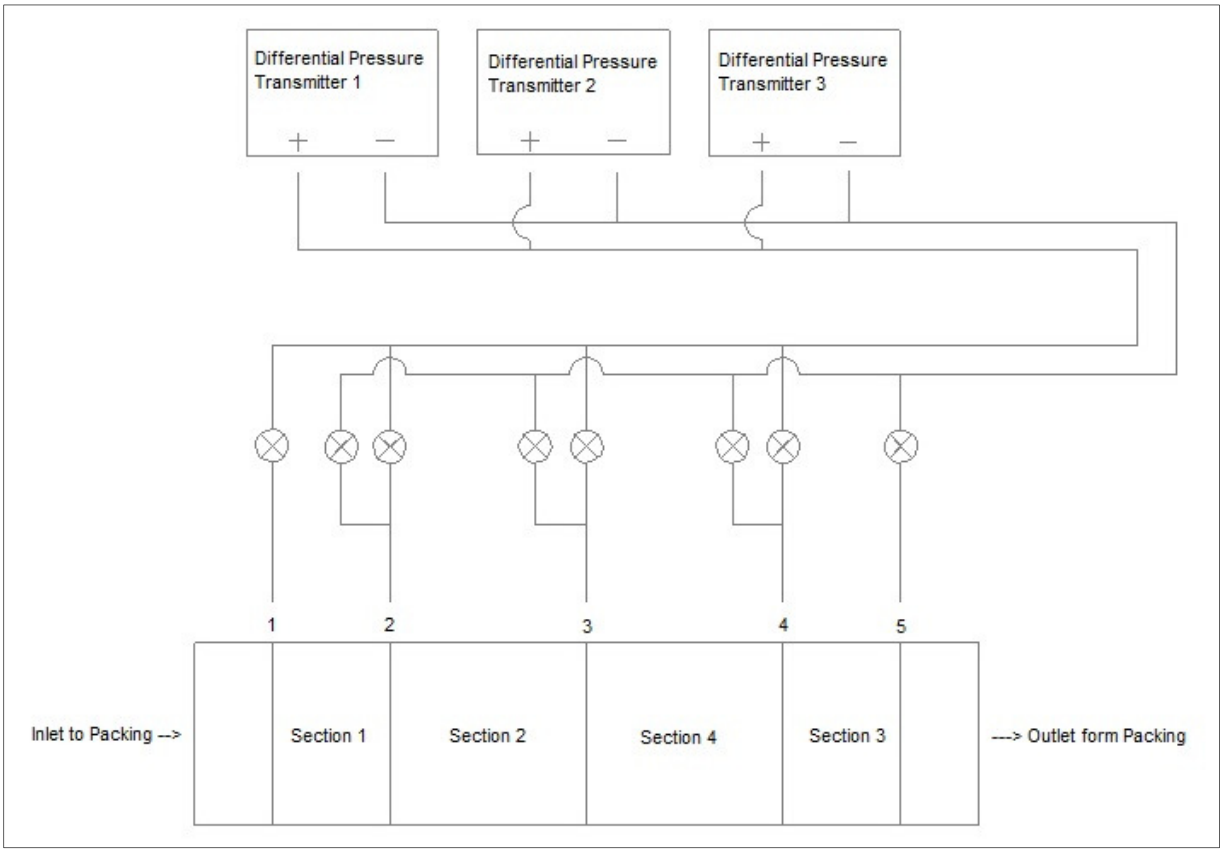

Figure 33: Pressure measurement system layout.

The piping configuration used for the pressure measurement system is shown in Figure 33. Numbers 1 to 5 in Figure 33 indicate where the pressure measurements are taken on the test section. Pressure tappings numbers 1 and 5, on the packing, only lead to the high and low pressure sides of the differential pressure transmitters respectively. The pipes that lead from pressure tappings numbers 1 and 5 are also the main lines that lead to the high and low

pressure sides of the differential pressure transmitters respectively. Pressure tapping numbers 2 to 4 had two pipes leading from the same measuring point. These two pipes were then connected to the two main lines respectively. Each of the two pipes also had their own valve to isolate it from the remainder of the piping system.

To be able to measure the pressure drop through section 2, the following valves had to be open:

- The valve that opens pressure tapping point number 2 to the line that leads to the high pressure side of each differential pressure transmitter;
- The valve that opens pressure tapping point number 3 to the line that leads to the low pressure side of each differential pressure transmitter; and
- All the other valves in the pressure measurement system need to be closed.

4.3.2 DETAIL DESIGN OF THE DATA ACQUISITION SYSTEM

All of the measurement instrumentation was selected for a 4 to 20 mA output signal. In order to interpret the 4 to 20 mA signal, an ADAM-4017 (Advantech Data Acquisition Module) module was used. The ADAM-4017 module is connected in series to the 12 V electricity line that powers the measuring instrument. The ADAM-4017 module can withstand 3000 V_{DC}. Only the Proline Promag 50W50 flow meter makes use of 220 V_{AC}. The 4 to 20 mA signal from the Proline Promag 50W50 flow meter was measured in a circuit separate to the power supply circuit.

The ADAM-4017 module makes use of a 250 Ω shunt resistance to convert the 4 to 20 mA signal to a 1 to 5 V_{DC} signal. The 250Ω shunt resistance is made up of a 100 Ω and a 150 Ω resistor. Each of these resistors had a tolerance of 99% with a 5 W rating.

The ADAM-4017 module made use of a RS-485 connection to send the data (the 1 to 5 V_{DC} signal) that it measured to an ADAM-4520 module. The ADAM-4520 module converted the RS-485 signal to a RS-232 signal that the PC could interpret. Labview (URS-13) was used to present and log the measurements of temperature, pressure and volume flow rate. The conversion performed by Labview was done with a linear relation obtained from the calibration certificate of each of the measurement instruments. In Labview, the test facility layout is shown on screen with instantaneous readouts for each of the measurement instruments. Continuous

graphs of all the measurements were also plotted during the experiment. A wiring diagram of the DAQ system can be seen in Figure 71 in APPENDIX A.

4.3.3 DETAIL DESIGN OF THE ELECTRICITY DISTRIBUTION SYSTEM

The design of the electricity distribution system was done with the help of wire diagrams. The electricity distribution system consists of two parts. The first part is the AC electrical system and the second one is the DC electrical system. The wire diagram for the AC and DC electrical system designs can be seen in Figure 72 and Figure 73 in APPENDIX A respectively.

In Figure 34 a flow chart illustrates how the electricity is distributed from the three phase (400 V) outlet to each of the components that require AC or DC electricity. The three phase five wire cable enters the distribution board (DB) where it first passes through a 63 A main switch. From there it passes through a 63 A earth leakage switch. The main switch and the earth leakage switch are connected in series. After the earth leakage switch all three the phases lead to the three phase circuit breaker switch. From the three phase circuit breaker switch it passed through a direct online switch that was used to start the pump.

Three single phase circuit breakers were connected in parallel with the 3-phase circuit breaker used exclusively for the pump. The three phases were divided between the three single phase circuit breakers. These three single phase circuit breakers supplied electricity to the PC, the Flow meter and the AC/DC transformer after passing through 3-pin plugs, each with its own switch and indicator light.

The AC/DC transformer supplied DC electricity to the following components:

- Differential pressure transmitter 1;
- Differential pressure transmitter 2;
- Differential pressure transmitter 3;
- PT-100 temperature meter;
- ADAM 4017 module; and
- ADAM 4520 module.

The three differential pressure transmitters and the temperature meter each had their own switch and indicator light. The entire electrical system was earthed.

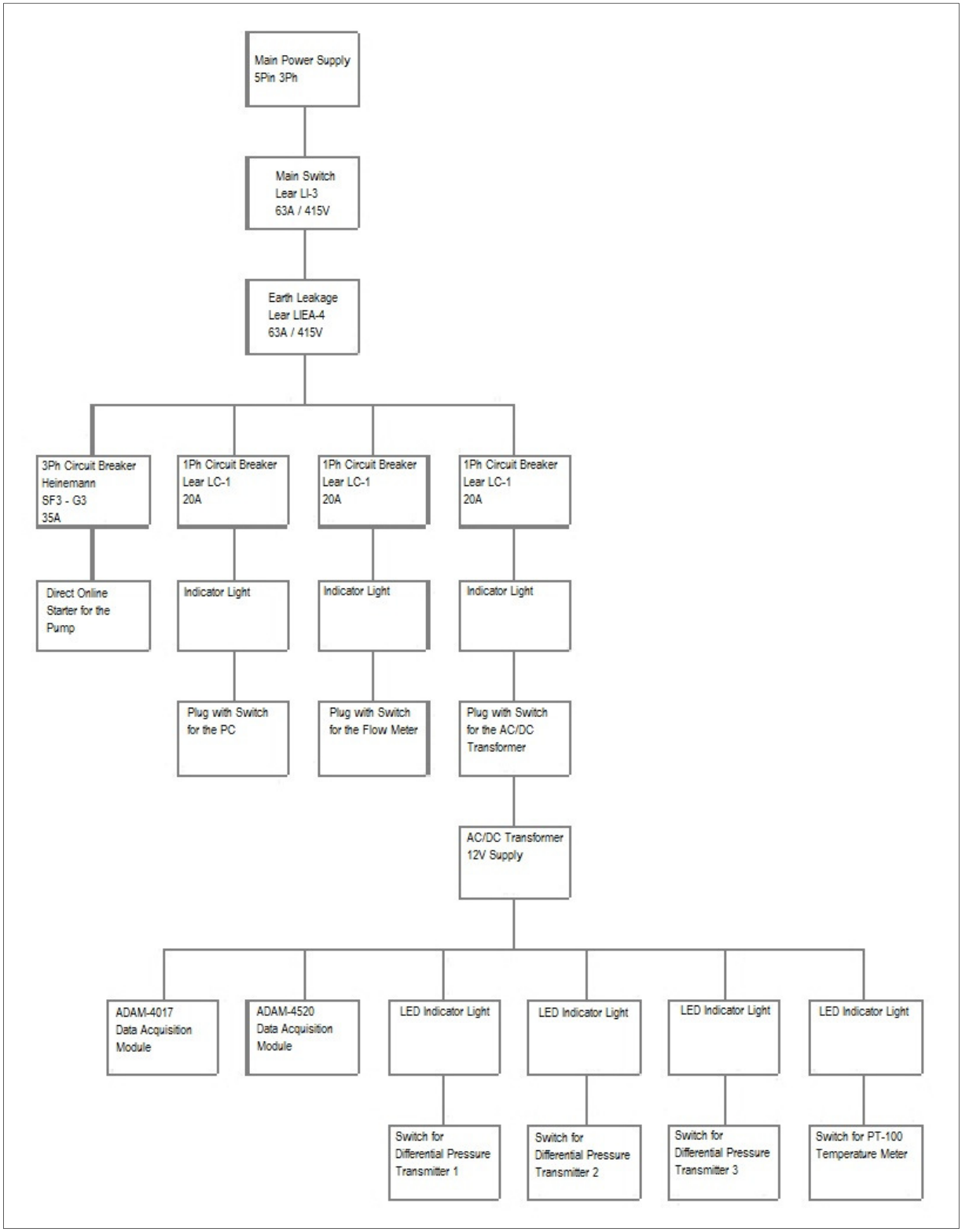

Figure 34: Layout of the electricity distribution system.

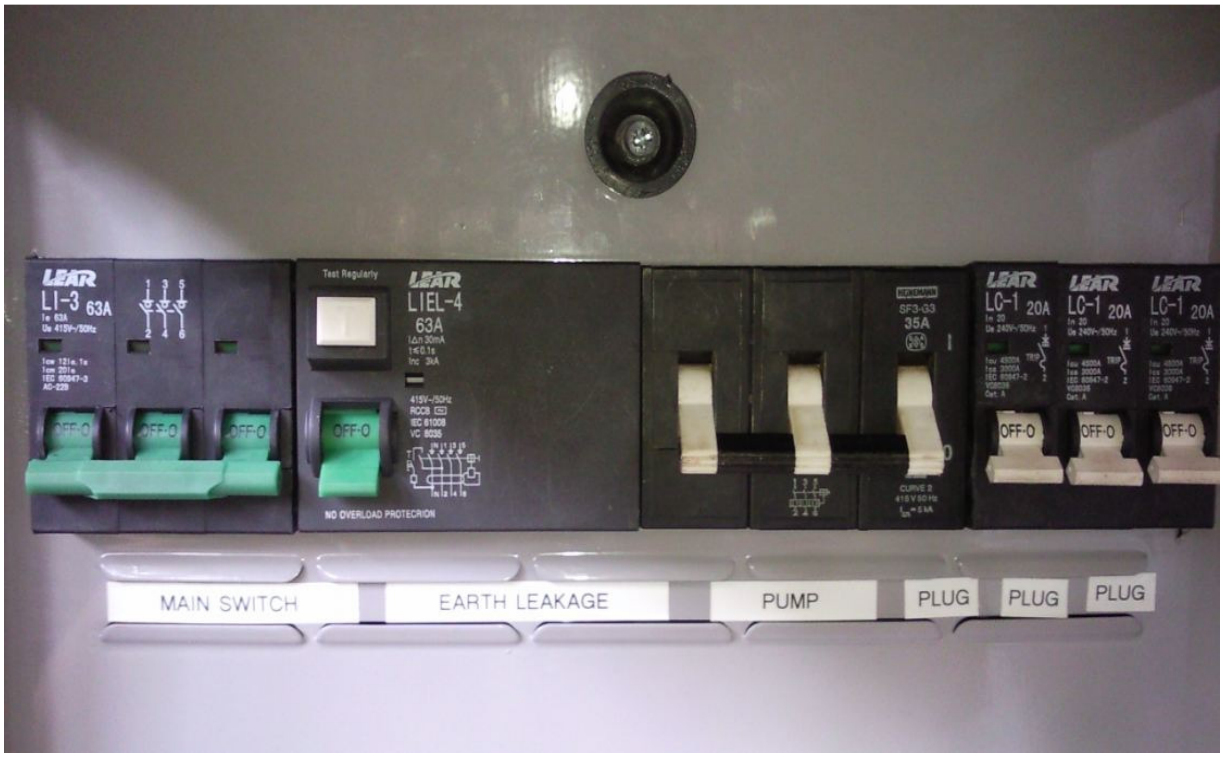

Figure 35: Inside of the distribution board.

Figure 36: Left – distribution board; Right – control box.

4.4 CONCLUSION

A detail description of the design of each of the sections and components that comprised the test facility was described in this chapter. The URS was developed during consultations with the promoters. It provides the specifications for the design of the testing facility. The conceptual design of testing facility was done to provide the outline of the project. The section on the detail design of the test facility was disaggregated into the three main sections of the test facility (These systems were the main system, the data acquisition system and the electricity distribution system.). Each of these sections was described in detail. The following chapter will discuss the experimental procedure for the testing facility.

CHAPTER 5 : EXPERIMENTAL PROCEDURE

For the purpose of this study an experimental setup was designed to perform pressure drop tests on packed beds of spheres. A description of how the experiment needs to be conducted is presented in this chapter. The process that needs to be followed will be referred to as the experimental procedure.

In Figure 37 to Figure 41 the experimental setup can be seen. The alphabetical notations added to the pictures of the experimental setup identify the components of the system that will be referred to during the description of the experimental procedure. In Table 9 a description of all the components shown in Figure 37 to Figure 41 is given.

Table 9: Description of the components of the experimental setup.

Notation	Name	Description
A	Brass bleed valve top	Brass bleed valves at the highest point in the system
B	Control valves – bed loop	Gate valves for flow control on the loop passing through the packed bed
C	Flow meter	Measures the flow through the packed bed
D	Inlet	Inlet to the system where the water is added
E	Distribution board	Electrical DB with switches for all the main areas
F	Control box	Distributes electricity to all components (Except the pump) and houses the DAQ modules.
G	Computer	Gives digital display of operations through Labview. Logs data.
H	Pump	Pumps water through system
I	Direct-online switch	Switch for starting the pump
J	Control valves – bypass loop	Controls flow through bypass loop
K	Brass bleed valve bottom	Brass bleed valves at the lowest point in the system
L	Isolation valve	Isolates the packed bed from the rest of the system
M	Packing bleed valves	Bleeds air from the inlet and outlet of the packing
N	Pressure meters	Measures differential pressure over packing
O	Pressure measurement	Used to measure differential pressure over different

	valves	sections of the packing at a constant flow rate
P	Temperature meter	Measures temperature of fluid before it enters the packed bed
Q	Pressure meter valves	Vents, Isolates and Equalises the fluid at the pressure meter. These functions are performed by three separate vales.
R	Pressure measurement system bleed valves	Bleeds the air from the pressure measurement system
S	Electrical plugs	These plugs supply AC electricity to the PC, AC/DC power supply and the flow meter
T	Component switches	These switches supply DC electricity to the three differential pressure transmitters and the temperature meter
U	Tensioner	Used to apply sufficient pressure to the packing to prevent it from leaking
V	Packing fasteners	Flanges where the packings are fastened to the galvanised pipes

Figure 37: Experimental setup designed to investigate the pressure drop through packed beds of spheres.

Figure 38: Layout of pressure drop measurement system with ball valve setup.

5.1 BLEEDING THE EXPERIMENTAL SETUP FOR AIR

Before conducting an experiment, water needs to be added to the piping system. To ensure that the water does not flow from the piping system, some of the valves need to be closed. The valves that need to be closed before the water can be added to the piping system are the following:

- The drain valves at K (Figure 37); and
- The ventilation valves at Q (Figure 38).

Some of the valves in the piping system need to be open for the water to completely fill the piping system and expel all the air from the pipes and cavities. These valves include the following:

- The bleed valves at A (Figure 37);
- The control valves at B (Figure 37);
- The control valve at J (Figure 37);
- The isolation valves at L (Figure 37);
- The bleed valves at M (Figure 37);
- All the pressure tapping valves at O (Figure 38);
- The vent valves at Q (Figure 38);
- The isolation valves at Q (Figure 38);
- The equaliser valves at Q (Figure 38); and
- The bleed valves at R (Figure 38).

Once all the valves in the piping system are in their correct positions, the water could be added to the piping system. The water is added at the inlet of the piping system at D (Figure 37). As the water level in the piping system starts to rise, the water will start to leak from the valves that are open. This leak means that the air has been pushed out of the piping section associated with that specific valve and that the valve can now be closed.

It is important to note that bleed valves A (Figure 37), M (Figure 37) and R (Figure 38) are connected to the inlet of the piping system at D (Figure 37). The reason for this connection is to continuously bleed the piping system as the water is circulated through the piping system when the pump is started. As the water in circulated through the piping system, air that is trapped in

cavities starts to move through the system. As the trapped air moves past an open bleed valve it will be released from the piping system. When the flow rate of water is increased through the piping system, all the air in the piping system will eventually be released by means of the bleed valves.

Note that before the pump can be switched, on the experimental setup needs to be plugged into a power supply. Once the experimental setup is connected, the main switch breaker and earth leakage in the DB at E (Figure 37) can be switched on. The three phase circuit breaker marked as “PUMP” must be switched on to supply electricity to the pump. The final step in switching on the pump is to push the green button on the direct-online switch at I (Figure 37). The pump must now run until all the air has been bled from the piping system. The best way to confirm whether all the air has been expelled from the piping system is to look into the transparent perspex pipe that houses the packed bed to establish if air bubbles are still moving through the packing. The vent valves of the pressure transmitters at Q (Figure 38) must also be opened and closed just to make sure that all the air has been bled from the pressure tapping piping system.

Due to the large size of the pump, the water is constantly heated (At a rate of about 3 ℃ per minute) while the pump is in operation. This is due to the fact that much of the mechanical work that the pump deliver to the water is converted into heat. Therefore the pump needs to be stopped as soon as all the air is bled for the piping system to allow the water to cool down before the experiment can be conducted. It takes approximately four hours for the water to cool down sufficiently for the experiment to be conducted. It is important to switch off the main switch and the earth leakage in the DB at E (Figure 37). It is also important to disconnect the experimental setup from the external power supply.

5.2 CONDUCTING THE EXPERIMENT

Once the water has cooled, down the experiment can be conducted. It is important to ensure that all of the bleed valves in the piping system are closed to force all the flow through the flow meter at C (Figure 37) and the packed bed. To supply electricity to all the components of the experimental setup, it needs to be connected to the external power supply and the main switch and the earth leakage in the DB at E (Figure 37) must also be switched on.

The same process needs to be followed as described above to turn on the pump to conduct the experiment. To supply electricity to the remainder of the components in the experimental setup, the three single phase circuit breakers, each labelled as “PLUG” in the DB at E (Figure 37), needs to be switched on. The indicator lights on the plugs at S (Figure 39) will show whether the plug receives electricity or not. Once a plug is switched on the component specified on the side of the plug will receive electricity.

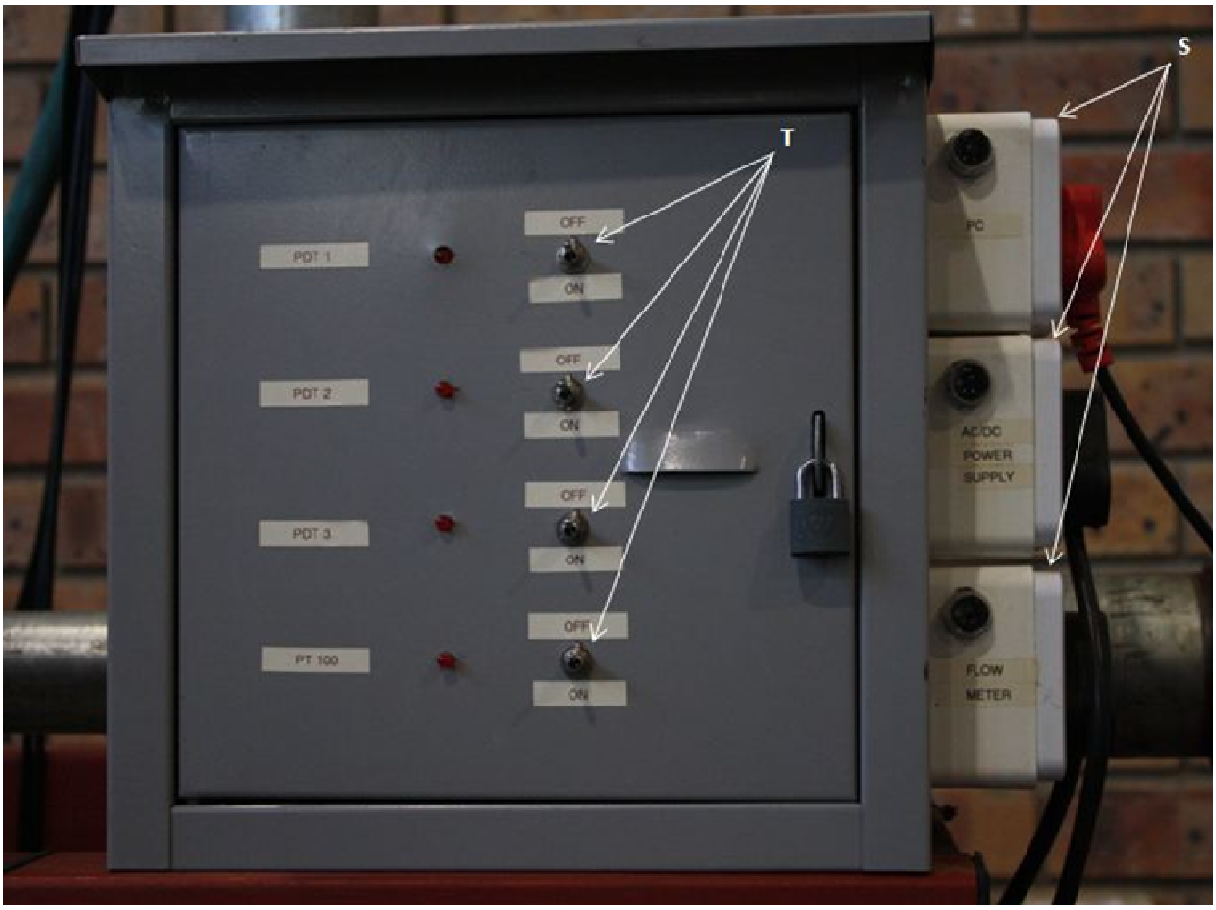

Figure 39: The control box and all the switches related to it.

When the AC/DC power supply receives electricity, it can supply DC electricity to the components. These components include the three differential pressure transmitters and the temperature meter. Each of these components has its own switch with an indicator light, which

can be seen at T (Figure 39), to show when the component is active. DC electricity is also supplied to the ADAM modules, without a switch, once the AC/DC power supply is switched on. These ADAM modules are situated inside the control box at F (Figure 37). To check whether all the components are operational once their switches has been switched on, check their displays or look for indicator lights on the individual components.

The PC can now be switched on. Once the PC has booted up, the software, in the form of Labview that will log the data of the experiment, can be launched. Labview will also display the operation of the system in real-time. The data for each meter will be logged and saved in a text file on the PC at a pre-determined location.

The three differential pressure transmitters should be reset to zero before taking any measurements. Labview can now be set to run continuously. On the graphs that Labview will plot for each of the components in operation it must be checked that the readings for each of the differential pressure transmitters and the flow meter is at zero. The reading of the temperature meter will give the temperature of the water at that time. A screen capture of the Labview interface can be seen in Figure 40.

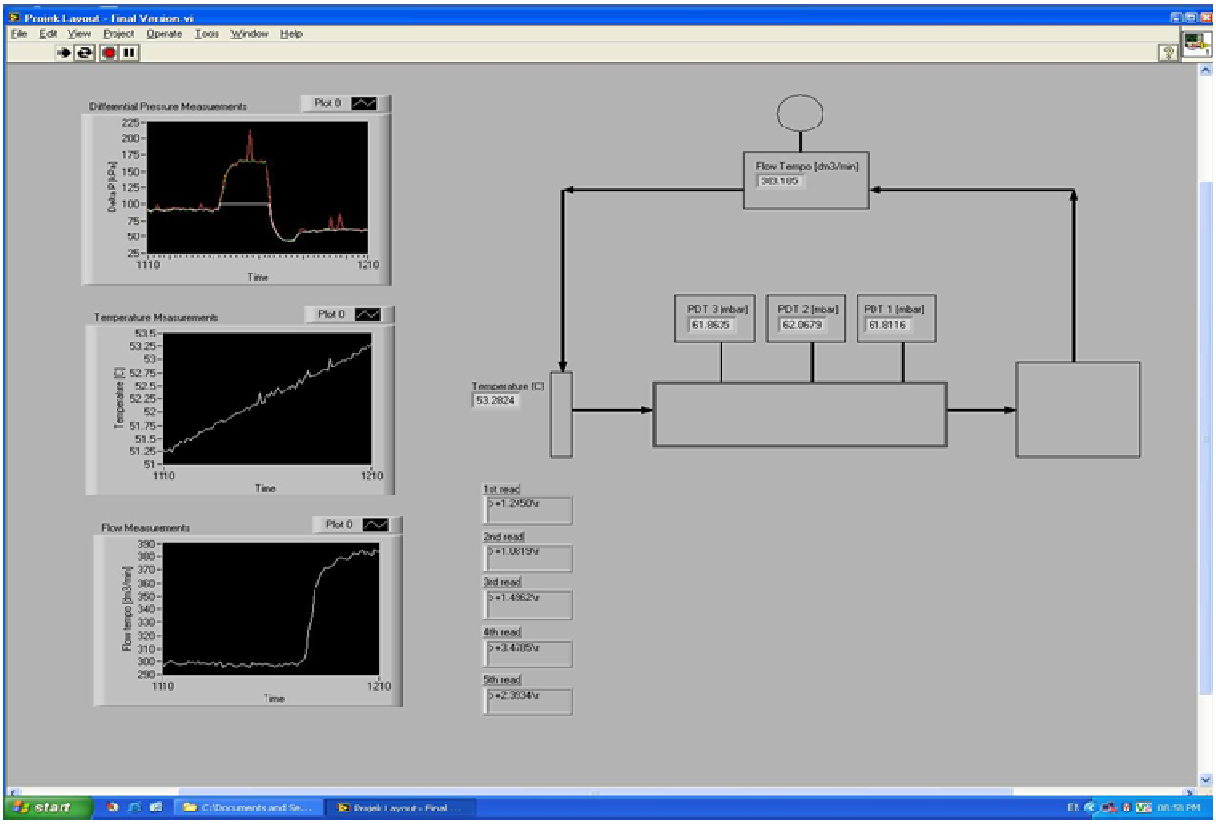

Figure 40: Screen shot of the Labview interface.

Before the pump can be started, the control valves at B (Figure 37) must first be closed and the control valve at J (Figure 37) must be fully opened. This is to allow the flow of water to circulate through the bypass section before allowing any flow to go through the test section. The pump can now be started and the smaller control valve at B (Figure 37) can now be opened slowly to allow water to start flowing through the test section. The small control valve at B (Figure 37) can now be adjusted to obtain the desired flow rate through the test section. Once the small valve at B (Figure 37) is fully opened and more flow is at the desired level, the large control valve at B (Figure 37) can be opened. When the point is reached where the large control valve at B (Figure 37) is also fully opened, and even more flow in desired through the test section, the control valve at J (Figure 37) must be adjusted to obtain the desired flow rate through the test section.

When the desired flow rate is obtained through the test section the different pressure drop measurements should be taken over the packed bed. At O (Figure 38) the pressure tapping

valves are shown. It can be seen from Figure 38 that the first pressure tapping on the left (inlet to packing) and the last pressure tapping on the right (outlet of packing) each have only one valve connected to them. The pressure tappings located on the inlet and outlet of the packing are connected to the two pressure sensors on the left and right hand side of each differential pressure transmitter respectively. The other three pressure tappings on the packing each have two valves connected to them. The valves on the left hand side of each pressure tapping feeds into the same pressure tapping line as the pressure tapping at the outlet of the packing. The valves on the right hand side each feed into the same pressure tapping line as the pressure tapping at the inlet of the packing.

This configuration of valves enables the operator of the system to achieve differential pressure measurements on any of the sections of the packing with any of the differential pressure transmitters. The differential pressure transmitters can each be isolated from the system by closing its isolation valves at Q (Figure 38). This also means that once the differential pressure measured by any meter exceeds what the meter can handle, it must be isolated from the system and vented by opening the vent valves. This will ensure that the meter is not damaged by pressures outside of its range of operation.

Once all the required measurements have been taken, the pump can be switched off. The Labview program can then be stopped and the data downloaded from the PC for further processing. The PC along with all the other components in the system can now be switched off and the testing facility can be disconnected from the external power supply.

If the test section has to be replaced with another one, all the water must first be drained from the piping system. This is done by opening the bottom drain valves at K (Figure 37). It is also important to open all the other bleed valves in the system so that a vacuum in the system does not prevent the water from flowing out of the piping system.

Once all the water has drained from the piping system, the bolts at V (Figure 41) can be loosened and removed. Then the tension applied by the tensioner at U (Figure 41) can be released. The test section should then be able to slide out of the piping system with ease. A different test section can then be inserted and fastened by the tensioner at U (Figure 41) and the bolts at V (Figure 41).

Figure 41: Illustration of where the test section needs to be unfastened and fastened for replacement.

5.3 CONCLUSION

In this chapter a detail description of the operation of the test facility was provided. Each component that is used during the operation of the testing facility was named and described. Then a step-by-step guide was given of the various stages, from adding the water to the system, up to when a complete set of experimental data is recorded. The steps of how to replace the test section with a different one were also described. In the following chapter the results that were obtained from the experiments done on the two differently structured packed beds are discussed.

CHAPTER 6 : RESULTS

6.1 INTRODUCTION

The results obtained for the experiments done on the test facility described in Chapter 4 will be discussed in this chapter. Dimensionless parameters in the form of the friction factor (f) and the modified Reynolds number (Re_m) are used to describe the hydrodynamic behaviour of each section of the test facility. The overall hydrodynamic behaviour of the packed beds will also be described by these dimensionless parameters. It is important to note that the D'arcy-Weisbach friction factor will be used for the purpose of this experiment and not the Fanning friction factor. The Fanning friction factor is four times less than the D'arcy-Weisbach friction factor. The D'acry-Weisbach friction factor for packed beds of spheres is given in Eq (24) and Eq (25), Du Toit (2008).

$$f = 2\frac{\Delta P}{\rho V_o^2}\frac{d_p}{L}\left(\frac{\varepsilon^3}{1-\varepsilon}\right) \tag{24}$$

$$f = \frac{320}{\left(\frac{Re_m}{1-\varepsilon}\right)} + \frac{6}{\left(\frac{Re_m}{1-\varepsilon}\right)^{0.1}} \tag{25}$$

The Reynolds number is defined as the ratio between the inertial and viscous forces that is acting on a fluid. The modified Reynolds number is a variation of the Reynolds number that describe the fluid flow through a packed bed of spheres. The modification is done with the help of the porosity of the packing, the particle diameter and the superficial velocity of the fluid. The modified Reynolds number is given in Eq (26), Du Toit (2008).

$$Re_m = \frac{\rho V_o d_p}{\mu}\left(\frac{1-\varepsilon}{\varepsilon^3}\right) \tag{26}$$

Each of the two packed beds was divided into sections. For each of the packings there were six sections to consider. A layout of how the packings were divided into sections is given in Figure 42. It can be seen from Figure 42 that the water would enter the packing on the left-hand side and pass through the packing before exiting on the right-hand side. The inlet and outlet sections of the packing form part of the packing and also consist of spherical particles.

Sections 1 through 6 form the regions where the pressure drop measurements were made on the packings. The pressure drop measurements for sections 1 and 3 were made to illustrate that the end effects were successfully eliminated by the inlet and outlet of the packings mentioned earlier. The core of each packing consist of sections 2 and 4. The combined impact of sections 2 and 4 were accounted for with the measurements taken on section 5. Section 6 was used to measure the pressure drop over the entire length of the packing without end effects.

The pressure measurements were taken on the boundaries between the sections into which the packing was divided. Pressure tapping 1 through 5 in Figure 42 shows where the pressure measurements were taken. At each pressure tapping position four pressure tapping insertions were made around the circumference of the packing at positions where the packing was open to the flow of water.

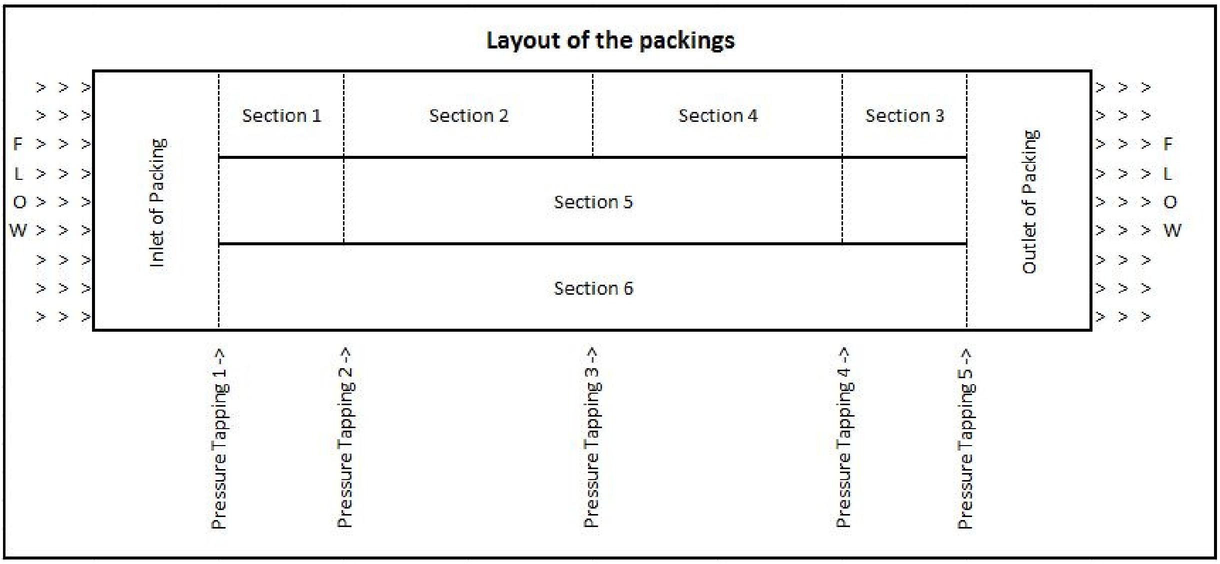

Figure 42: Description of the different sections of the packings.

All the raw data (temperature, differential pressure and flow rate) obtained by means of the DAQ system, combined with the fluid properties of water, were used to calculate the friction factors, modified Reynolds numbers and experimental errors for each section of each packing tested. It was possible to conduct all the experiments for modified Reynolds numbers ranging from about 10,000 to 85,000. This is well above the 50,000 modified Reynolds number required according

to the URS (URS-1). This means that all of the experiments were done in the turbulent flow range. To simplify the experimental procedure the increments in which the experiment was done depended on the flow rate through the packing. The measurements were done on flow increments of 100 and 200 dm^3/min. The fluid properties were calculated with the use of EES software and are shown in Table 10 below. For a change in temperature from 15°C to 60°C the density changes by 1.59% and the viscosity changes with 59%.

Table 10: Fluid property variation with water temperature.

Temp (°C)	**Density (kg/m^3)**	**Viscosity (kg/ms)**
15.00	999.20	0.00114
18.21	998.70	0.00105
21.43	998.00	0.00097
24.64	997.20	0.00090
27.86	996.40	0.00084
31.07	995.40	0.00078
34.29	994.30	0.00073
37.50	993.20	0.00069
40.71	992.00	0.00064
43.93	990.70	0.00061
47.14	989.40	0.00057
50.36	987.90	0.00054
53.57	986.40	0.00052
56.79	984.90	0.00049
60.00	983.30	0.00047

For an experiment to be valid, it must be proven to be repeatable. Therefore the experiments done on the random and structured packings were repeated three times to check the repeatability of the experiments. After each of the experimental repetition the test facility would be switched off and the water would be drained. A waiting period of at least three hours would pass before the next experiment was conducted on the test facility.

It is also important to compare the results obtained during an experiment with predicted values obtained from correlations derived from other sources. In the case of the pressure drop through

a random packing of spheres the Ergun (1952) (Eq (3)) and the KTA (1981) (Eq (1)) correlations were chosen for comparison. The correlation of Wentz and Thodos (1963) (Eq (2)) was chosen for comparison with the experimental data obtained from the tests done on the structured packing.

Each measurement point on all the graphs, representing the hydrodynamic behaviour of the random and structured packings, is an average of 26 measured values. The standard deviation of the 26 pressure drop measurements is indicated in all the graphs in section 6.2. Once the desired flow rate was attained the readings were allowed to stabilise and then 26 continuous measurements were logged with Labview. Labview was programmed to take a measurement every second. The number of 26 was chosen because it is the number of continuous measurements that could be made for each point while still having enough time to be able to complete a whole set of measurement before the water temperature reaches 60℃. All the dimensionless properties and errors were then calculated for each of the 26 measured points where after they were averaged to give the results as illustrated in the graphs in sections 6.3, 6.4, 6.5 and 6.6.

The accuracy of the DAQ system for the first two test runs was less than that of the third test run. The reason for the experimental accuracy of the third test run being higher than the other two test runs is due to the fact that for the third test run only two shunt resistors with 99% tolerance was used instead of the 6 shunt resistor with a tolerance of 90% as with the first two test runs for each of the meters.

6.2 REPEATABILITY

The repeatability of the experiments done with the random and structured packings will be discussed in this section. The average standard deviation of the 26 measured points for a few of the tests done with the random and structured packings can be seen in APPENDIX B. For both the random and structured packings, the graphs of sections 1, 2 and 4 are shown for the purpose of illustration. These sections were chosen because they represent the inlet and the core of the packings. Not all of the test runs had the same amount of measurement points. This was due to the fact that the water temperature reached 60℃ before the test runs could be completed.

The average standard deviation of the pressure drop measurements made for the random packing was 0.91%. The minimum and maximum standard deviations that were calculated for all the experimental runs of the random packing were 0.10% and 2.73% respectively. This shows that the tests that were done on the randomly packed bed have good repeatability. Shown in Figure 43 to Figure 45 are the graphical comparisons of the three pressure drop tests that were done for sections 1, 2 and 4 respectively. Also shown in the graphs are the standard deviations of each point in the form of error bars. The graphs for sections 3, 5 and 6 are shown in Figure 74 to Figure 76 in Appendix A.

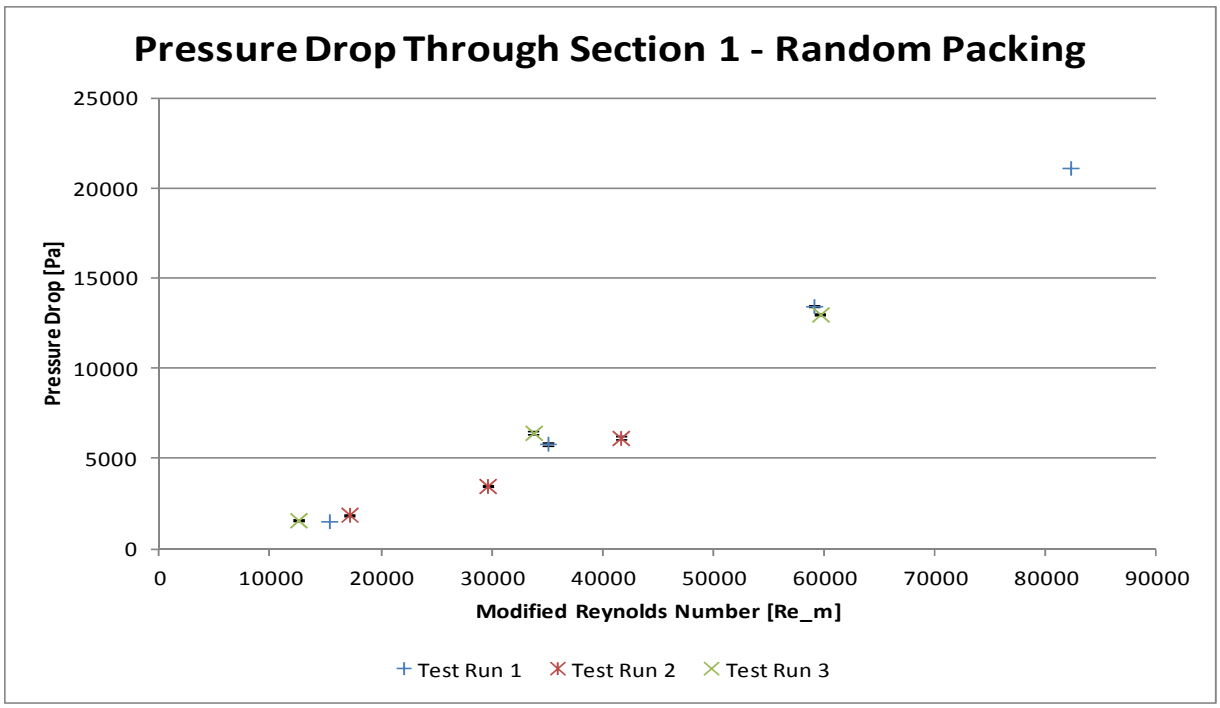

Figure 43: Pressure drop through section 1 of the random packing with standard deviation error bars.

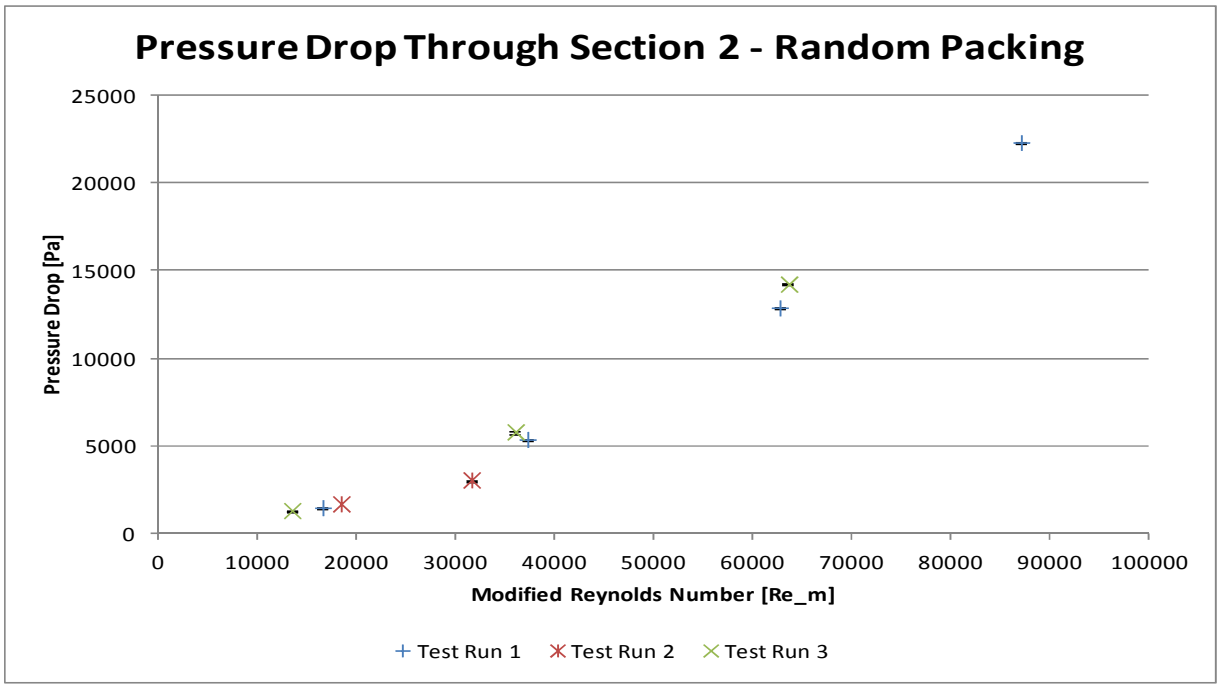

Figure 44: Pressure drop through section 2 of the random packing with standard deviation error bars.

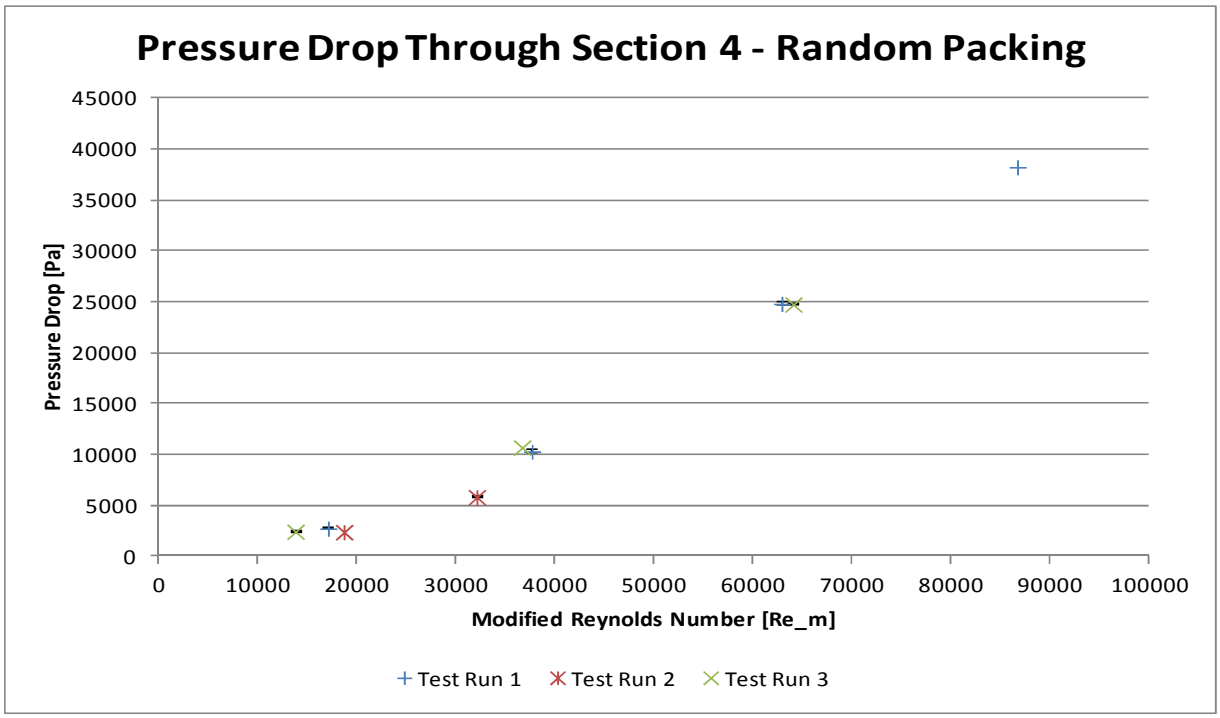

Figure 45: Pressure drop through section 4 of the random packing with standard deviation error bars.

The average standard deviation of the pressure drop measurements made was 0.74%. The minimum and maximum standard deviations that were calculated for all the experimental runs were 0.00% and 3.07% respectively. This shows that the tests that were done on the structured packed bed have good repeatability. Shown in Figure 46 to Figure 48 are the graphical comparisons of the three pressure drop tests that were done for sections 1, 2 and 4 respectively. Also shown in the graphs are the standard deviations of each point in the form of error bars. The graphs for sections 3, 5 and 6 are shown in Figure 80 to Figure 82 in Appendix A.

With the repeatability being proven for the experiments done with the two packings the results in the form of the dimensionless parameters will now be presented. These results will also be compared to friction factors predicted by trusted correlations from the literature.

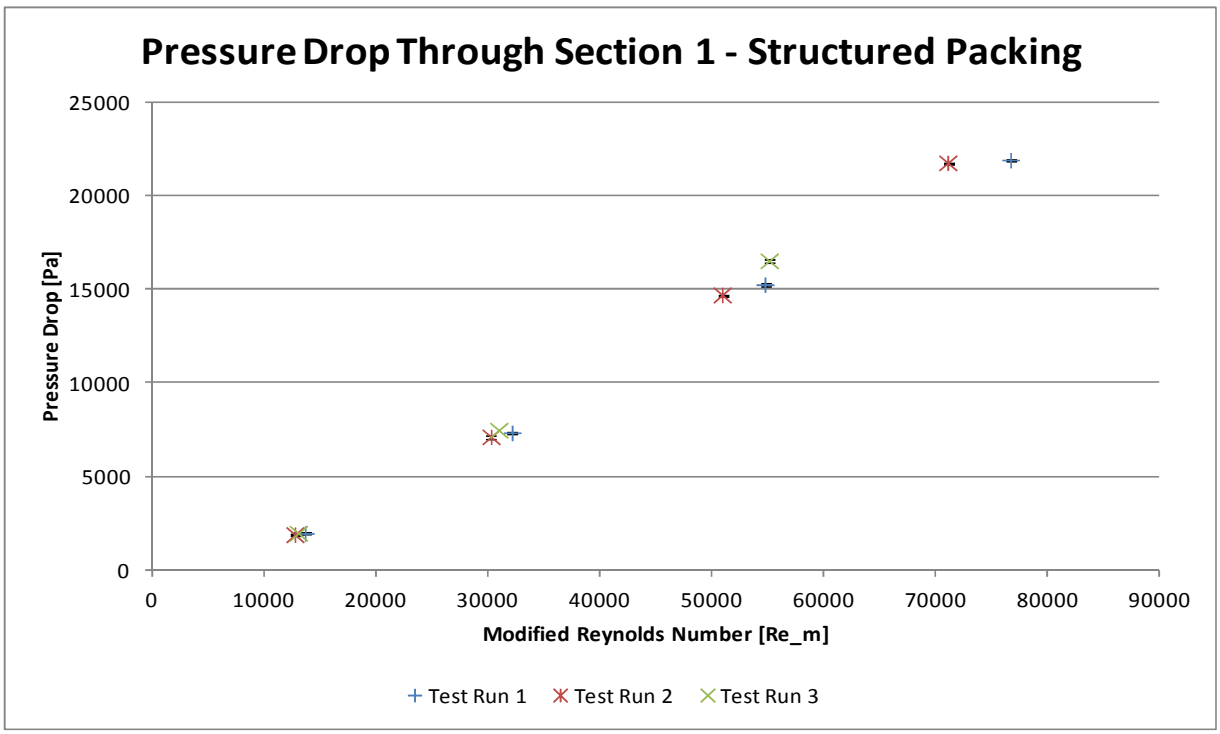

Figure 46: Pressure drop through section 1 of the structured packing with standard deviation error bars.

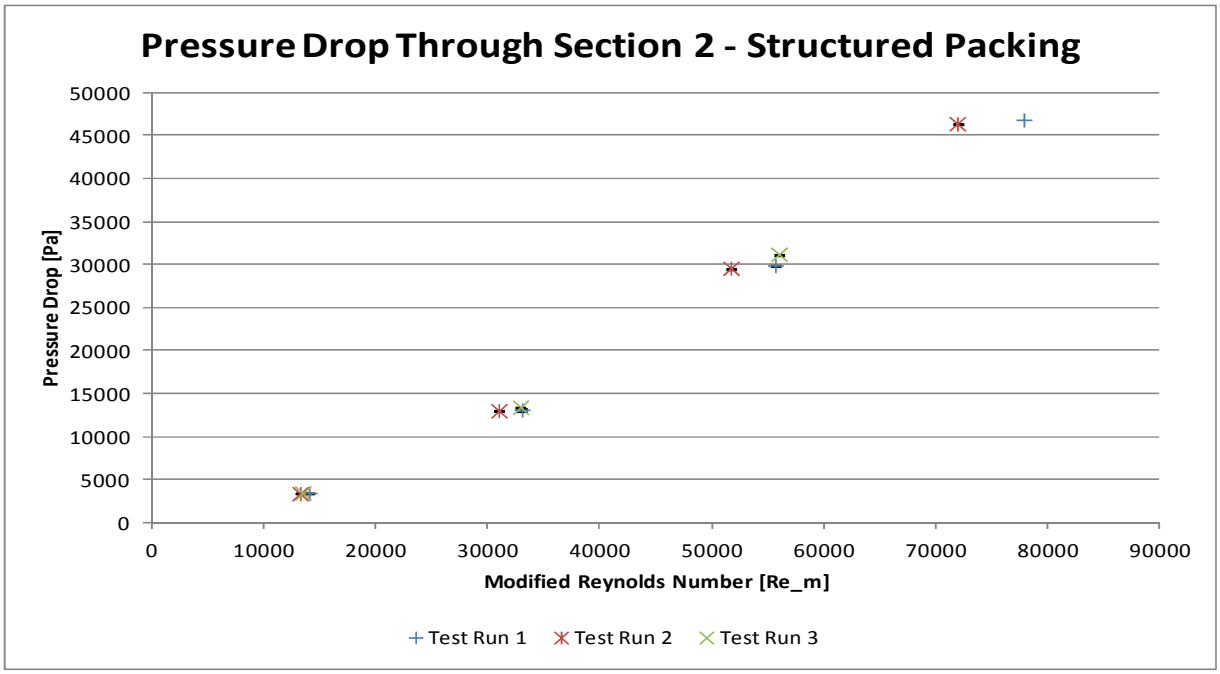

Figure 47: Pressure drop through section 2 of the structured packing with standard deviation error bars.

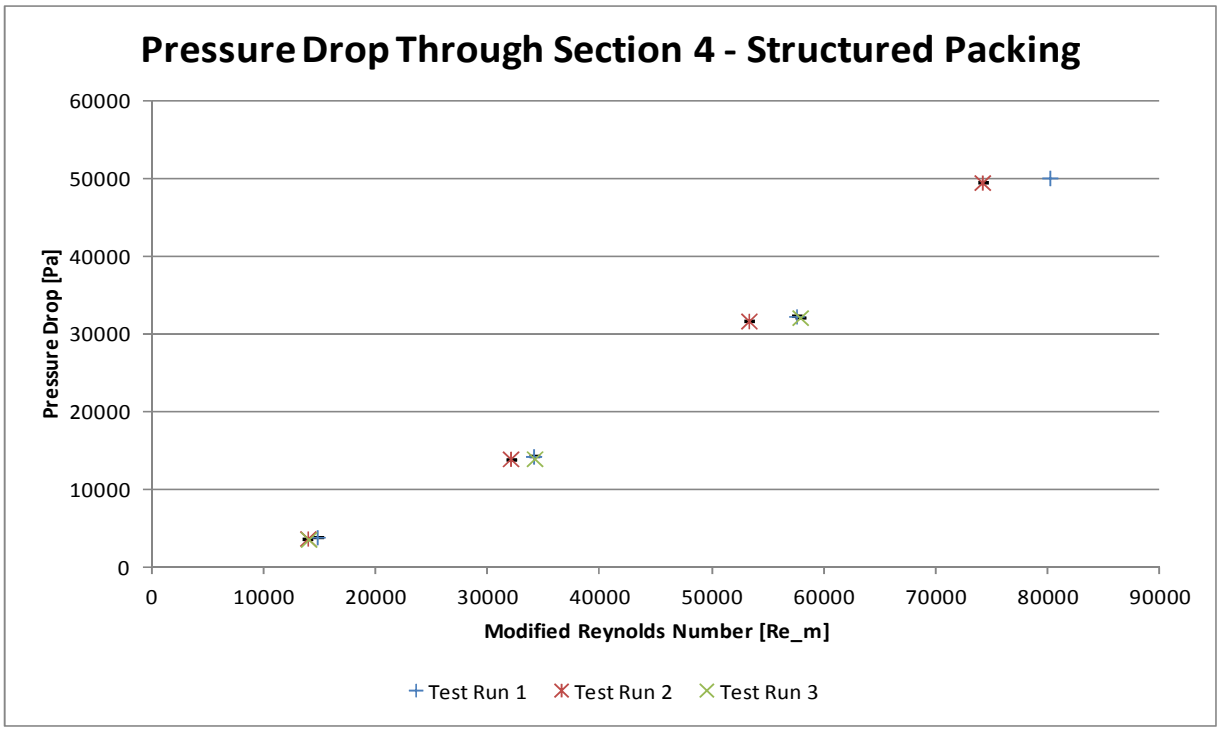

Figure 48: Pressure drop through section 4 of the structured packing with standard deviation error bars.

6.3 UNCERTAINTY ASSESSMENT

An example of how the uncertainties were calculated for the experimental results obtained during this experiment will be shown in this section. The principles discussed in chapter 3 for conducting an uncertainty assessment on experimental data, was used. Firstly, an example will be given of how the bias errors for the individual measurement instrumentation were calculated. These bias errors were calculated using Eq (20), (21) and (22) in section 3.2.1.

The bias errors was firstly converted to bias limits for a normal distribution with a confidence level of 95%. This was done by multiplying it by 2 (coverage factor) and dividing it by $\sqrt{6}$. All of the bias errors affecting each meter had to be taken into consideration. These errors included the accuracy of the meter, as well as the errors of the DAQ system. The bias errors of each meter was added by the RSS method as illustrated in Eq (21) in section 3.2.1 and shown in Table 11. The point that was chosen for that purpose of illustration was measurement point 1 of section 1 of the random packing's third test run. The first differential pressure transmitter with a

range of 0-100 mbar was chosen for the illustration in Table 11. The bias errors for all the other meters were calculated in exactly the same manner as explained above.

Table 11: Example of bias error calculation of a meter.

Section 1 - Test Run 3 - Point 1		
Bias Error		
Differential Pressure Transmitter - 0...100mbar		
Meter Error	0.075%	
100Ohm Error	1.000%	
150Ohm Error	1.000%	
Total Error	1.156%	Eq (20) & Eq (21)
Error on Set Span	1.156323196	mbar
	115.6323196	Pa

In order to determine the total bias error for each of the measurements, Eq (22) in section 3.2.1 was used. The combination of the bias errors of all the meters had to be used to determine the total bias error of the final result. The sensitivity coefficient for each of the variables in the DRE also had to be determined in order to calculate the total bias error of a measurement. The DRE for this experiment is given in Eq (27). The sensitivity coefficients for the pressure drop, flow velocity and the fluid density are given in Eq (28), (29) and (30) respectively.

$$DRE = \varphi = 2\frac{\Delta P}{\rho V_o^2}\left(\frac{\varepsilon^3}{1-\varepsilon}\right)\frac{d_p}{L} \tag{27}$$

$$\theta_{\Delta P} = \frac{\partial \varphi}{\partial \Delta P} = 2\frac{1}{\rho V_o^2}\left(\frac{\varepsilon^3}{1-\varepsilon}\right)\frac{d_p}{L} \tag{28}$$

$$\theta_{\rho} = \frac{\partial \varphi}{\partial \rho} = -2\frac{1}{\rho^2 V_o^2}\left(\frac{\varepsilon^3}{1-\varepsilon}\right)\frac{d_p}{L} \tag{29}$$

$$\theta_{V_o} = \frac{\partial \varphi}{\partial V_o} = -4\frac{1}{\rho V_o^3}\left(\frac{\varepsilon^3}{1-\varepsilon}\right)\frac{d_p}{L} \tag{30}$$

The combination of the sensitivity coefficients and the bias errors for each of the measurements, as shown by Eq (22) in section 3.2.1, were then used to calculate the total bias error for the measurement made. The column labelled as $B_{e\ Total}$ in Table 12 shows the total bias error as

calculated with Eq (22) in section 3.2.1. The value in green at the bottom of that column is the average bias error of the 26 measurement points that were taken at that specific condition.

The precision errors for each of the variables in the DRE were calculated in the same way as was shown in Table 11. The only difference is that the standard deviations calculated in Table 12 were multiplied by a coverage factor of 2 to convert it to a precision limit with a 95% confidence level. The total precision errors were calculated using Eq (19) in section 3.2. The sensitivity coefficients, as described in Eq (28) to (30), and the standard deviations, as calculated in Table 19 and Table 20, would both be needed in the determination of the total precision error. The precision errors for each of the 26 measured points are given in the column labelled as $P_{e\,\psi}$ in Table 12. The value at the bottom of that column is the average precision error for all of the 26 measured points.

The total uncertainty of each of the 26 measurements taken was calculated with the help of Eq (23) in section 3.2.2 where the RSS method is used to combine the effects of the two errors on the total error. The column labelled as U_{total} gives the total uncertainty of each measurement point. The bottom of that column provides the average uncertainty of all 26 measured points. The average uncertainty of 8.61% was predicted for the 26 measurement points under consideration.

Table 12: Measurement results for the random packing; test run 3, section 1, measurement point 1.

	Measured Variables				Constants			Sensitivity Coefficients			Bias Errors				Precision Errors				Final Results		
	ΔP [Pa]	ρ [kg/m3]	μ [Ns/m]	V_o [m/s]	Ɛ [-]	L [m]	dp [m]	dΨ/dΔP	dΨ/dρ	dΨ/dVo	B_e_ΔP	B_e_Vo	B_e_ρ	B_e_Total	P_e_ΔP	P_e_Vo	P_e_ρ	P_e_ψ	U_total	Re_o [-]	Ψ [-]
1	1587.5	997.5	0.0009	0.2119	0.4350	0.09	0.03	0.00217	-0.00345	-32.50	115.8	0.0138	50.2	0.2933	345.9	4.88E-08	1.33E-02	0.0048	0.2934	12398.9	3.44
2	1601.0	997.5	0.0009	0.2123	0.4350	0.09	0.03	0.00216	-0.00347	-32.58	115.8	0.0138	50.2	0.2941	26.2	4.07E-07	1.33E-02	0.0047	0.2942	12416.4	3.46
3	1621.9	997.5	0.0009	0.2120	0.4350	0.09	0.03	0.00217	-0.00352	-33.13	115.8	0.0138	50.2	0.3023	251.3	1.37E-07	1.33E-02	0.0048	0.3023	12413.1	3.51
4	1639.4	997.5	0.0009	0.2119	0.4350	0.09	0.03	0.00217	-0.00356	-33.56	115.8	0.0138	50.2	0.3086	1110.6	4.88E-08	1.33E-02	0.0048	0.3087	12416.7	3.55
5	1607.5	997.4	0.0009	0.2116	0.4350	0.09	0.03	0.00217	-0.00350	-33.03	115.8	0.0138	50.2	0.3013	1.9	2.20E-09	2.37E-04	0.0048	0.3013	12420.4	3.49
6	1607.0	997.4	0.0009	0.2115	0.4350	0.09	0.03	0.00218	-0.00351	-33.06	115.8	0.0138	50.2	0.3018	0.8	1.86E-08	2.37E-04	0.0048	0.3018	12413.8	3.50
7	1594.0	997.4	0.0009	0.2118	0.4350	0.09	0.03	0.00217	-0.00347	-32.65	115.8	0.0138	50.2	0.2955	146.6	3.66E-08	2.37E-04	0.0048	0.2955	12422.0	3.46
8	1590.0	997.4	0.0009	0.2114	0.4350	0.09	0.03	0.00218	-0.00347	-32.76	115.8	0.0138	50.2	0.2975	259.2	5.09E-08	2.37E-04	0.0048	0.2975	12414.0	3.46
9	1586.5	997.4	0.0009	0.2112	0.4350	0.09	0.03	0.00218	-0.00347	-32.79	115.8	0.0138	50.2	0.2982	384.0	2.15E-07	2.37E-04	0.0048	0.2983	12404.2	3.46
10	1608.2	997.4	0.0009	0.2116	0.4350	0.09	0.03	0.00217	-0.00351	-33.06	115.8	0.0138	50.2	0.3017	4.5	5.89E-09	2.37E-04	0.0048	0.3018	12432.4	3.50
11	1594.0	997.3	0.0009	0.2115	0.4350	0.09	0.03	0.00218	-0.00348	-32.80	115.8	0.0138	50.2	0.2980	146.6	1.86E-08	7.16E-03	0.0048	0.2981	12584.1	3.47
12	1597.5	997.4	0.0009	0.2115	0.4350	0.09	0.03	0.00218	-0.00349	-32.88	115.8	0.0138	50.2	0.2992	74.2	2.76E-08	2.37E-04	0.0048	0.2993	12442.4	3.48
13	1618.2	997.4	0.0009	0.2118	0.4350	0.09	0.03	0.00217	-0.00352	-33.18	115.8	0.0138	50.2	0.3033	146.6	1.04E-08	2.37E-04	0.0048	0.3033	12470.6	3.51
14	1627.9	997.4	0.0009	0.2119	0.4350	0.09	0.03	0.00217	-0.00354	-33.33	115.8	0.0138	50.2	0.3053	477.1	4.88E-08	2.37E-04	0.0048	0.3053	12483.2	3.53
15	1608.2	997.4	0.0009	0.2111	0.4350	0.09	0.03	0.00218	-0.00352	-33.29	115.8	0.0138	50.2	0.3054	4.5	3.06E-07	2.37E-04	0.0049	0.3054	12447.3	3.51
16	1606.0	997.4	0.0009	0.2110	0.4350	0.09	0.03	0.00219	-0.00352	-33.28	115.8	0.0138	50.2	0.3054	0.0	4.13E-07	2.37E-04	0.0049	0.3055	12448.9	3.51
17	1620.7	997.4	0.0009	0.2115	0.4350	0.09	0.03	0.00218	-0.00354	-33.36	115.8	0.0138	50.2	0.3061	213.3	2.76E-08	2.37E-04	0.0048	0.3062	12477.0	3.53
18	1601.7	997.4	0.0009	0.2118	0.4350	0.09	0.03	0.00217	-0.00349	-32.83	115.8	0.0138	50.2	0.2982	19.1	1.73E-08	2.37E-04	0.0048	0.2983	12507.1	3.48
19	1606.7	997.3	0.0009	0.2118	0.4350	0.09	0.03	0.00217	-0.00350	-32.95	115.8	0.0138	50.2	0.3000	0.4	1.04E-08	7.16E-03	0.0048	0.3000	12526.5	3.49
20	1572.8	997.4	0.0009	0.2111	0.4350	0.09	0.03	0.00218	-0.00344	-32.55	115.8	0.0138	50.2	0.2949	1110.6	3.06E-07	2.37E-04	0.0048	0.2949	12484.8	3.44
21	1591.5	997.3	0.0009	0.2114	0.4350	0.09	0.03	0.00218	-0.00348	-32.80	115.8	0.0138	50.2	0.2982	213.2	6.52E-08	7.16E-03	0.0048	0.2982	12541.8	3.47
22	1607.0	997.3	0.0009	0.2116	0.4350	0.09	0.03	0.00217	-0.00350	-33.03	115.8	0.0138	50.2	0.3012	0.8	2.20E-09	7.16E-03	0.0048	0.3012	12541.5	3.49
23	1616.5	997.3	0.0009	0.2120	0.4350	0.09	0.03	0.00217	-0.00351	-33.01	115.8	0.0138	50.2	0.3006	107.3	1.60E-07	7.16E-03	0.0048	0.3006	12584.9	3.50
24	1630.9	997.3	0.0009	0.2121	0.4350	0.09	0.03	0.00216	-0.00354	-33.28	115.8	0.0138	50.2	0.3044	616.9	2.11E-07	7.16E-03	0.0048	0.3044	12588.4	3.53
25	1602.0	997.3	0.0009	0.2120	0.4350	0.09	0.03	0.00217	-0.00348	-32.73	115.8	0.0138	50.2	0.2966	17.0	1.37E-07	7.16E-03	0.0048	0.2966	12601.5	3.47
26	1614.0	997.3	0.0009	0.2117	0.4350	0.09	0.03	0.00217	-0.00352	-33.13	115.8	0.0138	50.2	0.3026	61.8	1.80E-09	7.16E-03	0.0048	0.3026	12576.3	3.51
	1606.1	997.4	0.0009	0.2116	0.4350	0.09	0.03	0.0022	-0.0035	-33.0	115.8	0.0138	50.2	0.3005	30.3	0.0007	0.1350	0.0048	**0.3006**	12479.2	3.49

6.4 RANDOM PACKING RESULTS AND DISCUSSION

The results obtained for sections 2, 4 and 5 of the random packing for each of the three test runs are given in Figure 49, Figure 50 and Figure 51 respectively (see section 6.5 for the results of the structured packing). The error bars in these figures indicate the total experimental uncertainty that was calculated for each measurement point.

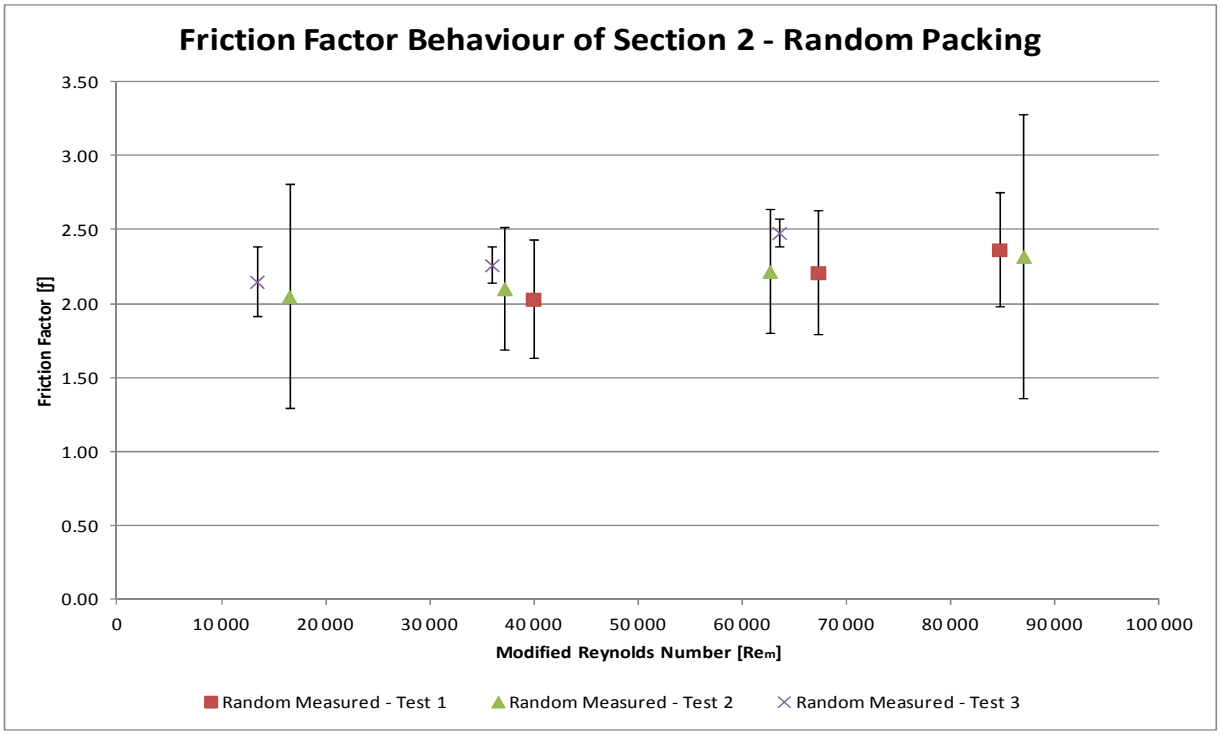

Figure 49: Friction factor behavior for section 2 of the random packing.

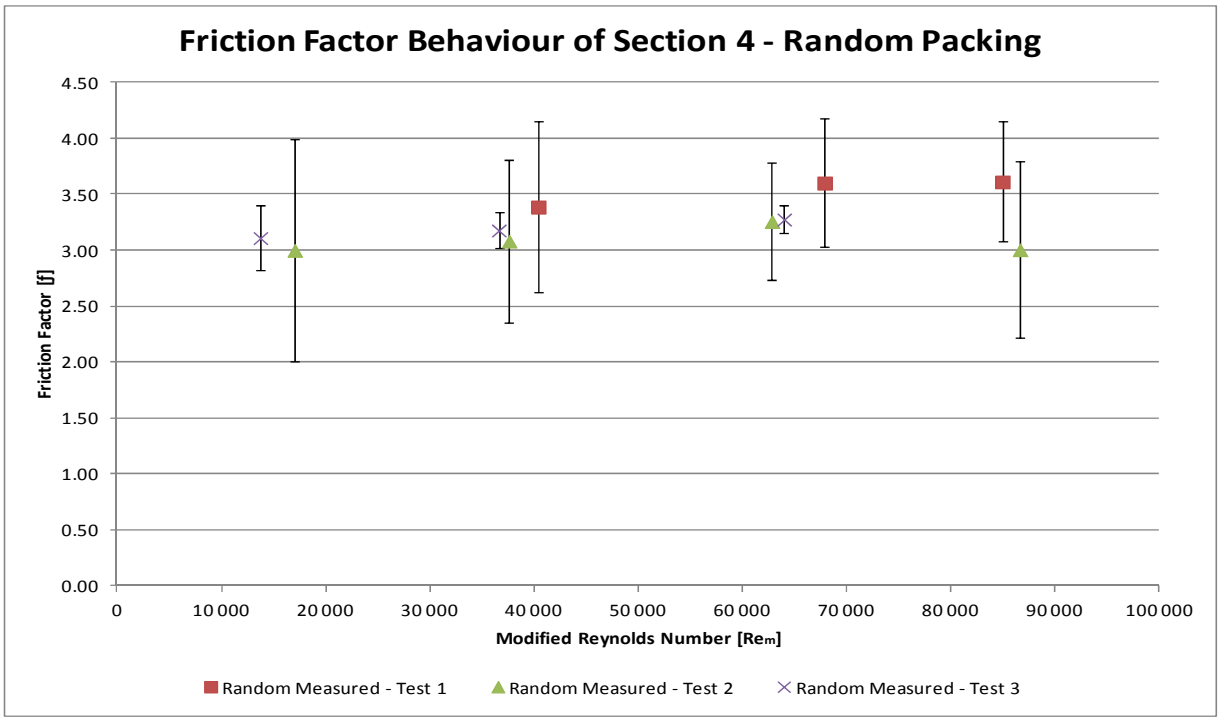

Figure 50: Friction factor behavior for section 4 of the random packing.

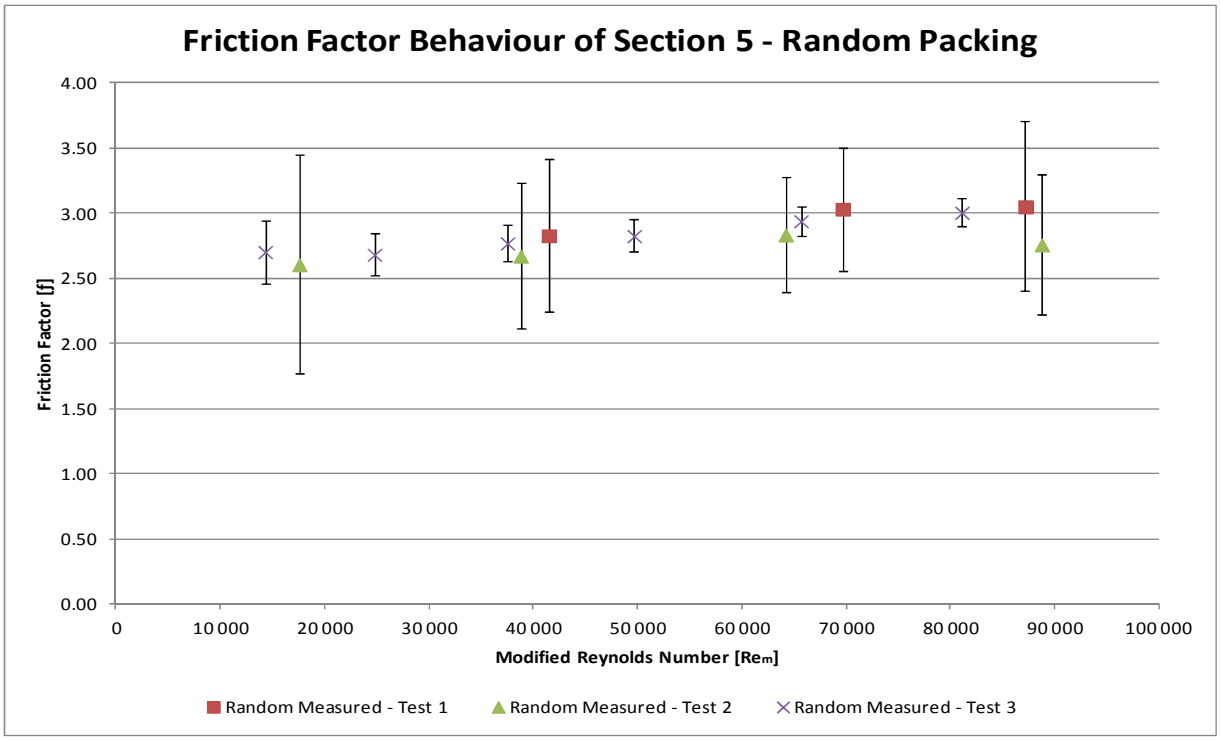

Figure 51: Friction factor behavior for section 5 of the random packing.

The average friction factor ranged between 2 and 2.5 with a constant rise in friction factor as the modified Reynolds number increased for the three test runs of section 2, as indicated in Figure 49. For the first and third test runs of section 4, as indicated in Figure 50, the friction factor seemed to stay constant at about 1.85. The second test run of section 4 seemed to follow the same tendency as the first and third test runs, but had a slightly lower friction factor of approximately 1.82.

The first test run of section 5, as indicated in Figure 51, seemed to give the highest friction factors which starting at 2.8 and increased with increasing modified Reynolds numbers before flattening out at a friction factor of approximately 3. The second and third test runs of section 5 seemed to follow the same tendency, but at lower friction factors. The slight rise in friction factor as the modified Reynolds number increases can also be seen for the other sections of the random packing that were tested. The results for the other sections are shown in Figure 77 to Figure 79 in APPENDIX A.

Test run three of section 1 for the random packing was the only experimental graph of which the friction factor decreased with increasing modified Reynolds numbers. For the remainder of the experimental data, the friction factors showed a slight increase as the modified Reynolds numbers increased. This increase in friction factor with increasing modified Reynolds number was an unexpected result. In the literature, this phenomenon was only encountered in an article by Carman (1937).

Carman (1937) represented many different results found in the literature concerning the packing of spheres and rings. From the results of packings of porcelain rings it was found, in some cases, that the friction factor would increase with an increase in modified Reynolds number. This was also seen for the results of stoneware rings and aluminium rings. Unfortunately the results he presented for spherical particles did not show the same tendency. The results presented by Carman (1937) for rings and spheres were in the laminar range and one cannot predict what its behaviour would have been in the turbulent range. This phenomenon of a slight increase in friction factor with an increase in modified Reynolds number, of the results found in this study, has been seen in the literature. However, it is not clear what the cause is of this phenomenon and further investigation is needed.

Test run three was chosen to be the representative test run for the random packing for comparison with the friction factors predicted by trusted correlations from the literature. The

reason for selecting test run three is that it stretched over the largest range of modified Reynolds numbers $(15{,}000 < Re_m < 85{,}000)$, and had the highest experimental accuracy.

Sections 5 and 6 of the random packing, as shown in Figure 52 and Figure 53, were chosen for comparison with the friction factors predicted by the correlations from the literature. There were two reasons for selecting these two sections. The first reason was that it can be illustrated that the end-effects have been eliminated by allowing the water to pass through the inlet and outlet sections of the packing before entering section 1 and leaving section 3 respectively. It can be seen from Figure 52 and Figure 53 that the profiles of the two experimental data sets look almost exactly similar with an average difference of 2% between each of the data points. It can also be seen that the friction factors for both the graphs range between 2.68 and 3.01. This gives an indication that the end-effects of the random packing had been eliminated and did not affect the experiment in any way.

The second reason for choosing sections 5 and 6 for comparison with the friction factors predicted by the correlations from the literature was because they represent the bulk of the packed bed used in the experiment.

When the results obtained for sections 5 and 6 of the random packing was compared with the friction factors predicted by the Ergun (1952) and KTA (1981) correlations, it was found to be higher. The results obtained from the experiment was on average 39% and 26% higher than that predicted by the Ergun (1952) and KTA (1981) correlations respectively. Such a large difference between the experimental and theoretical results was unexpected. A discussion of this phenomenon will follow in section 6.6.

The estimated error that was made during the course of the experiment is at an average of 5.2% for the entire range of measurements made. The maximum estimated error that was made during the course of the experiment was 8.9%. This uncertainty is within the 10% error limit as specified by the URS. The experimental data from which all the graphs for the random packing were constructed can be seen in Table 13 to Table 15 in APPENDIX B.

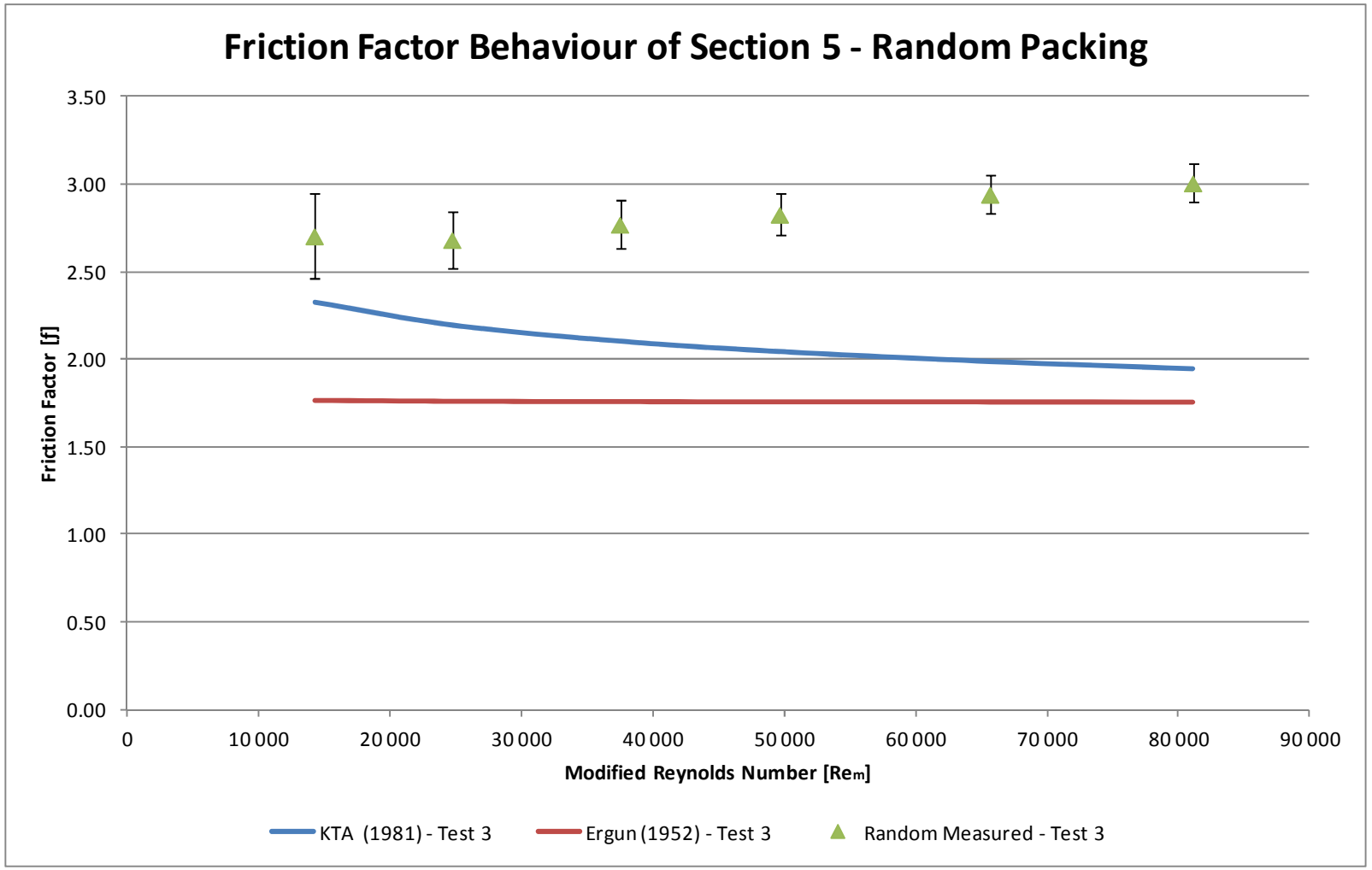

Figure 52: Friction factor behavior for section 5 of the random packing compared with the Ergun (1952) and KTA (1981) relations.

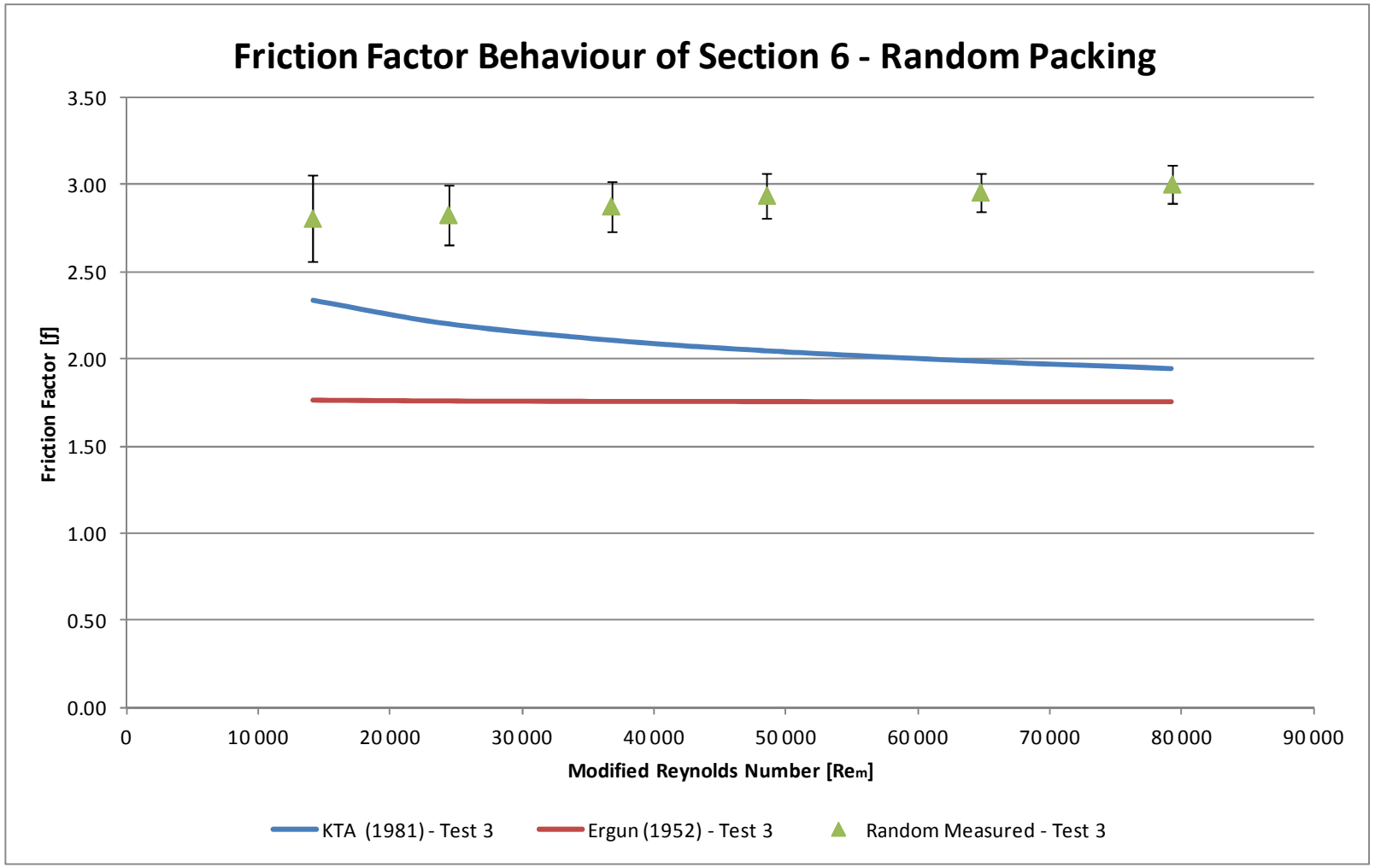

Figure 53: Friction factor behavior for section 6 of the random packing compared with the Ergun (1952) and KTA (1981) relations.

6.5 STRUCTURED PACKING RESULTS AND DISCUSSION

The results obtained for sections 2, 4 and 5 of the structured packing for each of the three test runs are given in Figure 54, Figure 55 and Figure 56 respectively. The error bars in these figures indicate the total experimental uncertainty that was calculated for each measurement point.

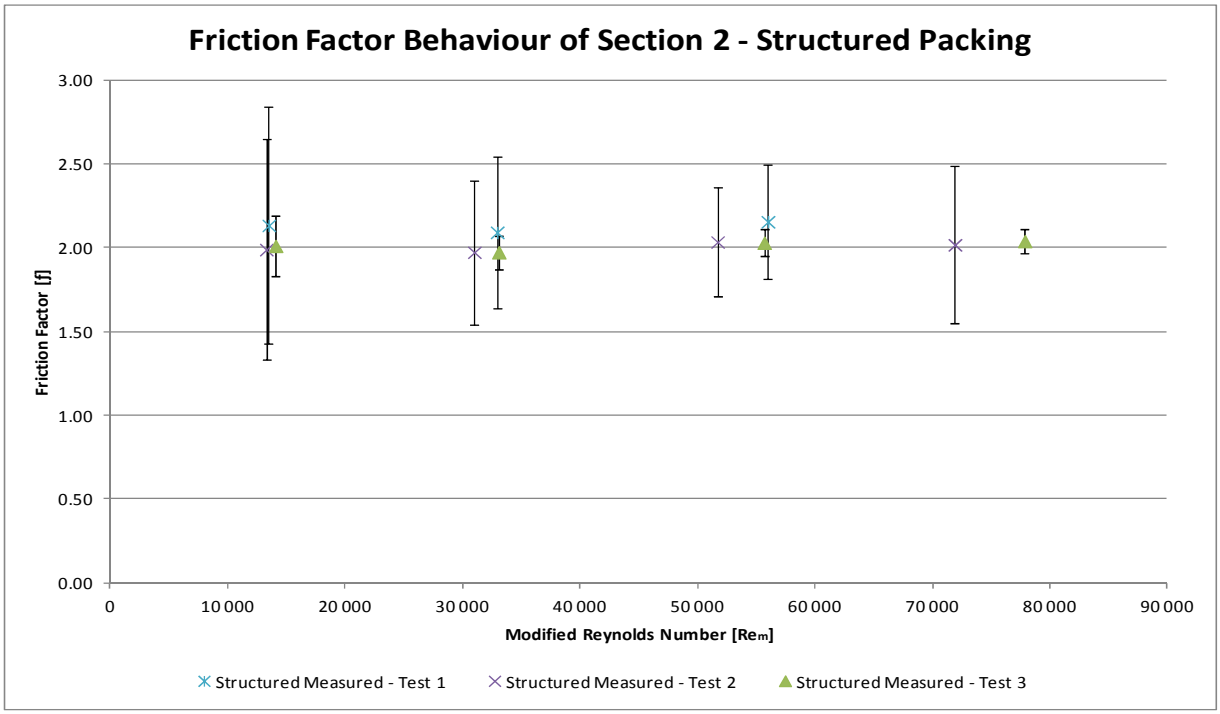

Figure 54: Friction factor behavior for section 2 of the structured packing.

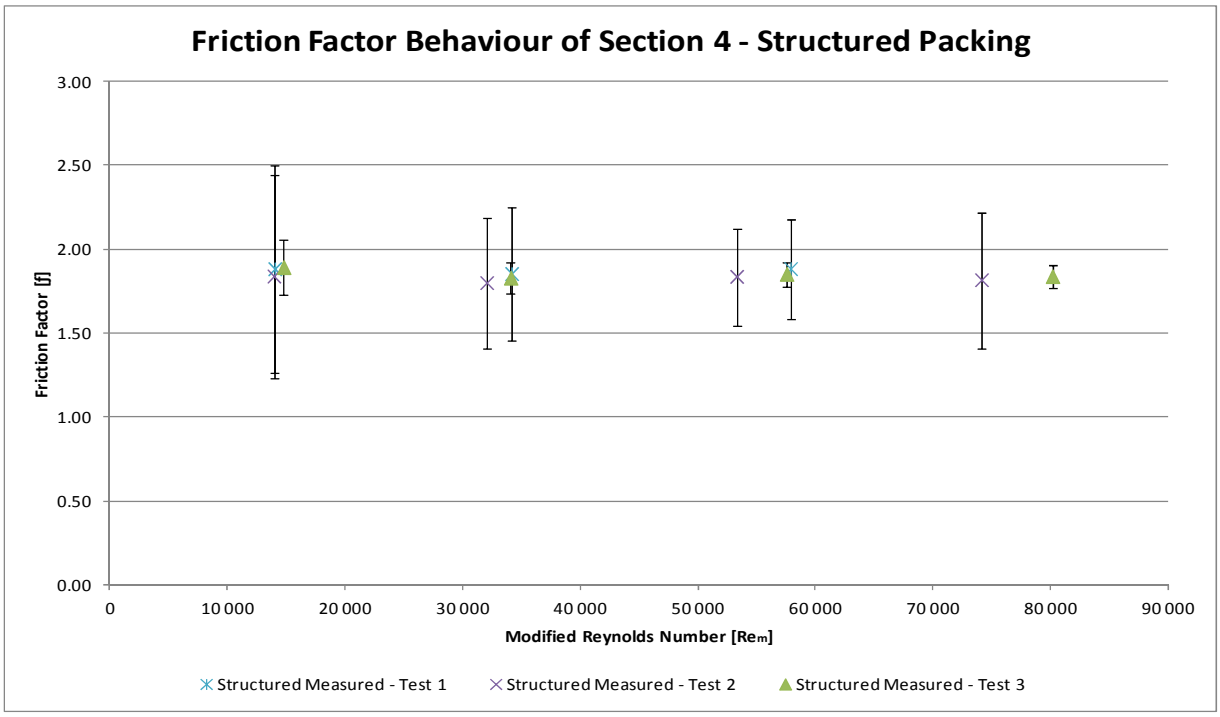

Figure 55: Friction factor behavior for section 4 of the structured packing.

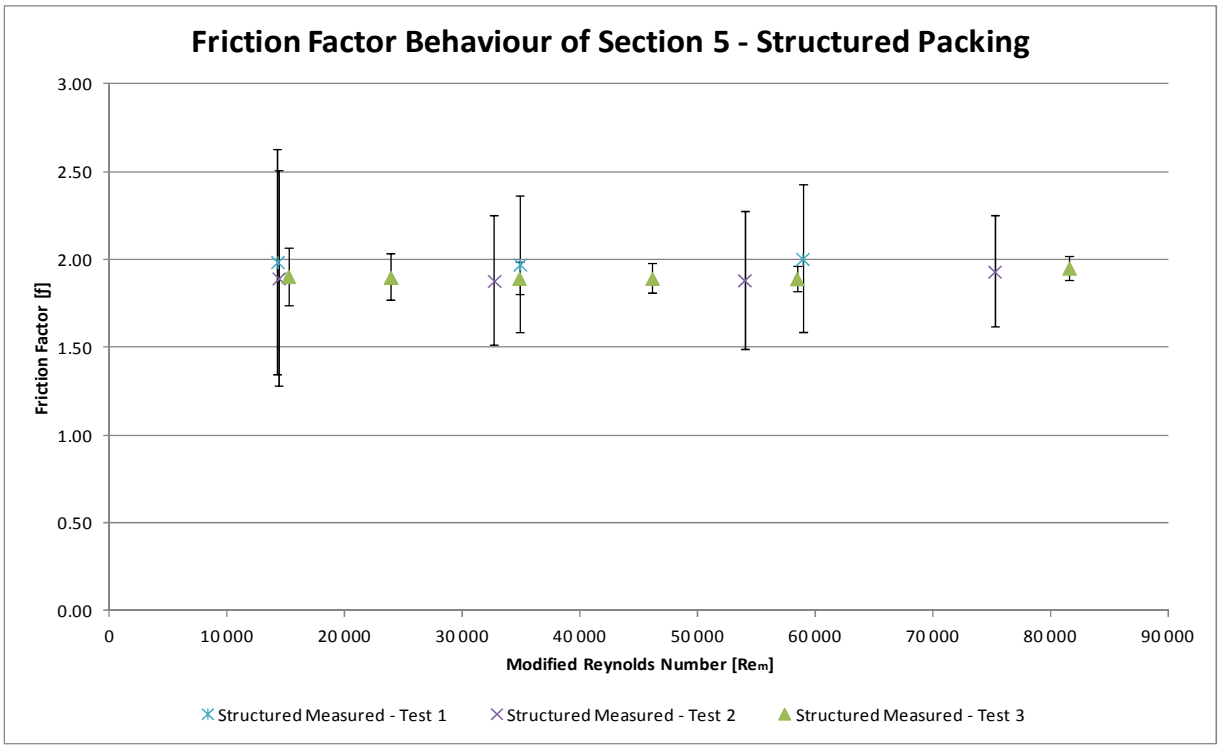

Figure 56: Friction factor behavior for section 5 of the structured packing.

For the first test run of section 2, the friction factor seemed to be almost constant at approximately 2.1 with the slightest of increase in the friction factor as the modified Reynolds number increased. The friction factors for the second and third test runs had the same tendency as the first test run which was to have a very slight increase with increasing modified Reynolds number. The friction factor for test runs two and three ranged from 2 to just above 2.

For all three the test runs of section 4 the friction factor seemed to follow the same pattern. As the modified Reynolds number increased to approximately 35,000 the friction factors decreased slightly. The friction factors of the three test runs then starts to increase again up to a modifies Reynolds number of 60,000. Beyond this point the friction factors of the second and third test runs decreased again with increasing modified Reynolds numbers. Throughout the test runs of section 4 the friction factor stayed in the average range of 1.85.

The test runs of section 5 seemed to stay constant for modified Reynolds numbers ranging up to about 55,000. Beyond this point the friction factors seemed to increase again with increasing modified Reynolds numbers. For the first test run the friction factors was at an average of 2.01. The friction factors of the second and third experimental runs the friction factors seemed to stay constant at about 1.87 after which it raised to a maximum of 1.92.

Test run three was chosen to be the representative test run for the structured packing for comparison with the friction factors predicted by trusted correlations from the literature. The reason for selecting test run three is because it stretched over the largest range of modified Reynolds numbers $(15{,}000 < Re_m < 85{,}000)$, and had the highest experimental accuracy.

Sections 5 and 6 of the structured packing were chosen for comparison with the friction factors predicted by the correlations from the literature. The graphs containing the comparisons can be seen in Figure 57 and Figure 58. There were two reasons for choosing these two sections. The first reason was that it could be illustrated that the end-effects have been eliminated by letting the water pass through the inlet and outlet sections of the packing before entering section 1 and leaving section 3 respectively. It can be seen from Figure 57 and Figure 58 that the profiles of the two experimental data look almost exactly alike with an average difference of 0.53% for each of the data points. It can also be seen that the friction factors for the experimental data of both the experiments range between 1.89 and 1.95. This gives an indication that the end-effects of the random packing had been eliminated and did not affect the experiment in any way. The second reason for choosing sections 5 and 6 for comparison with the friction factors

predicted by the correlations from the literature was because they represent the bulk of the packed bed used in the experiment.

When the results obtained for sections 5 and 6 of the structured packing was compared with the friction factors predicted by the correlation of Wentz and Thodos (1963), it was found to be higher. The results obtained from the experiment are on average 57.5% higher than that predicted by the correlation of Wentz and Thodos (1963).

One of the reasons for the structured packing having a higher friction factor than expected could be the distensions used to separate the spheres. Wentz and Thodos (1963) also used distended packings. The diameter of the distensions they used was 0.45 mm in diameter; whereas the distensions used for the structured packing in this study is 2 mm in diameter. This restriction in the flow could account for a somewhat higher friction factor. A further discussion of this phenomenon will follow in section 6.6.

The estimated error that was made during the course of the experiment is at an average of 5.4% for the entire range of measurements made. The maximum estimated error that was made during the course of the experiment was 8.7%. This uncertainty is within the 10% error limit as specified by the URS. The experimental data from which all the graphs for the random packing were constructed can be seen in Table 16 to Table 18 in APPENDIX B.

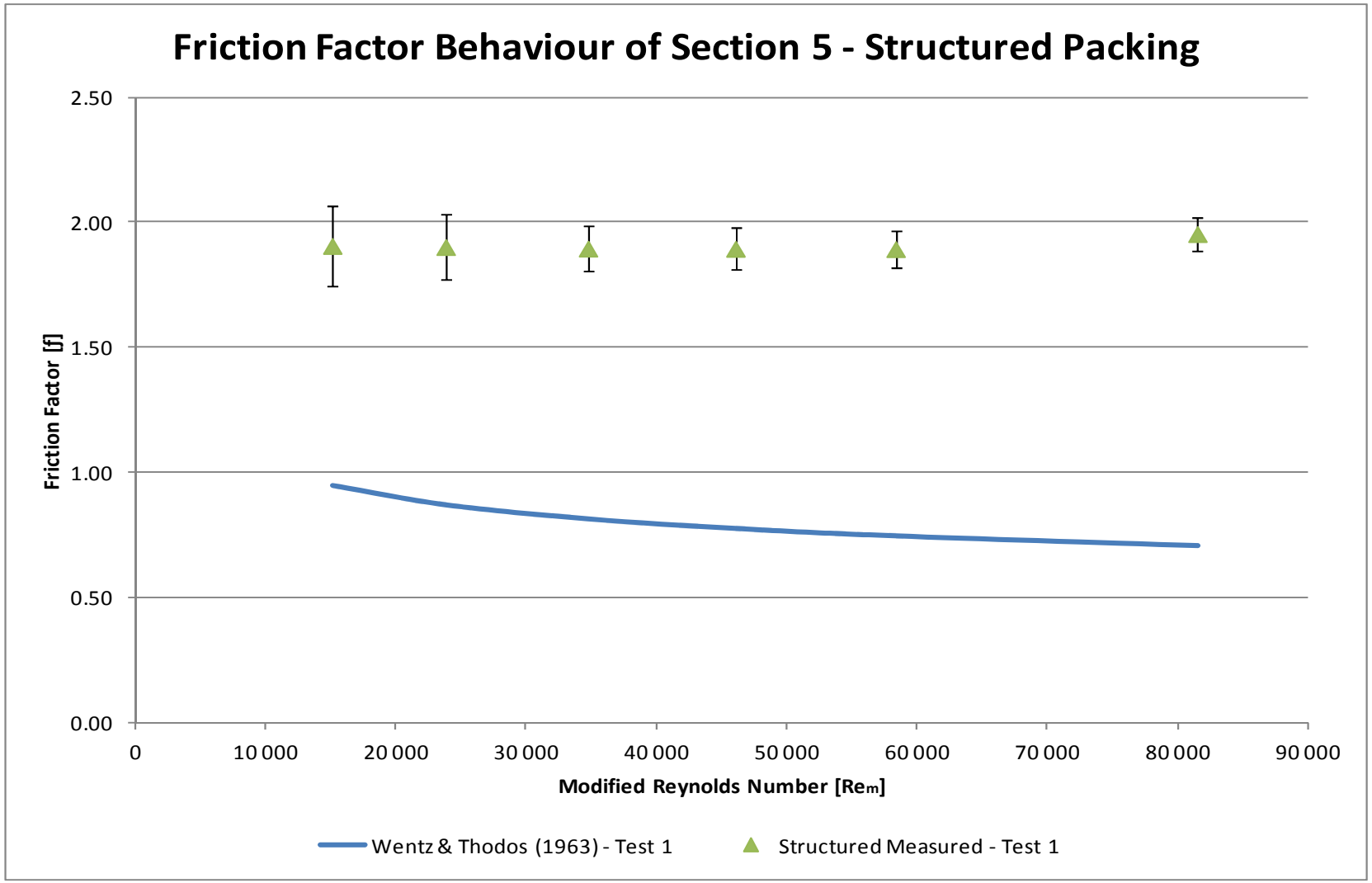

Figure 57: Results for section 5 of the structured packing compared with the relation of Wentz and Thodos (1963).

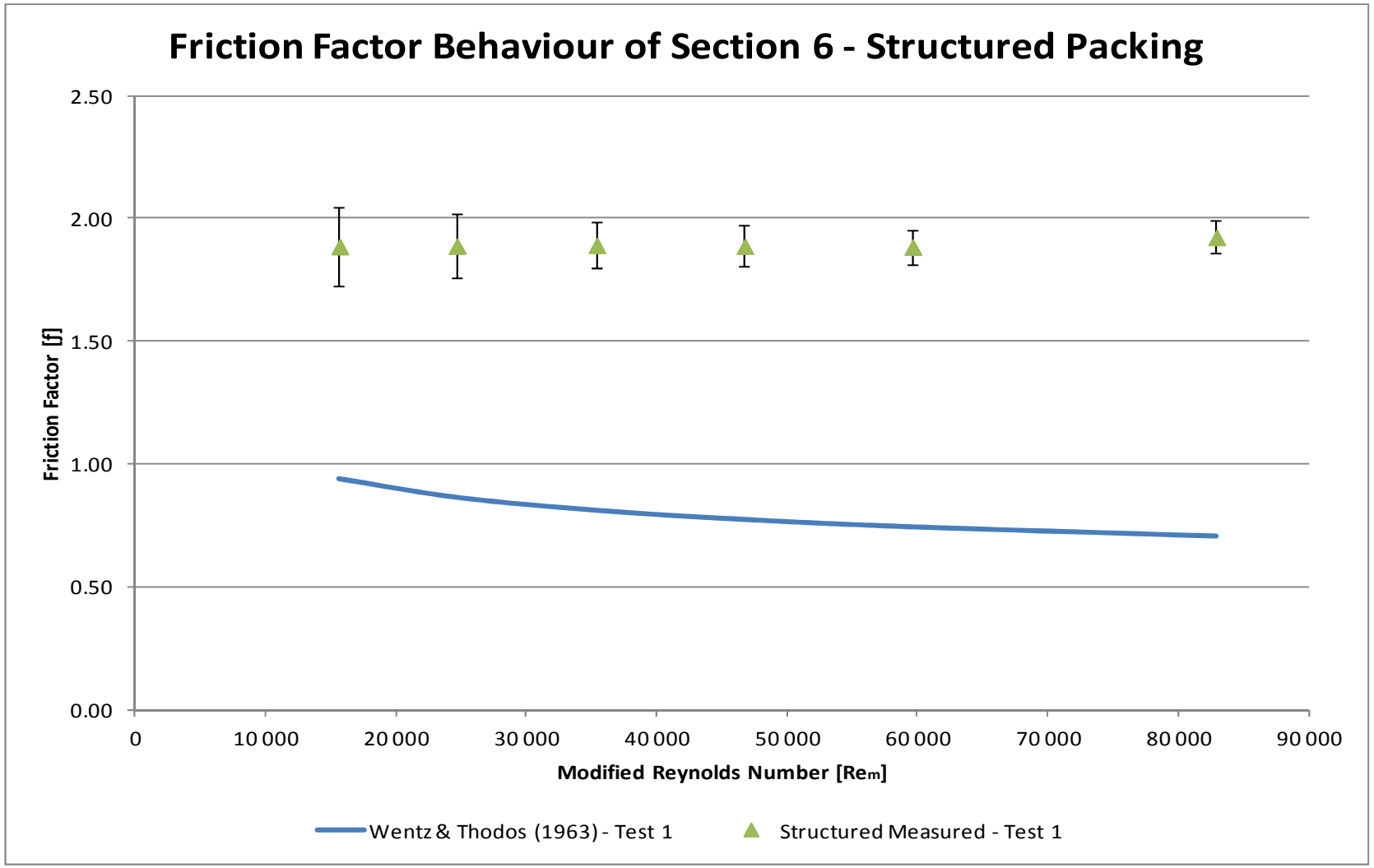

Figure 58: Results for section 6 of the structured packing compared with the relation of Wentz and Thodos (1963).

6.6 COMBINED RESULTS AND DISCUSSION

When considering the effects of structuredness on the pressure drop through a packed bed of spheres it was expected that the geometrically ordered packing would cause a smaller pressure drop than that of a random packing. In Figure 59 and Figure 60 the combined results for the random and structured packings are given. The expected friction factors as predicted by the KTA (1981) correlation (for comparison with the friction factors derived from the experimental data of the experiments done on the random packing) and the friction factors predicted by the correlation of Wentz and Thodos (1963) (for comparison with the friction factors derived from the experimental data of the experiments done on the structured packing) are also provided in Figure 59 and Figure 60.

The experimental results confirm that the pressure drop through a geometrically structured packing would be less than that of a random packing. However, the experimental results for the random and the structured packings were much higher than the expected results as predicted by the KTA (1981) correlation and the correlation of Wentz and Thodos (1963) respectively.

The results from the experiment done on the random packing were on average 26% higher than the results predicted by the KTA (1981) correlation. It can also be seen from Figure 59 that the friction factor seemed to increase as the modified Reynolds number increased. This was an unexpected occurrence as the KTA (1981) correlation predicted a decrease in the friction factor with an increase in the modified Reynolds number.

The experimental results from the structured packing showed that the friction factor remains constant through the largest part of the range of modified Reynolds numbers with a slight increase at the end. The results predicted by the correlation proposed by Wentz and Thodos (1963) also seemed to be quite constant but with a slight decrease in friction factor as the modified Reynolds number increased. There seemed to be some agreement between the profiles of the structured packing and the profile of the graph from the correlation of Wentz and Thodos (1963).

As with the results from the random packing the experimental results from the structured packing was also much higher than the predicted values. On average the experimental results from the structured packing was 57.4% higher than that predicted by the correlation of Wentz and Thodos (1963).

The phenomenon of the increasing friction factors with increasing modified Reynolds numbers was mentioned in sections 6.4 and 6.5. Carman (1937) found that for some ring type packings (Porcelain, stoneware and aluminium), an increasing friction factor occurred with an increasing modified Reynolds number. Unfortunately the same tendency was not found for packings of spheres. This phenomenon was also only encountered by Carman (1937) in the laminar flow range.

It was not expected that the pressure drop through the random and structured packings should be so much higher than the values predicted by the correlations found in the literature as was found in this experiment. One of the physical parameters that could have contributed to the two packed beds having such high friction factor could be the surface finish of the particles that were used. The surface finish was very rough as a result of the manufacturing process, which was rapid prototyping. The layers of plastic, from which the packings were constructed, were 0.5 mm thick. This meant that over the curvature of a sphere grooves formed that was 0.5 mm deep. Therefore the surface finish of the spheres that formed the packings under consideration was very rough.

The surface finishes of the particles that were used in the literature were predominantly smooth. Examples of articles that made use of smooth surface particles for the pressure drop tests that they conducted are listed below:

- Susskind and Becker (1967) made use of steel spheres that were manufactured with a diametric tolerance of ±0.001 in and a surface finish of 9 RMS (Root Mean Square) which is very smooth;
- Wentz and Thodos (1963) made use of plastic phenolic spheres which is expected to have a smooth surface finish;
- Handley and Heggs (1968) made use of steel, lead, bronze, lead glass and soda glass spheres. It is expected that these materials would give smooth surface finishes;
- Tobis (2000) made use of table tennis balls which has a smooth surface finish; and
- The test done at the North-West University's HPTU was done with acrylic and steel spheres, each of which has smooth surface finishes. Du Toit (2008)

It was expected that the roughness of the surface finish of the spheres under consideration would cause the friction factors of the packings to be higher than that predicted by the KTA (1981) correlation and the correlation of Wentz and Thodos (1963).

Another reason why the structured packing resulted in a higher pressure drop than was expected and proposed by the correlation of Wentz and Thodos (1963), was the size of the distensions used to obtain the porosity of the packing. As mentioned in section 6.5, Wentz and Thodos (1963) made use of distention which had diameters of 0.45 mm whereas the packing that was used in this study made use of distensions with diameters of 2 mm. It is expected that this large difference in distension diameter size could have an influence on the pressure drop through the structured packing.

For both the random and the structured packings enough superficial flow area was provided so that the container diameter-to-particle diameter would be larger than 4.5. Both the packing were also manufactured long enough so that the packing length-to-particle diameter would be equal to 20. The spheres near the wall of the container were cut into the shape of the container so that the packings would be able to fit into the container without the walls of the container affecting the porosity or structure of the packing, thus eliminating the wall effect.

The hollow spheres near the wall of the containers were filled with silicone before they were inserted into the containers. The silicone made the packings fit snugly into the containers and also eliminated the by-pass flow between the spheres and the container wall.

The porosities of both the packings were determined with the aid of the Solid Works™ models that they were manufactured from. These porosities were also verified by submerging the packings into a container filled with water and measuring the displacement of the water for each of the sections through which the pressure drop was measured.

All the measurement instrumentation used during the experiment was calibrated and in good working condition. The pressure tappings that were made in the perspex container housing the packings were made in open areas so that it would be open to the flow of the working fluid. The pressure tapping that penetrated the perspex container was inserted in such a manner that it would be flush with the inside surface of the container.

The DAQ system was able to record the experimental data to an acceptable level of accuracy as set out by the URS in section 4.1. The repeatability of the measurement was shown to be acceptable. All the preceding statement indicates that the trustworthiness of the data is good.

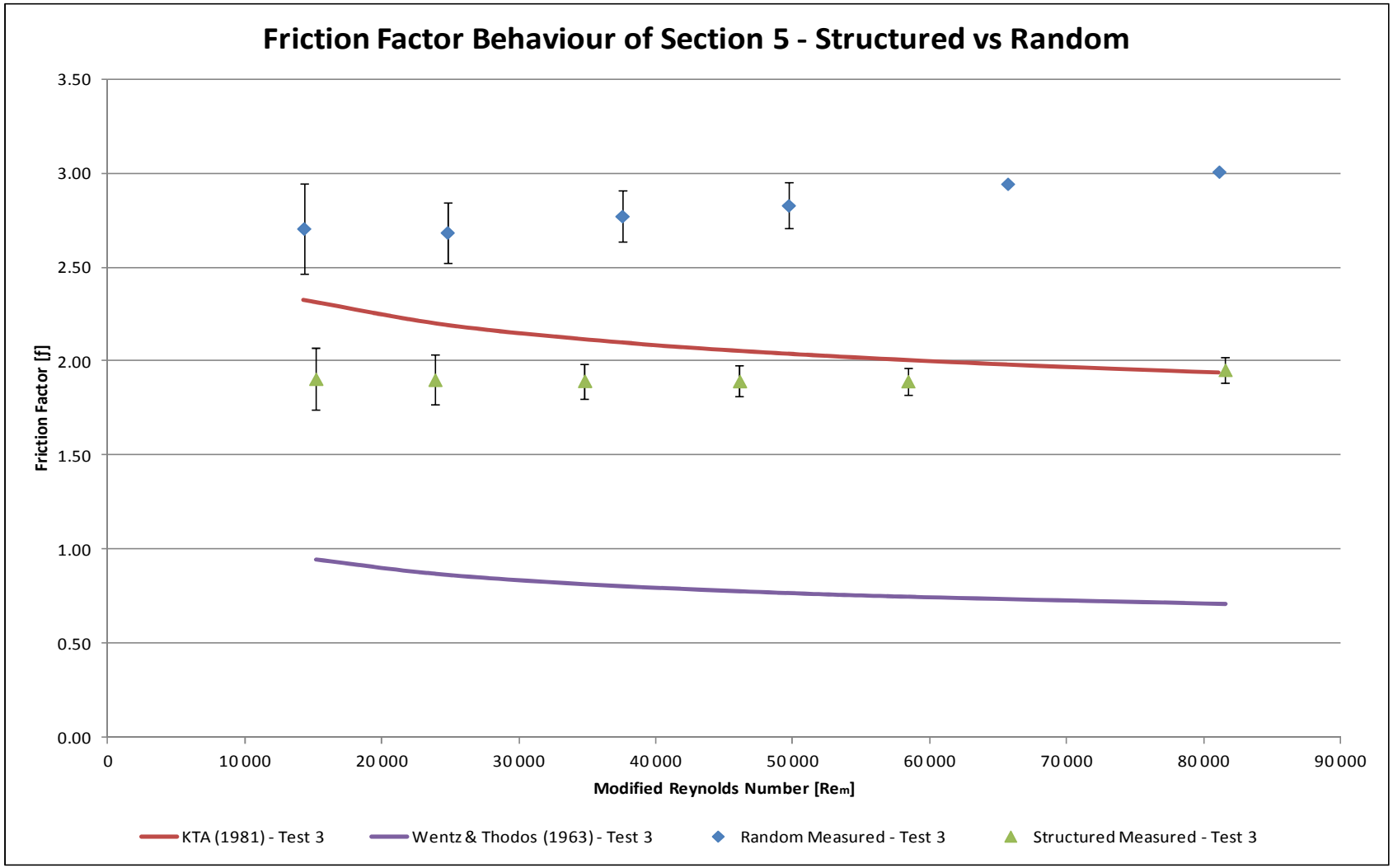

Figure 59: Comparison of the results of section 5 from the random and structured packings with KTA (1981) relation and the relation of Wentz and Thodos (1963) respectively.

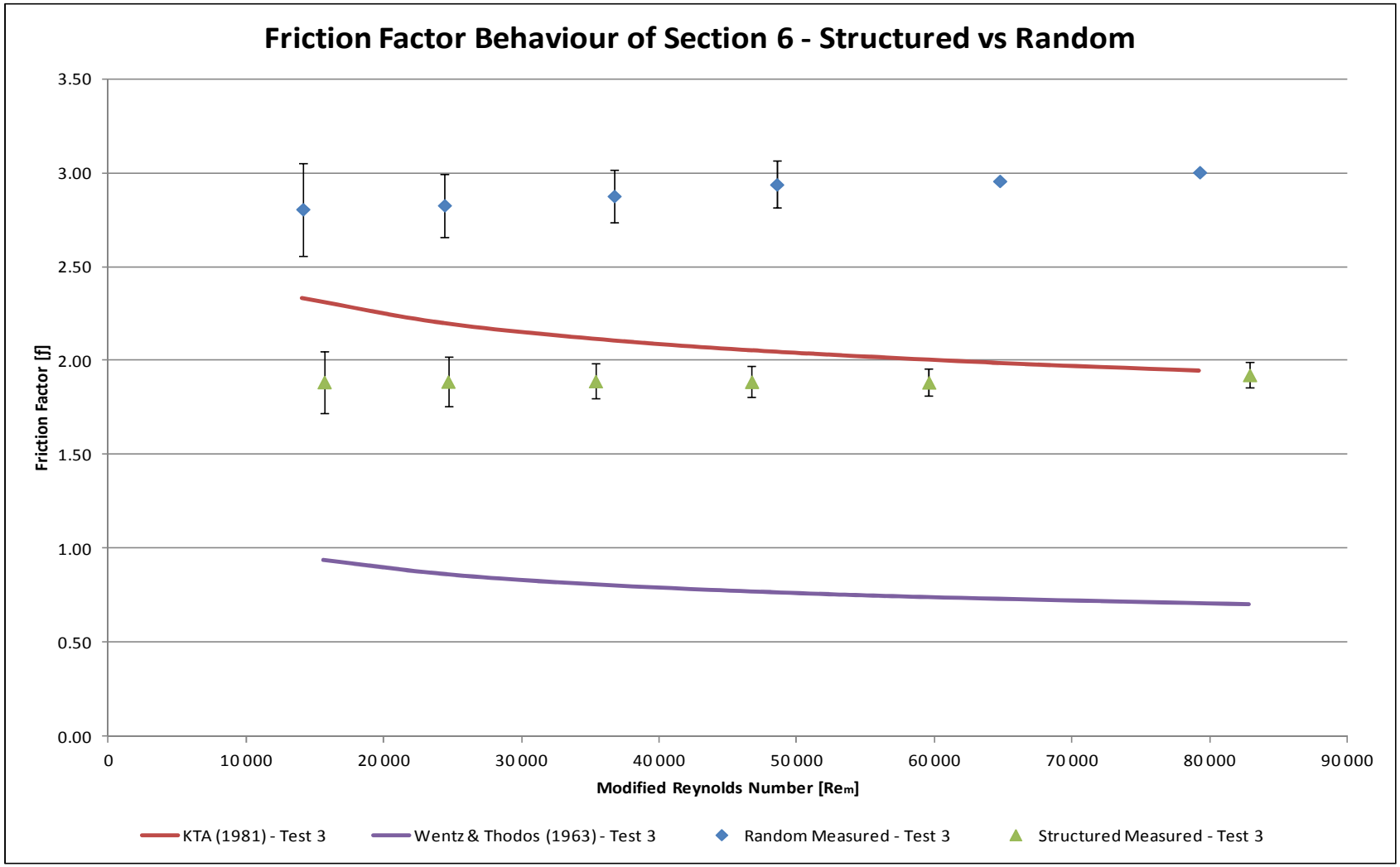

Figure 60: Comparison of the results of section 6 from the random and structured packings with KTA (1981) relation and the relation of Wentz and Thodos (1963) respectively.

6.7 CONCLUSIONS

In this chapter the experimental data that was obtained from this study was presented. It was found that the experiments were repeatable and that the trustworthiness of the measurements was acceptable.

The friction factors derived from the experimental data was compared with correlation found in the literature that was relevant for the specific applications. The friction factors obtained for the random packing was compared to the calculated friction factor of the KTA (1981) correlation. For the friction factors obtained for the structured packing was compared to the calculated friction factor of the correlation of Wentz and Thodos (1963).

The tendency of the friction factors, of the packings used in this experiment, to increase as the modified Reynolds number increases was an unexpected phenomenon. Carman (1937) also encountered this phenomenon. Unfortunately, Carman (1937) found this phenomenon to occur for packings of rings in the laminar flow region. It was unclear what caused this phenomenon and further study is needed in this matter.

As expected, it was found that the pressure drop through a structured packing was less than the pressure drop through a random packing. However, when the results for both the packing was compared to the theoretical results of the KTA (1981) correlation and the correlation of Wentz and Thodos (1963) it was found to be much higher. This difference could be attributed to the surface finish of the particles used in the experiment being very rough and increasing the pressure drop through the packings. In the case of the structured packing, the sizes of the distensions being larger than those used by Wentz and Thodos (1963) could also have caused the pressure drop to be higher.

CHAPTER 7 : CONCLUSIONS AND RECOMMENDATIONS

7.1 CONCLUSIONS

The main aim of the project described in this dissertation was to design and commission a test facility that could be used to conduct pressure drop test through packed beds of spheres with varying levels of structuredness. The basic outcomes of the test facility were that it had to be easy to use and that it had to be safe to operate. The experimental data that would be obtained from the tests done with the test facility had to have an experimental uncertainty of less than 10%.

The pressure drop was to be conducted on two packings of which the structure of the particles in the packing differed. One structured packed bed and one random packed bed was tested. The reason for choosing packings with different levels of structuredness was to investigate what the effect of the structuredness of a packing is on the pressure drop through a packed bed of spheres.

The main aim of the literature survey was to investigate what effect the structuredness of a packed bed of spheres has on its hydrodynamic properties. It was found that geometrically ordered packing resulted in lower pressure drops that that of randomly packed beds of spheres. It was also found that in cases where only the structure of the packing was changed, keeping all the other physical properties of the packing unchanged, that the hydrodynamic properties of the packing changed. It could therefore be concluded that the structure of a packed bed is a parameter that cannot be ignored when attempting to formulate a correlation that would fully characterise any packed bed of spheres.

Once the detail design of the testing facility was done it was built and commissioned. The pressure drop test, through the two packed bed, was then done with the use of the test facility. The tests done with the test facility were shown to be repeatable and it was found that the measurements done with the test facility are trustworthy.

The measurement data obtained from the experiment was used to derive the friction factors for the packed beds. These friction factors was then compared to friction factors as calculated with

the use of the KTA (1981) correlation and the correlation of Wentz and Thodos (1963) for the random and structures packings respectively.

It was found that the friction factors derived from the measured data slightly increased as the modified Reynolds numbers increased. A sharper increase in the friction factors was found for the random packing than for the structured packing. This phenomenon was unexpected and similar results were found by Carman (1937) for ring type packings in the laminar flow region. There was however no good explanation for this phenomenon.

When the friction factors obtained from the experiments for the random and structured packings were compared with the friction factors calculated from the KTA (1981) correlation and the correlation of Wentz and Thodos (1963), it was found that the experimental friction factors were higher than that proposed by the theory in both cases. One of the physical properties of the packed beds that could contribute to the experimental friction factors being higher than that of the theoretical friction factors was the surface finish of the particles in the packings. Most, if not all, of the particles that were used for pressure drop experiments in the literature had smooth surface finishes. Due to the manufacturing process that was used to manufacture the packings for the current study 0.5mm deep grooves cover all the particles. These grooves could cause the pressure drop through the packing to be higher.

Another physical parameter that could contribute to the friction factor of the structured packing being higher than that proposed by Wentz and Thodos (1963) is the size of the distensions that was used. Wentz and Thodos (1963) made use of 0.45mm diameter whereas the distensions used in this experiment was 2mm in diameter. This enlarged distension size could cause the pressure drop through the structured packing to be higher.

From the results that were obtained from the experiments done with the testing facility and the low experimental uncertainty of the results, it could be conclude that the test facility succeeded in its purpose that was set out for it. This test facility can be used to conduct further experiments on packed bed of spheres.

7.2 RECOMMENDATIONS

There was very little mention in the literature of friction factors increasing as the modified Reynolds number increases. This phenomenon is not fully understood. It is recommended that the phenomenon be investigates in more detail to get a better understanding of it.

The fact that the friction factor derived from the measured data from the random and structured packings was higher than the theoretical friction factors calculated from the KTA (1981) correlation and the correlation of Wentz and Thodos (1963) could be contributed to the fact that the surface finish of the particles used in the packings used for this experiment. Another factor that could contribute is the distensions that were used for the structured packing being larger than those used by Wentz and Thodos (1963). It is however recommended that further research be conducted to better understand the effect that the surface finish of the particles in a packed bed of spheres have on the pressure drop through the packing.

BIBLIOGRAPHY

Achenbach, E., 1995. Heat and Flow Characteristics of Packed Beds. *Experimental Thermal and Fluid Science*, Vol. 10, pp.17 - 27.

AIAA, 1995. Assessment of Wind Tunnel Data Uncertainty. *AIAA S-071-1995*.

Anon., 1981. *Reactor Core Design of High-Tmperature Gas-Cooled Reactors, Part 3: Loss of Pressure through Friction in Pebble Bed Cores*. Nuclear Safety Standard Commission (KTA). KTA 3102.3.

Atmakidis, T. & Kenig, E.Y., 2009. CFD-based Analysis of the Wall Effect on the Pressure Drop in Packed Beds With Moderate Tube/Particle Diameter Ratios in the Laminar Flow Regime. *Chemical Engineering Journal*, Vol. 155, pp.404 - 410.

Barthels, H., 1972. Druckverlust in Kugelschuttungen. *Brennstof-Warme-Kraft*, Vol. 24, pp.233 - 236.

Bernal, J.D. & Mason, J., 1960. Packing of Spheres. *Nature*, pp.908 - 911.

Blake, F.E., 1922. Resistance of Packing to Fluid Flow. *Transactions of American Institute of Chemical Engineers*, Vol. 14, pp.415 - 421.

Carman, P.C., 1937. Fluid Flow Through Granular Beds. *Trans. Inst. Chem. Eng.*, Vol. 15, pp.150 - 166.

Cohen, Y. & Metzner, A.B., 1981. Wall Effects in Laminar Flow of Fluids Through Packed Beds. *A.I.Ch.E Journal*, Vol. 27, pp.705 - 715.

Coleman, H.W. & Steele, W.G., 1999. *Experimentation and Uncertainty Analysis for Engineers*. 2nd ed. New York: John Wiley & Sons, Inc.

De Klerk, A., 2003. Voidage Variation in Packed Beds at Small Column to Particle Diameter Ratios. *A.I.Ch.E Journal*, Vol. 49, pp.2022 - 2029.

Devore, J. & Nicholas, F., 2005. *Applied Statistics for Engineers ans Scientists*. 2nd ed. California: Thompson Brooks Cole.

Du Toit, C.G., 2008. *HPTU Pressure Drop Tests Summary Report*. Potchefstroom: M-Tech Industrial (Pty) Ltd Report - HPTU002-0011 Rev 1A.

Du Toit, C.G., 2011. Uncertainty Assessment Interview.

Ergun, S., 1952. Fluid flow through packed columns. *Chemical Engineering Process*, pp.89 - 94.

Handley, D. & Heggs, P.J., 1968. Momentum and Heat Transfer Mechanisms in Regular Shaped Packings. *Trans. Instn Chem. Engrs*, Vol. 64, pp.251 - 264.

Jeschar, R., 1965. Drukverlust in Mehrkornschuttungen aus Kegeln. *Arch. Eisenhiittenw.*, Vol. 35, pp.91 - 108.

Longo, J. & Stern, F., 2005. Uncertainty Assssment for Towing Tank Testers With Example for Surface Combatent DTMB Model 5415. *Journal for Shipping Research*, pp.Vol. 49, No. 1. pp. 55-68.

Metha, D. & Hawley, M.C., 1969. Wall Effect in Packed Columns. *I&EC Process Design and Development*, pp.280 - 282.

PBMR, 2006. *News Release - November 2004*. [Online] Available at: http://www.pbmr.co.za/index.asp?Content=10&MSTate=DT&Article=48 [Accessed 5 October 2008].

PBMR, 2008. *Why PBMR*. [Online] Available at: http://www.pbmr.co.za/index.asp?Content=3& [Accessed 5 October 2008].

Reichelt, W., 1972. ZurBerechnun des Druckverlusten Einphasig Durchstromter Kugel- und Zylinderschuttungen. *Chem. Ing. Tech.*, Vol. 44, pp.1068 - 1071.

Rouseau, P.G., 2008. In *THERMAL-FLUID SYSTEMS MODELLING - Course Notes*. Potchefstroom: North-West University.

Sato, Y. & Hirose, T., 1973. Pressure Loss and Liquid Hold-up in Packed Reactors With Concurrent Gas-liquid Downflow. *Journal of Chemical Enginering Japan*, Vol. 6, pp.147 - 152.

Stern, F. & Muste, M., 1999. *Summary of Experimental Uncertainty Assessmnet Methodology with Example*. Iowa City: Iowa Institute of Hydraulic Research.

Susskind, H. & Becker, W., 1967. Pressure Drop in Geometrically Ordered Packed Beds of Spheres. *A.I.Ch.E Journal*, Vol.13(No. 6), pp.1155 - 1159.

Tobis, J., 2000. Influence of Bed Geometry on its Frictional Resistance Under Turbulent Flow Conditions. *Chemical Engineering Science*, Vol. 55, pp.5359 - 5366.

Wentz, C.A. & Thodos, G., 1963. Pressure Drop in the flow of gasses through packed and distended beds of spehrical particles. *A.I.Ch.E Journal*.

Wikipedia, 2011. *Accuracy and Precision*. [Online] Available at: http://en.wikipedia.org/wiki/Accuracy_and_precision [Accessed 7 July 2011].

Yang, J. & Wang, Q., 2010. Computational Study of Forced Convective Heat Transfer in Structured Packed Beds with Spherical or Ellipsoidal Particles. *Chemical Engineering Science*, Vol. 65, pp.726 - 738.

APPENDIX A

In Appendix A all the necessary documentation relating to the design of the testing facility is provided. This documentation includes the following:

- Material properties of the packed beds;
- Calibration certificates;
- Detail drawings of the piping system;
- Pumping curve and pump dimensions;
- Detail drawings of the frame; and
- Wiring diagrams of the all the electrical systems.

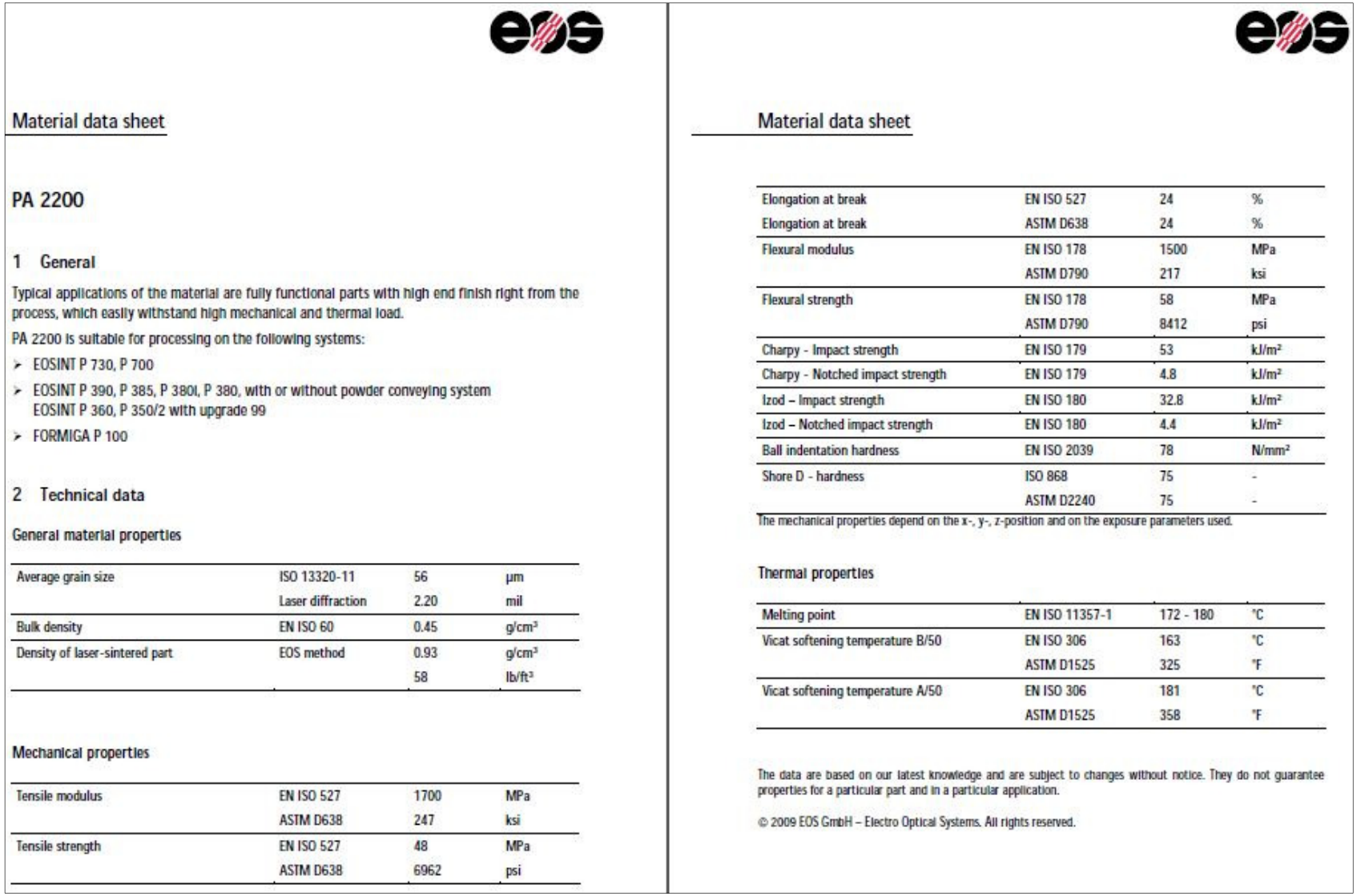

Material data sheet

PA 2200

1 General

Typical applications of the material are fully functional parts with high end finish right from the process, which easily withstand high mechanical and thermal load.

PA 2200 is suitable for processing on the following systems:

- EOSINT P 730, P 700
- EOSINT P 390, P 385, P 380i, P 380, with or without powder conveying system
  EOSINT P 360, P 350/2 with upgrade 99
- FORMIGA P 100

2 Technical data

General material properties

Average grain size	ISO 13320-11	56	µm
	Laser diffraction	2.20	mil
Bulk density	EN ISO 60	0.45	g/cm³
Density of laser-sintered part	EOS method	0.93	g/cm³
		58	lb/ft³

Mechanical properties

Tensile modulus	EN ISO 527	1700	MPa
	ASTM D638	247	ksi
Tensile strength	EN ISO 527	48	MPa
	ASTM D638	6962	psi

Material data sheet

Elongation at break	EN ISO 527	24	%
Elongation at break	ASTM D638	24	%
Flexural modulus	EN ISO 178	1500	MPa
	ASTM D790	217	ksi
Flexural strength	EN ISO 178	58	MPa
	ASTM D790	8412	psi
Charpy - Impact strength	EN ISO 179	53	kJ/m²
Charpy - Notched impact strength	EN ISO 179	4.8	kJ/m²
Izod – Impact strength	EN ISO 180	32.8	kJ/m²
Izod – Notched impact strength	EN ISO 180	4.4	kJ/m²
Ball indentation hardness	EN ISO 2039	78	N/mm²
Shore D - hardness	ISO 868	75	-
	ASTM D2240	75	-

The mechanical properties depend on the x-, y-, z-position and on the exposure parameters used.

Thermal properties

Melting point	EN ISO 11357-1	172 - 180	°C
Vicat softening temperature B/50	EN ISO 306	163	°C
	ASTM D1525	325	°F
Vicat softening temperature A/50	EN ISO 306	181	°C
	ASTM D1525	358	°F

The data are based on our latest knowledge and are subject to changes without notice. They do not guarantee properties for a particular part and in a particular application.

Figure 61: Material properties of PA 2200.

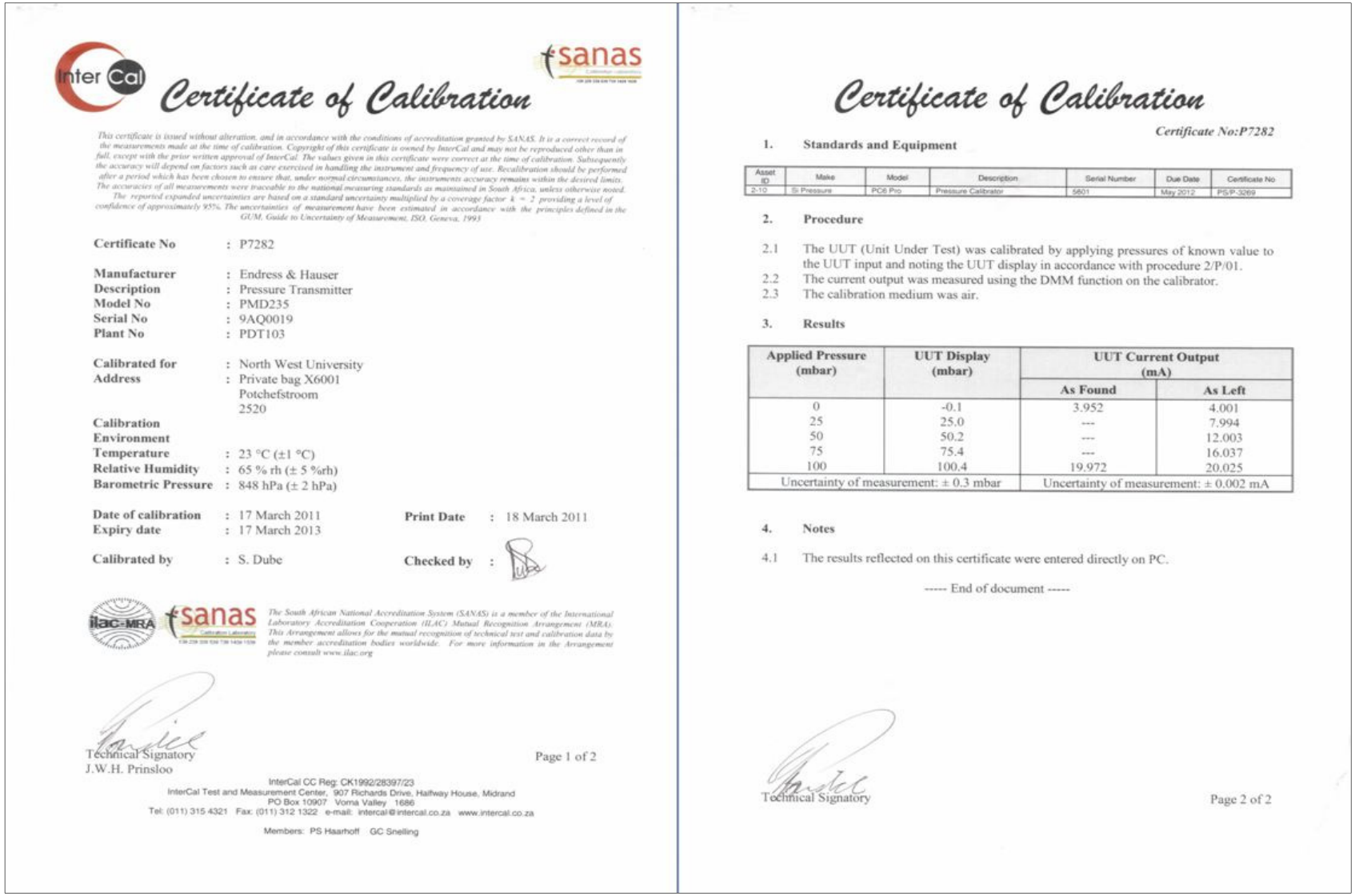

Certificate of Calibration

This certificate is issued without alteration, and in accordance with the conditions of accreditation granted by SANAS. It is a correct record of the measurements made at the time of calibration. Copyright of this certificate is owned by InterCal and may not be reproduced other than in full, except with the prior written approval of InterCal. The values given in this certificate were correct at the time of calibration. Subsequently the accuracy will depend on factors such as care exercised in handling the instrument and frequency of use. Recalibration should be performed after a period which has been chosen to ensure that, under normal circumstances, the instruments accuracy remains within the desired limits. The accuracies of all measurements were traceable to the national measuring standards as maintained in South Africa, unless otherwise noted. The reported expanded uncertainties are based on a standard uncertainty multiplied by a coverage factor k = 2 providing a level of confidence of approximately 95%. The uncertainties of measurement have been estimated in accordance with the principles defined in the GUM, Guide to Uncertainty of Measurement, ISO, Geneva, 1993.

Certificate No : P7282

Manufacturer : Endress & Hauser
Description : Pressure Transmitter
Model No : PMD235
Serial No : 9AQ0019
Plant No : PDT103

Calibrated for : North West University
Address : Private bag X6001
Potchefstroom
2520

Calibration Environment
Temperature : 23 °C (±1 °C)
Relative Humidity : 65 % rh (± 5 %rh)
Barometric Pressure : 848 hPa (± 2 hPa)

Date of calibration : 17 March 2011
Expiry date : 17 March 2013
Print Date : 18 March 2011

Calibrated by : S. Dube
Checked by :

The South African National Accreditation System (SANAS) is a member of the International Laboratory Accreditation Cooperation (ILAC) Mutual Recognition Arrangement (MRA). This Arrangement allows for the mutual recognition of technical test and calibration data by the member accreditation bodies worldwide. For more information in the Arrangement please consult www.ilac.org

Technical Signatory
J.W.H. Prinsloo

Page 1 of 2

InterCal CC Reg: CK1992/28397/23
InterCal Test and Measurement Center, 907 Richards Drive, Halfway House, Midrand
PO Box 10907 Vorna Valley 1686
Tel: (011) 315 4321 Fax: (011) 312 1322 e-mail: intercal@intercal.co.za www.intercal.co.za
Members: PS Haarhoff GC Snelling

Certificate of Calibration

Certificate No:P7282

1. Standards and Equipment

Asset ID	Make	Model	Description	Serial Number	Due Date	Certificate No
2-10	S Pressure	PC6 Pro	Pressure Calibrator	5601	May 2012	PS/P-3269

2. Procedure

2.1 The UUT (Unit Under Test) was calibrated by applying pressures of known value to the UUT input and noting the UUT display in accordance with procedure 2/P/01.
2.2 The current output was measured using the DMM function on the calibrator.
2.3 The calibration medium was air.

3. Results

Applied Pressure (mbar)	UUT Display (mbar)	UUT Current Output (mA)	
		As Found	As Left
0	-0.1	3.952	4.001
25	25.0	---	7.994
50	50.2	---	12.003
75	75.4	---	16.037
100	100.4	19.972	20.025
Uncertainty of measurement: ± 0.3 mbar		Uncertainty of measurement: ± 0.002 mA	

4. Notes

4.1 The results reflected on this certificate were entered directly on PC.

----- End of document -----

Technical Signatory

Page 2 of 2

Figure 62: Calibration certificate for the PMD 235 (0-100 mbar) differential pressure transmitter.

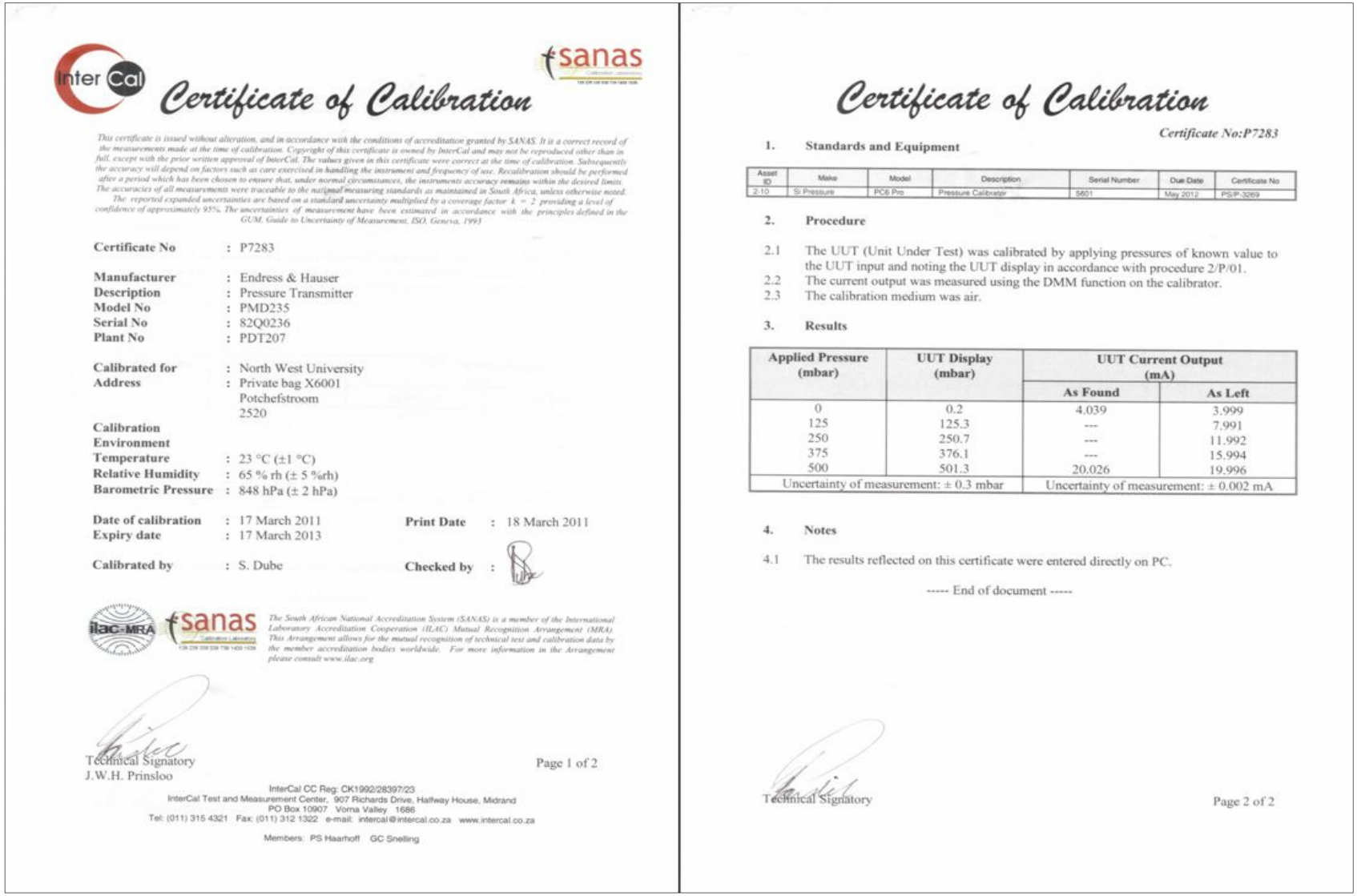

Certificate of Calibration

This certificate is issued without alteration, and in accordance with the conditions of accreditation granted by SANAS. It is a correct record of the measurements made at the time of calibration. Copyright of this certificate is owned by InterCal and may not be reproduced other than in full, except with the prior written approval of InterCal. The values given in this certificate were correct at the time of calibration. Subsequently the accuracy will depend on factors such as care exercised in handling the instrument and frequency of use. Recalibration should be performed after a period which has been chosen to ensure that, under normal circumstances, the instruments accuracy remains within the desired limits. The accuracies of all measurements were traceable to the national measuring standards as maintained in South Africa, unless otherwise noted. The reported expanded uncertainties are based on a standard uncertainty multiplied by a coverage factor k = 2 providing a level of confidence of approximately 95%. The uncertainties of measurement have been estimated in accordance with the principles defined in the GUM, Guide to Uncertainty of Measurement, ISO, Geneva, 1995

Certificate No : P7283

Manufacturer : Endress & Hauser
Description : Pressure Transmitter
Model No : PMD235
Serial No : 82Q0236
Plant No : PDT207

Calibrated for : North West University
Address : Private bag X6001
Potchefstroom
2520

Calibration Environment
Temperature : 23 °C (±1 °C)
Relative Humidity : 65 % rh (± 5 %rh)
Barometric Pressure : 848 hPa (± 2 hPa)

Date of calibration : 17 March 2011
Expiry date : 17 March 2013
Print Date : 18 March 2011

Calibrated by : S. Dube
Checked by :

The South African National Accreditation System (SANAS) is a member of the International Laboratory Accreditation Cooperation (ILAC) Mutual Recognition Arrangement (MRA). This Arrangement allows for the mutual recognition of technical test and calibration data by the member accreditation bodies worldwide. For more information in the Arrangement please consult www.ilac.org

Technical Signatory
J.W.H. Prinsloo

InterCal CC Reg: CK1992/28397/23
InterCal Test and Measurement Center, 907 Richards Drive, Halfway House, Midrand
PO Box 10907 Vorna Valley 1686
Tel: (011) 315 4321 Fax: (011) 312 1322 e-mail: intercal@intercal.co.za www.intercal.co.za
Members: PS Haarhoff GC Snelling

Certificate of Calibration

Certificate No:P7283

1. Standards and Equipment

Asset ID	Make	Model	Description	Serial Number	Due Date	Certificate No
2-10	Si Pressure	PC6 Pro	Pressure Calibrator	5601	May 2012	PS/P-3269

2. Procedure

2.1 The UUT (Unit Under Test) was calibrated by applying pressures of known value to the UUT input and noting the UUT display in accordance with procedure 2/P/01.
2.2 The current output was measured using the DMM function on the calibrator.
2.3 The calibration medium was air.

3. Results

Applied Pressure (mbar)	UUT Display (mbar)	UUT Current Output (mA)	
		As Found	As Left
0	0.2	4.039	3.999
125	125.3	---	7.991
250	250.7	---	11.992
375	376.1	---	15.994
500	501.3	20.026	19.996
Uncertainty of measurement: ± 0.3 mbar		Uncertainty of measurement: ± 0.002 mA	

4. Notes

4.1 The results reflected on this certificate were entered directly on PC.

----- End of document -----

Technical Signatory

Figure 63: Calibration certificate for the PMD 235 (0-500 mbar) differential pressure transmitter.

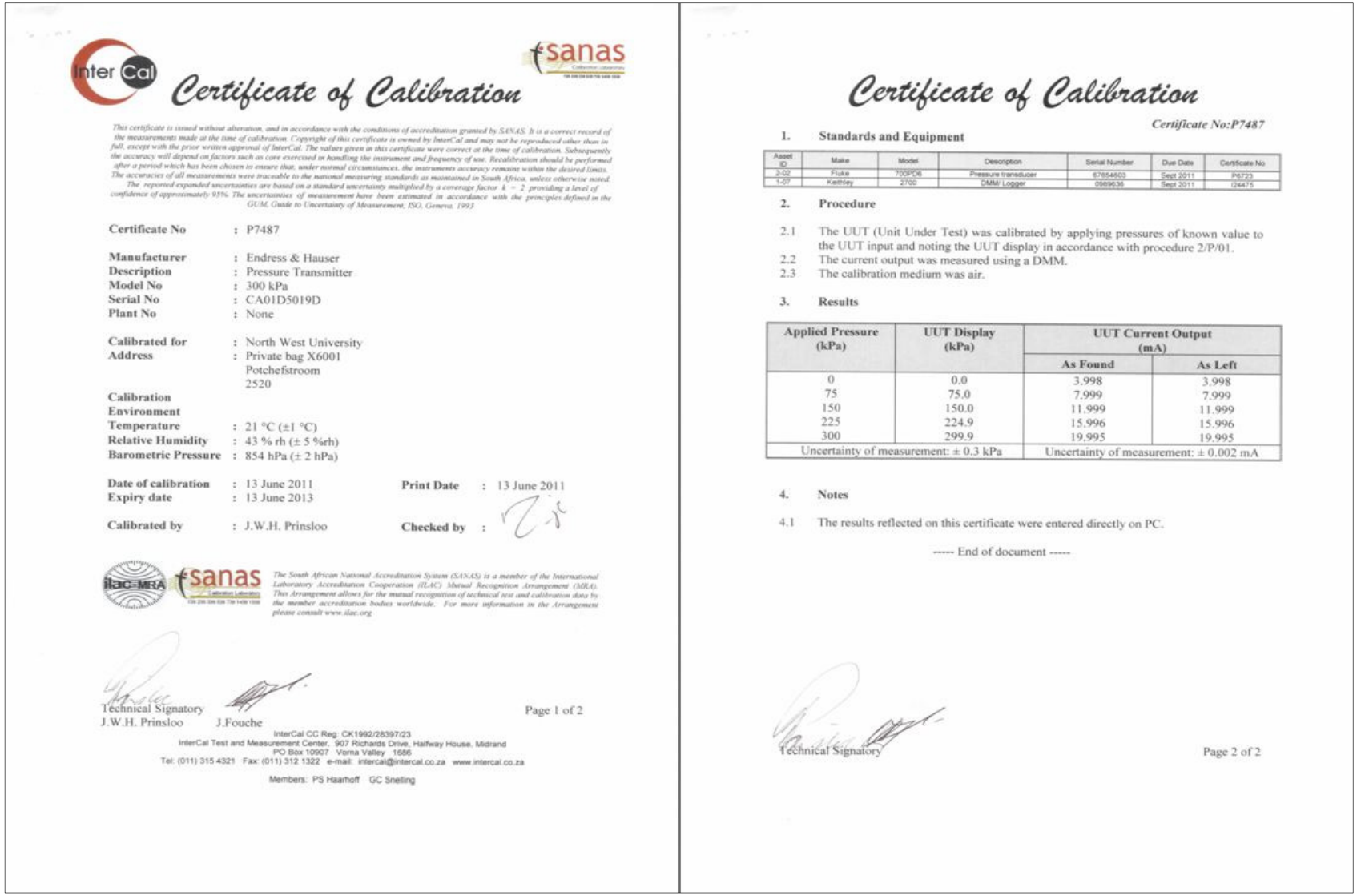

Certificate of Calibration

This certificate is issued without alteration, and in accordance with the conditions of accreditation granted by SANAS. It is a correct record of the measurements made at the time of calibration. Copyright of this certificate is owned by InterCal and may not be reproduced other than in full, except with the prior written approval of InterCal. The values given in this certificate were correct at the time of calibration. Subsequently the accuracy will depend on factors such as care exercised in handling the instrument and frequency of use. Recalibration should be performed after a period which has been chosen to ensure that, under normal circumstances, the instruments accuracy remains within the desired limits. The accuracies of all measurements were traceable to the national measuring standards as maintained in South Africa, unless otherwise noted. The reported expanded uncertainties are based on a standard uncertainty multiplied by a coverage factor $k = 2$ providing a level of confidence of approximately 95%. The uncertainties of measurement have been estimated in accordance with the principles defined in the GUM, Guide to Uncertainty of Measurement, ISO, Geneva, 1993

Certificate No	:	P7487
Manufacturer	:	Endress & Hauser
Description	:	Pressure Transmitter
Model No	:	300 kPa
Serial No	:	CA01D5019D
Plant No	:	None
Calibrated for	:	North West University
Address	:	Private bag X6001 Potchefstroom 2520
Calibration Environment		
Temperature	:	21 °C (±1 °C)
Relative Humidity	:	43 % rh (± 5 %rh)
Barometric Pressure	:	854 hPa (± 2 hPa)
Date of calibration	:	13 June 2011
Expiry date	:	13 June 2013
Print Date	:	13 June 2011
Calibrated by	:	J.W.H. Prinsloo
Checked by	:	

The South African National Accreditation System (SANAS) is a member of the International Laboratory Accreditation Cooperation (ILAC) Mutual Recognition Arrangement (MRA). This Arrangement allows for the mutual recognition of technical test and calibration data by the member accreditation bodies worldwide. For more information on the Arrangement please consult www.ilac.org

Technical Signatory
J.W.H. Prinsloo J.Fouche

Page 1 of 2

InterCal CC Reg: CK1992/28397/23
InterCal Test and Measurement Center, 907 Richards Drive, Halfway House, Midrand
PO Box 10907 Vorna Valley 1686
Tel: (011) 315 4321 Fax: (011) 312 1322 e-mail: intercal@intercal.co.za www.intercal.co.za

Members: PS Haarhoff GC Snelling

Certificate of Calibration

Certificate No:P7487

1. Standards and Equipment

Asset ID	Make	Model	Description	Serial Number	Due Date	Certificate No
2-02	Fluke	700PD6	Pressure transducer	67654803	Sept 2011	P6723
1-07	Keithley	2700	DMM/ Logger	0989636	Sept 2011	I24475

2. Procedure

2.1 The UUT (Unit Under Test) was calibrated by applying pressures of known value to the UUT input and noting the UUT display in accordance with procedure 2/P/01.
2.2 The current output was measured using a DMM.
2.3 The calibration medium was air.

3. Results

Applied Pressure (kPa)	UUT Display (kPa)	UUT Current Output (mA)	
		As Found	As Left
0	0.0	3.998	3.998
75	75.0	7.999	7.999
150	150.0	11.999	11.999
225	224.9	15.996	15.996
300	299.9	19.995	19.995
Uncertainty of measurement: ± 0.3 kPa		Uncertainty of measurement: ± 0.002 mA	

4. Notes

4.1 The results reflected on this certificate were entered directly on PC.

----- End of document -----

Technical Signatory

Page 2 of 2

Figure 64: Calibration certificate for the PMD 70 (-300…300 kPa) differential pressure transmitter.

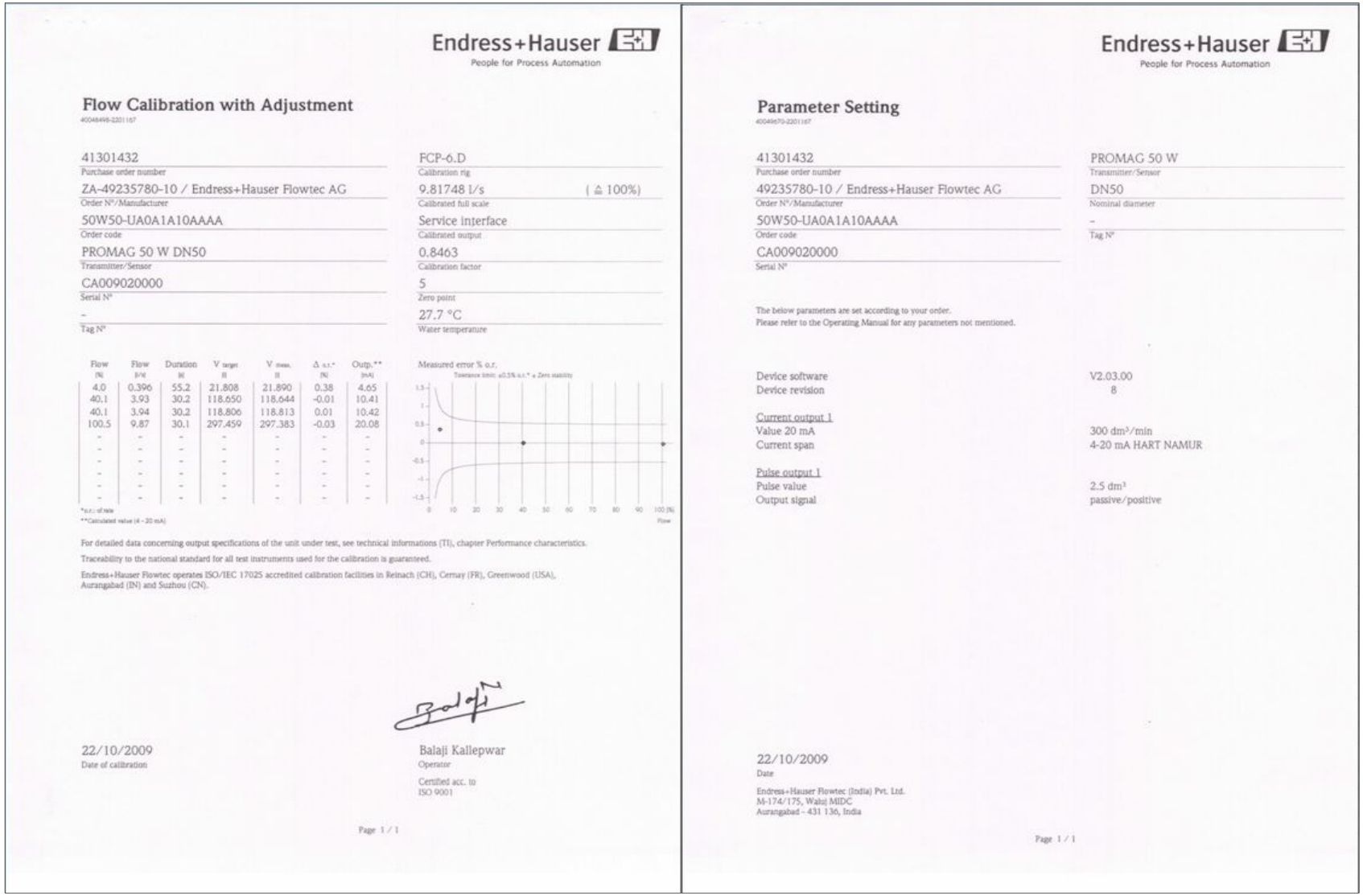

Endress+Hauser
People for Process Automation

Flow Calibration with Adjustment

40048498-2201167

41301432
Purchase order number

ZA-49235780-10 / Endress+Hauser Flowtec AG
Order N°/Manufacturer

50W50-UA0A1A10AAAA
Order code

PROMAG 50 W DN50
Transmitter/Sensor

CA009020000
Serial N°

–
Tag N°

FCP-6.D
Calibration rig

9.81748 l/s (≙ 100%)
Calibrated full scale

Service interface
Calibrated output

0.8463
Calibration factor

5
Zero point

27.7 °C
Water temperature

Flow [%]	Flow [l/s]	Duration [s]	V target [l]	V meas. [l]	Δ o.r.* [%]	Outp.** [mA]
4.0	0.396	55.2	21.808	21.890	0.38	4.65
40.1	3.93	30.2	118.650	118.644	-0.01	10.41
40.1	3.94	30.2	118.806	118.813	0.01	10.42
100.5	9.87	30.1	297.459	297.383	-0.03	20.08
–	–	–	–	–	–	–
–	–	–	–	–	–	–
–	–	–	–	–	–	–
–	–	–	–	–	–	–
–	–	–	–	–	–	–
–	–	–	–	–	–	–

*o.r.: of rate
**Calculated value (4 – 20 mA)

Measured error % o.r.

For detailed data concerning output specifications of the unit under test, see technical informations (TI), chapter Performance characteristics.

Traceability to the national standard for all test instruments used for the calibration is guaranteed.

Endress+Hauser Flowtec operates ISO/IEC 17025 accredited calibration facilities in Reinach (CH), Cernay (FR), Greenwood (USA), Aurangabad (IN) and Suzhou (CN).

22/10/2009
Date of calibration

Balaji Kallepwar
Operator

Certified acc. to ISO 9001

Page 1 / 1

Endress+Hauser
People for Process Automation

Parameter Setting

40049670-2201167

41301432
Purchase order number

49235780-10 / Endress+Hauser Flowtec AG
Order N°/Manufacturer

50W50-UA0A1A10AAAA
Order code

CA009020000
Serial N°

PROMAG 50 W
Transmitter/Sensor

DN50
Nominal diameter

–
Tag N°

The below parameters are set according to your order.
Please refer to the Operating Manual for any parameters not mentioned.

Device software	V2.03.00
Device revision	8
Current output 1	
Value 20 mA	300 dm³/min
Current span	4-20 mA HART NAMUR
Pulse output 1	
Pulse value	2.5 dm³
Output signal	passive/positive

22/10/2009
Date

Endress+Hauser Flowtec (India) Pvt. Ltd.
M-174/175, Waluj MIDC
Aurangabad - 431 136, India

Page 1 / 1

Figure 65: Calibration certificate for the Proline Promag 50W50 flow meter.

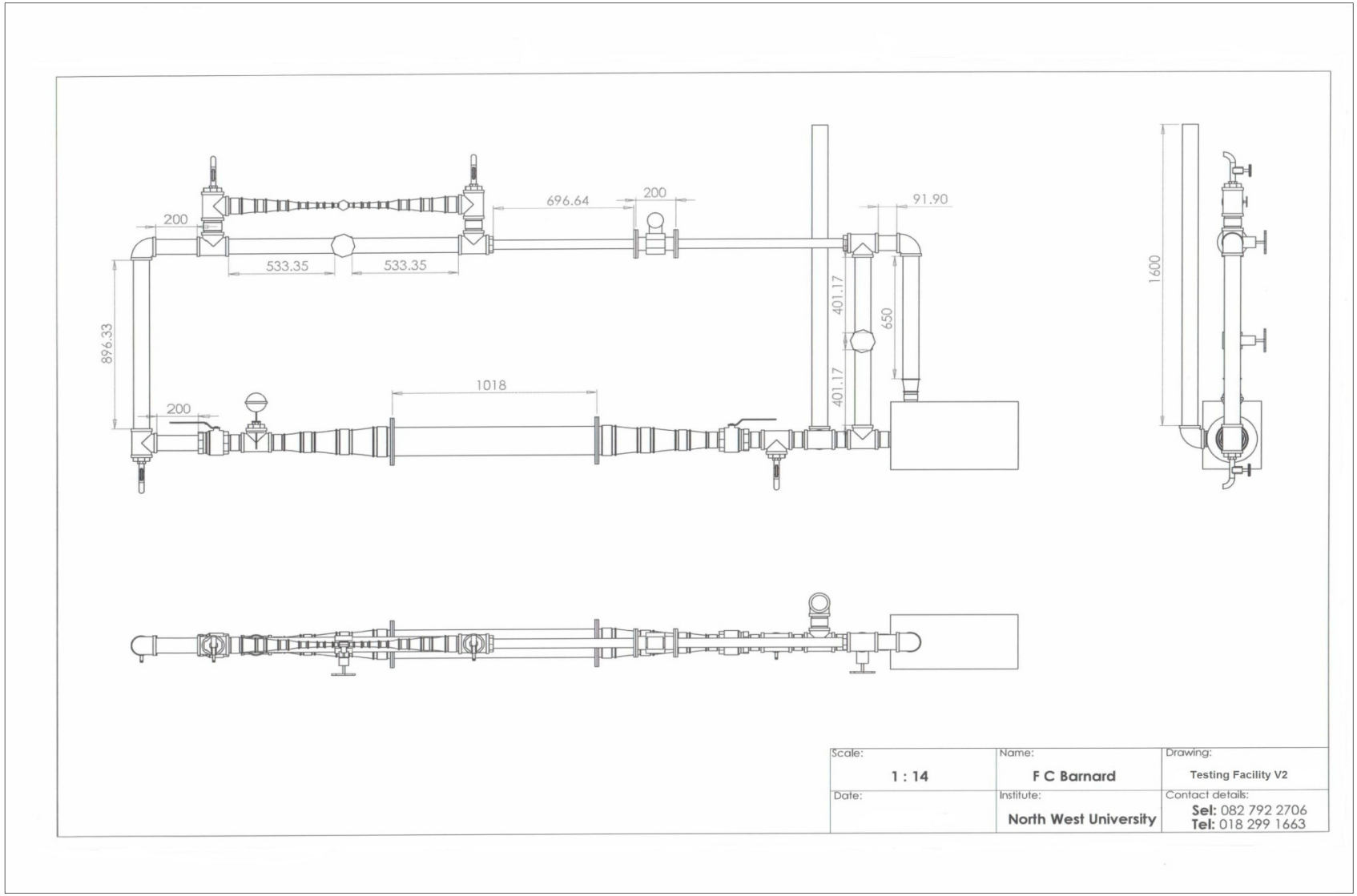

Figure 66: Detail design of the main system.

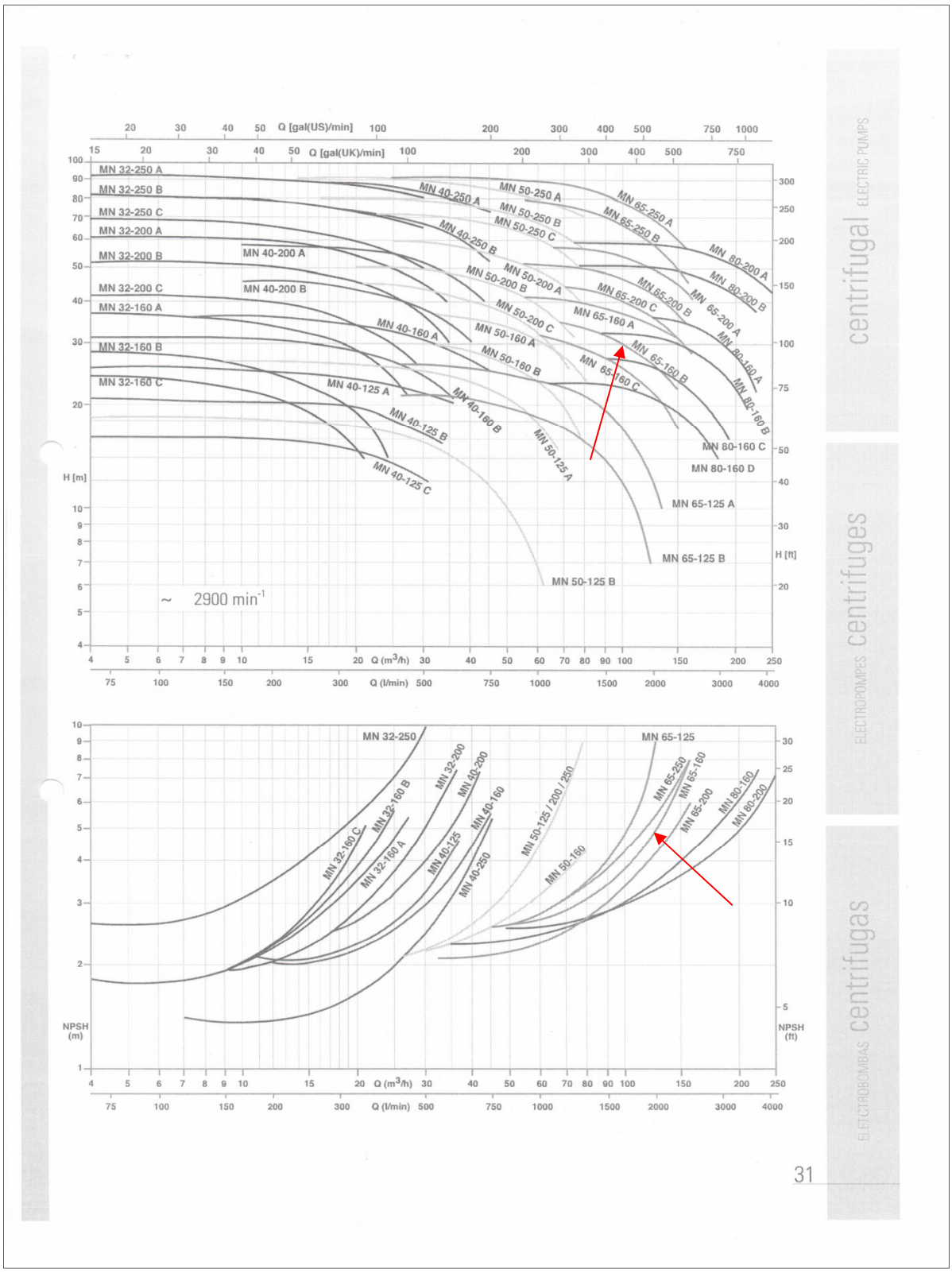

Figure 67: FORAS MN 65 – 160/B centrifugal pump operational curves.

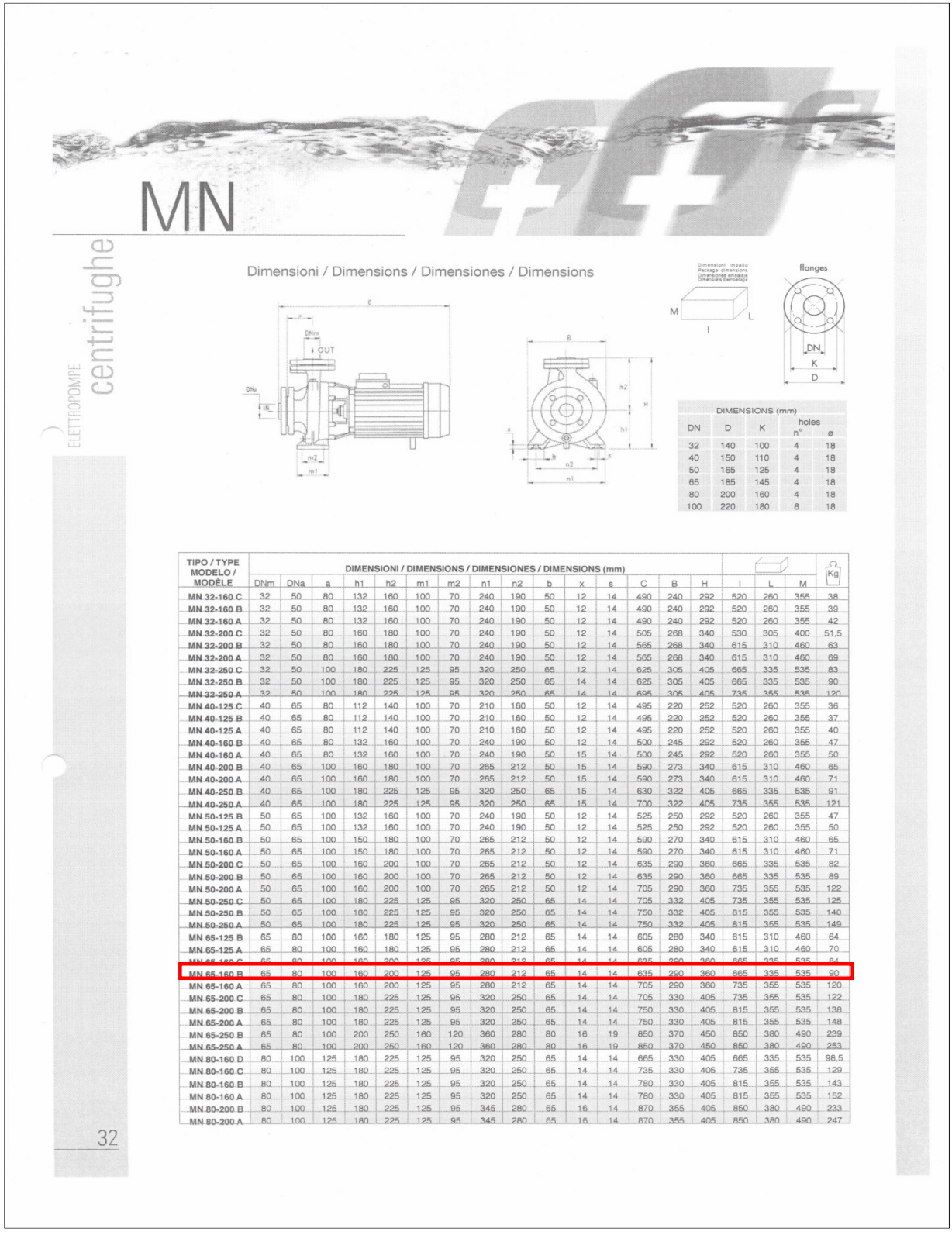

MN

ELETTROPOMPE centrifughe

Dimensioni / Dimensions / Dimensiones / Dimensions

flanges

DIMENSIONS (mm)

DN	D	K	holes n°	holes ø
32	140	100	4	18
40	150	110	4	18
50	165	125	4	18
65	185	145	4	18
80	200	160	4	18
100	220	180	8	18

TIPO / TYPE MODELO / MODÈLE	DIMENSIONI / DIMENSIONS / DIMENSIONES / DIMENSIONS (mm)																		Kg
	DNm	DNa	a	h1	h2	m1	m2	n1	n2	b	x	s	C	B	H	I	L	M	
MN 32-160 C	32	50	80	132	160	100	70	240	190	50	12	14	490	240	292	520	260	355	38
MN 32-160 B	32	50	80	132	160	100	70	240	190	50	12	14	490	240	292	520	260	355	39
MN 32-160 A	32	50	80	132	160	100	70	240	190	50	12	14	490	240	292	520	260	355	42
MN 32-200 C	32	50	80	160	180	100	70	240	190	50	12	14	505	268	340	530	305	400	51,5
MN 32-200 B	32	50	80	160	180	100	70	240	190	50	12	14	565	268	340	615	310	460	63
MN 32-200 A	32	50	80	160	180	100	70	240	190	50	12	14	565	268	340	615	310	460	69
MN 32-250 C	32	50	100	180	225	125	95	320	250	65	12	14	625	305	405	665	335	535	83
MN 32-250 B	32	50	100	180	225	125	95	320	250	65	14	14	625	305	405	665	335	535	90
MN 32-250 A	32	50	100	180	225	125	95	320	250	65	14	14	695	305	405	735	355	535	120
MN 40-125 C	40	65	80	112	140	100	70	210	160	50	12	14	495	220	252	520	260	355	36
MN 40-125 B	40	65	80	112	140	100	70	210	160	50	12	14	495	220	252	520	260	355	37
MN 40-125 A	40	65	80	112	140	100	70	210	160	50	12	14	495	220	252	520	260	355	40
MN 40-160 B	40	65	80	132	160	100	70	240	190	50	12	14	500	245	292	520	260	355	47
MN 40-160 A	40	65	80	132	160	100	70	240	190	50	15	14	500	245	292	520	260	355	50
MN 40-200 B	40	65	100	160	180	100	70	265	212	50	15	14	590	273	340	615	310	460	65
MN 40-200 A	40	65	100	160	180	100	70	265	212	50	15	14	590	273	340	615	310	460	71
MN 40-250 B	40	65	100	180	225	125	95	320	250	65	15	14	630	322	405	665	335	535	91
MN 40-250 A	40	65	100	180	225	125	95	320	250	65	15	14	700	322	405	735	355	535	121
MN 50-125 B	50	65	100	132	160	100	70	240	190	50	12	14	525	250	292	520	260	355	47
MN 50-125 A	50	65	100	132	160	100	70	240	190	50	12	14	525	250	292	520	260	355	50
MN 50-160 B	50	65	100	150	180	100	70	265	212	50	12	14	590	270	340	615	310	460	65
MN 50-160 A	50	65	100	150	180	100	70	265	212	50	12	14	590	270	340	615	310	460	71
MN 50-200 C	50	65	100	160	200	100	70	265	212	50	12	14	635	290	360	665	335	535	82
MN 50-200 B	50	65	100	160	200	100	70	265	212	50	12	14	635	290	360	665	335	535	89
MN 50-200 A	50	65	100	160	200	100	70	265	212	50	12	14	705	290	360	735	355	535	122
MN 50-250 C	50	65	100	180	225	125	95	320	250	65	14	14	705	332	405	735	355	535	125
MN 50-250 B	50	65	100	180	225	125	95	320	250	65	14	14	750	332	405	815	355	535	140
MN 50-250 A	50	65	100	180	225	125	95	320	250	65	14	14	750	332	405	815	355	535	149
MN 65-125 B	65	80	100	160	180	125	95	280	212	65	14	14	605	280	340	615	310	460	64
MN 65-125 A	65	80	100	160	180	125	95	280	212	65	14	14	605	280	340	615	310	460	70
MN 65-160 C	65	80	100	160	200	125	95	280	212	65	14	14	635	290	360	665	335	535	84
MN 65-160 B	65	80	100	160	200	125	95	280	212	65	14	14	635	290	360	665	335	535	90
MN 65-160 A	65	80	100	160	200	125	95	280	212	65	14	14	705	290	360	735	355	535	120
MN 65-200 C	65	80	100	180	225	125	95	320	250	65	14	14	705	330	405	735	355	535	122
MN 65-200 B	65	80	100	180	225	125	95	320	250	65	14	14	750	330	405	815	355	535	138
MN 65-200 A	65	80	100	180	225	125	95	320	250	65	14	14	750	330	405	815	355	535	148
MN 65-250 B	65	80	100	200	250	160	120	360	280	80	16	19	850	370	450	850	380	490	239
MN 65-250 A	65	80	100	200	250	160	120	360	280	80	16	19	850	370	450	850	380	490	253
MN 80-160 D	80	100	125	180	225	125	95	320	250	65	14	14	665	330	405	665	335	535	98,5
MN 80-160 C	80	100	125	180	225	125	95	320	250	65	14	14	735	330	405	735	355	535	129
MN 80-160 B	80	100	125	180	225	125	95	320	250	65	14	14	780	330	405	815	355	535	143
MN 80-160 A	80	100	125	180	225	125	95	320	250	65	14	14	780	330	405	815	355	535	152
MN 80-200 B	80	100	125	180	225	125	95	345	280	65	16	14	870	355	405	850	380	490	233
MN 80-200 A	80	100	125	180	225	125	95	345	280	65	16	14	870	355	405	850	380	490	247

32

Figure 68: FORAS MN 65 – 160/B centrifugal pump physical dimensions.

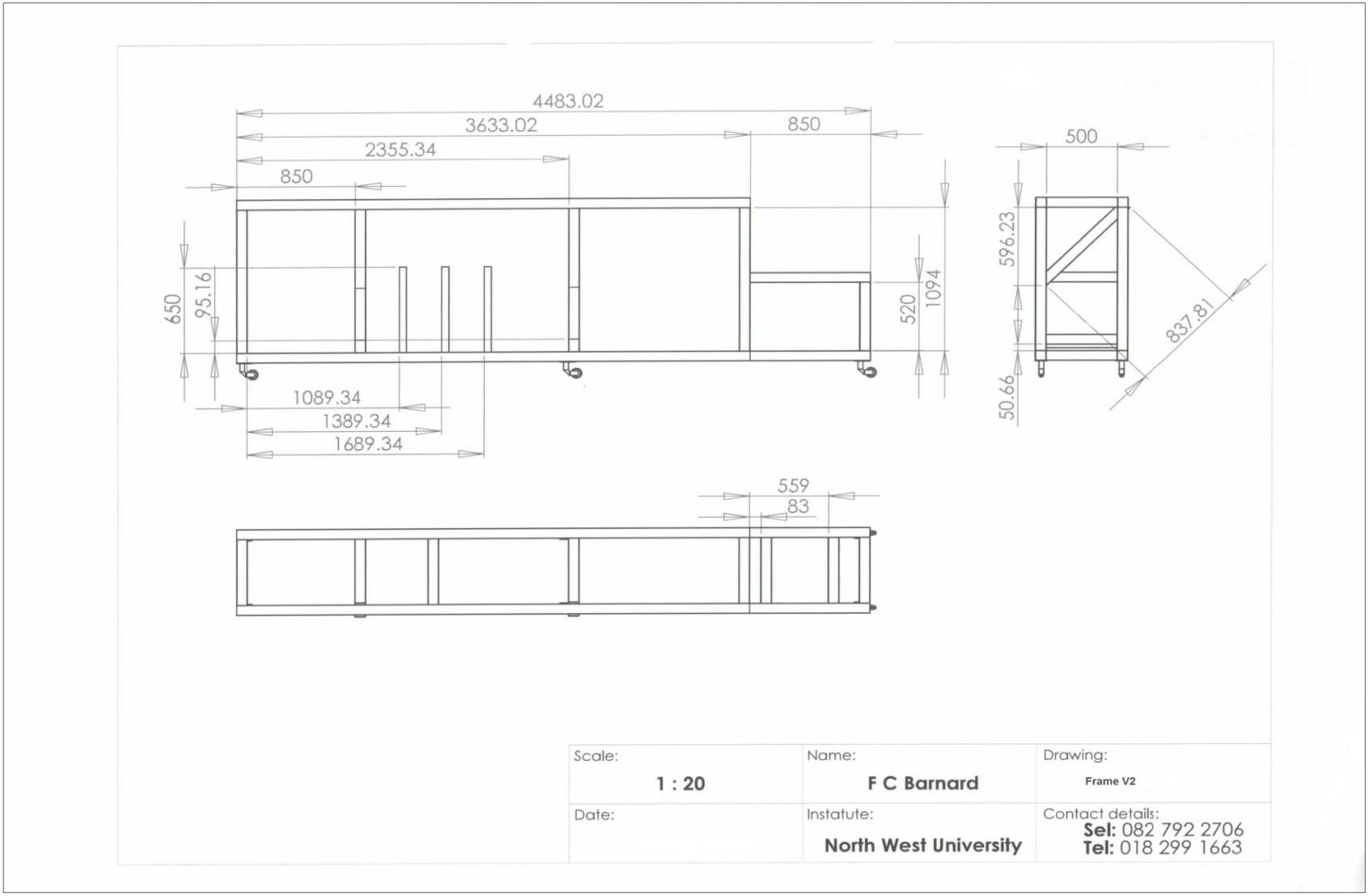

Figure 69: Detail dimensions of the frame.

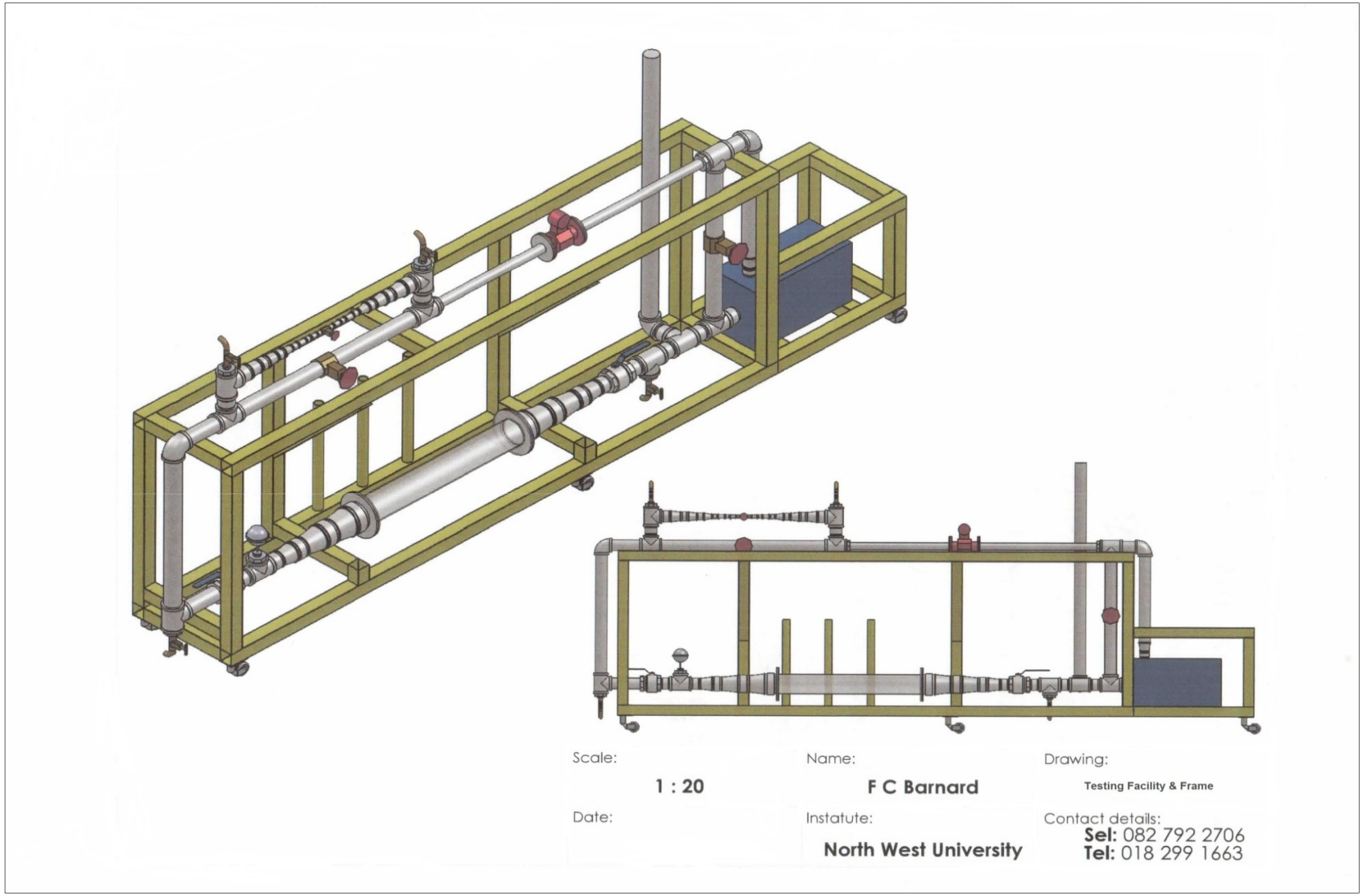

Figure 70: Combination of the testing facility and the frame.

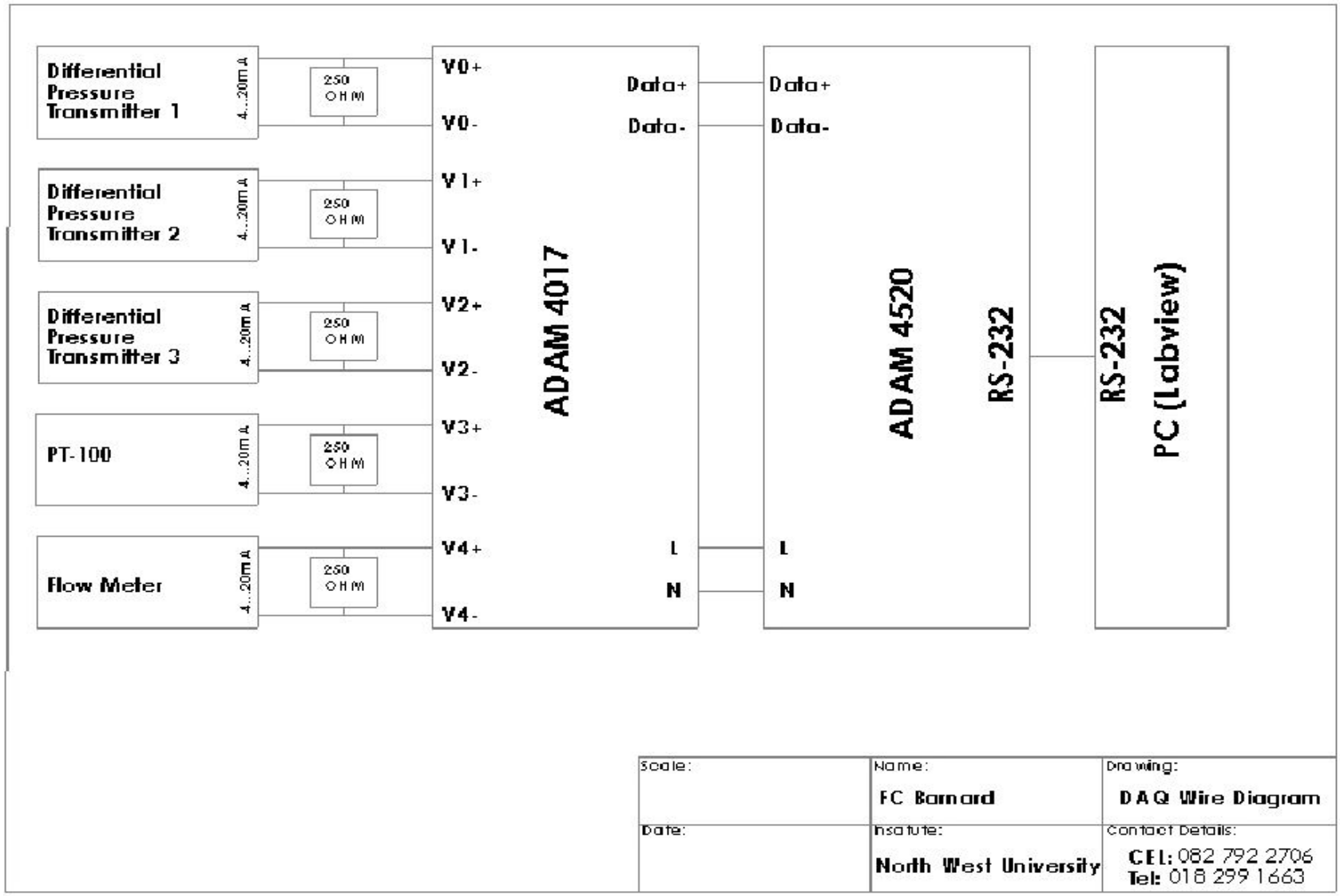

Figure 71: Wire diagram of DAQ system.

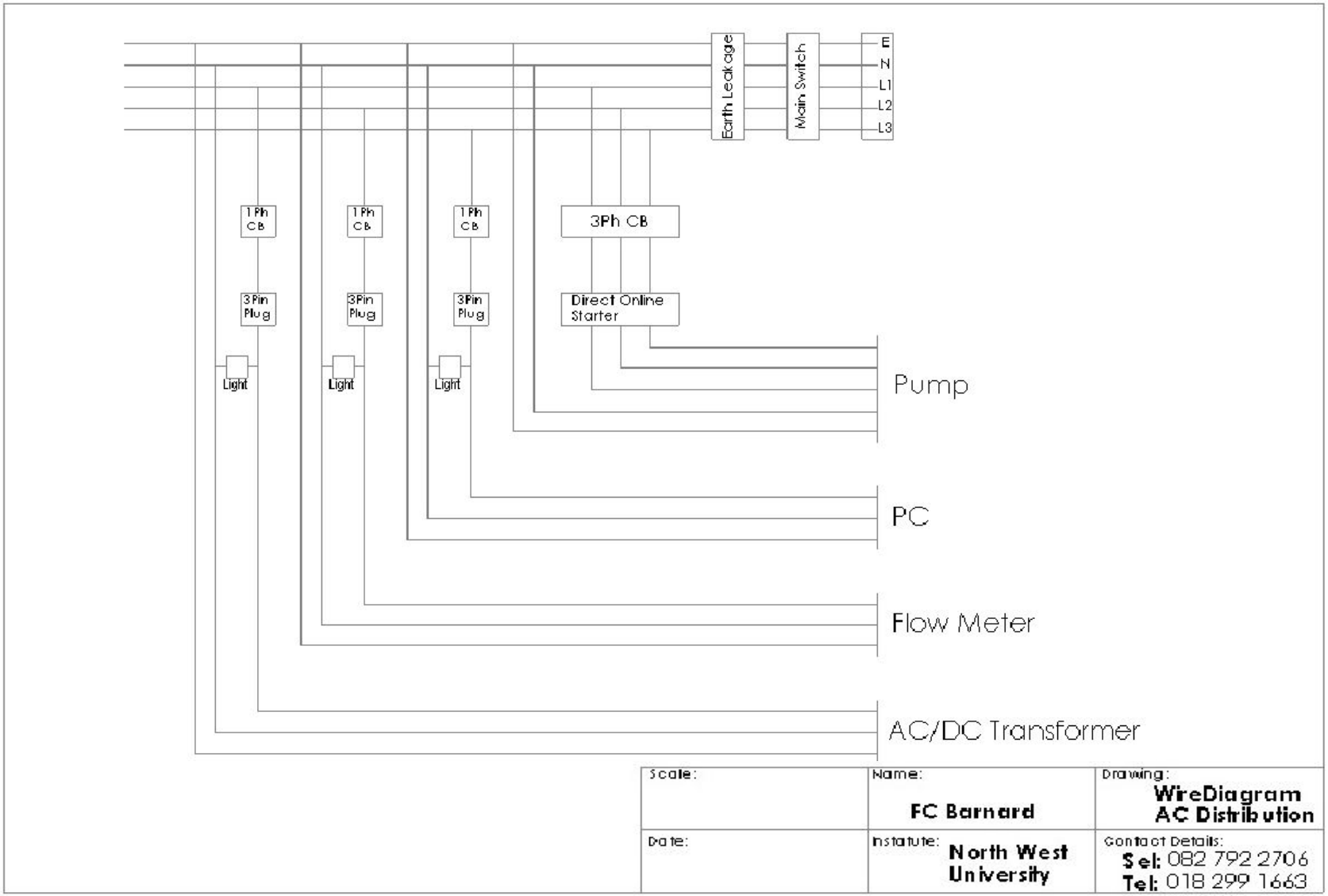

Figure 72: Wiring diagram of AC electricity distribution system.

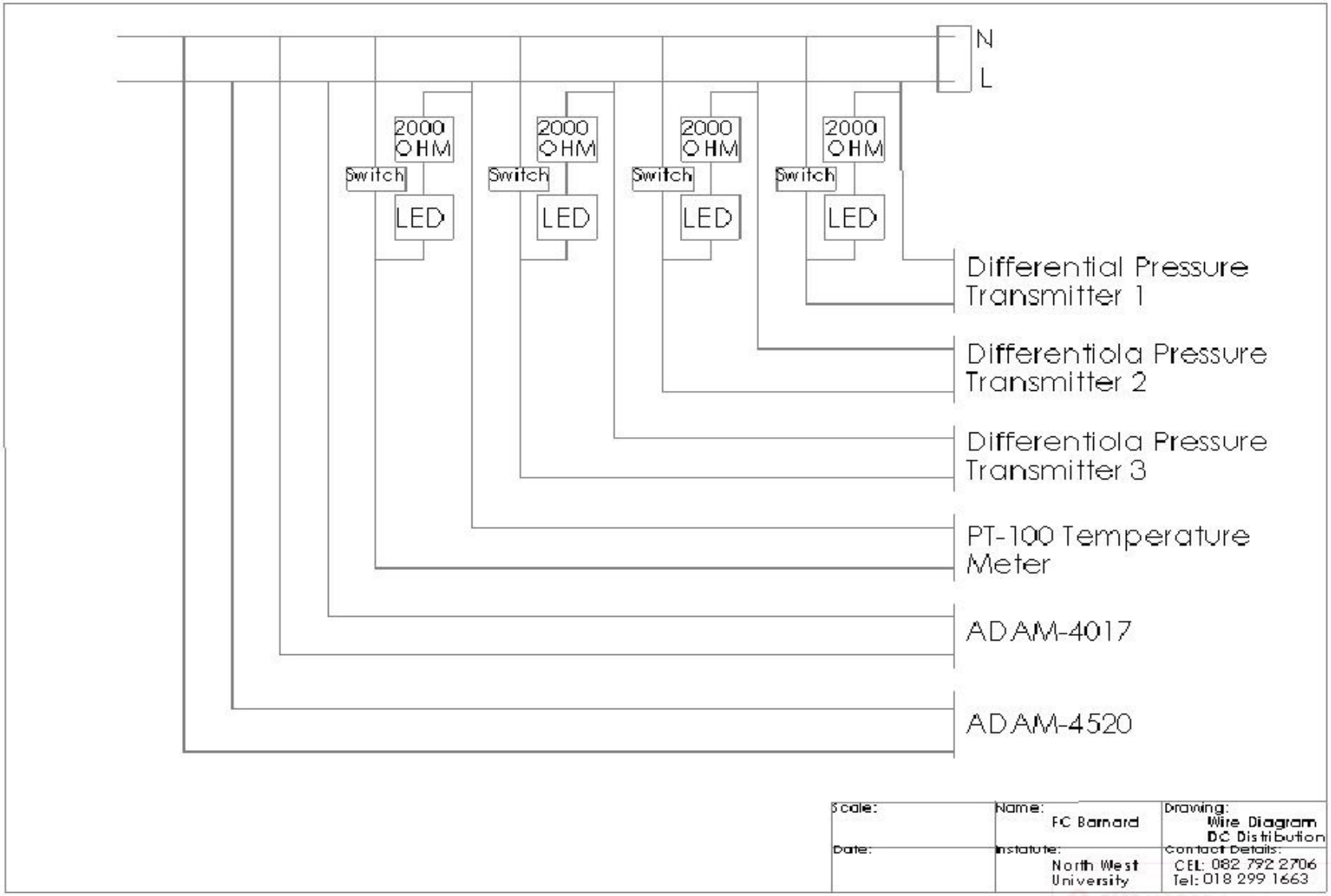

Figure 73: Wire diagram of DC electricity distribution system.

APPENDIX B

Appendix B contain all the additional results from the experiments conducted on the random and structured packings. These results are summarised in the form of graphs and tables. The results for the randomly packed bed are provided first, which is then followed by the results of the structured packed bed.

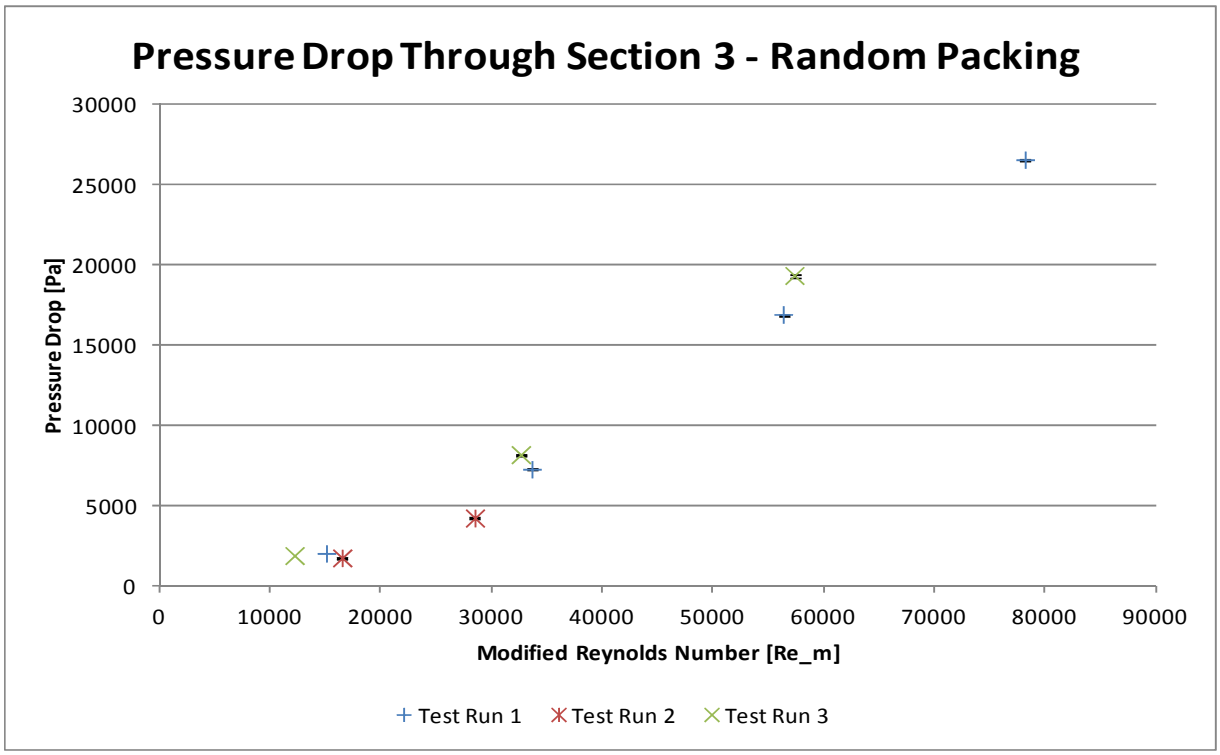

Figure 74: Pressure drop results for section 3 of the random packing.

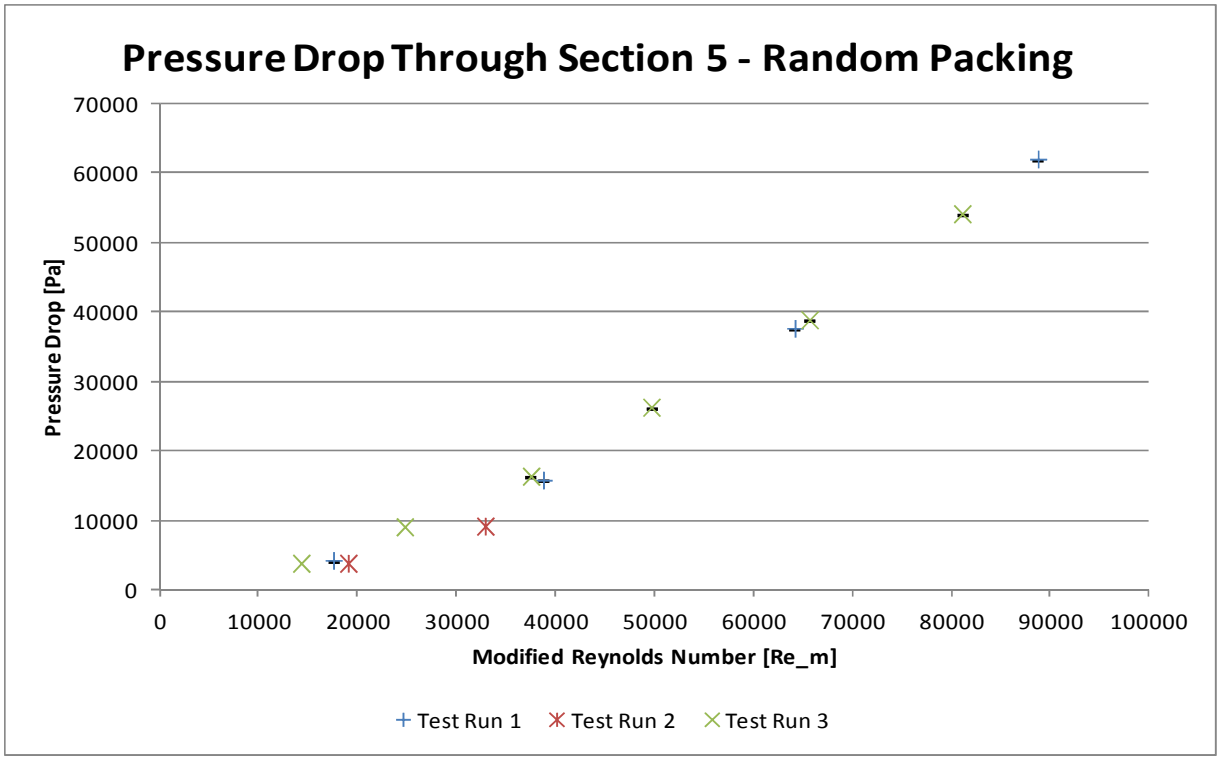

Figure 75: Pressure drop results for section 5 of the random packing.

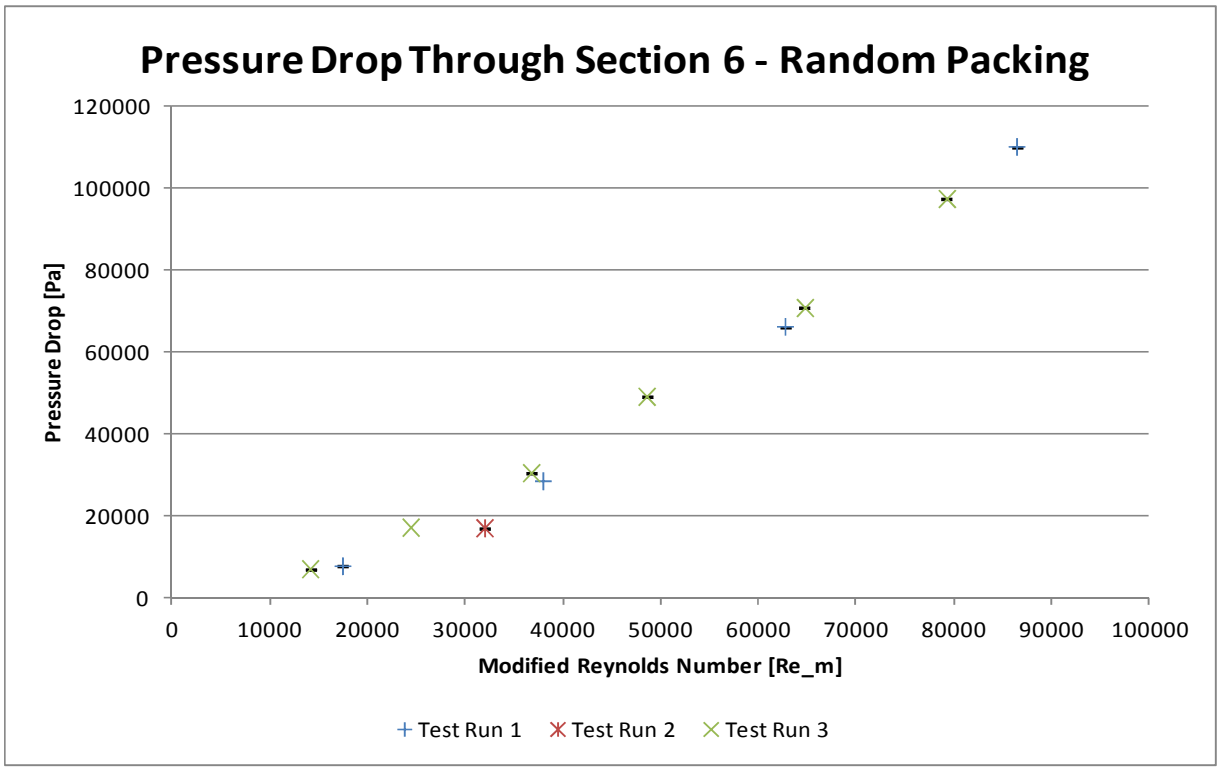

Figure 76: Pressure drop results for section 6 of the random packing.

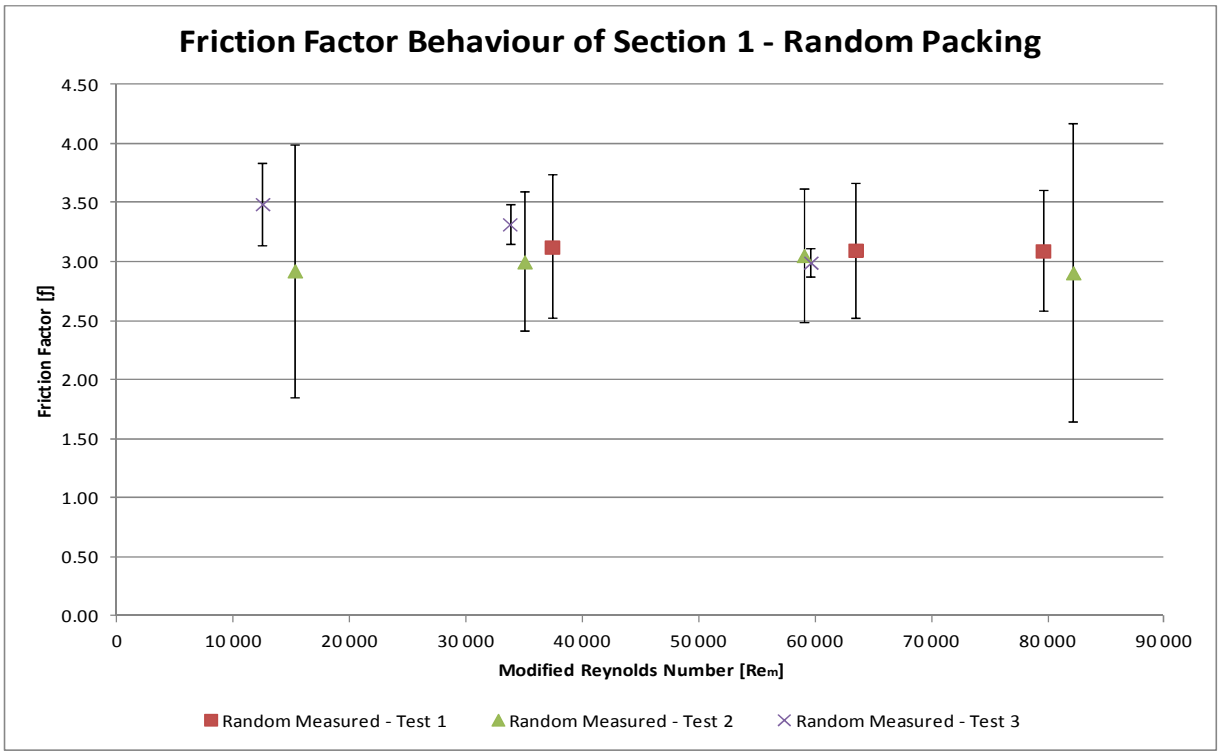

Figure 77: Results for section 1 of the random packing.

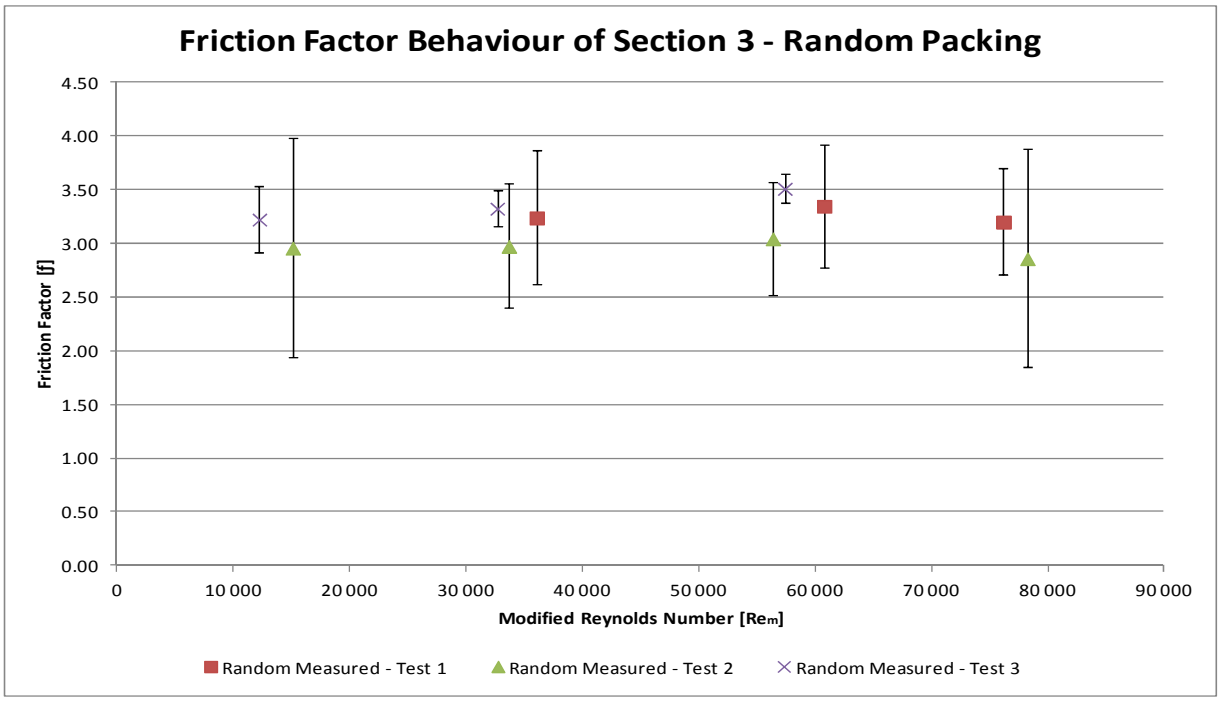

Figure 78: Results for section 3 of the random packing.

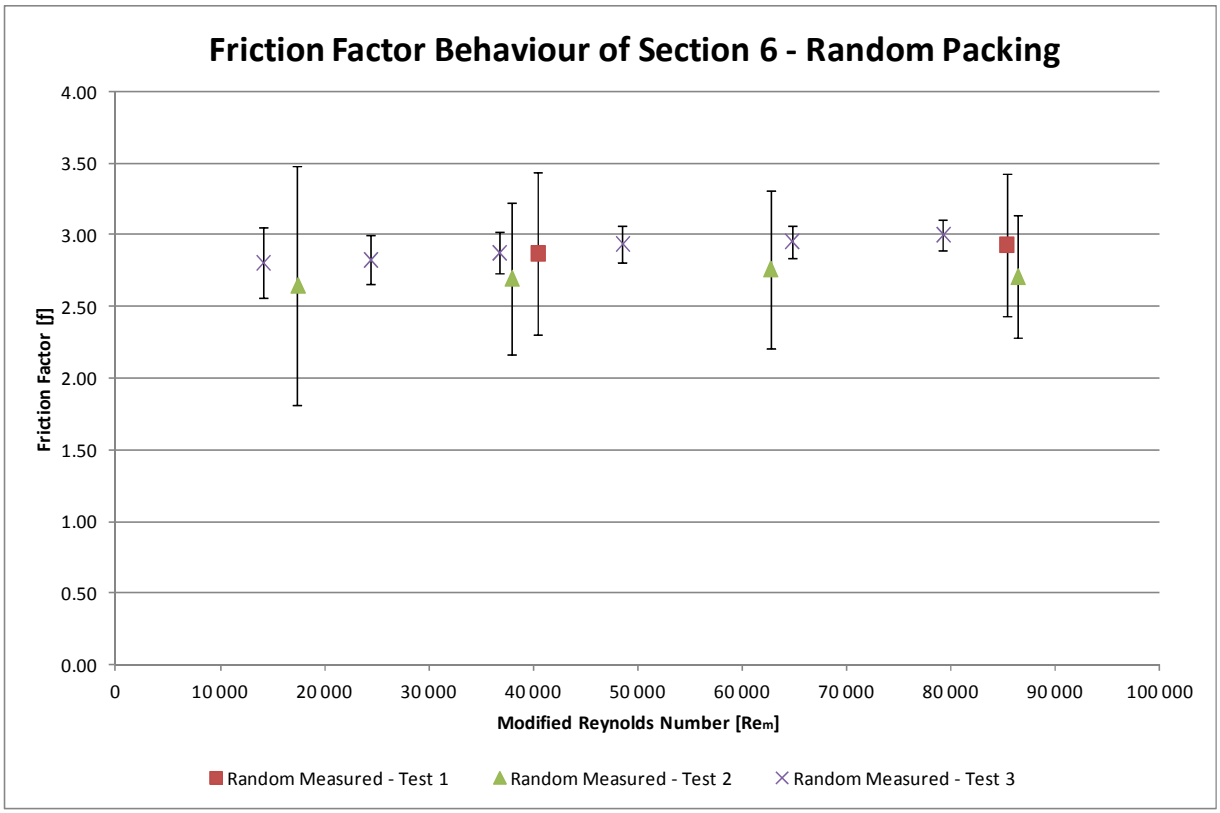

Figure 79: Results for section 6 of the random packing.

Table 13: Experimental data from the first experimental test done on the random packing.

Random Packing - Test 1											
Section 1	Error	Re	Random Measured - Test 1	KTA - Test 1	Ergun - Test 1	Section 4	Error	Re	Random Measured - Test 1	KTA - Test 1	Ergun - Test 1
1	0.61	37365.41	3.13	2.10	1.75	1	0.77	40415.93	3.39	2.09	1.75
2	0.57	63456.88	3.10	1.99	1.75	2	0.58	67900.55	3.60	1.98	1.75
3	0.51	79568.85	3.09	1.95	1.75	3	0.53	84966.27	3.61	1.93	1.75
Section 2	Error	Re	Random Measured - Test 1	KTA - Test 1	Ergun - Test 1	Section 5	Error	Re	Random Measured - Test 1	KTA - Test 1	Ergun - Test 1
1	0.40	39912.76	2.03	2.09	1.75	1	0.59	41490.38	2.83	2.08	1.75
2	0.42	67259.76	2.21	1.98	1.75	2	0.47	69670.72	3.03	1.97	1.75
3	0.38	84662.32	2.37	1.93	1.75	3	0.65	87191.46	3.05	1.93	1.75
Section 3	Error	Re	Random Measured - Test 1	KTA - Test 1	Ergun - Test 1	Section 6	Error	Re	Random Measured - Test 1	KTA - Test 1	Ergun - Test 1
1	0.62	36053.26	3.24	2.11	1.75	1	0.56	40421.70	2.87	2.09	1.75
2	0.57	60764.50	3.35	2.00	1.75	2	0.49	85312.10	2.93	1.93	1.75
3	0.49	76179.11	3.20	1.95	1.75						

Table 14: Experimental data from the second experimental test done on the random packing.

Random Packing - Test 2											
Section 1	Error	Re	Random Measured - Test 2	KTA - Test 2	Ergun - Test 2	Section 4	Error	Re	Random Measured - Test 2	KTA - Test 2	Ergun - Test 2
1	1.07	15265.16	2.93	2.31	1.76	1	0.99	17033.03	3.00	2.28	1.76
2	0.59	35007.99	3.00	2.12	1.75	2	0.73	37623.28	3.08	2.10	1.75
3	0.57	59022.86	3.05	2.01	1.75	3	0.53	62856.07	3.26	1.99	1.75
4	1.26	82177.95	2.91	1.94	1.75	4	0.79	86663.77	3.01	1.93	1.75
Section 2	Error	Re	Random Measured - Test 2	KTA - Test 2	Ergun - Test 2	Section 5	Error	Re	Random Measured - Test 2	KTA - Test 2	Ergun - Test 2
1	0.76	16492.79	2.05	2.29	1.76	1	0.84	17556.69	2.61	2.28	1.76
2	0.42	37162.10	2.11	2.10	1.75	2	0.56	38783.28	2.67	2.09	1.75
3	0.42	62629.91	2.22	1.99	1.75	3	0.44	64199.00	2.84	1.99	1.75
4	0.96	87004.19	2.32	1.93	1.75	4	0.54	88768.20	2.76	1.92	1.75
Section 3	Error	Re	Random Measured - Test 2	KTA - Test 2	Ergun - Test 2	Section 6	Error	Re	Random Measured - Test 2	KTA - Test 2	Ergun - Test 2
1	1.02	15087.86	2.96	2.31	1.76	1	0.84	17415.34	2.65	2.28	1.76
2	0.58	33663.51	2.98	2.13	1.75	2	0.53	37919.76	2.70	2.10	1.75
3	0.53	56357.29	3.05	2.02	1.75	3	0.55	62687.79	2.76	1.99	1.75
4	1.01	78241.08	2.86	1.95	1.75	4	0.43	86390.55	2.71	1.93	1.75

Table 15: Experimental data from the third experimental test done on the random packing.

Random Packing - Test 3											
Section 1	Error	Re	Random Measured - Test 3	KTA - Test 3	Ergun - Test 3	Section 4	Error	Re	Random Measured - Test 3	KTA - Test 3	Ergun - Test 3
1	0.30	12479.16	3.49	2.36	1.76	1	0.29	13729.20	3.11	2.34	1.76
2	0.17	33728.38	3.32	2.12	1.75	2	0.16	36624.73	3.18	2.11	1.75
3	0.12	59616.39	3.00	2.00	1.75	3	0.12	64018.11	3.28	1.99	1.75
Section 2	Error	Re	Random Measured - Test 3	KTA - Test 3	Ergun - Test 3	Section 5	Error	Re	Random Measured - Test 3	KTA - Test 3	Ergun - Test 3
1	0.23	13386.75	2.15	2.34	1.76	1	0.24	14284.11	2.70	2.33	1.76
2	0.12	35956.95	2.26	2.11	1.75	2	0.16	24759.68	2.68	2.19	1.76
3	0.10	63550.79	2.48	1.99	1.75	3	0.14	37518.97	2.77	2.10	1.75
						4	0.12	49672.83	2.83	2.04	1.75
						5	0.11	65672.66	2.94	1.98	1.75
						6	0.11	81102.25	3.01	1.94	1.75
Section 3	Error	Re	Random Measured - Test 3	KTA - Test 3	Ergun - Test 3	Section 6	Error	Re	Random Measured - Test 3	KTA - Test 3	Ergun - Test 3
1	0.31	12212.79	3.23	2.37	1.76	1	0.25	14106.09	2.81	2.33	1.76
2	0.17	32666.33	3.33	2.13	1.75	2	0.17	24390.20	2.83	2.20	1.76
3	0.14	57379.43	3.51	2.01	1.75	3	0.14	36723.17	2.88	2.11	1.75
						4	0.13	48533.81	2.94	2.05	1.75
						5	0.11	64730.94	2.96	1.99	1.75
						6	0.11	79252.07	3.00	1.95	1.75

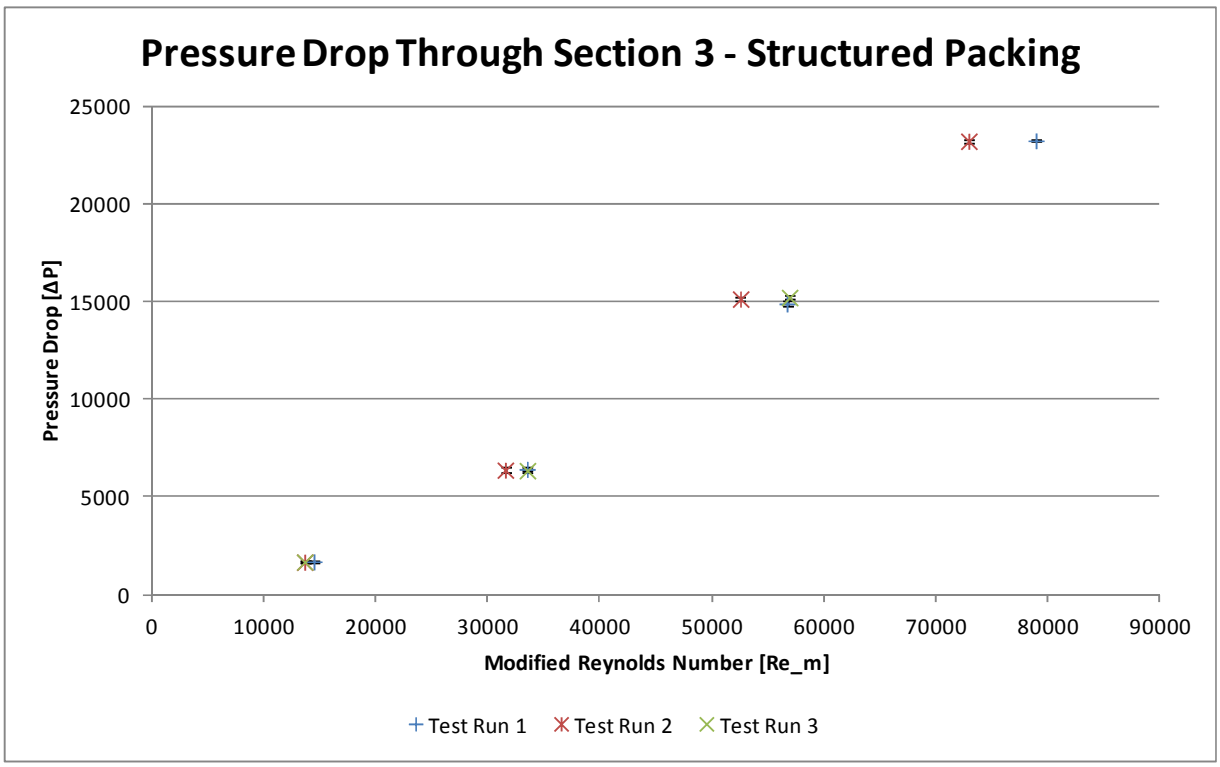

Figure 80: Pressure drop results for section 3 of the structured packing.

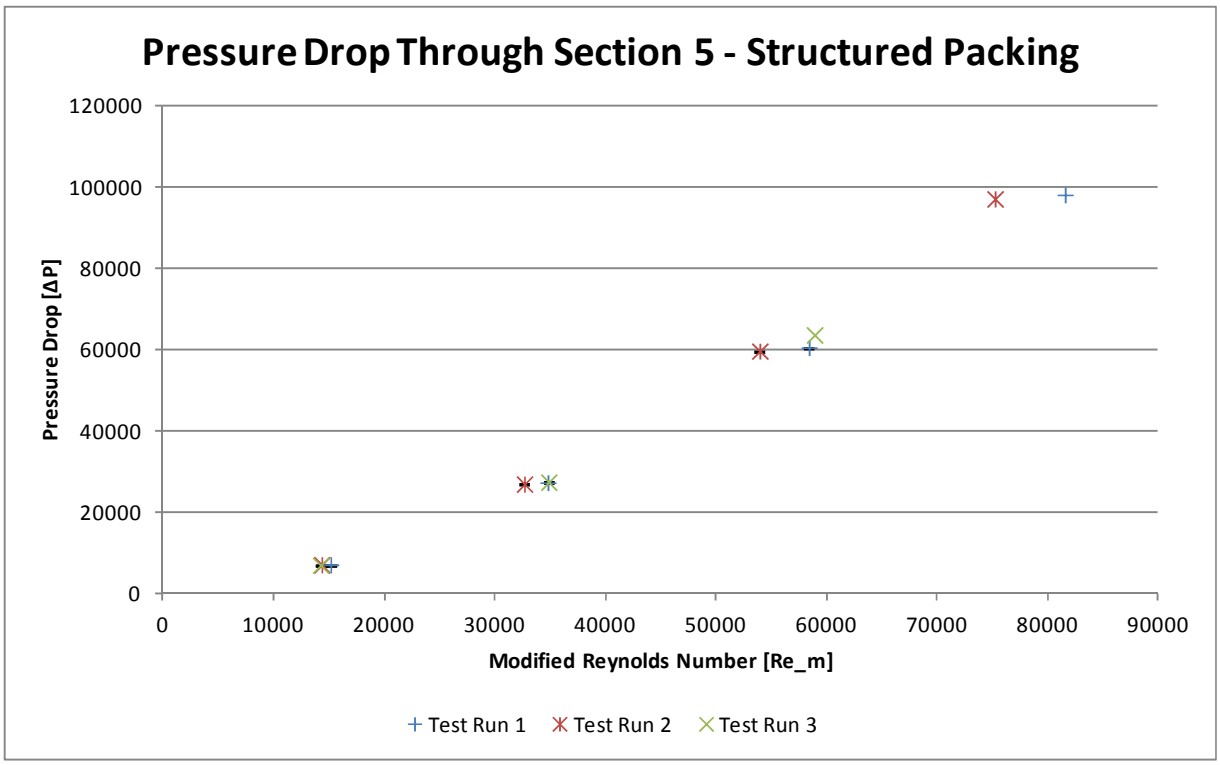

Figure 81: Pressure drop results for section 5 of the structured packing.

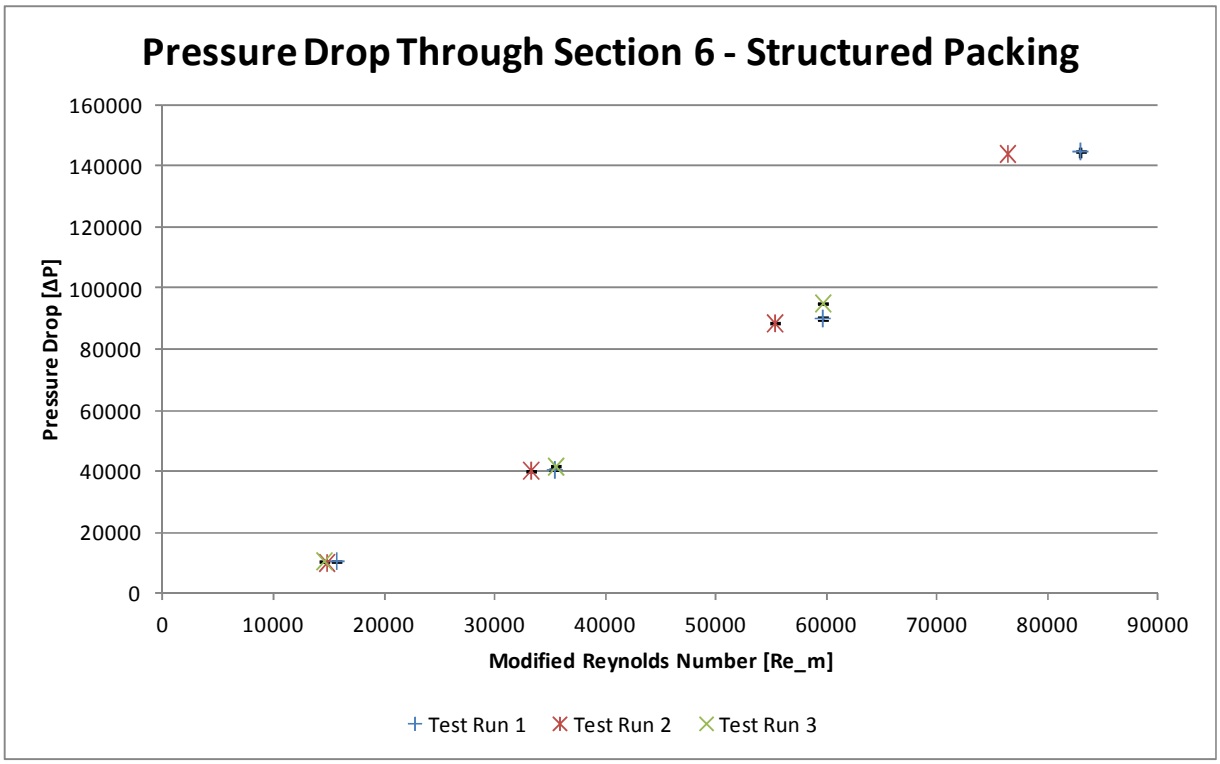

Figure 82: Pressure drop results for section 6 of the structured packing.

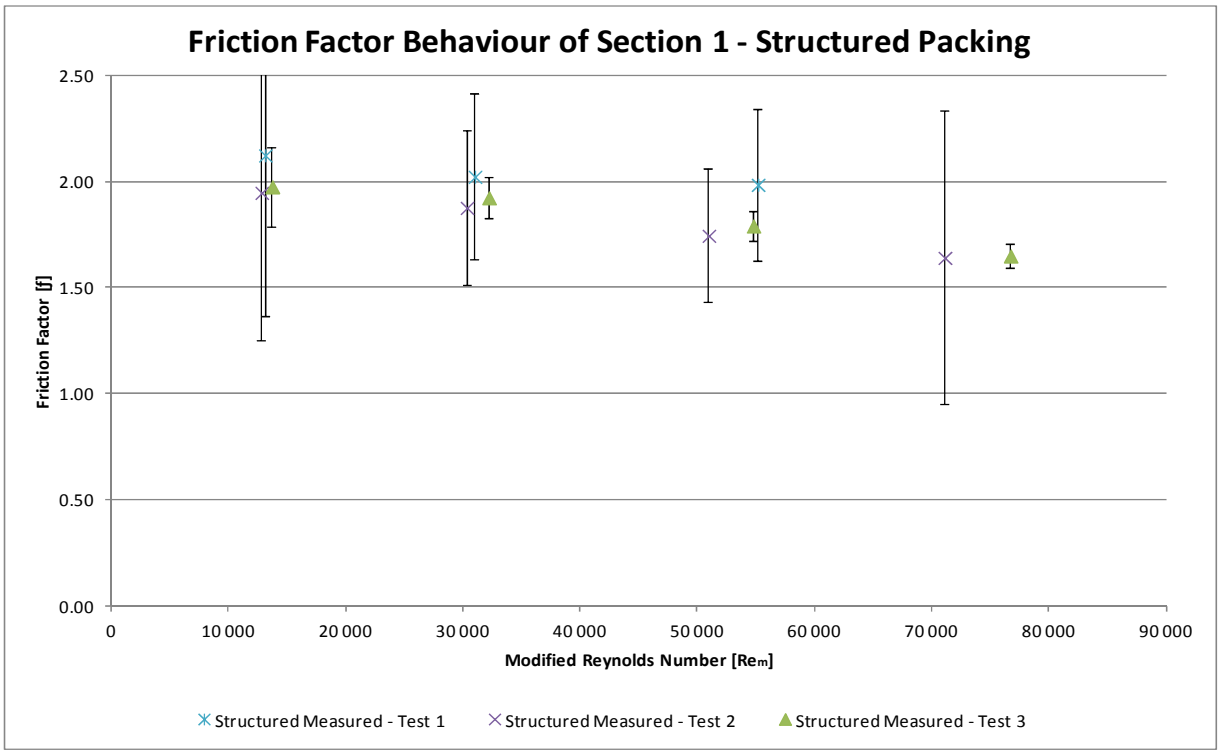

Figure 83: Results for section 1 of the structured packing.

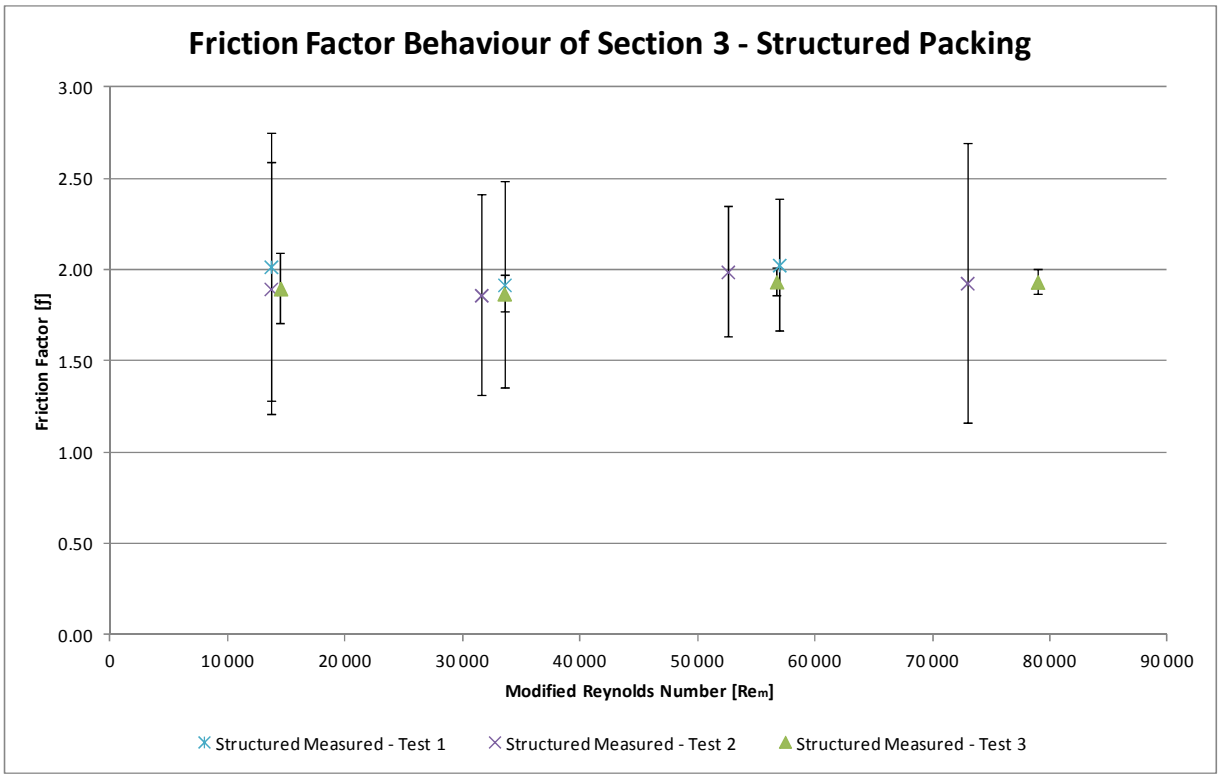

Figure 84: Results for section 3 of the structured packing.

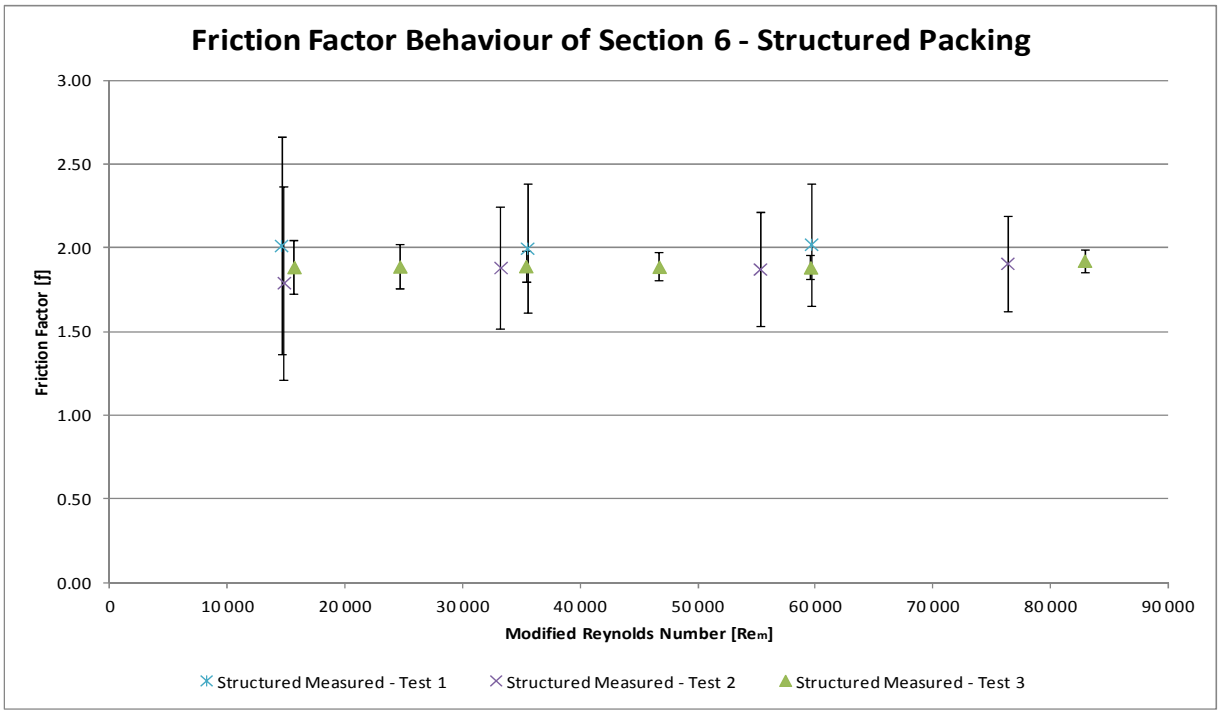

Figure 85: Results for section 6 of the structured packing.

Table 16: Experimental data from the first experimental test done on the structured packing.

Structured Packing - Test 1									
Section 1	Error	Re	Structured Measured - Test 1	Wentz & Thodos - Test 1	Section 4	Error	Re	Structured Measured - Test 1	Wentz & Thodos - Test 1
1	0.76	13085.29	2.12	0.97	1	0.62	14012.95	1.88	0.96
2	0.39	30977.08	2.02	0.83	2	0.40	34162.85	1.85	0.82
3	0.36	55129.57	1.99	0.75	3	0.30	57883.42	1.88	0.75
Section 2	Error	Re	Structured Measured - Test 1	Wentz & Thodos - Test 1	Section 5	Error	Re	Structured Measured - Test 1	Wentz & Thodos - Test 1
1	0.71	13481.69	2.13	0.97	1	0.64	14244.63	1.99	0.96
2	0.46	32930.02	2.09	0.82	2	0.39	34862.23	1.97	0.81
3	0.34	55986.47	2.15	0.75	3	0.42	58886.64	2.01	0.74
Section 3	Error	Re	Structured Measured - Test 1	Wentz & Thodos - Test 1	Section 6	Error	Re	Structured Measured - Test 1	Wentz & Thodos - Test 1
1	0.73	13663.88	2.02	0.97	1	0.65	14547.13	2.01	0.95
2	0.57	33550.55	1.92	0.82	2	0.38	35477.28	2.00	0.81
3	0.36	56942.79	2.03	0.75	3	0.36	59631.90	2.02	0.74

Table 17: Experimental data from the second experimental test done on the structured packing.

Structured Packing - Test 2									
Section 1	Error	Re	Structured Measured - Test 2	Wentz & Thodos - Test 2	Section 4	Error	Re	Structured Measured - Test 2	Wentz & Thodos - Test 2
1	0.69	12778.27	1.95	0.98	1	0.61	13936.96	1.84	0.96
2	0.36	30294.18	1.88	0.83	2	0.39	32035.96	1.80	0.83
3	0.31	50930.77	1.74	0.76	3	0.29	53299.32	1.84	0.76
4	0.69	71075.35	1.64	0.72	4	0.40	74129.84	1.82	0.72
Section 2	Error	Re	Structured Measured - Test 2	Wentz & Thodos - Test 2	Section 5	Error	Re	Structured Measured - Test 2	Wentz & Thodos - Test 2
1	0.66	13272.53	1.99	0.97	1	0.61	14347.30	1.89	0.96
2	0.43	30992.43	1.97	0.83	2	0.37	32669.38	1.88	0.82
3	0.32	51704.10	2.03	0.76	3	0.40	53944.36	1.88	0.76
4	0.47	71904.64	2.02	0.72	4	0.32	75223.00	1.93	0.72
Section 3	Error	Re	Structured Measured - Test 2	Wentz & Thodos - Test 2	Section 6	Error	Re	Structured Measured - Test 2	Wentz & Thodos - Test 2
1	0.69	13659.40	1.90	0.97	1	0.58	14779.86	1.79	0.95
2	0.55	31569.10	1.86	0.83	2	0.36	33225.13	1.88	0.82
3	0.36	52559.41	1.99	0.76	3	0.34	55282.75	1.87	0.75
4	0.77	72943.77	1.93	0.72	4	0.29	76328.92	1.91	0.71

Table 18: Experimental data from the third experimental test done on the structured packing.

Structured Packing - Test 3									
Section 1	Error	Re	Structured Measured - Test 3	Wentz & Thodos - Test 3	Section 4	Error	Re	Structured Measured - Test 3	Wentz & Thodos - Test 3
1	0.19	13688.66	1.98	0.97	1	0.17	14770.50	1.89	0.95
2	0.10	32178.53	1.92	0.82	2	0.09	34082.00	1.83	0.82
3	0.07	54742.37	1.79	0.75	3	0.07	57554.00	1.85	0.75
4	0.06	76688.28	1.65	0.71	4	0.06	80166.57	1.84	0.71
Section 2	Error	Re	Structured Measured - Test 3	Wentz & Thodos - Test 3	Section 5	Error	Re	Structured Measured - Test 3	Wentz & Thodos - Test 3
1	0.18	14064.49	2.01	0.96	1	0.16	15161.89	1.91	0.95
2	0.10	33069.03	1.97	0.82	2	0.13	23867.95	1.90	0.87
3	0.08	55670.35	2.03	0.75	3	0.09	34792.25	1.90	0.81
4	0.07	77851.48	2.04	0.71	4	0.08	46103.62	1.89	0.78
					5	0.07	58396.95	1.89	0.75
					6	0.07	81557.35	1.95	0.71
Section 3	Error	Re	Structured Measured - Test 3	Wentz & Thodos - Test 3	Section 6	Error	Re	Structured Measured - Test 3	Wentz & Thodos - Test 3
1	0.19	14484.72	1.90	0.96	1	0.16	15652.61	1.89	0.94
2	0.10	33524.85	1.87	0.82	2	0.13	24644.90	1.89	0.86
3	0.08	56718.16	1.94	0.75	3	0.09	35363.89	1.89	0.81
4	0.07	78940.78	1.94	0.71	4	0.08	46708.41	1.89	0.77
					5	0.07	59583.61	1.88	0.74
					6	0.07	82887.46	1.92	0.71

Table 19: Average standard deviations for the pressure drop test done on the random packing at Re_m=15 500 (Numbers rounded).

Section 1 of Test Run 3 - Point 1																											
Count	1	2	3	4	5	6	7	8	9	10	11	12	13	14	15	16	17	18	19	20	21	22	23	24	25	26
ΔP [Pa]	1587	1601	1622	1639	1607	1607	1594	1590	1586	1608	1594	1597	1618	1628	1608	1606	1621	1602	1607	1573	1591	1607	1616	1631	1602	1614
Average ΔP [ẍ]	1606																									
$(ẍ-x)^2$	346	26	251	1111	2	1	147	259	384	5	147	74	147	477	5	0	213	19	0	1111	213	1	107	617	17	62
Standard Deviation sqrt{sum[$(ẍ-x)^2$]/ (26-1)}	15	0.94%																								
Section 2 of Test Run 3 - Point 1																											
Count	1	2	3	4	5	6	7	8	9	10	11	12	13	14	15	16	17	18	19	20	21	22	23	24	25	26
ΔP [Pa]	1321	1305	1319	1309	1290	1301	1293	1295	1299	1302	1305	1287	1278	1268	1268	1273	1298	1305	1290	1281	1279	1324	1298	1289	1292	1301
Average ΔP [ẍ]	1295																									
$(ẍ-x)^2$	698	109	596	201	23	32	5	0	16	55	94	69	290	729	743	463	10	99	23	204	265	821	7	36	11	32
Standard Deviation sqrt{sum[$(ẍ-x)^2$]/ (26-1)}	15	1.16%																								
Section 3 of Test Run 3 - Point 1																											
Count	1	2	3	4	5	6	7	8	9	10	11	12	13	14	15	16	17	18	19	20	21	22	23	24	25	26
ΔP [Pa]	1838	1844	1842	1837	1876	1877	1875	1861	1871	1860	1864	1861	1866	1858	1859	1891	1897	1884	1882	1893	1885	1884	1889	1908	1893	1892
Average ΔP [ẍ]	1873																									
$(ẍ-x)^2$	1167	836	925	1254	14	18	8	137	4	149	71	131	42	223	181	324	576	121	91	410	151	133	273	1277	410	381
Standard Deviation sqrt{sum[$(ẍ-x)^2$]/ (26-1)}	19	1.03%																								
Section 4 of Test Run 3 - Point 1																											
Count	1	2	3	4	5	6	7	8	9	10	11	12	13	14	15	16	17	18	19	20	21	22	23	24	25	26
ΔP [Pa]	2467	2480	2455	2492	2505	2510	2480	2487	2490	2479	2483	2493	2462	2484	2474	2468	2468	2496	2458	2464	2467	2467	2469	2468	2447	2467
Average ΔP [ẍ]	2476																									
$(ẍ-x)^2$	78	17	432	237	834	1130	12	124	186	7	41	294	212	67	7	65	65	376	317	158	82	78	54	65	829	78
Standard Deviation sqrt{sum[$(ẍ-x)^2$]/ (26-1)}	15	0.62%																								

Table 20: Average standard deviations for the pressure drop tests done on the structured packing at Re_m=13 000 (Numbers rounded).

Section 1 of Test Run 3 - Point 1																											
Count	1	2	3	4	5	6	7	8	9	10	11	12	13	14	15	16	17	18	19	20	21	22	23	24	25	26
ΔP [Pa]	1950	1946	1954	1962	1939	1943	1957	1945	1938	1949	1943	1962	1959	1960	1979	1975	1964	1980	1925	1951	1981	1991	1975	1983	1957	1992
Average ΔP [ẍ]	1960																									
$(ẍ-x)^2$	96	184	37	3	432	290	11	219	497	111	274	3	2	0	357	237	14	396	1226	73	458	939	215	513	11	1017
Standard Deviation sqrt{sum[$(ẍ-x)^2$]/ (26-1)}	17	0.89%																								
Section 2 of Test Run 3 - Point 1																											
Count	1	2	3	4	5	6	7	8	9	10	11	12	13	14	15	16	17	18	19	20	21	22	23	24	25	26
ΔP [Pa]	3367	3388	3435	3498	3528	3497	3493	3439	3452	3451	3467	3459	3400	3383	3392	3396	3432	3460	3513	3506	3400	3395	3391	3396	3398	3412
Average ΔP [ẍ]	3437																									
$(ẍ-x)^2$	4892	2374	3	3827	8384	3674	3234	5	246	201	955	525	1332	2832	1979	1660	21	572	5866	4809	1332	1721	2046	1619	1482	613
Standard Deviation sqrt{sum[$(ẍ-x)^2$]/ (26-1)}	47	1.38%																								
Section 3 of Test Run 3 - Point 1																											
Count	1	2	3	4	5	6	7	8	9	10	11	12	13	14	15	16	17	18	19	20	21	22	23	24	25	26
ΔP [Pa]	1860	1785	1761	1756	1712	1693	1664	1646	1641	1664	1668	1662	1644	1650	1643	1653	1652	1664	1694	1687	1671	1662	1681	1671	1675	1652
Average ΔP [ẍ]	1685																									
$(ẍ-x)^2$	30728	9982	5805	5034	730	65	437	1531	1947	437	278	536	1692	1200	1775	1049	1066	437	86	2	208	536	20	194	104	1115
Standard Deviation sqrt{sum[$(ẍ-x)^2$]/ (26-1)}	52	3.07%																								
Section 4 of Test Run 3 - Point 1																											
Count	1	2	3	4	5	6	7	8	9	10	11	12	13	14	15	16	17	18	19	20	21	22	23	24	25	26
ΔP [Pa]	3583	3628	3565	3527	3525	3533	3538	3530	3538	3495	3501	3505	3574	3557	3620	3618	3576	3570	3586	3588	3559	3543	3536	3538	3531	3532
Average ΔP [ẍ]	3554																									
$(ẍ-x)^2$	833	5558	119	692	801	433	250	566	235	3451	2783	2402	405	13	4365	4137	479	260	1047	1164	32	107	308	250	509	465
Standard Deviation sqrt{sum[$(ẍ-x)^2$]/ (26-1)}	36	1.00%																								

APPENDIX C

In Appendix C the EES program for the design of the testing facility is provided.

```
"Fluid Properties
-------------------------"

rho[1] = DENSITY(Water,T=T[1],P=P[1])
mu[1] = VISCOSITY(Water,T=T[1],P=P[1])

{T[1] = 60}
P[1] = 600

"Conservation of Mass
---------------------------------"

m_._P = m_._TSL + m_._BPL
m_._FM = m_._TSL
{m_._P = 1}
{m_._TSL = 0.7}

"Test Section Loop
-----------------------------"

DELTAP_TSL = ((f_TSL*(l_TSL/d_TSL))+K_TSL) * ((abs(m_._TSL)*m_._TSL)/(2*rho[1]*A_pipe_TSL)) +
((f_FM*(l_FM/d_FM)) * ((abs(m_._FM)*m_._FM)/(2*rho[1]*A_pipe_FM)))
DELTAP_TSL_CV = (K_TSL_CV * ((abs(m_._TSL)*m_._TSL)/(2*rho[1]*A_pipe_TSL)))

Re_TSL = (rho[1]*V_TSL*d_TSL)/mu[1]
Re_FM = (rho[1]*V_FM*d_FM)/mu[1]
epsilon_pipe = 0.15                    {Galv = 0.15;  PVC = 0.0015}
RR_TSL = epsilon_pipe / d_TSL
RR_FM = epsilon_pipe / d_FM
f_TSl = MoodyChart(Re_TSL, RR_TSL)
f_FM = MoodyChart(Re_FM, RR_FM)

K_TSL = 0.9+7+7+0.9+0.9+2+2+0.9+0.05+7+7+0.05+0.9+0.9+0.9
l_TSL = 1.7+1.7+1.3+0.5
d_TSL = 0.08
A_pipe_TSL = (pi/4)*d_TSL^2
m_._TSL = rho[1] * V_TSL * A_pipe_TSL
m_._TSL = q_._TSL/60

{K_TSL_CV = 10000}

l_FM = 1.5
d_FM = 0.05
A_pipe_FM = (pi/4)*d_FM^2
m_._FM = rho[1] * V_FM * A_pipe_FM

"By Pass Loop
----------------------"
DELTAP_BPL = ((f_BPL*(l_BPL/d_BPL))+K_BPL) * ((abs(m_._BPL)*m_._BPL)/(2*rho[1]*A_pipe_BPL))
DELTAP_BPL_CV = (K_BPL_CV) * ((abs(m_._BPL)*m_._BPL)/(2*rho[1]*A_pipe_BPL))

Re_BPL = (rho[1]*V_BPL*d_BPL)/mu[1]
RR_BPL = epsilon_pipe / d_BPL
f_BPL = MoodyChart(Re_BPL, RR_BPL)

{K_BPL_CV = 10000}
```

```
K_BPL = 4
l_BPL = 1.5
d_BPL = 0.08
A_pipe_BPL = (pi/4)*d_BPL^2
m_._BPL = rho[1] * V_BPL * A_pipe_BPL
m_._BPL = q_._BPL/60

"Packed Bed
--------------------"
    "Bed Parameters
    -------------------------"
    epsilon = 0.36
    d_p = 0.03
    n = 20
    L = n * d_p
    A_o = pi * (0.14/2)^2
    m_._TSL = rho[1] * V_o * A_o
    Re_o = (rho[1] * V_o * d_p) / mu[1]
    Re_m = Re_o/(1-epsilon)

    "Pressure Drop Parameters
    ----------------------------------------"
    psi_A = (320/(Re_o/(1-epsilon)))
    psi_B = 1.8 {(6/((Re_o/(1-epsilon))^(0.1)))}

    psi = psi_A + psi_B

    Eu = 0.5 * psi * ((1-epsilon)/(epsilon^3))*(L/d_p)
    DELTAP_Packing = (Eu * rho[1] * V_o^2)
    F_TS = (DELTAP_Packing*A_o)/9.81


"Pump Loop
--------------------"
{q_._p = 2000}
h_p  = (-0.000004*q_._p^2) + (0.006*q_._p) + 32.508
DELTAP_pump = rho[1]*9.81*h_p

m_._P = q_._p/60

DELTAP_PL = ((f_PL*(l_PL/d_PL))+K_PL) * ((abs(m_._P)*m_._P)/(2*rho[1]*A_pipe_PL))

Re_PL = (rho[1]*V_PL*d_PL)/mu[1]
RR_PL = epsilon_pipe / d_PL
f_PL = MoodyChart(Re_PL, RR_PL)

K_PL = 1+1.5+7
l_PL = 1.5
d_PL = 0.08
A_pipe_PL = (pi/4)*d_PL^2
m_._P = rho[1] * V_PL * A_pipe_PL

DELTAP_pump = DELTAP_PL + DELTAP_BPL_CV + DELTAP_BPL {+ DELTAP_TSL_CV +
DELTAP_TSL + DELTAP_Packing}
DELTAP_BPL_CV + DELTAP_BPL = DELTAP_TSL_CV + DELTAP_TSL + DELTAP_Packing
```

```
h_inlet = 2
P_MAX = (rho[1]*9.81*h_inlet)+DELTAP_pump
F_MAX = (P_MAX*A_pipe_FM)/9.81
```